Design Earthquakes Based on Probabilistic Seismic Hazard Analysis

by

Shun-Hao Ni

A thesis
presented to the University of Waterloo
in fulfilment of the
thesis requirement for the degree of
Doctor of Philosophy
in
Civil Engineering

Waterloo, Ontario, Canada, 2012

Author's Declaration

I hereby declare that I am the sole author of this thesis. This is a true copy of the thesis, including any required final revisions, as accepted by my examiners.

I understand that my thesis may be made electronically available to the public.

Abstract

Earthquake is one of the most destructive natural disasters leading to financial, environmental, and even human losses. The most effective approach to prevent losses induced by structural damage is seismic design for structures, in which the determination of design earthquakes, including seismic design spectra and seismic design ground motions, is of great importance.

Probabilistic Seismic Hazard Analysis (PSHA) has been widely used for the determination and selection of design earthquakes. However, there are a number of issues on the engineering application of PSHA in obtaining the design earthquakes, which need to be addressed before it can be readily implemented into reliability- and performance-based seismic design. In this research, based on the PSHA, the generation of seismic design spectra and spectrum-compatible earthquake ground motions is studied.

The PSHA-based seismic design spectra mainly include Uniform Hazard Spectrum (UHS), predicted spectrum based on Ground-Motion Prediction Equations (GMPEs), and Conditional Mean Spectrum considering ε (CMS-ε). These existing design spectra, however, do not or only partially provide probabilistic knowledge about the simultaneous occurrence of spectral accelerations at multiple vibration periods. The lack of such probabilistic knowledge of the design spectra may prevent them from being incorporated into reliability- and performance-based seismic design.

The purpose of this study is to bridge the gaps between seismological analyses and engineering applications, i.e., to find suitable representations of design earthquakes from the PSHA so that they can be readily applied in reliability- and performance-based seismic design procedure. A generalized approach is developed to generate seismic design spectra using both scalar and vector-valued PSHA, which overcomes the deficiencies and preserves certain advantages of the existing PSHA-based seismic design spectra. To simplify the approach to the generation of seismic design spectra so that they can be easily incorporated into structural design and further performance-based seismic design, an approximate approach is also developed.

On the other hand, spectrum-compatible earthquake ground motions, which are generated by manipulating recorded ground motions, have been widely used for seismic design verification and seismic qualification of structures. The existing spectral matching algorithms in frequency-domain, however, may distort the valuable information contained in recorded earthquake ground motions due to the deficiency of the transformation methodologies on which they are based.

To properly preserve the frequency contents and nonstationary characteristics of recorded ground motions, a signal processing method called Hilbert-Huang Transform (HHT) is used to generate spectrum-compatible earthquake ground motions. In the proposed generation procedures, the strategy of the selection of recorded ground motions is based on the PSHA so that the generated ground motions reflect realistic seismic hazard for the site of interest.

Acknowledgments

I would like to thank all people who have helped and inspired me during my doctoral study.

I especially like to express my sincere appreciation to my supervisors, Professor Wei-Chau Xie and Professor Mahesh D. Pandey, whose encouragement, guidance, and support from the initial to the final level enabled me to develop an understanding of the subject.

I would like to extend my gratitude to Professors Gail Atkinson, Gordon J. Savage, Giovanni Cascante, and Jeffrey S. West, for serving as my thesis committee members, and for their insightful comments and cares for my research.

I was delighted to interact with Dr. Binh-Le Ly, Dr. Tarek S. Aziz, Mr. Wei Liu, Dr. Zhi-Hua Chen, Mr. Sudip Adhikari, Dr. Yu-Xin Liu, Mrs. Yi-Ming Jiang, and Dr. Ying An, of Candu Energy Inc., by sharing conversations to nuclear industry. Their engineering experiences and valuable suggestions have had a remarkable influence on this research.

Thanks also go to my friends and colleagues, Dr. Tian-Jin Cheng, Dr. Dong-Liang Lu, Arun Veeramany, Dr. Min Wang, Richard Wiebe, Jin Zhou, Lu Xin, Xu-Fang Zhang, Jian Deng, De-Yi Zhang, Bo Li, Zhao-Liang Wang, Yu-Song Xue, Dritan Topuzi, Chao Jin, Dr. Wei-Wei Du, Dr. Lei Liu, and other graduate students in the Department of Civil and Environmental Engineering, with whom I shared the unforgettable days in Waterloo.

The financial support by the Natural Sciences and Engineering Research Council of Canada (NSERC) and the University Network of Excellence in Nuclear Engineering (UNENE) in the form of a Research Assistantship is greatly appreciated.

Last but not least, without the unflagging love, support, and encouragement from my parents, parents-in-law, and my wife, Qi Sun, throughout these years, this thesis would not be possible.

TO

My Family

Contents

List of Figures x

Nomenclature xvi

1 **Introduction** 1

1.1 Overview 1

1.2 Objectives of This Study 7

1.3 Organization of This Study 7

2 **Seismic Hazard Analysis** 10

2.1 Engineering Seismology 10

2.1.1 Ground-Motion Prediction Equations 11

2.1.2 Correlation Coefficients of Spectral Accelerations 19

2.1.3 Probability Distribution of Spectral Accelerations 23

2.2 Deterministic Seismic Hazard Analysis 25

2.3 Probabilistic Seismic Hazard Analysis 26

2.3.1 Probability Distribution of Source-site Distance 30

2.3.2 Probability Distribution of Earthquake Magnitude 33

2.3.3 Scalar Probabilistic Seismic Hazard Analysis 36

2.3.4 Vector-valued Probabilistic Seismic Hazard Analysis 39

2.4 Seismic Hazard Deaggregation 42

2.4.1 Scalar Seismic Hazard Deaggregation 42

2.4.2 Vector-valued Seismic Hazard Deaggregation 49

2.5 Treatment of Epistemic Uncertainty 51

2.6 Summary 53

3 Seismic Design Spectra **54**
3.1 Existing Seismic Design Spectra Based on PSHA 55
3.1.1 Uniform Hazard Spectrum 56
3.1.2 Predicted Spectrum Based on GMPEs 57
3.1.3 Conditional Mean Spectrum Considering Epsilon 58
3.2 Generalized Approach for Generating Design Spectra 60
3.2.1 Vector-valued Uniform Hazard Spectrum 63
3.2.2 Vector-valued Non-Uniform Hazard Spectrum 64
3.2.3 Vector-valued Conditional Uniform Hazard Spectrum 66
3.2.4 Approximation of Generalized Approach 69
3.2.5 Numerical Examples 73
3.3 Summary 87

4 Spectrum-Compatible Ground Motions **89**
4.1 Existing Spectral Matching Algorithms 90
4.2 Hilbert-Huang Transform 93
4.2.1 Empirical Mode Decomposition 94
4.2.2 Hilbert Spectral Analysis 96
4.3 Spectral Matching for Single Motions 104
4.3.1 Generation of Single Ground Motions 107
4.3.2 Numerical Examples 109
4.4 Spectral Matching for Multiple Motions 129
4.4.1 Generation of Multiple Ground Motions 130
4.4.2 Numerical Examples 135
4.5 Spectral Matching for Tri-directional Motions 152
4.5.1 Generation of Tri-directional Ground Motions 154
4.5.2 Numerical Examples 158
4.6 Summary 166

5 **Conclusions and Future Research** **179**
5.1 Vector-valued Seismic Hazard Deaggregation 179
5.2 Generalized Approach for Generating Design Spectra 180
5.3 Spectral Matching Algorithms Based on HHT 181
5.4 Future Research 182

Bibliography **184**

A **Appendix** **194**
A.1 Earthquake Response Spectrum 194
A.2 Seismic Analysis of Linear Systems 196
A.2.1 Modal Analysis 196
A.2.2 Seismic Response History Analysis 200
A.2.3 Seismic Response Spectrum Analysis 201
A.3 Combination Rules for Modal Superposition Method 202
A.4 Fourier Spectral Analysis 204
A.4.1 Fourier Series 204
A.4.2 Discrete Fourier Transform 205

List of Figures

1.1	Reliability- and performance-based seismic design	3
2.1	Correlation coefficients of spectral accelerations by Baker and Cornell (2006)	22
2.2	Correlation coefficients of spectral accelerations by Baker and Jayaram (2008)	22
2.3	Procedure of deterministic seismic hazard analysis	27
2.4	Procedure of probabilistic seismic hazard analysis	29
2.5	Geometries of seismic source zones modeled in seismic hazard analysis	30
2.6	Geometry of line seismic source zone	32
2.7	Bounded Gutenberg-Richter recurrence relationship	35
2.8	Hypothetical configuration of seismic source zones	39
2.9	Seismic hazard curve for spectral acceleration at vibration period of 0.1 sec	40
2.10	Seismic hazard curve for spectral acceleration at vibration period of 1 sec	40
2.11	Contours (denoting the joint probability of exceedance) of vector-valued probabilistic seismic hazard analysis	41
2.12	Scalar seismic hazard deaggregation for spectral acceleration at vibration period of 0.1 sec	48
2.13	Scalar seismic hazard deaggregation for spectral acceleration at vibration period of 1 sec	48
2.14	Vector-valued seismic hazard deaggregation for spectral accelerations at multiple vibration periods	50
2.15	Logic tree for characterizing epistemic uncertainty of seismic hazard models	52

3.1 Concept of uniform hazard spectrum 56

3.2 Seismic design spectra for dominant period of 0.1 sec at annual probability of exceedance of 4×10^{-4} 75

3.3 Seismic design spectra for dominant periods between 1 and 5 sec at annual probability of exceedance of 4×10^{-4} 75

3.4 Vector-valued uniform hazard spectra using approximate generalized approach 78

3.5 Vector-valued non-uniform hazard spectra using approximate generalized approach 79

3.6 Vector-valued conditional uniform hazard spectra using approximate generalized approach 80

3.7 Vector-valued uniform hazard spectra with different controlling periods 82

3.8 Approximate VUHS with different controlling periods using ground-motion prediction equation by Abrahamson and Silva (1997) 84

3.9 Approximate VUHS with different controlling periods using ground-motion prediction equation by Boore and Atkinson (2008) 85

4.1 Earthquake ground motion recorded in Imperial Valley Earthquake, 1940 97

4.2 Eight intrinsic mode functions of El-Centro ground motion through empirical mode decomposition 97

4.3 Final residue of El-Centro ground motion through empirical mode decomposition 98

4.4 Difference between original and reconstructed El-Centro ground motion 98

4.5 Eight time-dependent amplitudes of intrinsic mode functions of the El-Centro motion 100

4.6 Eight instantaneous frequencies of intrinsic mode functions of the El-Centro motion 101

4.7 Eight normalized response spectra of intrinsic mode functions of the El-Centro ground motion 102

4.8 Hilbert energy spectrum of El-Centro ground motion 103

4.9 Quebec City: target uniform hazard spectrum, response spectrum of generated earthquake ground motion, and response spectra of seed recorded earthquake ground motions 114

4.10 La Malbaie: target uniform hazard spectrum, response spectrum of generated earthquake ground motion, and response spectra of seed recorded earthquake ground motions 114

4.11 New York City: target RG 1.60 design spectrum, response spectrum of generated earthquake ground motion, and response spectra of seed recorded earthquake ground motions 115

4.12 Chicago: target RG 1.60 design spectrum, response spectrum of generated earthquake ground motion, and response spectra of seed recorded earthquake ground motions 115

4.13 Seed and generated earthquake ground motions for UHS at Quebec City 116

4.14 Hilbert energy spectrum of generated earthquake ground motion for UHS at Quebec City 116

4.15 Seed and generated earthquake ground motions for UHS at Quebec City 117

4.16 Seed and generated earthquake ground motions for UHS at Quebec City 118

4.17 Seed and generated earthquake ground motions for UHS at La Malbaie 119

4.18 Hilbert energy spectrum of generated ground motion for UHS at La Malbaie 119

4.19 Seed and generated earthquake ground motions for UHS at La Malbaie 120

4.20 Seed and generated earthquake ground motions for UHS at La Malbaie 121

4.21 Seed and generated earthquake ground motions for CDS at New York City 122

4.22 Hilbert energy spectrum of generated ground motion for CDS at New York City 122

4.23 Seed and generated earthquake ground motions for CDS at New York City 123

4.24 Seed and generated earthquake ground motions for CDS at New York City 124

4.25 Seed and generated earthquake ground motions for CDS at Chicago 125

4.26 Hilbert energy spectrum of generated ground motion for CDS at Chicago 125

4.27 Seed and generated earthquake ground motions for CDS at Chicago 126

4.28 Seed and generated earthquake ground motions for CDS at Chicago 127

4.29 21 normalized response spectra of intrinsic mode functions for Quebec City 128

4.30 Comparison of response spectra based on full intrinsic mode functions and selected intrinsic mode functions 128

4.31 Response spectra of recorded ground motions and seed spectrum-compatible earthquake ground motion 138

4.32 Seed recorded ground motions and seed spectrum-compatible earthquake ground motion 138

4.33 Seed recorded ground motions and seed spectrum-compatible earthquake ground motion 139

4.34 Seed recorded ground motions and seed spectrum-compatible earthquake ground motion 140

4.35 10 resulting response spectra with coefficients of variation constrained 141

4.36 15 resulting response spectra with coefficients of variation constrained 141

4.37 10 resulting response spectra with amplitude scaling parameters constrained 142

4.38 5 resulting response spectra with amplitude scaling parameters constrained 142

4.39 10 generated spectrum-compatible earthquake ground motions (COV constrained) 143

4.40 10 generated spectrum-compatible earthquake ground motions (COV constrained) 144

4.41 10 generated spectrum-compatible earthquake ground motions (COV constrained) 145

4.42 10 generated spectrum-compatible earthquake ground motions (Amplitude constrained) 146

4.43 10 generated spectrum-compatible earthquake ground motions (Amplitude constrained) 147

4.44 10 generated spectrum-compatible earthquake ground motions (Amplitude constrained) 148

4.45 Resulting spectral correlation matrices with COV constrained 149

4.46 Resulting spectral correlation matrices with amplitude constrained 150

4.47 Horizontal response spectra for Quebec City 162

4.48 Ratio of resulting horizontal response spectra to target horizontal design spectrum for Quebec City 162

4.49 Horizontal earthquake ground motions for Quebec City 163

4.50 Horizontal earthquake ground motions for Quebec City 164

4.51 Horizontal earthquake ground motions for Quebec City 165

4.52 Hilbert energy spectrum of generated horizontal ground motions for Quebec City 166

4.53 Vertical response spectra for Quebec City 167

4.54 Ratio of resulting vertical response spectrum to target vertical design spectrum for Quebec City 167

4.55 Vertical earthquake ground motions for Quebec City 168

4.56 Hilbert energy spectrum of generated vertical ground motion for Quebec City 168

4.57 Vertical earthquake ground motions for Quebec City 169

4.58 Vertical earthquake ground motions for Quebec City 169

4.59 Horizontal response spectra for eastern North America 170

4.60 Ratio of resulting horizontal response spectra to target horizontal UHS for ENA 170

4.61 Horizontal earthquake ground motions for ENA 171

4.62 Horizontal earthquake ground motions for ENA 172

4.63 Horizontal earthquake ground motions for ENA 173

4.64 Hilbert energy spectrum of generated horizontal ground motions for ENA 174

4.65 Vertical response spectra for ENA 175

4.66 Ratio of resulting vertical response spectrum to target vertical UHS for ENA 175

4.67 Vertical earthquake ground motions for ENA 176

4.68 Hilbert energy spectrum of generated vertical ground motion for ENA 176

4.69 Vertical earthquake ground motions for ENA 177

4.70 Vertical earthquake ground motions for ENA 177

A.1 Single degree-of-freedom (SDOF) system 195

A.2 Concept of the earthquake response spectrum 197

A.3 An n-storey shear building modelled as an n degrees-of-freedom system 198

Nomenclature

CDF	Cumulative Distribution Function
CDS	Conventional Design Spectrum
CMS-ε	Conditional Mean Spectrum considering ε
COV	Coefficient of Variation
CQC	Complete Quadratic Combination
DOF	Degree-Of-Freedom
DSHA	Deterministic Seismic Hazard Analysis
ENA	Eastern North America
EMD	Empirical Mode Decomposition
FSA	Fourier Spectral Analysis
FT	Fourier Transform
GMPE	Ground-Motion Prediction Equation
GSC	Geological Survey of Canada
HAS	Hilbert Amplitude Spectrum
HES	Hilbert Energy Spectrum
HHT	Hilbert-Huang Transform
HSA	Hilbert Spectral Analysis
IMF	Intrinsic Mode Function
NGA	Next Generation Attenuation
NRCAN	Natural Resources Canada
OBE	Operating Basis Earthquake
PDF	Probability Density Function

PEER	Pacific Earthquake Engineering Research
PGA	Peak Ground Acceleration
PMF	Probability Mass Function
PSHA	Probabilistic Seismic Hazard Analysis
SDC	Seismic Design Category
SHD	Seismic Hazard Deaggregation
SP	Sifting Process
SRHA	Seismic Response History Analysis
SRSA	Seismic Response Spectral Analysis
SRSS	Square-Root-of-Sum-of-Squares
SSC	Structure, System, or Component
SSE	Safe Shutdown Earthquake
UHS	Uniform Hazard Spectrum
USGS	U.S. Geological Survey
VCUHS	Vector-valued Conditional Uniform Hazard Spectrum
VNUHS	Vector-valued Non-Uniform Hazard Spectrum
VUHS	Vector-valued Uniform Hazard Spectrum

CHAPTER 1

Introduction

Earthquake is one of the most destructive natural disasters leading to financial, environmental, and even human losses. The most effective approach to prevent losses induced by structural damage caused by earthquakes is seismic design for structures.

In Section 1.1, the general seismic design procedure is introduced, in which several issues regarding engineering applications are identified. Based on the problems stated in Section 1.1, the objectives of this study are presented in Section 1.2. The organization of this thesis is then described in Section 1.3.

1.1 Overview

In the last two decades, a large number of destructive earthquakes have occurred and caused tremendous casualties and property losses, such as 1994 Northridge, 1995 Kobe, 1999 Turkey, 1999 Chi-Chi, 2001 Gujarat, 2003 Southeastern Iran, 2004 Sumatra, 2005 Kashmir, 2008 Si-Chuan, 2010 Haiti, and 2011 Tohoku earthquakes. These earthquakes have prompted the re-evaluation of the entire seismic design process, with more focus on the issue of uncertainty in the seismic design.

A comprehensive seismic design (reliability- and performance-based seismic design) procedure involves several steps:

1. selection of performance objectives, including expected levels of damage resulting from expected levels of design earthquakes;

2. site suitability and seismic hazard analysis;
3. conceptual overall seismic design, including the selections of structural configuration, structural layout, structural system, structural materials, and non-structural components and their materials;
4. comprehensive numerical seismic design
   (a) establishment of design earthquakes (including seismic design spectra and seismic design ground motions) based on seismic hazard analysis in Step 2,
   (b) numerical preliminary seismic design,
      (i) statement of the problem and its preliminary analysis,
      (ii) preliminary sizing and detailing,
      (iii) acceptability checks of the preliminary design,
   (c) the final design (Bertero and Bertero, 2002).

The design procedure is illustrated in Figure 1.1.

Design earthquakes, including seismic design spectra and seismic design ground motions, are determined in Step 4(a), which is based on the seismic hazard analysis in Step 2. From the point of view of seismic design, a structural system is designed to withstand several single design earthquake excitations separately, which is consistent with the fact that the structure will be subjected to only a single earthquake excitation at one time. To account for the uncertainties in the ground motions induced by earthquakes, design earthquakes are usually a combination of effects of ground motions observed from many earthquakes, in which certain conservatism is introduced. It is required that the probability of exceedance (i.e., the performance objective of the expected level selected in Step 1) of the resulting single design earthquake is provided.

Having obtained the design earthquakes, the numerical preliminary seismic design in Step 4(b) is conducted. The structure is modeled as a linear n degrees-of-freedom (DOF) system following the conceptual overall seismic design in Step 3. The structural responses are then obtained based on the n-DOF system model subjected to the seismic design spectra determined in Step 4(a), using Seismic Response Spectral Analysis (SRSA).

The SRSA procedure is an approximate predictor of peak responses of a structure. The n degrees-of-freedom (DOF) model of the structure is decoupled into n single DOF systems

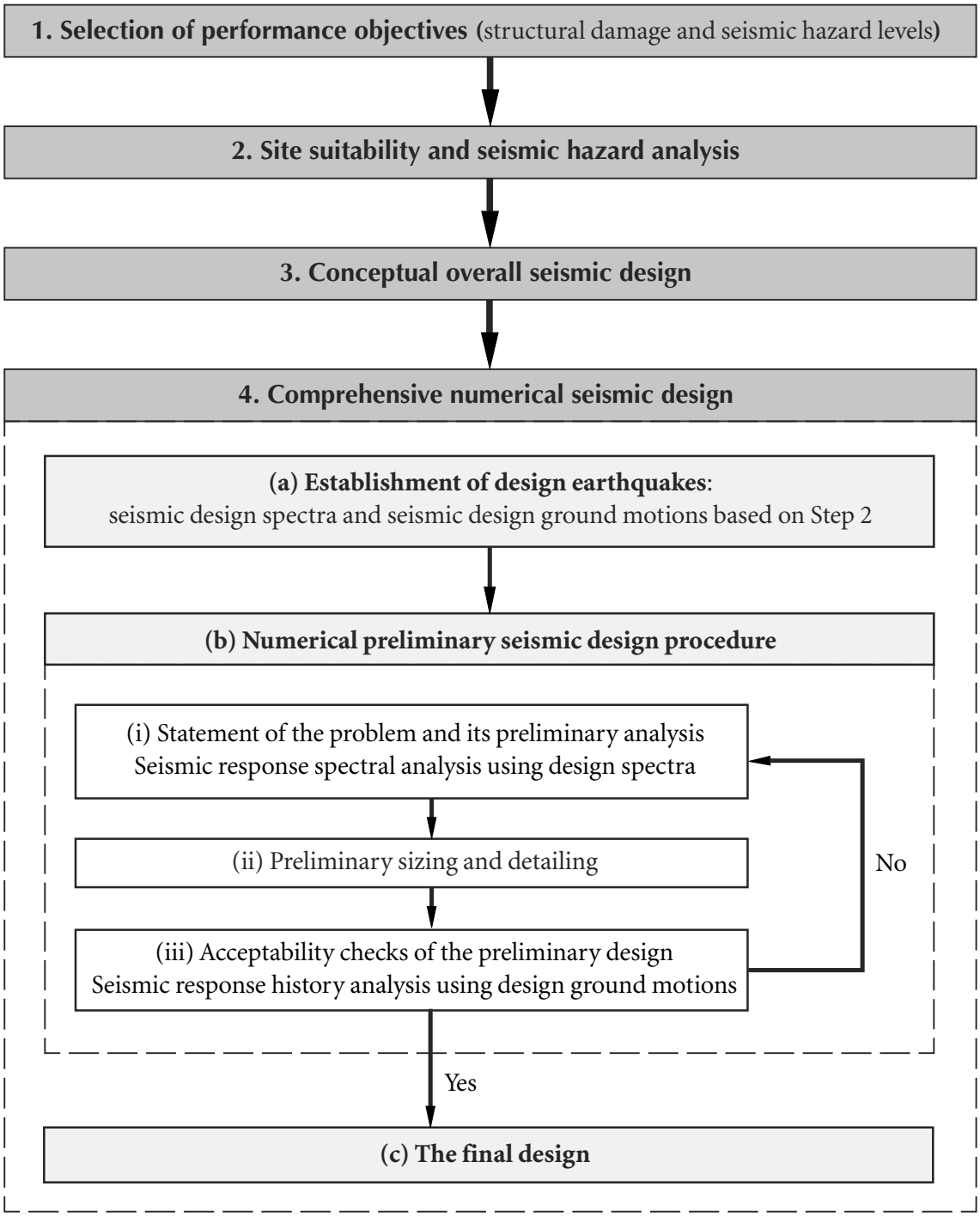

Figure 1.1 Reliability- and performance-based seismic design

(n modes) using modal analysis, as discussed in Appendix A.2.1. Using the seismic design spectrum, the peak response of each single DOF system (each mode) is determined directly, as described in Appendix A.2.3. The peak response of the structure can then be obtained by combining the peak responses of the n single DOF systems (or n modes of the structure) using a suitable modal combination rule, such as the Square-Root-of-Sum-of-Squares (SRSS) or Complete Quadratic Combination (CQC), as presented in Appendix A.3.

It should be emphasized that the structure is under the excitation of the design earthquake (a single earthquake). When the modal analysis is applied, each single DOF system or each mode is also under the excitation of this single design earthquake. Therefore, the peak response of each single DOF system or each mode must be caused by this single design earthquake. When the method of spectral analysis is applied to determine the peak response of each mode, it is required that spectral accelerations at all vibration periods on a seismic design spectrum be caused by a single earthquake or occur simultaneously. It is noted that, in this thesis, the wording of "simultaneously" represents a time period within the duration of excitation of an earthquake ground motion rather than the exact time instance.

This terminology is used to distinguish certain response spectra, such as the uniform hazard spectra discussed in Chapter 3, in which the spectral acceleration at one vibration period is caused by one earthquake while the spectral acceleration at a different vibration period is caused by another earthquake; in such a case, the spectral accelerations on the response spectrum are said to not occur simultaneously, because they are caused by different earthquakes occurring at different times. These response spectra should not be employed directly in SRSA, since it is inappropriate to obtain the peak first mode response from one earthquake, the peak second mode response from a different earthquake, the peak third mode response from yet another earthquake, and then combine these peak modal responses to obtain the peak response of the structure.

Furthermore, when discussing the crucial requirement of a response spectrum in the spectral analysis, it is more intuitive to state that spectral accelerations at all vibration periods on a seismic design spectrum must be caused by a single earthquake. On the other hand, when formulating joint probabilities in the generalized approach for generating

design spectra in Chapter 3, it is much more convenient mathematically to state that spectral accelerations at all vibration periods on a seismic design spectrum occur simultaneously.

Using the estimated peak structural responses (seismic demand) obtained in Step 4b(i), the structural and non-structural members are sized and detailed, such as the cross-sections of steel structural members and the reinforcement of reinforced concrete structural members, in Step 4b(ii). Typical structural response parameters may include stress ratios, deformation and inter-storey drift ratios, response accelerations, ductility demand ratios, damage index, and energy dissipation.

Having obtained the overall structure with detailed configuration of members, the preliminary design is checked and verified based on the seismic design ground motions obtained in Step 4(a), using Seismic Response History Analysis (SRHA), in Step 4b(iii). The SRHA procedure is concerned with the calculation of structural response as a function of time when the system is subjected to a given ground acceleration. Detailed SRHA procedure is described in Appendix A.2.2. It is noted that the SRHA is also often used for seismic qualification of existing critical structures, such as nuclear power plants (ASCE, 1998).

The numerical preliminary seismic design in Step 4(b) is based on the fundamental principles of structural dynamics considering the real behaviour of the entire structural system. It leads to a preliminary design that is as close as possible to the desired final design in Step 4(c). The procedure from Step 4b(i) to Step 4b(iii) may be iterated for several times to reach the final design.

In the seismic design procedure presented above, there are several gaps between the establishment of design earthquakes in Step 4(a) and the numerical preliminary seismic design procedure in Step 4(b). In general, the establishment of design earthquakes is conducted by seismologists while the numerical preliminary seismic design is carried out by structural engineers. The gaps are discussed in the following.

1. In Step 4(a), Probabilistic Seismic Hazard Analysis (PSHA) has been widely used for the determination and selection of design earthquakes. The primary advantage of the PSHA is that it provides a framework in which uncertainties in the location of earthquakes, the size of earthquakes, the rate of occurrence of earthquakes, and the variation of ground-motion characteristics with earthquake size and location can be

identified, quantified, and combined in a mathematically rigorous manner to describe the seismic hazard at a given site.

PSHA-based seismic design spectra include mainly Uniform Hazard Spectrum (UHS), predicted spectrum based on Ground-Motion Prediction Equations (GMPEs), and Conditional Mean Spectrum considering ε (CMS-ε). These design spectra, however, do not or only partially provide probabilistic knowledge about the simultaneous occurrence of spectral accelerations at multiple vibration periods. As a result, the seismic design probability level of a single design earthquake (the entire seismic design spectrum) is not provided. The lack of such probabilistic knowledge of the design spectra may prevent them from being properly incorporated into Step 4b(i) of the numerical preliminary seismic design.

2. Due to large uncertainties in the frequency contents of recorded ground motions, to achieve consistent frequency contents between a seismic design ground motion and a seismic design spectrum, a recorded ground motion is often manipulated so that the response spectrum of the resulting design ground motion closely matches the target design spectrum. The spectrum-compatible earthquake ground motions (seismic design ground motions) have been widely used for seismic design verification and seismic qualification of structures.

   However, the existing spectral matching algorithms in frequency domain may significantly distort the valuable information contained in the recorded ground motions due to the deficiency of the transformation methodologies on which they are based. Furthermore, the selection of recorded ground motions based on the PSHA may not be compatible with the physical meanings of several PSHA-based seismic design spectra, which is seldom mentioned in the existing algorithms. These issues create a gap between Step 4(a) and Step 4b(iii), in which seismic response history analysis is performed.

1.2 Objectives of This Study

The purpose of this study is to bridge the gaps between seismological analyses and engineering applications, i.e., to find suitable representations of design earthquakes from the PSHA so that they can be readily applied in reliability- and performance-based seismic design procedure. The seismic design spectrum should provide the probability level of a single design earthquake. The seismic design ground motions should preserve the valuable information contained in the recorded ground motions and be also consistent with the physical meanings of the PSHA-based seismic design spectra.

1.3 Organization of This Study

In this study, a number of issues in the determination of design earthquakes (seismic design spectra and seismic design ground motions) based on PSHA are investigated.

In Chapter 2, the basic concept of seismic hazard analysis is introduced. The core contents of the seismic hazard analysis, ground-motion prediction equations (GMPEs), correlation coefficients of spectral accelerations, and probability distribution of spectral accelerations, are presented. From the point of view of uncertainty treatment, seismic hazard analysis is classifies as Deterministic Seismic Hazard Analysis (DSHA) and Probabilistic Seismic Hazard Analysis (PSHA). In most engineering practice, to avoid unnecessary conservatism in DSHA, PSHA has been widely used for the determination of design earthquakes, which is the focus of this study.

In terms of dimensions, PSHA is classified as scalar (one dimensional) PSHA and vector-valued (multiple dimensional) PSHA. Mathematically, the scalar PSHA is a special case of the vector-valued PSHA. The PSHA combines all possible and relevant earthquake scenarios and probability levels through integration, which is an "aggregation" procedure. To study the contribution of earthquake parameters (e.g., magnitude, distance, epsilon, and occurrence rate) to the seismic hazard at a given site, a "deaggregation" procedure corresponding to the PSHA, i.e., seismic hazard deaggregation (SHD), is often performed. The SHD is also classified as scalar SHD and vector-valued SHD. The terminologies of "PSHA" and "SHD"

are adopted for aggregation and deaggregation procedures, respectively, although both the aggregation and deaggregation procedures are actually under the framework of PSHA.

In Chapter 3, the existing PSHA-based seismic design spectra, including UHS, predicted spectra, and CMS-ε, are presented. Their primary properties and limitations are discussed. To overcome the deficiencies of these design spectra, a generalized approach is developed to generate seismic design spectra using both scalar and vector-valued PSHA. The generated seismic design spectra are called Vector-valued Uniform Hazard Spectra (VUHS), Vector-valued Non-Uniform Hazard Spectra (VNUHS), and Vector-valued Conditional Uniform Hazard Spectra (VCUHS), based on their specific mathematical properties.

The spectral shapes of these generated design spectra can be narrowed and concentrated at a specified vibration period or a range of vibration periods based on the information of structural modes or the specific requirements of engineering projects. The seismic hazard level, i.e., annual probability of exceeding spectral accelerations simultaneously at multiple vibration periods of engineering interest, of each design spectrum is provided by the vector-valued PSHA. Each spectrum can then be interpreted as a single "design earthquake" via the joint probability. Through the PSHA, the resulting design spectra reflect the seismic hazard environment surrounding a given site and also take the dynamic characteristics of structures into consideration.

To simplify the approach for the generation of seismic design spectra so that they can be easily incorporated into structural design and further performance-based seismic design, an approximate approach is also developed using SHD. Based on several numerical studies, it is concluded that the selection of controlling vibration periods does not affect the resulting seismic design spectra and the results of the SHD significantly, as long as the selected periods cover the entire range of vibration period of engineering interest roughly uniformly.

In Chapter 4, the existing spectral matching algorithms in both time domain and frequency domain are discussed. A signal processing method, Hilbert-Huang Transform (HHT), is described, and its characteristics in processing earthquake ground motions are analyzed. Based on the HHT, three methodologies are developed for generating single, multiple, and tri-directional spectrum-compatible earthquake ground motions. The primary advantage of using the HHT in the compatibility algorithm is that the basis functions of

the HHT transformation are empirically derived from the recorded ground motions themselves, which guarantees the adaptivity of the transformation method and thus preserves the nonstationary characteristics of the seed recorded ground motions. Strategies for the selection of the recorded ground motions based on the PSHA are also provided, which are compatible with the physical meanings of the PSHA-based seismic design spectra.

Chapter 5 presents some conclusions from this study and directions for future research.

CHAPTER 2

Seismic Hazard Analysis

Seismic hazard analyses involve the quantitative estimation of ground-shaking hazards at a particular site. Seismic hazards may be analyzed deterministically using Deterministic Seismic Hazard Analysis (DSHA), or probabilistically using Probabilistic Seismic Hazard Analysis (PSHA). In this chapter, the primary components of engineering seismology relevant to seismic hazard analysis are introduced, based on which the DSHA and PSHA are presented.

2.1 Engineering Seismology

The study of seismic hazard requires an understanding of various processes from the occurrence of earthquakes to the corresponding effects on ground motions. Engineering seismology is an integral part of earthquake engineering covering a wide range of topics regarding the earthquakes and their effects. It mainly includes mechanism of sources and occurrences of earthquakes, measurements and parameters of earthquakes and their induced ground motions, effects of local site conditions on ground motions, prediction of intensity measures of ground motions, and historical seismicity (Kramer, 1996, McGuire, 2004).

Ground-Motion Prediction Equations (GMPEs) from engineering seismology for the intensity measures of ground motions are the core component for both DSHA and PSHA. The uncertainty descriptions (probability distributions) of the intensity measures of ground

motions based on GMPEs are required in PSHA. Hence, this section focuses on the GMPEs and their corresponding outcomes. Other components of engineering seismology, including identification and characterization of seismic sources, probability distribution of earthquake magnitude, and seismicity, are discussed with the DSHA or PSHA in Sections 2.2 and 2.3.

In Section 2.1.1, GMPEs for intensity measures of ground motions (spectral accelerations for horizontal components are used as the intensity measures in this study) are described. In Section 2.1.2, to account for the statistical correlation between spectral accelerations, the correlation coefficients of spectral accelerations are introduced. Based on the GMPEs and the correlation coefficients of spectral accelerations, the marginal and joint probability distributions of spectral accelerations for a given scenario earthquake are presented in Section 2.1.3.

2.1.1 Ground-Motion Prediction Equations

Ground-motion prediction equations (GMPEs) for ground-motion intensity measures, such as Peak Ground Acceleration (PGA) and spectral acceleration at individual vibration period (see Appendix A.1), as functions of earthquake magnitude, source-site distance, and some other variables, are important tools in seismic hazard analysis. GMPEs are typically developed empirically by regression analyses of recorded strong-motion amplitude data versus magnitude, distance, and possibly other predictor variables. Some GMPEs were also determined based on simulated ground motions (Atkinson and Boore, 2006). The GMPEs provide a connection between the intensity measures (e.g., spectral accelerations) of earthquake-induced ground motions, which are directly correlated to seismic analysis and design, and the parameters (e.g., magnitude and distance) of earthquakes.

A typical GMPE for spectral acceleration $S_a(T_j)$ at vibration period T_j can be expressed as

$$\ln S_a(T_j) = f(m, r, T_j, \boldsymbol{\theta}) + \sigma\, \varepsilon(T_j), \tag{2.1.1}$$

where $f(m, r, T_j, \boldsymbol{\theta})$ is the expected value of the prediction equation, in which, besides the essential parameters (earthquake magnitude m and source-site distance r), various predictor variables $\boldsymbol{\theta}$, such as fault type, hanging wall effect, seismic wave propagation path, and local

site condition, may be considered. σ is the total standard deviation of the prediction equation model, which could be a combination of intra-event (ground motions within the same earthquake event) and inter-event (ground motions between different earthquake events) aleatory uncertainties and a function of m, T_j, and other predictor variables. $\varepsilon(T_j)$ is the number of standard deviations σ by which the logarithmic spectral acceleration $\ln S_a(T_j)$ deviates from the expected value $f(m, r, T_j, \boldsymbol{\theta})$ (Abrahamson and Silva, 1997, Atkinson and Boore, 2006, Boore and Atkinson, 2008). Given a set of predictor variables m, r, and $\boldsymbol{\theta}$, $\varepsilon(T_j)$ has been verified to follow standard normal distribution; consequently, $\ln S_a(T_j)$ follows normal distribution conditional on m, r, and $\boldsymbol{\theta}$ (Baker and Jayaram, 2008). Detailed discussion on the probability distribution of spectral accelerations is presented in Section 2.1.3.

The functional form of the prediction equation $f(m, r, T_j, \boldsymbol{\theta})$ in equation (2.1.1) is usually selected to reflect the mechanisms of the ground-motion process as closely as possible. However, ground motions are complicated; they are influenced by, and consequently reflect, characteristics of the seismic source, the rupture process, the source-site travel path, and local site conditions (Kramer, 1996). Various functional forms of the prediction equation have been adopted to account for different ground-motion mechanisms, based on the availability of regional recorded ground motions and engineering practice (Douglas, 2011). To introduce the basic concept of GMPE, three examples of typical GMPEs are given below.

GMPEs by Abrahamson and Silva (1997)

Abrahamson and Silva (1997) developed GMPEs for spectral accelerations. The GMPEs are derived for the geometric average of two horizontal components and vertical component for shallow earthquakes in active tectonic regions. A database of 655 sets of tri-directional recorded ground motions from 58 earthquakes are used in the regression analysis. The functional form $f(m, r, T_j, \boldsymbol{\theta})$ in equation (2.1.1) of the GMPE is given by

$$\ln S_a = f_1(m, r_{\text{rup}}) + \text{F} \cdot f_3(m) + \text{HW} \cdot f_4(m, r_{\text{rup}}) + \text{S} \cdot f_5(\overline{\text{PGA}}_{\text{rock}}), \tag{2.1.2}$$

where S_a is spectral acceleration at a specific vibration period, m is moment magnitude, r_{rup} is the closest distance to the rupture plane, F is a coefficient for the fault type (1 for reverse, 0.5 for reverse/oblique, and 0 otherwise), HW is a coefficient for hanging wall sites (1 for

sites over the hanging wall and 0 otherwise), and S is a coefficient for local site conditions (0 for rock or shallow soil, and 1 for deep soil).

Function $f_1(m, r_{\text{rup}})$ in equation (2.1.2), which is the basic functional form of the GMPE for strike-slip events recorded at rock sites, is given by

$$f_1(m, r_{\text{rup}}) = a_1 + a(m-6.4) + a_{12}(8.5-m)^n + \left[a_3 + a_{13}(m-6.4)\right] \ln \sqrt{r_{\text{rup}}^2 + c_4^2}, \quad (2.1.3)$$

where $a = a_2$ for $m \leqslant 6.4$ and $a = a_4$ for $m > 6.4$.

Function $f_3(m)$ in equation (2.1.2), which allows for magnitude and period dependence of the type of fault, is given by

$$f_3(m) = \begin{cases} a_5, & \text{for } m \leqslant 5.8, \\ a_5 + \dfrac{a_6 - a_5}{6.4 - 5.8}, & \text{for } 5.8 < m < 6.4, \\ a_6, & \text{for } m \geqslant 6.4. \end{cases} \quad (2.1.4)$$

Function $f_4(m, r_{\text{rup}})$ in equation (2.1.2) that allows for magnitude and distance dependence of the effect of hanging wall is given by

$$f_4(m, r_{\text{rup}}) = f_{\text{HW}}(m) \cdot f_{\text{HW}}(r_{\text{rup}}), \quad (2.1.5)$$

where

$$f_{\text{HW}}(m) = \begin{cases} 0, & \text{for } m \leqslant 5.5, \\ m - 5.5, & \text{for } 5.5 < m < 6.5, \\ 1, & \text{for } m \geqslant 6.5, \end{cases}$$

$$f_{\text{HW}}(r_{\text{rup}}) = \begin{cases} 0, & \text{for } r_{\text{rup}} \leqslant 4 \text{ km}, \\ \frac{1}{4}\, a_9\, (r_{\text{rup}} - 4), & \text{for } 4 \text{ km} < r_{\text{rup}} \leqslant 8 \text{ km}, \\ a_9, & \text{for } 8 \text{ km} < r_{\text{rup}} \leqslant 18 \text{ km}, \\ a_9 \left[1 - \frac{1}{7}(r_{\text{rup}} - 18)\right], & \text{for } 18 \text{ km} < r_{\text{rup}} \leqslant 24 \text{ km}, \\ 0, & \text{for } r_{\text{rup}} > 24 \text{ km}. \end{cases}$$

The nonlinear soil response term $f_5(\overline{\text{PGA}}_{\text{rock}})$ in equation (2.1.2) is modeled by

$$f_5(\overline{\text{PGA}}_{\text{rock}}) = a_{10} + a_{11} \ln\left(\overline{\text{PGA}}_{\text{rock}} + c_5\right), \quad (2.1.6)$$

where $\overline{\text{PGA}}_{\text{rock}}$ is the expected value of peak ground acceleration (PGA) on rock, as predicted by the expected prediction equation (2.1.2) with S = 0.

The total standard deviation σ in equation (2.1.1) of the GMPE, including intra-event and inter-event aleatory uncertainties, is magnitude dependent and is modeled by

$$\sigma_{\text{total}}(m) = \begin{cases} b_5, & \text{for } m \leqslant 5.0, \\ b_5 - b_6(m-5), & \text{for } 5.0 < m < 7.0, \\ b_5 - 2\,b_6, & \text{for } m \geqslant 7.0. \end{cases} \tag{2.1.7}$$

In equation (2.1.7), the total standard deviation $\sigma_{\text{total}}(m)$ for the horizontal ground motions is determined by calculating the geometric average of two horizontal components. The total standard deviation can also be obtained for arbitrary horizontal components of ground motions by inflating $\sigma_{\text{total}}(m)$ using a functional fit developed by Baker and Cornell (2006c). Consequently, the standard deviation for arbitrary horizontal components, in terms of magnitude m and vibration period T, is given by

$$\sigma_{\text{total,arb}}(m, T) = \sigma_{\text{total}}(m)\sqrt{\frac{2}{1.78 - 0.039 \ln T}}. \tag{2.1.8}$$

In equations (2.1.2)-(2.1.7), $a_1, \ldots, a_6, a_9, \ldots, a_{13}, c_4, c_5, n, b_5$, and b_6 are period dependent parameters of regression analysis.

GMPEs by Atkinson and Boore (2006)

Atkinson and Boore (2006) developed GMPEs for horizontal ground motions at hard rock and soil sites in eastern North America (ENA). The GMPEs are obtained by regression analysis of a database of simulated ground motions using a stochastic finite-fault model. The GMPE model incorporates information obtained from new ENA seismographic data, including tri-directional broadband ground motions that provide new information on ENA source and path effects. The functional form of the GMPE is given by

$$\log_{10} S_a = c_1 + c_2\, m + c_3\, m^2 + (c_4 + c_5\, m)\cdot f_1 + (c_6 + c_7\, m)\cdot f_2 + (c_8 + c_9\, m)\cdot f_0 + c_{10}\, r_{\text{cd}} + S, \tag{2.1.9a}$$

$$f_0 = \max\left(\log_{10}\frac{10}{r_{\text{cd}}},\ 0\right), \quad f_1 = \min\left(\log_{10} r_{\text{cd}},\ \log_{10} 70\right), \quad f_2 = \max\left(\log_{10}\frac{R_{\text{cd}}}{140},\ 0\right), \tag{2.1.9b}$$

where S_a is spectral acceleration at a specific vibration period, m is the moment magnitude, and r_{cd} is the closest distance to the fault rupture.

To account for soil amplification in both linear and nonlinear ranges, a piecewise soil amplification factor S in equation (2.1.9a), as a function of shear wave velocity in the upper 30 m (V_{30}), is modeled as

$$S = \begin{cases} 0, & \text{for hard-rock sites,} \\ \log_{10}\left[\exp\left(b_{\text{lin}} \cdot \ln\dfrac{V_{30}}{760} + b_{\text{nl}} \cdot \ln\dfrac{60}{100}\right)\right], & \text{for } \text{pgaBC} \leqslant 60 \text{ cm/sec}^2, \\ \log_{10}\left[\exp\left(b_{\text{lin}} \cdot \ln\dfrac{V_{30}}{760} + b_{\text{nl}} \cdot \ln\dfrac{\text{pgaBC}}{100}\right)\right], & \text{for } \text{pgaBC} > 60 \text{ cm/sec}^2, \end{cases} \tag{2.1.10}$$

where pgaBC is the predicted value of PGA for $V_{30} = 760$ m/sec, b_{lin} is the linear factor of soil amplification, and the nonlinear soil amplification factor b_{nl} is given by

$$b_{\text{nl}} = \begin{cases} b_1, & \text{for } V_{30} \leqslant 180 \text{ m/sec,} \\ (b_1 - b_2)\dfrac{\ln V_{30} - \ln 300}{\ln 180 - \ln 300} + b_2, & \text{for } 180 \text{ m/sec} < V_{30} \leqslant 300 \text{ m/sec,} \\ b_2\dfrac{\ln V_{30} - \ln 760}{\ln 300 - \ln 760}, & \text{for } 300 \text{ m/sec} < V_{30} \leqslant 760 \text{ m/sec,} \\ 0, & \text{for } V_{30} > 760 \text{ m/sec.} \end{cases} \tag{2.1.11}$$

In equation (2.1.9a), the spectral acceleration is predicted for an event with fault stress of 140 bars. For stress values other than 140 bars (within the tested range from 35 to 560 bars), the spectral acceleration $\log_{10} S_{a,\text{adj}}$ is obtained by adjusting $\log_{10} S_a$ in equation (2.1.9a) as

$$\log_{10} S_{a,\text{adj}} = \log_{10} S_a + \text{SF}_1 \cdot \log_{10} \text{SF}_2, \tag{2.1.12a}$$

$$\text{SF}_1 = \frac{\log_{10} \text{Stress} - \log_{10} 140}{\log_{10} 2}, \tag{2.1.12b}$$

$$\log_{10} \text{SF}_2 = \min\left\{\left[\Delta + 0.05\right], \left[0.05 + \frac{\Delta \cdot \max[(m - M_1), 0]}{M_{\text{h}} - M_1}\right]\right\}. \tag{2.1.12c}$$

The standard deviations of $\log_{10} S_a$ for all vibration periods are 0.3. In equations (2.1.9)-(2.1.12), $c_1, \ldots, c_{10}, b_{\text{lin}}, b_1, b_2, \Delta, M_1$, and M_{h} are period dependent parameters of regression analysis.

GMPEs by Boore and Atkinson (2008)

Boore and Atkinson (2008) developed GMPEs for the geometric average values of two horizontal components of ground motions as a function of earthquake magnitude, source-site distance, local average shear wave velocity, and fault type. The geometric average is determined from the 50th percentile value of the geometric mean values computed for all non-redundant rotation angles, which is approximately identical to the geometric mean in most cases (Boore *et al.*, 2006). The GMPEs are derived by regression analysis of an extensive strong-motion database compiled by the Next Generation Attenuation (NGA) project of the Pacific Earthquake Engineering Research (PEER) Center. For periods less than 1 sec, the analysis uses 1574 recorded ground motions from 58 main-shocks in the distance range from 0 km to 400 km (the number of available data decreases with increasing vibration period).

The functional form $f(m, r, T_j, \boldsymbol{\theta})$ in equation (2.1.1) of the GMPE is given by

$$\ln S_a = F_{\text{M}}(m) + F_{\text{D}}(r_{\text{JB}}, m) + F_{\text{S}}(V_{30}, r_{\text{JB}}, m), \tag{2.1.13}$$

where F_{M}, F_{D}, and F_{S} represent the magnitude scaling, distance, and site amplification functions, respectively. m is the moment magnitude, r_{JB} is the Joyner-Boore distance (defined as the closest distance to the surface projection of the fault, which is approximately equal to the epicentral distance for events of $m < 6$), and V_{30} is the average shear wave velocity from the surface to a depth of 30 m.

The magnitude scaling function F_{M} in equation (2.1.13) is given by

$$F_{\text{M}}(m) = \begin{cases} e_1 \cdot \text{U} + e_2 \cdot \text{SS} + e_3 \cdot \text{NS} + e_4 \cdot \text{RS} + e_5(m - M_h) + e_6(m - M_h)^2, & \text{for } m \leqslant M_h, \\ e_1 \cdot \text{U} + e_2 \cdot \text{SS} + e_3 \cdot \text{NS} + e_4 \cdot \text{RS} + e_7(m - M_h), & \text{for } m > M_h, \end{cases} \tag{2.1.14}$$

where U, SS, NS, and RS are coefficients (1 for unspecified, strike-slip, normal-slip, and reverse-slip fault type, respectively, and 0 otherwise) and M_h, the "hinge magnitude" for the shape of the magnitude scaling, is a coefficient to be determined during the analysis.

The distance function F_{D} in equation (2.1.13) is given by

$$F_{\mathrm{D}}(r_{\mathrm{JB}}, m) = \left[c_1 + c_2(m - 4.5)\right] \ln\sqrt{r_{\mathrm{JB}}^2 + h^2} + c_3\left(\sqrt{r_{\mathrm{JB}}^2 + h^2} - 1\right). \tag{2.1.15}$$

The site amplification function F_{S} in equation (2.1.13) is given by

$$F_{\mathrm{S}}(V_{30}, r_{\mathrm{JB}}, m) = F_{\mathrm{LIN}} + F_{\mathrm{NL}}, \tag{2.1.16}$$

where the linear term F_{LIN} is

$$F_{\mathrm{LIN}} = b_{\mathrm{lin}}(\ln V_{30} - \ln 760), \tag{2.1.17}$$

and the nonlinear term F_{NL} is

$$F_{\mathrm{NL}} = \begin{cases} b_{\mathrm{nl}} \ln\left(\dfrac{0.06}{0.1}\right), & \text{for } \ \mathrm{pga4nl} \leqslant 0.03g, \\ b_{\mathrm{nl}} \ln\left(\dfrac{0.06}{0.1}\right) + c\left[\ln\left(\dfrac{\mathrm{pga4nl}}{0.03}\right)\right]^2 + d\left[\ln\left(\dfrac{\mathrm{pga4nl}}{0.03}\right)\right]^3, & \\ & \text{for } \ 0.03g < \mathrm{pga4nl} \leqslant 0.09g, \\ b_{\mathrm{nl}} \ln\left(\dfrac{\mathrm{pga4nl}}{0.1}\right), & \text{for } \ \mathrm{pga4nl} > 0.09g, \end{cases} \tag{2.1.18}$$

in which

$$c = \frac{1}{(\ln 0.09 - \ln 0.03)^2}\left[3b_{\mathrm{nl}}(\ln 0.09 - \ln 0.06) - b_{\mathrm{nl}}(\ln 0.09 - \ln 0.03)\right],$$

$$d = \frac{-1}{(\ln 0.09 - \ln 0.03)^3}\left[2b_{\mathrm{nl}}(\ln 0.09 - \ln 0.06) - b_{\mathrm{nl}}(\ln 0.09 - \ln 0.03)\right],$$

$$b_{\mathrm{nl}} = \begin{cases} b_1, & \text{for } \ V_{30} \leqslant 180 \text{ m/sec}, \\ \dfrac{(b_1 - b_2)(\ln V_{30} - \ln 300)}{\ln 180 - \ln 300} + b_2, & \text{for } \ 180 \text{ m/sec} < V_{30} \leqslant 300 \text{ m/sec}, \\ \dfrac{b_2(\ln V_{30} - \ln 760)}{\ln 300 - \ln 760}, & \text{for } \ 300 \text{ m/sec} < V_{30} < 760 \text{ m/sec}, \\ 0, & \text{for } \ V_{30} \geqslant 760 \text{ m/sec}. \end{cases}$$

The total standard deviation σ for $\ln S_a$ in equation (2.1.13), including intra-event and inter-event aleatory uncertainties, has been tabulated for fault type specified and unspecified (Boore and Atkinson, 2008).

In equation (2.1.18), pga4nl is the predicted PGA for $V_{30} = 760$ m/sec using equation (2.1.13) with the site amplification function $F_S = 0$. In equations (2.1.14)-(2.1.18), $e_1, \ldots, e_7, c_1, \ldots, c_3, b_1, b_2, M_h, h$, and b_{lin} are period dependent parameters of regression analysis.

As can be seen in these three examples of GMPE, various functional forms have been used to characterize the ground-motion mechanisms based on the availability of recorded ground motions and the corresponding geographical locations, over which the recorded ground motions were collected. Historically, the functional forms of GMPE used in regression analysis have been revised significantly with the increase of recorded ground motions since 1960s (Douglas, 2011). Most GMPEs are updated in the literature every 3 to 5 years or shortly after the occurrences of major earthquakes in well-instrumented regions (Kramer, 1996).

In this situation, it is infeasible to have the "correct" functional form of a GMPE with 100% confidence. In other words, each GMPE contains epistemic uncertainty to a varying extent. It is therefore important to include multiple GMPEs in seismic hazard analysis or risk analysis with weights (McGuire, 2004).

One useful procedure is to (1) determine the magnitude-distance range that are most critical to seismic hazard analysis, (2) collect a set of recorded ground motions relevant to the site of interest, and (3) compare the selected GMPEs with the ground-motion data in the magnitude-distance range. GMPEs that fit the ground-motion data better are given high weights, and GMPEs that fit less well are given low weights. The weight can be calculated proportionally to the inverse of the residual of the data around each GMPE (McGuire, 2004).

On the other hand, when applying any GMPE, it is very important to ensure that parameters, such as spectral acceleration, magnitude, and distance, are defined and used consistently with the application. For example, the horizontal spectral acceleration of a GMPE can be predicted for the geometric average of two horizontal components, arbitrary horizontal component, or the 50th percentile values of the geometric means of two horizontal components computed for all non-redundant rotation angles. Typically, GMPE for arbitrary horizontal component should be used for horizontal ground motion when structural responses are predicted by engineers (Baker and Cornell, 2006c).

2.1.2 Correlation Coefficients of Spectral Accelerations

Ground-motion prediction equations (GMPEs) describe the probability distributions of spectral accelerations at individual vibration periods, given a set of predictor variables, such as magnitude and distance. However, the statistical correlations between spectral accelerations at multiple periods are not addressed by GMPEs. Since the correlations of spectral accelerations at multiple periods are required in determining the joint distribution functions of spectral accelerations in vector-valued probabilistic seismic hazard analysis (PSHA), the Pearson product-moment correlation coefficients of spectral accelerations have been obtained empirically based on a large number of recorded ground motions (Baker and Cornell, 2006a, Baker and Jayaram, 2008).

In equation (2.1.1), only $\varepsilon(T_j)$ and $\ln S_a(T_j)$ are random variables, which follow standard normal distribution and normal distribution conditional on predictor variables (m, r, and $\boldsymbol{\theta}$), respectively. Hence, the determination of correlation coefficients of spectral accelerations is equivalent to that of correlation coefficients of ε.

By rearranging equation (2.1.1), $\varepsilon(T_j)$ can be expressed as

$$\varepsilon(T_j) = \frac{1}{\sigma}\big[\ln S_a(T_j) - f(m, r, T_j, \boldsymbol{\theta})\big]. \tag{2.1.19}$$

For a given sample (a recorded ground motion with known $S_a(T_j)$, m, r and $\boldsymbol{\theta}$), $\varepsilon(T_j)$ in equation (2.1.19) is a known number. Equation (2.1.19) then eliminates the impact of predictor variables (m, r, and $\boldsymbol{\theta}$) on the variability of $\varepsilon(T_j)$, i.e., the variability of $\varepsilon(T_j)$ is independent of the predictor variables. In practice, it is thus convenient to study on $\varepsilon(T_j)$, instead of $S_a(T_j)$, in statistical and regression analysis (Baker and Cornell, 2006a). It is noted that, since the normalized residual $\varepsilon(T_j)$ is used in the analysis, any outcomes are in principle dependent on the GMPEs selected.

The Pearson product-moment correlation coefficient between $\varepsilon(T_u)$ and $\varepsilon(T_v)$, at vibration periods T_u and T_v, is given by

$$\rho_{\varepsilon(T_u),\varepsilon(T_v)} = \frac{\sum_{i=1}^{M}\left[\varepsilon^{(i)}(T_u) - \overline{\varepsilon(T_u)}\right]\left[\varepsilon^{(i)}(T_v) - \overline{\varepsilon(T_v)}\right]}{\sqrt{\sum_{i=1}^{M}\left[\varepsilon^{(i)}(T_u) - \overline{\varepsilon(T_u)}\right]^2 \sum_{i=1}^{M}\left[\varepsilon^{(i)}(T_v) - \overline{\varepsilon(T_v)}\right]^2}}, \tag{2.1.20}$$

where $\varepsilon^{(i)}(T_u)$ is the number of standard deviations departing from $f(m, r, T_u, \boldsymbol{\theta})$ of the ith recorded ground motion at period T_u using equation (2.1.19), $\overline{\varepsilon(T_u)}$ is the mean value of ε of all M recorded ground motions at T_u, and M is the total number of recorded ground motions used in the statistical and regression analysis. Using equation (2.1.20), a symmetric positive semi-definite matrix of the correlation coefficients can be determined from all the combinations of ε at different periods.

Given a set of predictor variables (m, r, and $\boldsymbol{\theta}$) in equation (2.1.19), by substituting equation (2.1.19) into equation (2.1.20), the correlation coefficient between spectral accelerations $\ln S_a(T_u)$ and $\ln S_a(T_v)$ at any two periods T_u and T_v is obtained as

$$\rho_{\ln S_a(T_u),\ln S_a(T_v)} = \frac{\sum_{i=1}^{M}\left[\ln S_a^{(i)}(T_u) - \overline{\ln S_a(T_u)}\right]\left[\ln S_a^{(i)}(T_v) - \overline{\ln S_a(T_v)}\right]}{\sqrt{\sum_{i=1}^{M}\left[\ln S_a^{(i)}(T_u) - \overline{\ln S_a(T_u)}\right]^2 \sum_{i=1}^{M}\left[\ln S_a^{(i)}(T_v) - \overline{\ln S_a(T_v)}\right]^2}}, \quad (2.1.21)$$

where $\ln S_a^{(i)}(T_u)$ is the natural logarithmic spectral acceleration of the ith recorded ground motion at period T_u, and $\overline{\ln S_a(T_u)}$ is the mean value of logarithmic spectral acceleration of all M recorded ground motions at T_u. Hence, the correlation coefficients of ε and those of spectral accelerations conditional on a given scenario earthquake (known predictor variables m, r, and $\boldsymbol{\theta}$) are identical.

Using equations (2.1.19) and (2.1.20), a number of models of correlation coefficients of spectral accelerations (abbreviated as spectral correlation models) have been developed based on different databases of recorded ground motions (Inoue and Cornell, 1990, Baker and Cornell, 2006a, Baker and Jayaram, 2008). Two recent correlation models are described below.

Spectral correlation model by Baker and Cornell (2006)

Baker and Cornell (2006a) developed a spectral correlation model empirically based on 267 sets of recorded ground motions. An approximate analytical equation for the correlation coefficients between horizontal spectral accelerations at any two vibration periods is determined using nonlinear regression. The spectral correlation model is equally valid for both arbitrary component and geometric mean of two horizontal components of spectral accelerations. The valid range of vibration period of this correlation model is between 0.05

sec and 5 sec. It is observed that the resulting spectral correlations do not vary significantly when different GMPEs are used, which suggests that the correlation model are applicable regardless of the GMPEs chosen.

The correlation coefficient between the horizontal spectral accelerations $\ln S_a(T_u)$ and $\ln S_a(T_v)$ at any two periods T_u and T_v ($T_u \leqslant T_v$) is estimated as

$$\rho_{\ln S_a(T_u),\ln S_a(T_v)} = 1 - \cos\left\{\frac{\pi}{2} - \left[0.359 + 0.163\, I_{(T_u<0.189)} \cdot \ln\left(\frac{T_u}{0.189}\right)\right] \cdot \ln\left(\frac{T_v}{T_u}\right)\right\}, \tag{2.1.22}$$

where $I_{(T_u<0.189)}$ is an indicator function equal to 1 if $T_u < 0.189$ sec and equal to 0 otherwise. The matrix of correlation coefficients of spectral accelerations of this model is shown as contours in Figure 2.1.

As can be seen in Figure 2.1, the spectral correlations decrease with increasing separation of vibration periods when the periods are larger than around 0.2 sec, which cover the range of period of general engineering interest. However, the spectral correlations increase when one period is fixed and the other one approaches shorter periods less than around 0.2 sec. For example, the correlation between spectral accelerations at $T_u = 0.05$ sec and $T_v = 1$ sec is larger than the correlation at $T_u = 0.2$ sec and $T_v = 1$ sec. A similar phenomenon can also be observed in the following spectral correlation model.

Spectral correlation model by Baker and Jayaram (2008)

Baker and Jayaram (2008) developed a spectral correlation model empirically using the NGA ground-motion library and new NGA GMPEs (Abrahamson and Silva, 2008, Boore and Atkinson, 2008, Campbell and Bozorgnia, 2008, Chiou and Youngs, 2008). The spectral correlation model is valid for a variety of definitions of horizontal spectral acceleration, including spectral acceleration of arbitrary component, the geometric average of spectral accelerations from two orthogonal horizontal components, and the 50th percentile value of the geometric means computed for all non-redundant rotation angles. The valid range of vibration period of this correlation model is between 0.01 sec and 10 sec.

The correlation model of spectral correlations has the following properties: (1) it is not sensitive to the choice of accompanying GMPE models; (2) intra-event (ground motions within the same earthquake event) error, inter-event (ground motions between different

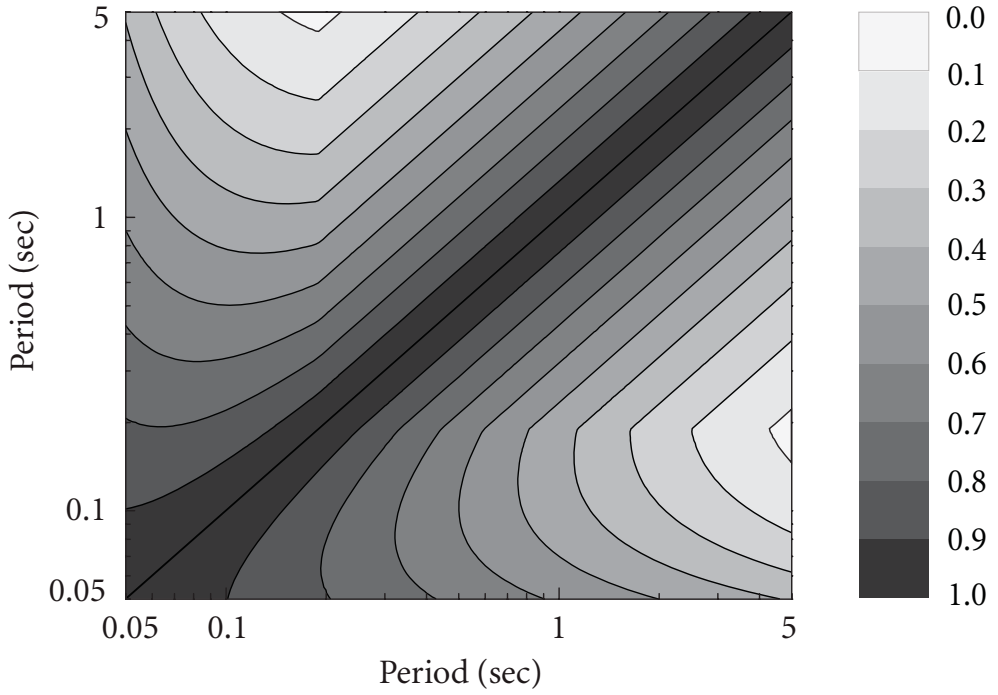

Figure 2.1 Correlation coefficients of spectral accelerations by Baker and Cornell (2006)

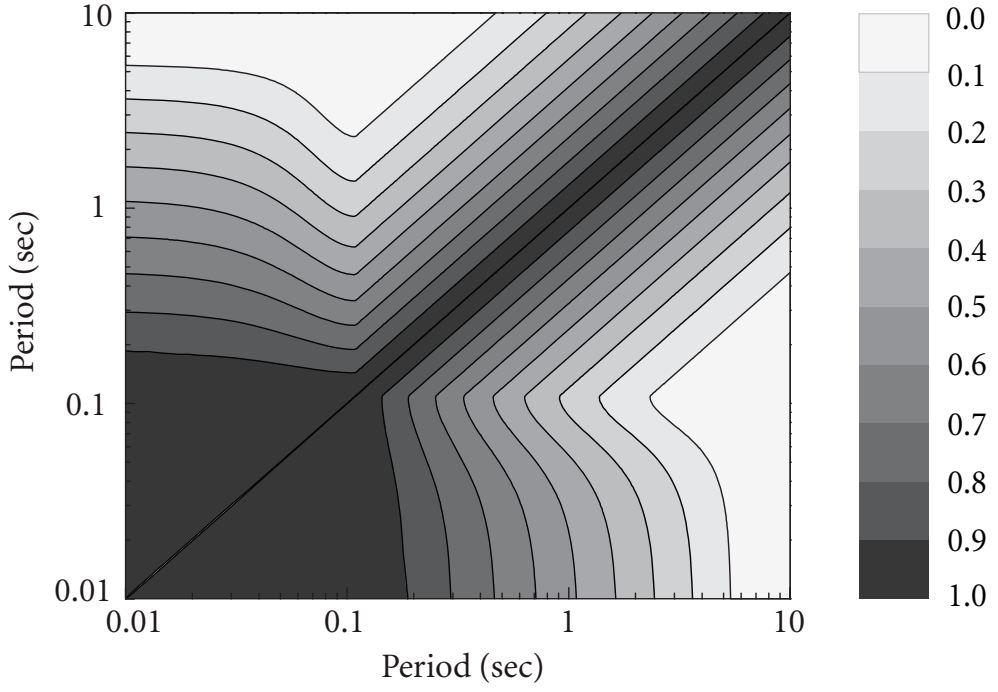

Figure 2.2 Correlation coefficients of spectral accelerations by Baker and Jayaram (2008)

earthquake events) error, and total error in the regression analysis of the GMPEs all exhibit similar correlation structure.

The correlation coefficient between the horizontal spectral accelerations $\ln S_a(T_u)$ and $\ln S_a(T_v)$ at any two periods T_u and T_v ($T_u \leqslant T_v$) is estimated as

$$\rho_{\ln S_a(T_u),\ln S_a(T_v)} = \begin{cases} C_2, & \text{if } \ T_v < 0.109, \\ C_1, & \text{else if } \ T_u > 0.109, \\ \min\big(C_2, C_4\big), & \text{else if } \ T_v < 0.2, \\ C_4, & \text{else,} \end{cases} \tag{2.1.23}$$

where

$$C_1 = 1 - \cos\left\{\frac{\pi}{2} - 0.366 \ln\left[\frac{T_v}{\max\big(T_u, 0.109\big)}\right]\right\},$$

$$C_2 = \begin{cases} 1 - 0.105\left[1 - \dfrac{1}{1+\exp(100T_v - 5)}\right]\left(\dfrac{T_v - T_u}{T_v - 0.0099}\right), & \text{if } \ T_v < 0.2, \\ 0, & \text{otherwise,} \end{cases}$$

$$C_3 = \begin{cases} C_2, & \text{if } \ T_v < 0.109, \\ C_1, & \text{otherwise,} \end{cases}$$

$$C_4 = C_1 - 0.5\big(\sqrt{C_3} - C_3\big)\left[1 + \cos\left(\frac{\pi T_u}{0.109}\right)\right].$$

The matrix of correlation coefficients of spectral accelerations of this model is shown as contours in Figure 2.2.

2.1.3 Probability Distribution of Spectral Accelerations

In Sections 2.1.1 and 2.1.2, the ground-motion prediction equations (GMPEs) and correlation coefficients of spectral accelerations are described. In this section, they are used to determine probability distributions of spectral accelerations, which are the core components of probabilistic seismic hazard analysis (PSHA).

For a given set of GMPEs for spectral accelerations at different vibration periods as in equation (2.1.1), based on a large number of recorded ground motions, the same number of samples is obtained for $\varepsilon(T_j)$ at each period T_j. Using normal Q-Q plots ("Q" standing for Quantile), univariate normality of the samples of $\varepsilon(T_j)$ (including inter-events and intra-events) at individual period T_j are tested. The normal Q-Q plots show strong linearity, indicating that the residuals $\varepsilon(T_j)$ are well represented by a standard normal distribution marginally. Thus, spectral acceleration $S_a(T_j)$ at individual period T_j follows lognormal distribution marginally, for a given scenario earthquake in terms of m, r, $\boldsymbol{\theta}$ (Jayaram and Baker, 2008),

$$\mathcal{P}\left\{S_a(T_j) > s_j \,\middle|\, m, r\right\} = 1 - \Phi\left(\frac{\ln s_j - \mu_{\ln S_a(T_j)\,|\,m,r}}{\sigma_{\ln S_a(T_j)\,|\,m}}\right), \tag{2.1.24}$$

where $\Phi(\cdot)$ is the standard normal distribution function and s_j is the threshold value. In the distribution function (2.1.24), the mean and standard deviation values of $\ln S_a(T_j)$ are

$$\mu_{\ln S_a(T_j)\,|\,m,r} = f(m, r, T_j, \boldsymbol{\theta}), \quad \sigma_{\ln S_a(T_j)\,|\,m} = \sigma, \tag{2.1.25}$$

where $f(m, r, T_j, \boldsymbol{\theta})$ and σ are obtained from the GMPE in equation (2.1.1). It is noted that the marginal lognormal distribution in equation (2.1.24) is conditional on a scenario earthquake, which may be represented by magnitude m, source-site distance r, and other predictor variables $\boldsymbol{\theta}$. Only m and r are expressed explicitly in equation (2.1.24) to represent a scenario earthquake, because m and r are treated as random variables in the PSHA in most cases. In this study, m and r are used to represent a scenario earthquake explicitly, while other predictor variables $\boldsymbol{\theta}$ are considered implicitly.

Based on the samples of $\varepsilon(T_j)$ (including inter-events and intra-events) at different periods T_j ($j = 1, 2, \ldots, k$), using Henze–Zirkler test, Mardia's tests of skewness and kurtosis, it is shown that the residuals $\varepsilon(T_j)$ at different periods T_j follow a multivariate standard normal distribution. Consequently, spectral accelerations $S_a(T_j)$ at different periods T_j conditional on a scenario earthquake follow multivariate lognormal distribution (Jayaram

and Baker, 2008)

$$\begin{aligned}&\mathcal{P}\left\{S_a(T_1) > s_1, \ldots, S_a(T_k) > s_k \,|\, m, r\right\} \\ &\qquad = \int_{s_k}^{\infty} \cdots \int_{s_1}^{\infty} f_{S_a(T_1),\ldots,S_a(T_k)}(s_1, \ldots, s_k \,|\, m, r)\, \mathrm{d}s_1 \ldots \mathrm{d}s_k,\end{aligned} \tag{2.1.26}$$

where $s_1, \ldots, s_k$ are threshold values of spectral accelerations at different periods and $f_{S_a(T_1),\ldots,S_a(T_k)}(s_1, \ldots, s_k \,|\, m, r)$ is the Probability Density Function (PDF) of multivariate lognormal distribution of k spectral accelerations conditional on m and r.

In the conditional multivariate lognormal distribution of spectral accelerations in equation (2.1.26), the mean and standard deviation values of $\ln S_a(T_j)$ in terms of m and r are obtained from the GMPE for each vibration period using equation (2.1.25). The correlation coefficient between the natural logarithmic spectral accelerations at any two periods given a scenario earthquake (m and r), as in equation (2.1.21), has been empirically obtained as discussed in Section 2.1.2.

The marginal and joint probability distributions of spectral accelerations governed by equations (2.1.24) and (2.1.26), respectively, will be used in the PSHA.

2.2 Deterministic Seismic Hazard Analysis

Seismic hazard can be analyzed either deterministically or probabilistically. In this section, Deterministic Seismic Hazard Analysis (DSHA) is introduced. DSHA involves the determination of a particular scenario earthquake, called controlling earthquake, on which a ground-motion hazard evaluation is based, through a ground-motion prediction equation (GMPE) as discussed in Section 2.1.1. The scenario earthquake consists of the postulated occurrence of an earthquake having a specified size and occurring at a specified location. A typical DSHA can be performed following four steps (Reiter, 1990, Kramer, 1996):

1. Identify and characterize all seismic sources, capable of producing significant ground motions, surrounding the site of interest, including determining the geometry (the seismic source zone) of each seismic source and earthquake potential (earthquake magnitude m) of each source.

2. Select a source-site distance parameter r for each source, usually the shortest distance between the seismic source zone and the site of interest. The distance may be expressed as the closest distance to the rupture plane, the closest distance to the fault rupture, the Joyner-Boore distance, or others, depending on the measure of distance of the GMPE used in Steps 3 and 4.
3. Select the controlling earthquake in terms of magnitude and source-site distance. For each seismic source i, determine the ground-motion parameter, such as spectral acceleration $S_{a,i}(T_j)$ at a specified vibration period T_j at the site of interest, produced by an earthquake with magnitude m_i (identified in Step 1) and occurring at source-site distance r_i (identified in Step 2), using a selected GMPE. The earthquake occurring at the seismic source producing the largest ground-motion parameter $S_{a,i}(T_j)$ is the controlling earthquake.
4. Determine the seismic hazard at the site of interest in terms of ground-motion intensity measures, such as PGA or design spectrum, by substituting the controlling earthquake (identified in Step 3) into the GMPE.

The DSHA procedure is shown schematically in Figure 2.3. When applied to structures for which failure could have catastrophic consequences, such as nuclear power plants and large dams, DSHA provides a straightforward framework for evaluation of the worst-case design earthquakes. However, it provides no information on the likelihood of occurrence of the controlling earthquake, the likelihood of occurrence at the assumed location, the level of shaking that might be expected during a finite period of time (e.g., useful lifetime of a particular structure or facility), and the effects of uncertainties in the various steps in the determination of the resulting ground-motion characteristics (Kramer, 1996).

2.3 Probabilistic Seismic Hazard Analysis

To analyze seismic hazard at a given site under a probabilistic framework rather than deterministically as in the deterministic seismic hazard analysis (DSHA) in Section 2.2, Probabilistic Seismic Hazard Analysis (PSHA) can be performed. PSHA has been widely used in earthquake engineering for decades. The primary advantage of the PSHA is that

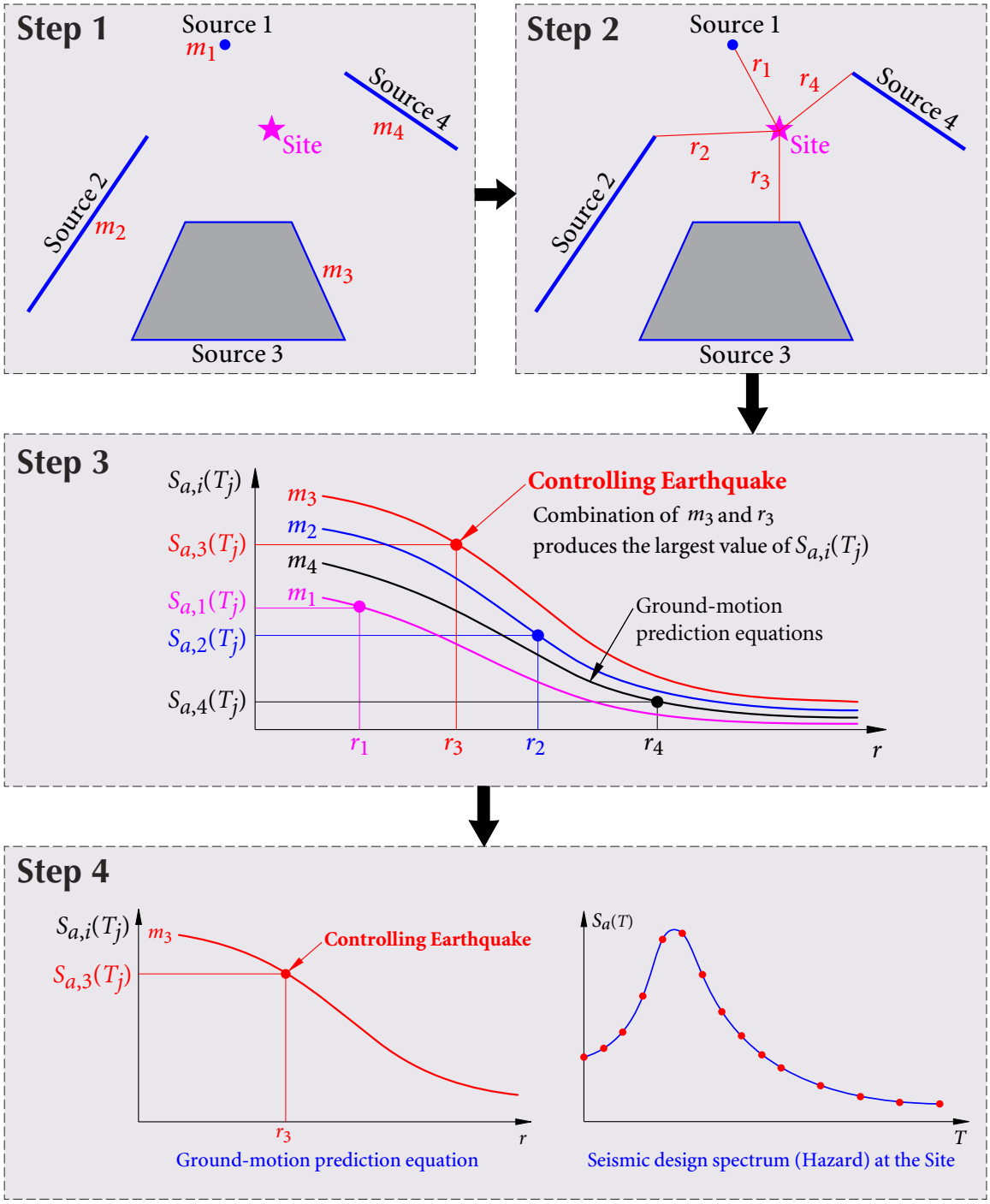

Figure 2.3 Procedure of deterministic seismic hazard analysis

it provides a framework in which uncertainties in the location of earthquakes, the size of earthquakes, the rate of occurrence of earthquakes, and the variation of ground-motion characteristics with earthquake size and location can be identified, quantified, and combined in a mathematically rigorous manner to describe the seismic hazard at a given site. The framework of the PSHA was established by Cornell (1968). The current well-known PSHA method is recognized as the Cornell-McGuire PSHA (McGuire, 2004).

Generally, the PSHA consists of a procedure of four steps (Reiter, 1990, Kramer, 1996, McGuire, 2004), as illustrated in Figure 2.4, each of which is similar to the step of the DSHA procedure:

1. Identify and characterize potential seismic sources surrounding the site of interest, which is identical to the first step of the DSHA, except that the probability distribution of potential rupture locations within the source must also be characterized. In most cases, uniform probability distribution is assigned to each seismic source zone, implying that earthquakes are equally likely to occur at any point within the source zone. The distribution of the rupture locations is then combined with the source geometry to obtain the corresponding probability distribution of source-site distance. The DSHA, on the other hand, implicitly assumes that the probability of occurrence is 1 at the points in each source zone closest to the site, and zero elsewhere. This step is elaborated in Section 2.3.1.

2. Characterize seismicity of each seismic source (i.e., temporal distribution of earthquake recurrence, from which mean rate of earthquake occurrence and probability distribution of earthquake magnitude are obtained). The temporal distribution of earthquake recurrence is called a recurrence relationship, which specifies the average rate at which an earthquake of some magnitude will be exceeded. The DSHA, on the other hand, implicitly assumes that the maximum magnitude earthquake will occur with probability 1. This step is discussed in Section 2.3.2

3. Determine the ground motions (in terms of ground-motion intensity measures, such as spectral accelerations) produced at the site by earthquakes of any possible magnitude, occurring at any possible point in the source zone, using ground-motion predic-

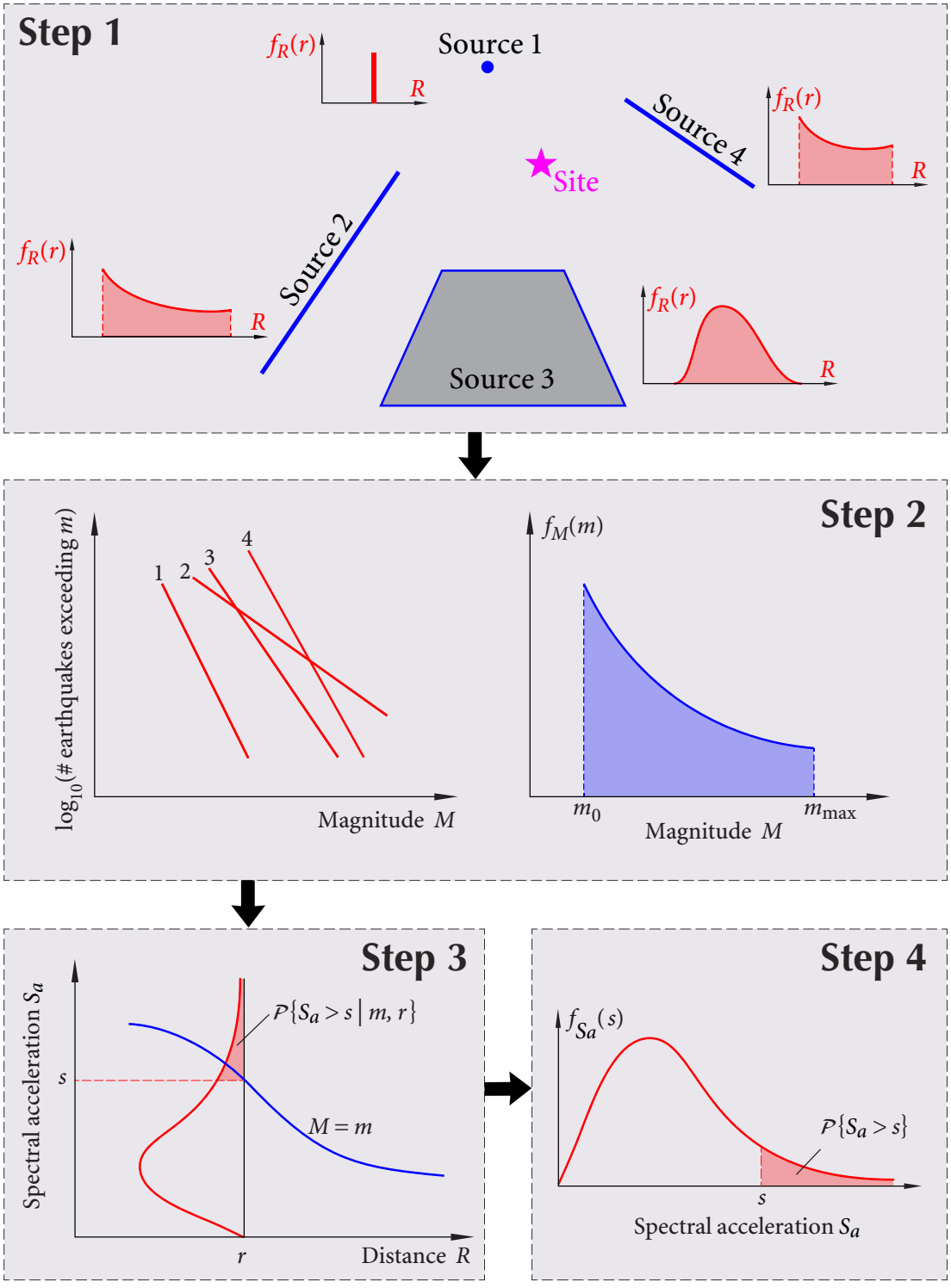

Figure 2.4 Procedure of probabilistic seismic hazard analysis

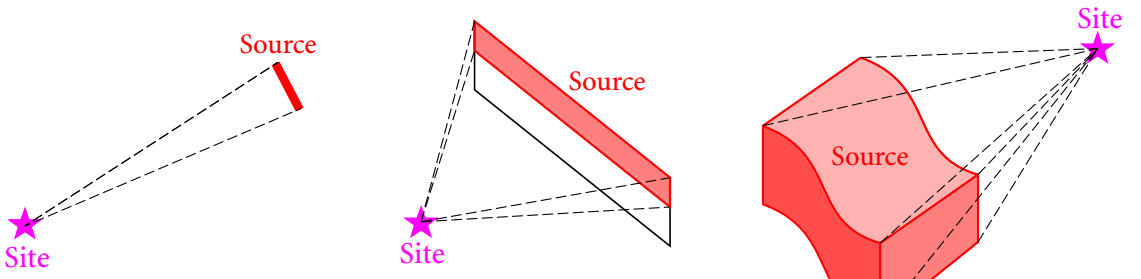

(a) Short fault modelled as a point source

(b) Shallow fault modelled as a line source

(c) Three-dimensional source zone

Figure 2.5 Geometries of seismic source zones modeled in seismic hazard analysis

tion equations (GMPEs). The uncertainty inherent in the GMPEs is also considered. This step has been discussed in Section 2.1.3.

4. Obtain the probability that ground-motion intensity measures are exceeded marginally (scalar probabilistic seismic hazard analysis) or jointly (vector-valued probabilistic seismic hazard analysis) during a time period by combining the uncertainties in the location of earthquakes, the size of earthquakes, the rate of occurrence of earthquakes, and the variation of ground-motion intensity measures with earthquake size and location. Details of this step are presented in Sections 2.3.3 and 2.3.4.

2.3.1 Probability Distribution of Source-site Distance

The geometries of seismic sources are dependent on the tectonic processes. For example, zones near volcanoes, in which earthquakes associated with volcanic activities originate, are small enough to be characterized as point seismic sources. Well-defined fault planes, on which earthquakes can occur at many different locations, can be considered as two-dimensional seismic area sources. Areas where earthquake mechanisms are poorly defined, where faulting is so extensive as to preclude distinction between individual faults, or where diffuse seismicity that are not amenable to modelling by specific faults exists, can be treated as three-dimensional seismic volume sources (Kramer, 1996).

For seismic hazard analysis, a seismic source zone may be an approximation of the actual source, depending on the relative geometry of the source and site of interest, and the quality

of information available for the source. For example, as shown in Figure 2.5(a), the relatively short fault can be modeled as a point source since the distance between any point along the fault and the site of interest is almost constant. Similarly, as shown in Figure 2.5(b), the depth of the fault plane is sufficiently small so that it does not significantly affect the source-site distance along the direction of the depth; as a result, the planar source can be approximated as a line source. In Figure 2.5(c), the available data are not sufficient to determine accurately the actual geometry of the source so that it is represented as a volume source (Kramer, 1996).

The occurrences of earthquakes are usually assumed to be uniformly distributed within a seismic source zone, i.e., earthquakes are considered equally likely to occur at any location within the source. It is also assumed that all the energy of the earthquake is released at the hypocenter of the earthquake. Based on these two assumptions, the probability distribution of the source-site distance can be determined using the geometrical relations between the source and the site of interest.

For illustration purpose, a simple line seismic source (linear fault) is used to obtain the probability distribution of source-site distance. As shown in Figure 2.6(a), the site of interest is assumed to be located at a perpendicular distance Δ from line $A'C'$ on the ground surface, along which the epicenter F' of the scenario earthquake is expected to lie. Line $A'C'$ is vertically above the fault AC of length l, located at the focal depth h. The site D is located symmetrically with respect to the fault AC.

Figure 2.6(b) shows the ABD plane of the fault. The geometrical relations between the fault and the site of interest are

$$d = \sqrt{h^2 + \Delta^2}, \tag{2.3.1a}$$

$$R = \sqrt{d^2 + X^2}, \tag{2.3.1b}$$

where d is the perpendicular slant distance from site D to fault AC, and R is the hypocentral distance, which is the distance from site D to any scenario hypocenter F located at a distance X from point B.

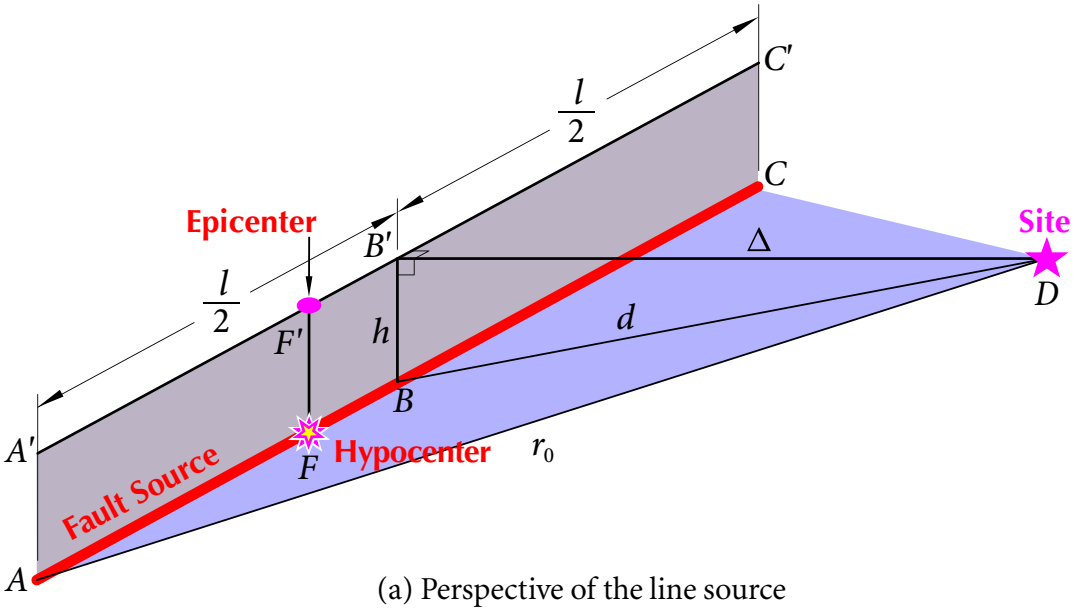

(a) Perspective of the line source

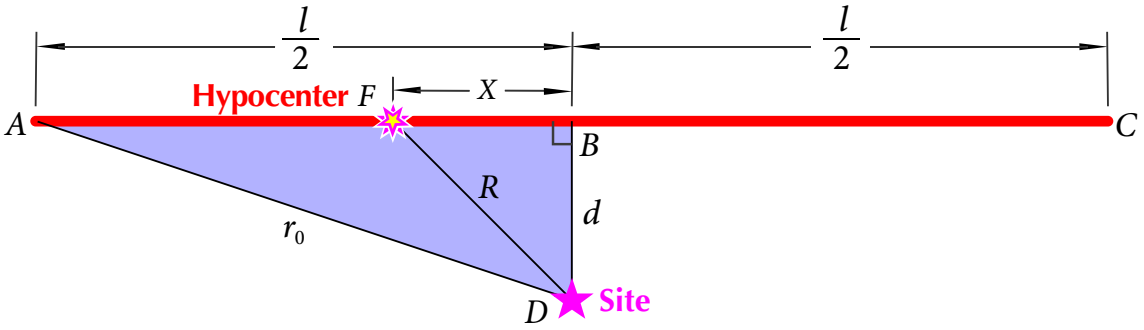

(b) *ABD* plane of the perspective of the line source

Figure 2.6 Geometry of line seismic source zone

By setting point B as the origin, it is observed that $-l/2 \leqslant X \leqslant l/2$ in Figure 2.6(b). Thus, the source-site distance R is restricted to $d \leqslant R \leqslant r_0$, in which

$$r_0 = \sqrt{d^2 + \frac{l^2}{4}}. \tag{2.3.2}$$

Based on the assumption that an earthquake is equally likely to occur anywhere along the fault, the location variable X is uniformly distributed on the interval $[-l/2, l/2]$, and $|X|$

is then uniformly distributed on the interval $[0, l/2]$. Thus, the Cumulative Distribution Function (CDF) of random variable $\left|X\right|$ can be expressed as

$$\mathcal{P}\left\{\left|X\right| \leqslant |x|\right\} = \frac{2|x|}{l}, \quad 0 \leqslant |x| \leqslant \frac{l}{2}. \tag{2.3.3}$$

By solving for X in equation (2.3.1b) and substituting X into equation (2.3.3), the CDF of source-site distance R is determined as

$$F_R(r) = \mathcal{P}\left\{R \leqslant r\right\} = \mathcal{P}\left\{\sqrt{R^2 - d^2} \leqslant \sqrt{r^2 - d^2}\right\} = \frac{2\sqrt{r^2 - d^2}}{l}, \quad d \leqslant r \leqslant r_0, \tag{2.3.4}$$

where r is threshold value of R. By differentiating equation (2.3.4), the probability density function (PDF) of R is given by

$$f_R(r) = \frac{\mathrm{d}}{\mathrm{d}r} F_R(r) = \frac{2r}{l\sqrt{r^2 - d^2}}, \quad d \leqslant r \leqslant r_0. \tag{2.3.5}$$

For seismic source zones with more complex geometries, the probability density function $f_R(r)$ can be evaluated numerically. By dividing the irregular source zone into a large number of discrete elements with equal length (for line source), area (for area source), or volume (for volume source), distance R from the site of interest to the center of each element is obtained. The percentages that the source-site distances R fall into predefined bins of the source-site distance are then determined. A histogram, in which the percentage of distance in each bin is plotted against the distance R, is then constructed to approximate $f_R(r)$ (Kramer, 1996).

2.3.2 Probability Distribution of Earthquake Magnitude

When a seismic source zone is identified, the earthquake magnitudes that the source zone is expected to produce need to be evaluated. In general, the source zone will produce earthquakes of different magnitudes up to the maximum possible value, with smaller earthquake occurring more frequently than larger ones. To characterize the temporal distribution of earthquake recurrence in terms of earthquake magnitude, occurrence relationships are established based on the database of historical seismicity.

Gutenberg and Richter (1944) organized the data of historical seismicity in southern California according to the number of earthquakes that exceeded different earthquake

magnitudes over a period of many years. By dividing the number of exceedance of each magnitude by the length of the time period, a mean annual rate λ_m of occurrence of an earthquake exceeding earthquake magnitude m is determined. When the logarithm of the mean annual rate of exceedance λ_m for southern California earthquakes is plotted against earthquake magnitude m, a linear relationship is observed. Consequently, the Gutenberg-Richter recurrence relationship is expressed as

$$\log_{10} \lambda_m = a - b\, m, \tag{2.3.6}$$

where 10^a is the mean annual number of earthquakes of magnitude larger than or equal to zero, and b describes the relative likelihood of large and small earthquakes. Generally, parameters a and b are obtained by regression analysis on a database of historical seismicity for the source zone of interest.

The Gutenberg-Richter recurrence relationship governed by equation (2.3.6) can also be expressed as

$$\lambda_m = 10^{a-b\,m} = \mathrm{e}^{\alpha - \beta m}, \tag{2.3.7}$$

where $\alpha = a \ln 10$ and $\beta = b \ln 10$. The Gutenberg-Richter recurrence relationship (2.3.7) implies that earthquake magnitudes are exponentially distributed and magnitude m is valid for the semi-infinite range of $[0, +\infty)$.

For engineering purpose, however, it is common to disregard very small earthquakes since they seldom cause significant damage. On the other hand, a seismic source zone has a maximum earthquake magnitude $m_{\max}$ that it is capable to produce due to its geological conditions. Thus, the bounded Gutenberg-Richter recurrence relationship was established to eliminate earthquake magnitudes lower than threshold $m_{\min}$ and larger than threshold $m_{\max}$ for the source zone of interest (McGuire, 2004)

$$\lambda_m = \nu\, \frac{\mathrm{e}^{-\beta(m-m_{\min})} - \mathrm{e}^{-\beta(m_{\max}-m_{\min})}}{1 - \mathrm{e}^{-\beta(m_{\max}-m_{\min})}}, \quad m_{\min} \leqslant m \leqslant m_{\max}, \tag{2.3.8}$$

where $\nu = \exp\left(\alpha - \beta m_{\min}\right)$ is the mean annual rate of occurrence of earthquakes above the minimum earthquake magnitude $m_{\min}$ for the source zone. The bounded Gutenberg-Richter recurrence relationship (2.3.8) is illustrated in Figure 2.7 for $\nu = 1$ and $\beta = 2$.

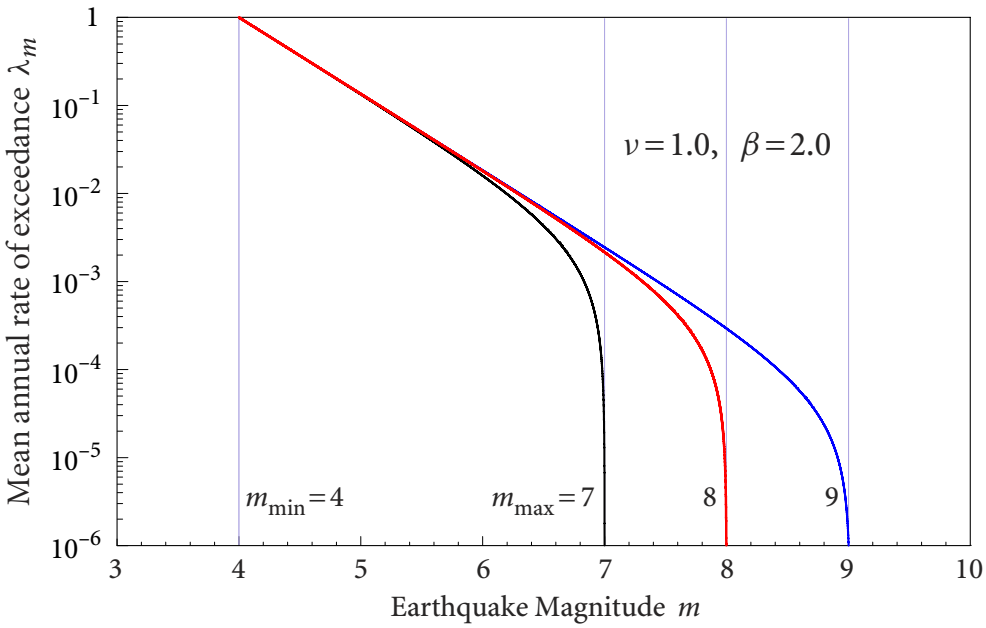

Figure 2.7 Bounded Gutenberg-Richter recurrence relationship

Based on equation (2.3.8), the CDF of earthquake magnitude M between $m_{\min}$ and $m_{\max}$ is given by

$$F_M(m) = \mathcal{P}\left\{M \leqslant m \,\middle|\, m_{\min} \leqslant m \leqslant m_{\max}\right\} = \frac{\lambda_{m_{\min}} - \lambda_m}{\lambda_{m_{\min}}} = \frac{1 - \mathrm{e}^{-\beta(m-m_{\min})}}{1 - \mathrm{e}^{-\beta(m_{\max}-m_{\min})}}. \quad (2.3.9)$$

By differentiating equation (2.3.9), the PDF of M is given by

$$f_M(m) = \frac{\mathrm{d}}{\mathrm{d}m} F_M(m) = \frac{\beta \mathrm{e}^{-\beta(m-m_{\min})}}{1 - \mathrm{e}^{-\beta(m_{\max}-m_{\min})}}. \quad (2.3.10)$$

Probabilistic seismic hazard analysis (PSHA) is usually conducted by considering seismic hazard environment surrounding specific sites. The earthquake-generating characteristics of individual faults are then important. Individual faults repeatedly generate earthquakes of similar size (within about one-half magnitude unit), known as characteristic earthquakes, at or near their maximum earthquake magnitude. Geological evidence indicates that the characteristic earthquakes occur more frequently than implied by extrapolating the Gutenberg-Richter recurrence relationship from high rates of exceedance (low magnitude) to low rates of exceedance (high magnitude). This results in a more complex recurrence

law governed by seismicity data at low magnitudes and geologic data at high magnitudes (Kramer, 1996).

2.3.3 Scalar Probabilistic Seismic Hazard Analysis

Having characterized the uncertainties in the location of earthquakes in Section 2.3.1, the size and occurrence rate of earthquakes in Section 2.3.2, and the variation of individual ground-motion intensity measure in Section 2.1.3, scalar probabilistic seismic hazard analysis (PSHA) can be performed in a mathematically rigorous manner.

Take spectral acceleration $S_a(T_j)$ at vibration period T_j as the ground-motion intensity measure, and assume that earthquake magnitude M and source-site distance R are statistically independent. For a given occurrence of an earthquake at a seismic source zone i, the probability that $S_a(T_j)$ exceeds a threshold s_j at the site of interest can be calculated using the total probability theorem

$$\begin{aligned}&\mathcal{P}\left\{S_a(T_j) > s_j \,\middle|\, \text{an earthquake occurring at source } i\right\}\\ &\qquad = \left\{ \int_r \int_m \mathcal{P}\left\{S_a(T_j) > s_j \,|\, m, r\right\} f_M(m) f_R(r) \mathrm{d}m \,\mathrm{d}r \right\}_i,\end{aligned} \tag{2.3.11}$$

where $\mathcal{P}\left\{S_a(T_j) > s_j \,|\, m, r\right\}$ is the CDF of spectral acceleration $S_a(T_j)$ conditional on a scenario earthquake in terms of m and r, given by equation (2.1.24), and $f_M(m)$ and $f_R(r)$ are the PDF of magnitude M and source-site distance R, determined in Sections 2.3.2 and 2.3.1, respectively.

Multiplying equation (2.3.11) by ν_i (the mean annual rate of occurrence of earthquakes above the minimum earthquake magnitude $m_{\min}$ for the source zone i), the mean annual rate that $S_a(T_j)$, produced by source i, exceeds a threshold s_j at the site of interest is given by

$$\lambda_{s_j}^{(i)} = \nu_i \left\{ \int_r \int_m \mathcal{P}\left\{S_a(T_j) > s_j \,|\, m, r\right\} f_M(m) f_R(r) \mathrm{d}m \,\mathrm{d}r \right\}_i. \tag{2.3.12}$$

For the seismic hazard evaluated at a site having N_S potential seismic source zones, the mean annual rate of exceedance of spectral acceleration $S_a(T_j)$ is

$$\lambda_{s_j} = \sum_{i=1}^{N_S} \lambda_{s_j}^{(i)} = \sum_{i=1}^{N_S} \nu_i \left\{ \int_r \int_m \mathcal{P}\left\{S_a(T_j) > s_j \,|\, m, r\right\} f_M(m) f_R(r) \mathrm{d}m \,\mathrm{d}r \right\}_i. \tag{2.3.13}$$

In equation (2.3.12), the mean annual rate of spectral acceleration $S_a(T_j)$ exceeding a threshold value s_j is calculated by summing up the probabilities for all possible earthquake magnitudes and distances, multiplied by the earthquake occurrence rate, for source zone i. The seismic hazards for all the sources are then combined in equation (2.3.13) to obtain the aggregate hazard at the site. It is noted that for regions where the causative structures of seismicity are largely unknown, smoothed historical seismicity method can be used to obtain a combination of magnitude and distance distributions, and the mean rate of occurrence, without drawing seismic source zones (Frankel, 1995).

Having obtained the mean annual rate of exceedance of spectral acceleration $S_a(T_j)$ in equation (2.3.13), the temporal uncertainties of the occurrence of such earthquakes are often modelled using Poisson process (Kramer, 1996). Assume that the event can occur randomly at any time and the occurrence of an event in a given time interval is independent of that in any other non-overlapping intervals, the probability of n events (i.e., spectral acceleration $S_a^t(T_j)$ exceeding s_j) occurring in a time period of t is given by

$$p_{N_E} = \mathcal{P}\{N_E = n\} = \frac{(\lambda_{s_j} t)^n}{n!} \mathrm{e}^{-\lambda_{s_j} t}, \quad n = 0, 1, 2, \ldots, \tag{2.3.14}$$

where the superscript "t" in $S_a^t(T_j)$ indicates the time period t.

From equation (2.3.14), the probability of at least one event occurring (i.e., the event of spectral acceleration $S_a^t(T_j)$ exceeding s_j occurring at least once) during time period t is given by

$$\mathcal{P}\{S_a^t(T_j) > s_j\} = 1 - \mathcal{P}\{N_E = 0\} = 1 - \mathrm{e}^{-\lambda_{s_j} t}. \tag{2.3.15}$$

In most earthquake engineering practices, the time period t is taken as one year or 50 years. For simplicity of notation, in this study, the time period t is taken as one year and the notation "$S_a(T_j)$" is used for $t = 1$.

When the value of the mean annual rate of exceedance λ_{s_j} in equation (2.3.13) is small, which is almost always the case in reality, λ_{s_j} and the annual ($t = 1$) probability of exceedance $\mathcal{P}\{S_a(T_j) > s_j\}$ in equation (2.3.15) are numerically identical. The commonly used terminology of "annual probability of exceedance" is then employed directly for λ_{s_j} in equation (2.3.13) in this study, instead of the mean annual rate of exceedance.

From equation (2.3.13), the annual probability (or mean annual rate) of exceedance plotted against spectral acceleration $S_a(T_j)$ is known as a *seismic hazard curve*, as shown in Figures 2.9 and 2.10. For a given annual probability of spectral acceleration $S_a(T_j)$ exceeding s_j, a plot of the threshold s_j for a number of vibration periods T_j of engineering interest at a site gives a uniform hazard spectrum (UHS). The properties and limitations of the UHS are discussed in Section 3.1.1.

Since the simultaneous exceedance of spectral accelerations at multiple periods in vector-valued probabilistic seismic hazard analysis (PSHA) can also be treated as an event of interest in the time interval t, the Poisson process in equation (2.3.15) and the terminology of "annual probability of exceedance" are also employed in the vector-valued PSHA presented in Section 2.3.4.

The scalar PSHA is demonstrated by a numerical example, which is based on a hypothetical configuration of seismic source zones as shown in Figure 2.8. The probability distribution of source-site distance in equation (2.3.5) is used for each seismic source zone. Equation (2.3.10) is taken as the probability distribution of earthquake magnitude, in which $m_{\min}$, $m_{\max}$, and β are assumed to be 5, 6, and 2.07, respectively, for Source 1, and 5, 8, and 2.07, respectively, for Source 2. The mean annual rates ν for Sources 1 and 2 are taken as 0.01 and 0.09, respectively. It is noted that the site of interest can be located inside an area source, which is the most common situation in Canada. However, the computation of the PSHA does not depend on seismic hazard configuration.

The ground-motion prediction equation (GMPE), proposed by Abrahamson and Silva (1997) as presented in Section 2.1.1, is used for obtaining the mean and standard deviation values in the conditional probability distribution of spectral acceleration at individual vibration period in equation (2.1.24). In the selected GMPE, parameters are set for rock site condition, reverse fault, any geological condition except for hanging wall, and sigma for arbitrary component.

By performing the scalar PSHA for the hypothetical configuration of seismic source zones, the seismic hazard curves for spectral accelerations at 0.1 and 1 sec are plotted in Figures 2.9 and 2.10, respectively. For a given annual probability of exceedance, 4×10^{-4} for

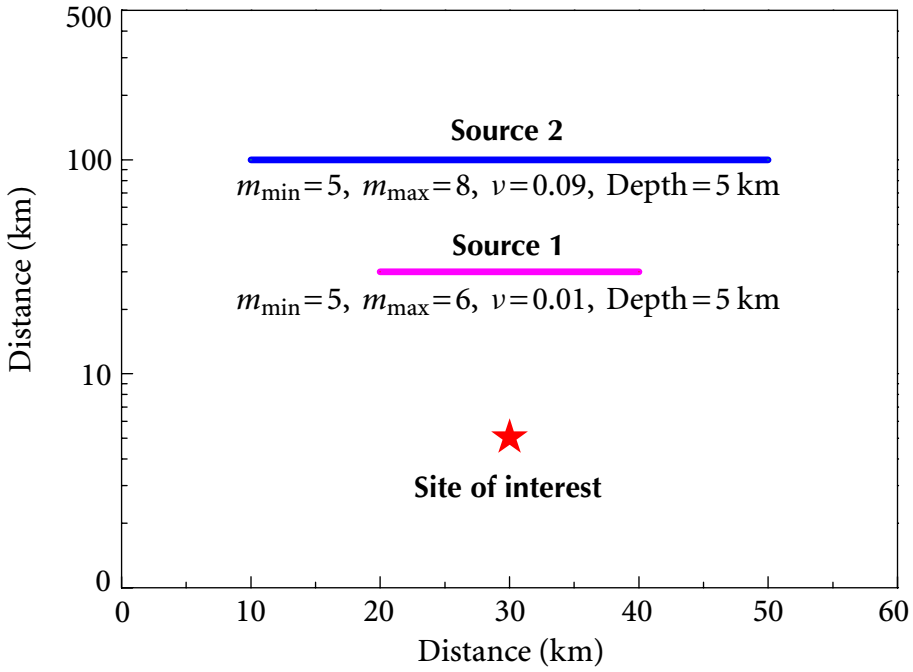

Figure 2.8 Hypothetical configuration of seismic source zones

example, the corresponding threshold values of spectral accelerations at 0.1 and 1 sec can be determined as $0.464\,g$ and $0.155\,g$ in Figures 2.9 and 2.10, respectively.

2.3.4 Vector-valued Probabilistic Seismic Hazard Analysis

The scalar PSHA for a specific site, as discussed in Section 2.3.3, provides the marginal annual probability of exceeding a threshold value of spectral acceleration at individual period. To improve the accuracy in predicting structural response induced by earthquakes, the vector-valued probabilistic seismic hazard analysis (PSHA), from which the joint annual probability of simultaneously exceeding threshold values of spectral accelerations at multiple vibration periods can be determined, was first proposed by Bazzurro and Cornell (2002).

In the k-dimensional case, replace the marginal probability distribution of spectral acceleration conditional on a scenario earthquake in equation (2.3.12) using the joint conditional probability distribution governed by equation (2.1.26). The joint annual probability (joint mean annual rate in actuality) of simultaneously exceeding spectral accelerations

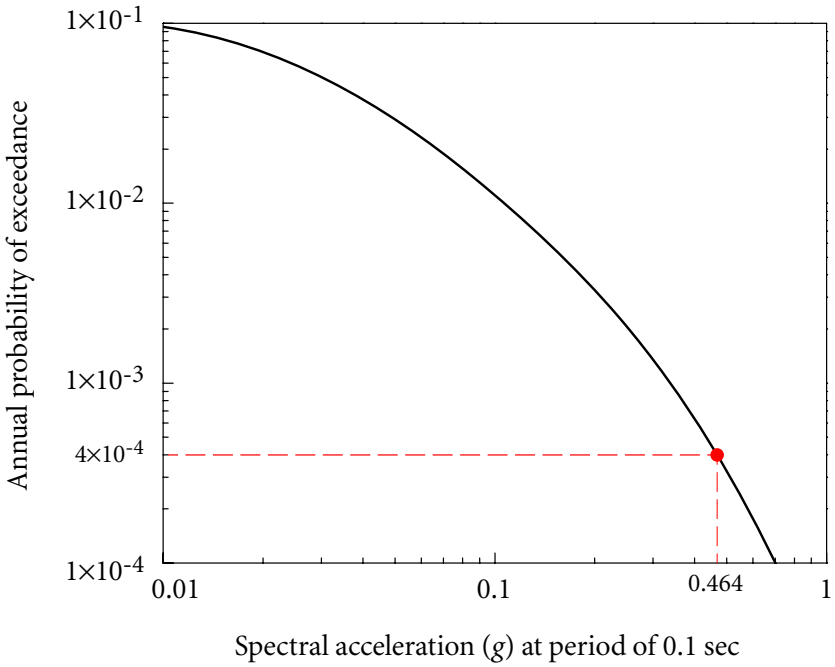

Figure 2.9 Seismic hazard curve for spectral acceleration at vibration period of 0.1 sec

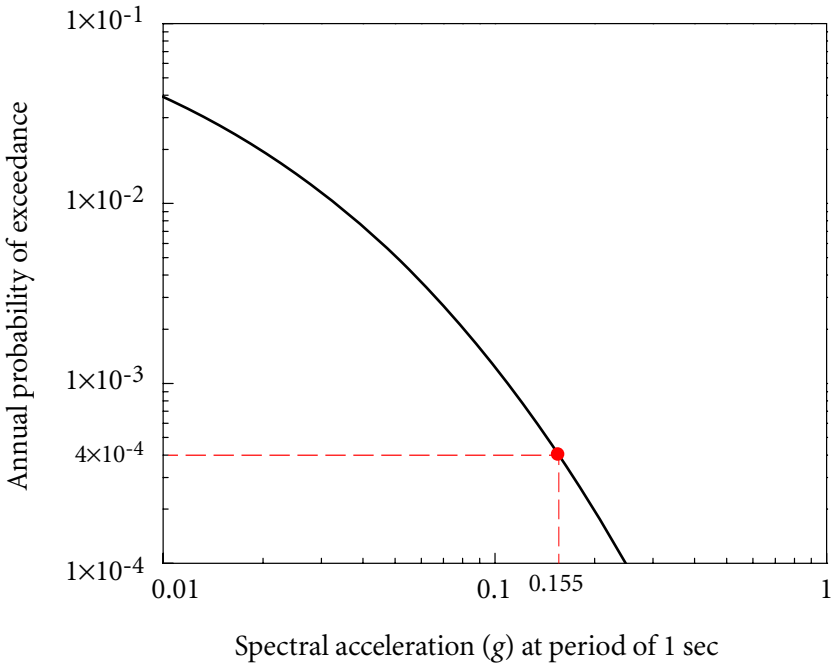

Figure 2.10 Seismic hazard curve for spectral acceleration at vibration period of 1 sec

$S_a(T_1), \ldots, S_a(T_k)$ at vibration periods $T_1, \ldots, T_k$ for the source zone i is given by

$$\lambda^{(i)}_{s_1 \ldots s_k} = \nu_i \Big\{ \int_r \int_m \mathcal{P}\left\{ S_a(T_1) > s_1, \ldots, S_a(T_k) > s_k \,\middle|\, m, r \right\} f_M(m) f_R(r) \mathrm{d}m \, \mathrm{d}r \Big\}_i . \quad (2.3.16)$$

For the seismic hazard evaluated at a site having N_S potential seismic source zones, the joint probability of simultaneously exceeding spectral accelerations is

$$\lambda_{s_1 \ldots s_k} = \sum_{i=1}^{N_S} \nu_i \Big\{ \int_r \int_m \mathcal{P}\left\{ S_a(T_1) > s_1, \ldots, S_a(T_k) > s_k \,\middle|\, m, r \right\} f_M(m) f_R(r) \mathrm{d}m \, \mathrm{d}r \Big\}_i . \quad (2.3.17)$$

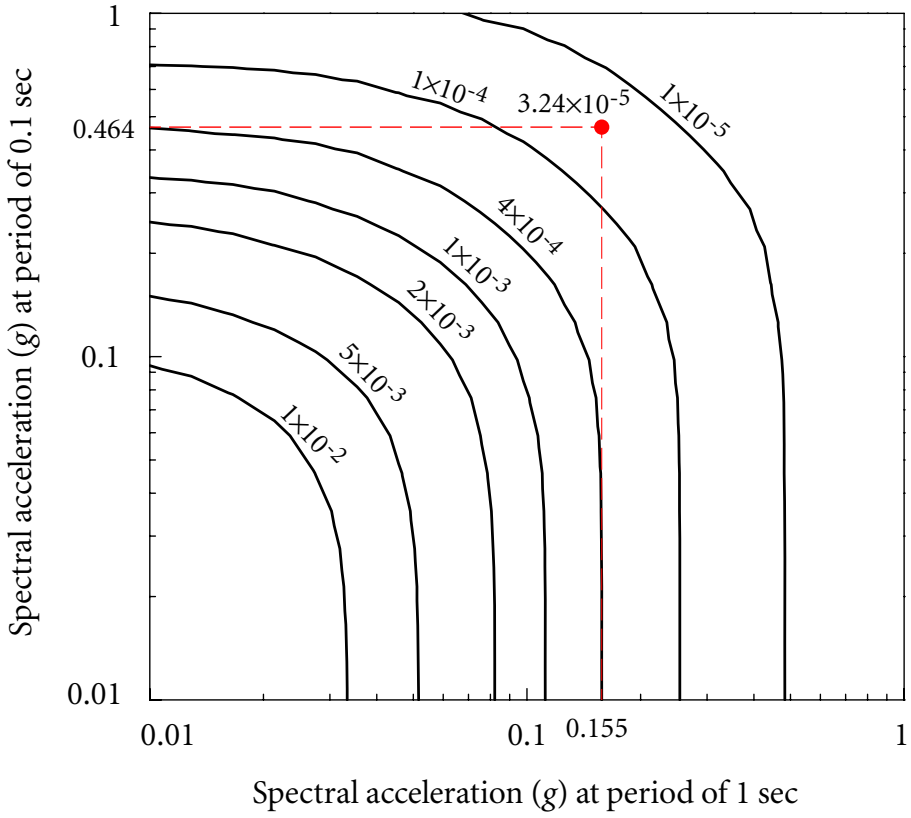

Figure 2.11 Contours (denoting the joint probability of exceedance) of vector-valued probabilistic seismic hazard analysis

To illustrate the vector-valued PSHA, the hazard analysis for the hypothetical configuration of seismic source zones, shown in Figure 2.8, is performed for spectral accelerations at vibration periods of 0.1 and 1 sec. In the joint conditional probability distribution governed

by equation (2.1.26), the most current matrix of spectral correlation developed by Baker and Jayaram (2008) is adopted. All other information required in the hazard evaluation is the same as used in Section 2.3.3.

Figure 2.11 shows the contours of the vector-valued PSHA for the hypothetical seismic hazard environment. The contours denote the joint annual probability of exceeding spectral accelerations at 0.1 and 1 sec simultaneously. For the marginal probability of exceedance of 4×10^{-4}, spectral accelerations at 0.1 and 1 sec are $0.464\,g$ and $0.155\,g$, respectively. As can be seen in Figure 2.11, the joint probability that the events of spectral acceleration at 0.1 sec exceeding 0.464 g and spectral acceleration at 1 sec exceeding 0.155 g occur at the same time is 3.24×10^{-5}, which is much smaller than the marginal probability for spectral accelerations at individual vibration periods.

2.4 Seismic Hazard Deaggregation

The PSHA combines all possible and relevant earthquake scenarios and probability levels through integration, which is an "aggregation" procedure. To study the contributions of parameters (such as earthquake magnitude, source-site distance, epsilon, and the rate of occurrence) of earthquake scenarios to the seismic hazard at a given site, a "deaggregation" procedure for equation (2.3.13) or (2.3.17), known as seismic hazard deaggregation (SHD), is often performed (McGuire, 1995, Bazzurro and Cornell, 1999). The SHD can be classified as scalar SHD and vector-valued SHD, corresponding to the scalar PSHA and vector-valued PSHA, respectively. The scalar and vector-valued SHD are discussed in Sections 2.4.1 and 2.4.2, respectively.

2.4.1 Scalar Seismic Hazard Deaggregation

To investigate not only the relative seismic hazard contributions from earthquake magnitude m and source-site distance r but also the number of standard deviations ε in equation (2.1.1), the standard formulation of scalar PSHA given by equation (2.3.13) can be extended to

$$\lambda_{s_j} = \sum_{i=1}^{N_S} \nu_i \left\{ \int_{\varepsilon} \int_{r} \int_{m} P\left\{ S_a(T_j) > s_j \,\middle|\, m, r, \varepsilon \right\} f_M(m) f_R(r) f_{\epsilon}(\varepsilon) \mathrm{d}m \, \mathrm{d}r \, \mathrm{d}\varepsilon \right\}_i . \qquad (2.4.1)$$

In equation (2.4.1), $f_\epsilon(\varepsilon)$ is the PDF of standard normal distribution as discussed in Section 2.1.3, and the first term in the integrand is the Heaviside step function,

$$\mathcal{P}\left\{S_a(T_j) > s_j \,\middle|\, m, r, \varepsilon\right\} = H\Big[\ln S_a(T_j) \,\Big|\, m, r, \varepsilon - \ln s_j\Big], \tag{2.4.2}$$

which is equal to 1 if $\ln S_a(T_j) \,|\, m, r, \varepsilon$, as computed from equation (2.1.1), is greater than $\ln s_j$ and 0 otherwise. From equations (2.4.1) and (2.4.2), the relative seismic hazard contributions can be calculated towards the probability of $S_a(T_j)$ exceeding (not equal to) s_j, as will be presented later.

In some cases, the relative seismic hazard contributions towards the probability of $S_a(T_j)$ equal to (not exceeding) s_j may be desired (McGuire, 1995, Baker and Cornell, 2006b). Equation (2.4.2) can be replaced by

$$\mathcal{P}\left\{S_a(T_j) = s_j \,\middle|\, m, r, \varepsilon\right\} = \mathrm{I}\Big[\ln S_a(T_j) \,\Big|\, m, r, \varepsilon,\ \ln s_j\Big], \tag{2.4.3}$$

where I denotes an indicator function, which is equal to 1 when $\ln S_a(T_j) \,|\, m, r, \varepsilon = \ln s_j$ and 0 otherwise. Since the probability of equal to a threshold is always zero for a continuous probability distribution function, equation (2.4.3) exits only when numerical discretization is applied so that equation (2.4.3) becomes a Probability Mass Function (PMF).

Using equation (2.4.1) along with equation (2.4.2) or (2.4.3), the annual probability of spectral acceleration exceeding (or equal to) a given value s_j (determined from a specified annual probability of exceedance using a seismic hazard curve) for the intervals $m_{x-1} \leqslant m \leqslant m_x$, $r_{y-1} \leqslant r \leqslant r_y$, and $\varepsilon_{z-1} \leqslant \varepsilon \leqslant \varepsilon_z$ ($1 \leqslant x \leqslant x_N$, $1 \leqslant y \leqslant y_N$, and $1 \leqslant z \leqslant z_N$, in which x_N, y_N, and z_N are the numbers of intervals for m, r, and ε, respectively) is given by

$$\lambda_{s_j,x,y,z} = \sum_{i=1}^{N_S} \nu_i \Big\{ \int_{\varepsilon_{z-1}}^{\varepsilon_z} \int_{r_{y-1}}^{r_y} \int_{m_{x-1}}^{m_x} \mathcal{P}\left\{S_a(T_j) > s_j \,\middle|\, m, r, \varepsilon\right\} f_M(m) f_R(r) f_\epsilon(\varepsilon) \mathrm{d}m\, \mathrm{d}r\, \mathrm{d}\varepsilon \Big\}_i. \tag{2.4.4}$$

Dividing these annual probabilities of exceedance (or equal) $\lambda_{s_j,x,y,z}$ for different cubic intervals of m-r-ε by the total annual probability of exceedance (or equal) λ_{s_j} in equation (2.4.1), a 4-dimensional histogram of relative contributions to the seismic hazard against the coordinates of m, r, and ε can be plotted.

Representative earthquake

From the relative seismic hazard contributions towards a given spectral acceleration s_j, the representative earthquake, in terms of modal or mean values of earthquake magnitude m, source-site distance r, and the number of standard deviations ε, can be obtained. For the cubic interval having the largest relative hazard contribution, the corresponding set of $\hat{m}_j$-$\hat{r}_j$-$\hat{\varepsilon}_j$ is known as the modal (most-likely) earthquake towards s_j.

The mean earthquake towards s_j, represented by the weighted average values of magnitude $\bar{m}_j$, distance $\bar{r}_j$, and the number of standard deviations $\bar{\varepsilon}_j$, is expressed as

$$\bar{m}_j = \sum_{x=1}^{x_N} \sum_{y=1}^{y_N} \sum_{z=1}^{z_N} \frac{\left(m_{x-1} + m_x\right)}{2} \frac{\lambda_{s_j,x,y,z}}{\lambda_{s_j}}, \tag{2.4.5a}$$

$$\bar{r}_j = \sum_{x=1}^{x_N} \sum_{y=1}^{y_N} \sum_{z=1}^{z_N} \frac{\left(r_{y-1} + r_y\right)}{2} \frac{\lambda_{s_j,x,y,z}}{\lambda_{s_j}}, \tag{2.4.5b}$$

$$\bar{\varepsilon}_j = \sum_{x=1}^{x_N} \sum_{y=1}^{y_N} \sum_{z=1}^{z_N} \frac{\left(\varepsilon_{z-1} + \varepsilon_z\right)}{2} \frac{\lambda_{s_j,x,y,z}}{\lambda_{s_j}}, \tag{2.4.5c}$$

where $\lambda_{s_j,x,y,z}$ and λ_{s_j} are given by equations (2.4.4) and (2.4.1), respectively.

In engineering practice, to achieve certain engineering objective, modifications or manipulations may be applied to the procedure of the scalar SHD.

Beta earthquake

McGuire (1995) proposed a procedure of scalar SHD to obtain the most-likely combination of m_β, r_β, and ε_β, known as the beta earthquake, to accurately replicate the uniform hazard spectrum (UHS) in some manner. The procedure for generating the beta earthquake is summarized as follows.

- Calculate seismic hazard curves of spectral accelerations at 0.1 sec (representing short period portion of the UHS) and 1 sec (representing long period portion of the UHS) for each seismic source zone separately using equation (2.3.12) and for all the seismic zones using equation (2.3.13).

- Specify an annual probability of exceedance (e.g., 4.0×10^{-4}) and determine the spectral acceleration threshold corresponding to this specified probability of exceedance on each calculated seismic hazard curve.

- **One Dominant Seismic Source:** If one seismic source is the dominant hazard contributor at both 0.1 and 1 sec, i.e., the largest threshold values of spectral accelerations at both 0.1 and 1 sec are from the same seismic source (dominant seismic source), one beta earthquake is used to represent the seismic hazard. In this case,

    1. Draw two 4-dimensional histograms of hazard contributions by m, r, and ε, using equations (2.4.3) and (2.4.4), for vibration periods of 0.1 and 1 sec at the specified annual probability of exceedance for the dominant seismic source.
    2. Draw a composite 4-dimensional histogram from the two histograms obtained in Step 1 by (a) considering only intervals in which there is a nonzero contribution in both histograms, (b) adding the contributions in the corresponding intervals for the two histograms, and (c) assigning zero to the remaining intervals, in which one or both histograms have a zero contribution.
    3. Determine the modal (or most-likely) earthquake in terms of m_β, r_β, and ε_β from the composite 4-dimensional histogram obtained in Step 2.
    4. Substitute m_β, r_β, and ε_β, obtained in Step 3, into the GMPEs in equation (2.1.1) at both 0.1 and 1 sec. Adjust the value of ε_β so that the resulting spectral accelerations at 0.1 and 1 sec are greater than or equal to the threshold values of spectral accelerations (corresponding to the specified probability of exceedance) calculated for all the seismic zones at 0.1 and 1 sec, respectively.
    5. Obtain the beta earthquake in terms of m_β, r_β, and the adjusted ε_β.

- **Two Dominant Seismic Sources:** If different seismic sources are the dominant hazard contributors at 0.1 and 1 sec, i.e., the largest threshold values of spectral accelerations at 0.1 and 1 sec, respectively, are from two different seismic sources (dominant seismic sources), two beta earthquakes are used to represent the seismic hazard at the portions of short period and long period, respectively. In this case,

1. Draw a 4-dimensional histogram of hazard contributions by m, r, and ε, using equations (2.4.3) and (2.4.4), for vibration period of 0.1 sec at the specified annual probability of exceedance for the corresponding dominant seismic source.

2. Determine the modal (or most-likely) earthquake in terms of m_β, r_β, and ε_β from the 4-dimensional histogram obtained in Step 1.

3. Substitute m_β, r_β, and ε_β, obtained in Step 2, into the GMPE in equation (2.1.1) at 0.1 sec and adjust the ε_β so that the resulting spectral acceleration at 0.1 sec is equal to the threshold value of spectral acceleration (corresponding to the specified probability of exceedance) calculated for all the seismic zones at 0.1 sec.

4. Obtain the beta earthquake in terms of m_β, r_β, and the adjusted ε_β for spectral acceleration at 0.1 sec.

5. Repeat Steps 1-4 to determine the beta earthquake in terms of m_β, r_β, and the adjusted ε_β for spectral acceleration at 1 sec.

There are initially two distributions (for spectral accelerations at 0.1 and 1 sec) contributing to seismic hazard by m, r, and ε. If the two distributions are close, similar earthquakes drive the hazard at both 0.1 and 1 sec, as treated in the case of one dominant source. If the distributions are different, different earthquakes drive the hazards for 0.1 and 1 sec, as treated in the case of two dominant sources. The beta earthquakes determined are used for replicating the UHS, as discussed in Section 3.1.2.

Representative earthquake for CMS-ε

Baker and Cornell (2005) proposed the concept of Conditional Mean Spectrum considering ε (CMS-ε). The CMS-ε is obtained based on the GMPEs, correlation coefficients of spectral accelerations, and the representative earthquake from the scalar SHD. The representative earthquake in terms of mean values $\bar{m}_j$, $\bar{r}_j$, and $\bar{\varepsilon}_j$ is obtained for equal to spectral acceleration at the fundamental period of the structure of interest using equations (2.4.3)-(2.4.5). The value of $\bar{\varepsilon}_j$ is then adjusted so that the resulting spectral acceleration at the structural fundamental period using GMPE matches the UHS at the fundamental period. The CMS-ε is discussed in Section 3.1.3.

Controlling earthquake

As presented previously, to replicate $S_a(T_j)$ on a UHS, representative earthquake in terms of m, r, and ε are substituted into a GMPE. However, ε is often reassigned to the value that gives a prediction of the target $S_a(T_j)$, because the resulting $S_a(T_j)$ using GMPE dose not necessarily match the target $S_a(T_j)$ on the UHS (McGuire, 1995, Baker and Cornell, 2005). In this situation, it may be unnecessary to disaggregate the seismic hazard for ε.

On the other hand, as shown in equation (2.1.1) and discussed in Section 2.1.3, the random variable $\varepsilon(T_j)$ in a GMPE characterizes only the probability level of $S_a(T_j)$ conditional on the occurrence of an earthquake in terms of m and r. The uncertainty of the occurrence of the earthquake itself, i.e., the occurrence rate of the earthquake, is not considered in the prediction of $S_a(T_j)$ on the UHS using GMPE.

From equation (2.3.13), the probability level of $S_a(T_j)$ on a UHS is a summation of the products of the annual probabilities of exceedance conditional on the earthquake occurrence and the earthquake occurrence rates. It is therefore inappropriate to predict $S_a(T_j)$ on a UHS by using only the GMPE and ε, without considering the occurrence rate of such an earthquake; in other words, it is inappropriate to implicitly characterize the probability level of $S_a(T_j)$ and the occurrence rate by only $\varepsilon(T_j)$.

Ni *et al.* (2011D) proposed the concept of controlling earthquake in terms of earthquake magnitude m_C, source-site distance r_C, and the rate of occurrence ν_C. The values of m_C and r_C are determined for the exceedance of a threshold of spectral acceleration using equations (2.4.5a), (2.4.5b), and (2.4.2). Similar to equations (2.4.5), the weighted average value of the rate of occurrence ν_C is given by

$$\nu_C = \sum_{i=1}^{N_S} \nu_i \frac{\lambda_{s_j}^{(i)}}{\lambda_{s_j}}, \tag{2.4.6}$$

where $\lambda_{s_j}^{(i)}$ is the seismic hazard contribution from seismic source i in equation (2.3.12) and λ_{s_j} is given by equation (2.3.13).

The use of the controlling earthquake from the scalar SHD, and the vector-valued SHD as presented in Section 2.4.2, for approximating several seismic design spectra is discussed in

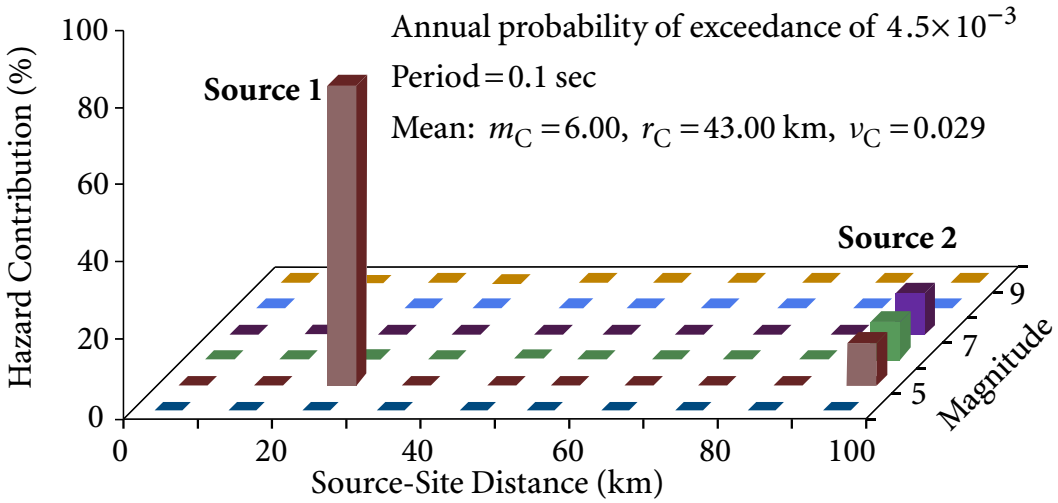

Figure 2.12 Scalar seismic hazard deaggregation for spectral acceleration at vibration period of 0.1 sec

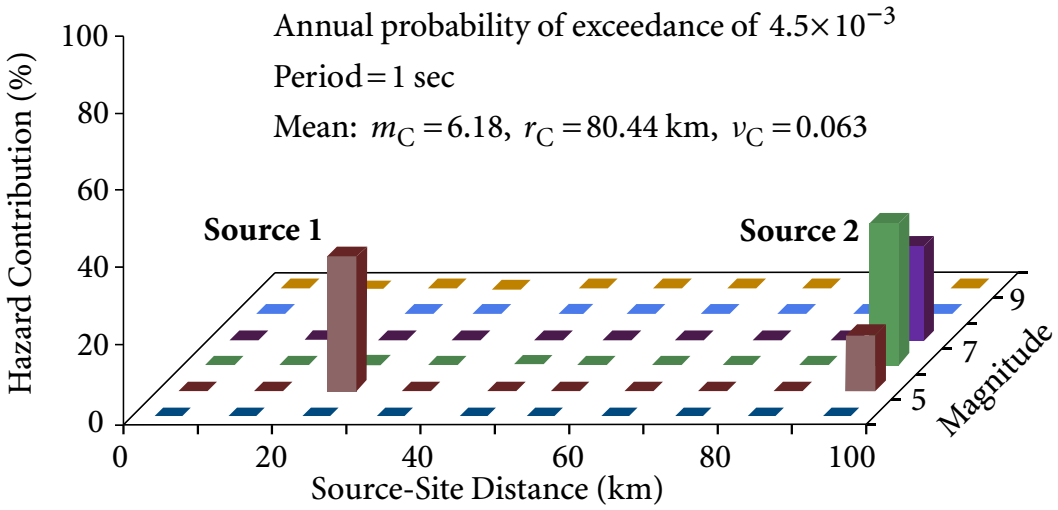

Figure 2.13 Scalar seismic hazard deaggregation for spectral acceleration at vibration period of 1 sec

Section 3.2.4. It is noted that the concept of "controlling earthquake" proposed by Ni *et al.* (2011D) is different from the one mentioned in the DSHA in Section 2.2.

For the hypothetical configuration of seismic source zones illustrated in Figure 2.8, the 3-dimensional histograms of relative seismic hazard contributions from m and r for spectral accelerations at vibration periods of 0.1 and 1 sec, respectively, are shown in Figures 2.12

and 2.13. The annual probability of exceedance is selected as 4.5×10^{-3} and all other parameters are the same as used in Section 2.3.3.

In Figure 2.12, Source 1 (producing small near-field earthquake) is the dominant seismic hazard contributor to the spectral acceleration at 0.1 sec (short period portion) so that the resulting controlling earthquake has relatively small magnitude and short distance. In contrast, as shown in Figure 2.13, Source 2 (producing large far-field earthquake) is the dominant seismic hazard contributor to the spectral acceleration at 1 sec (long period portion) so that the resulting controlling earthquake possesses relatively large magnitude and long distance. This phenomenon has been widely observed in seismic hazard analysis (McGuire, 1995, Frankel, 1995, Halchuk and Adams, 2004, Atkinson and Elgohary, 2007).

2.4.2 Vector-valued Seismic Hazard Deaggregation

In Section 2.4.1, the scalar seismic hazard deaggregation (SHD) does not consider the simultaneous exceedance of spectral accelerations at multiple vibration periods, as shown in equation (2.4.4), i.e., the representative earthquakes are extracted for spectral accelerations at individual periods separately. In this section, the scalar SHD procedure is extended to vector-valued SHD for determining the controlling earthquake that contributes seismic hazard to spectral accelerations at multiple periods simultaneously (Ni *et al.*, 2011D).

In comparison with the scalar SHD in equation (2.4.4), replacing the conditional marginal distribution of spectral acceleration at individual period in equation (2.1.24) by the conditional joint distribution of spectral accelerations at multiple periods in equation (2.1.26), the formulation of the vector-valued SHD is expressed as

$$\lambda_{s_1 \ldots s_k, x, y} = \sum_{i=1}^{N_S} \nu_i \left\{ \int_{r_{y-1}}^{r_y} \int_{m_{x-1}}^{m_x} \mathcal{P}\left\{ S_a(T_1) > s_1, \ldots, S_a(T_k) > s_k \,\middle|\, m, r \right\} f_M(m) f_R(r) \mathrm{d}m \, \mathrm{d}r \right\}_i . \tag{2.4.7}$$

It is noted that, in equation (2.4.7), the variable ε is not disaggregated when compared to equation (2.4.4).

The quotient of annual probability of exceedance $\lambda_{s_1 \ldots s_k, x, y}$ for various pairs of m and r divided by the total seismic hazard $\lambda_{s_1 \ldots s_k}$ obtained from equation (2.3.17) gives a 3-dimensional histogram of the relative seismic hazard contributed by different m-r pairs.

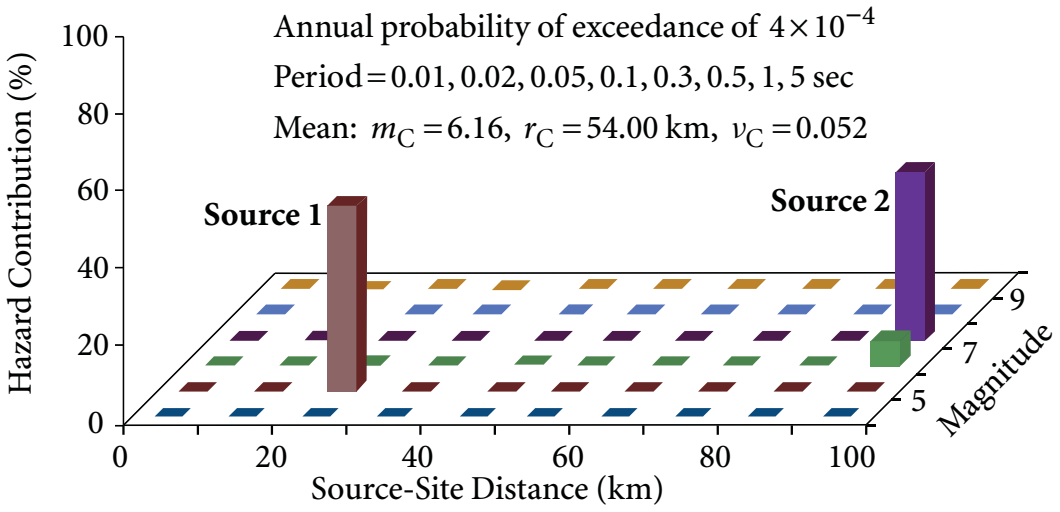

Figure 2.14 Vector-valued seismic hazard deaggregation for spectral accelerations at multiple vibration periods

Since the multivariate distribution of spectral accelerations is used in equation (2.4.7), the simultaneous exceedance of spectral accelerations at multiple periods is then considered in the vector-valued SHD, which corresponds to the vector-valued PSHA in equation (2.3.17). Each bar in the histogram in Figure 2.14 (for the same hazard configuration and parameters used in Section 2.4.1), for example, represents the relative seismic hazard contribution to the spectral accelerations $s_1, s_2, \ldots, s_k$ simultaneously, provided by the corresponding m-r pair.

Having obtained the distribution of the relative seismic hazard contributions, the weighted average values of magnitude and distance, which contribute the dominant seismic hazard to the spectral accelerations $s_1, s_2, \ldots, s_k$ simultaneously, is given by

$$m_C = \sum_{x=1}^{x_N} \sum_{y=1}^{y_N} \frac{(m_{x-1} + m_x)}{2} \frac{\lambda_{s_1 \ldots s_k, x, y}}{\lambda_{s_1 \ldots s_k}}, \tag{2.4.8a}$$

$$r_C = \sum_{x=1}^{x_N} \sum_{y=1}^{y_N} \frac{(r_{y-1} + r_y)}{2} \frac{\lambda_{s_1 \ldots s_k, x, y}}{\lambda_{s_1 \ldots s_k}}. \tag{2.4.8b}$$

Similarly, the weighted average value of the rate of occurrence for the resulting earthquake (m_C and r_C) can be obtained

$$\nu_C = \sum_{i=1}^{N_S} \nu_i \frac{\lambda_{s_1 \ldots s_k}^{(i)}}{\lambda_{s_1 \ldots s_k}}. \tag{2.4.9}$$

2.5 Treatment of Epistemic Uncertainty

In previous discussions, all the uncertainties in the location of earthquakes, the size of earthquakes, the rate of occurrence of earthquakes, and the variation of ground-motion characteristics with earthquake size and location are characterized by the corresponding probability distribution models. However, the determination of these distribution models may vary with the knowledge of professionals. This variation due to the professional knowledge is known as the epistemic uncertainty, while the intrinsic variation described by certain distribution model is known as the aleatory uncertainty. It is noted that the term "uncertainty" stands for the aleatory uncertainty in this study.

To properly characterize the epistemic uncertainty, the logic tree approach is often performed in the seismic hazard analysis (Kramer, 1996, McGuire, 2004). It allows the use of alternative models, each of which is assigned a weight factor that is interpreted as the relative likelihood of the model being correct. A logic tree consists of a series of nodes, representing points at which models are specified, and branches, representing the different models specified at each node. The sum of the probabilities of all branches connected to a given node (i.e., all the branches on the right-hand side of the given node) is 1.

A simple logic tree, considering the epistemic uncertainty in selection of models for GMPE, probability distribution of earthquake magnitude, and maximum magnitude, is illustrated in Figure 2.15. In this logic tree, two GMPEs, according to Abrahamson and Silva (1997) and Atkinson and Boore (2006), are considered equally likely to be correct; each GMPE is therefore assigned a relative likelihood of 0.5. Proceeding to the next level of nodes, the Gutenberg-Richter model is considered to be more likely to be correct than the characteristic earthquake model. At the final level of nodes, different values of relative likelihood are assigned to the maximum magnitude.

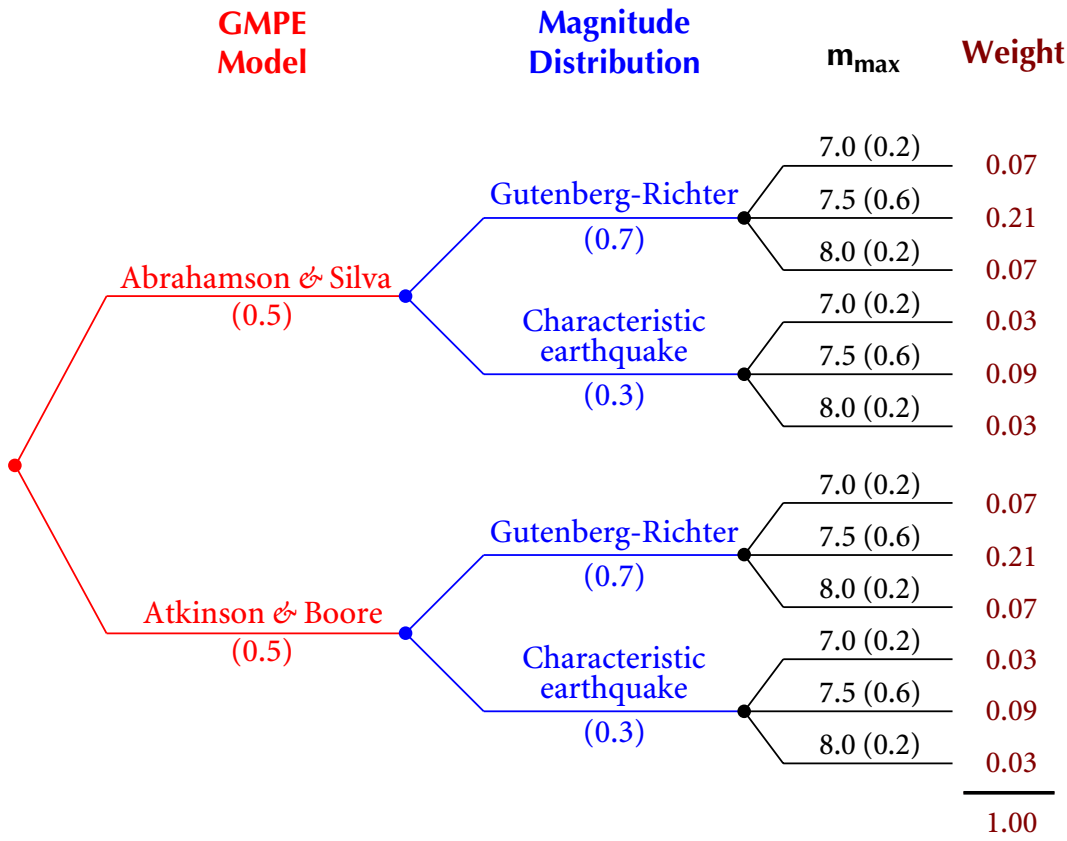

Figure 2.15 Logic tree for characterizing epistemic uncertainty of seismic hazard models

As can be seen in Figure 2.15, the logic tree terminates with a total of $2 \times 2 \times 3 = 12$ (number of GMPE models $\times$ number of magnitude distribution models $\times$ number of maximum magnitudes) branches. The relative likelihood of the combination of models and parameters implied by each terminal branch is given by the product of the relative likelihood of the terminal branch and all prior branches leading to it. For example, the relative likelihood of the combination of Abrahamson and Silva (1997) model, Gutenberg-Richter model, and maximum magnitude of 7.0 is $0.5 \times 0.7 \times 0.2 = 0.07$. The sum of the relative likelihoods of the terminal branches is equal to 1.

To use the logic tree, a PSHA or SHD is performed for the combination of models and/or parameters associated with each terminal branch. The resulting quantity (for example, annual probability of exceedance for a given spectral acceleration, spectral acceleration

from the PSHA, and representative earthquake in terms of m, r, ε, and ν from the SHD) is weighted by the relative likelihood of this terminal branch. The resulting quantities associated with their corresponding weight factors (relative likelihoods of the terminal branches) give the probability mass function (PMF) of the quantity. The mean, median, or any percentile value of the quantity can then be obtained using the PMF.

For the procedure of the determination of the beta earthquake discussed in Section 2.4.1, when different models (e.g., GMPEs, magnitude distributions, or maximum magnitudes) are considered to account for the epistemic uncertainties, the mean values of the beta earthquakes from all the combinations of the models, in terms of m_β, r_β, and ε_β, are obtained first using the logic tree approach presented above. The resulting beta earthquake is substituted into each GMPE. The ε_β is then adjusted so that the weighted average values of spectral accelerations using the GMPEs satisfy the target matching criteria as presented in Section 2.4.1 (McGuire, 1995).

2.6 Summary

In this chapter, the basics of engineering seismology, including ground-motion prediction equation (GMPE), correlation of spectral accelerations, probability distribution of spectral accelerations, and probability distributions of earthquake location and size, are introduced. The deterministic seismic hazard analysis (DSHA), and the scalar and vector-valued probabilistic seismic hazard analyses (PSHA) and their corresponding seismic hazard deaggregation (SHD) are presented with examples. The treatment of epistemic uncertainty of the PSHA and SHD is also discussed.

Based on the PSHA and SHD presented in this chapter, various seismic design spectra are discussed in Chapter 3.

CHAPTER 3

Seismic Design Spectra

Probabilistic seismic hazard analysis (PSHA), discussed in Chapter 2, has been widely used for the establishment of seismic design spectra, including uniform hazard spectrum (UHS) (ASCE, 2005, NBCC, 2010), predicted spectrum based on ground-motion prediction equations (GMPEs) (McGuire, 1995), and conditional mean spectrum considering ε (CMS-ε) (Baker and Cornell, 2006c). These seismic design spectra can be used as input design earthquakes in seismic response spectral analysis (SRSA) (see Appendix A.2.3) or target spectra for the selection or generation of earthquake ground motions.

The primary advantage of the PSHA is that it provides a framework in which uncertainties in the location of earthquakes, the size of earthquakes, the rate of occurrence of earthquakes, and the variation of ground-motion characteristics with earthquake size and location can be identified, quantified, and combined in a mathematically rigorous manner to describe the seismic hazard at a given site.

However, the existing PSHA-based seismic design spectra (UHS, predicted spectra, and CMS-ε) fail to represent single design earthquakes or provide complete probabilistic knowledge on the simultaneous occurrence of spectral accelerations at multiple vibration periods, which is a crucial requirement in the application of modal superposition methods in structural dynamics, and reliability- and performance-based seismic design (Ni *et al.*, 2011d).

To overcome the deficiencies of the existing PSHA-based seismic design spectra, a generalized approach (Ni *et al.*, 2012) is developed to generate seismic design spectra using both

scalar and vector-valued PSHA. The resulting spectral shapes can be made narrower and to concentrate at a specified vibration period or a range of vibration periods based on the information of structural modes or the specific requirements of engineering projects. The seismic hazard level, i.e., annual probability of exceeding spectral accelerations simultaneously at multiple periods of engineering interest, of each design spectrum is provided by the vector-valued PSHA. Each spectrum can then be interpreted as a single "design earthquake" via the joint probability. Through the PSHA, the resulting design spectra not only reflect the seismic hazard environment surrounding a given site but also take the dynamic characteristics of structures into consideration.

To simplify the approach for the generation of seismic design spectra so that they can be easily incorporated into structural design and performance-based seismic design, an approximate approach is also developed using seismic hazard deaggregation (SHD). Based on several numerical studies, it is concluded that the selection of controlling vibration periods does not significantly affect the resulting seismic design spectra and the results of the SHD, as long as the selected periods cover the entire range of vibration period of engineering interest roughly uniformly.

In Section 3.1, the properties and limitations of the existing PSHA-based seismic design spectra are discussed. In Section 3.2, a generalized approach and its approximation are developed to establish site- and structure-specific seismic design spectra based on both scalar and vector-valued PSHA. The proposed approach is then demonstrated by numerical examples. Some conclusions are summarized in Section 3.3.

3.1 Existing Seismic Design Spectra Based on PSHA

A number of seismic design spectra have been developed based on the PSHA. They mainly include uniform hazard spectrum (UHS), predicted spectrum based on GMPEs, and conditional mean spectrum considering ε (CMS-ε). In this section, the properties and limitations of these existing PSHA-based seismic design spectra are presented and discussed.

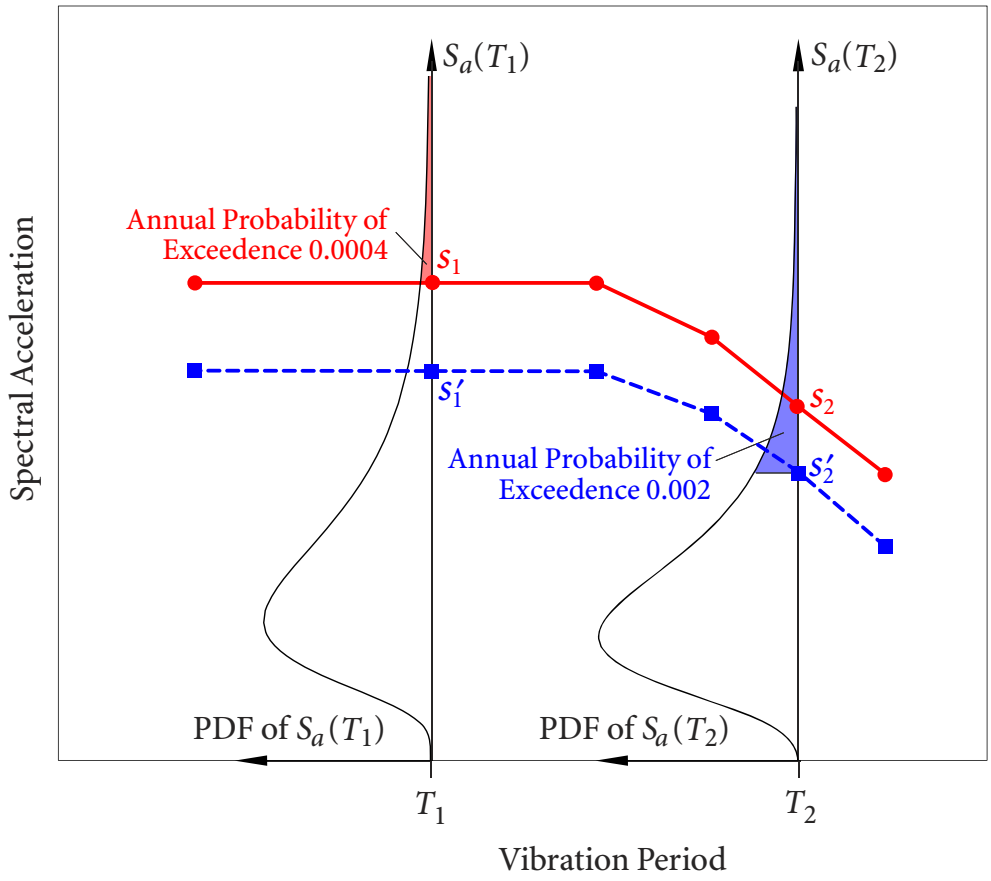

Figure 3.1 Concept of uniform hazard spectrum

3.1.1 Uniform Hazard Spectrum

As discussed in Section 2.3.3, based on the scalar PSHA in equation (2.3.13), for a given probability p_{M} (the subscript "M" standing for Marginal) of spectral acceleration $S_a(T_j)$ exceeding s_j, a plot of the threshold s_j for a number of vibration periods T_j of engineering interest ($j=1,2,\ldots,k$) at a site gives a uniform hazard spectrum (UHS). The concept of the UHS is schematically illustrated in Figure 3.1. It is called "uniform hazard" spectrum because the probability of exceedance p_{M} of spectral acceleration at each period is consistent.

The probability of exceedance p_{M} for an individual spectral acceleration, however, is not the probability of exceedance for a design earthquake (i.e., the entire design spectrum

with spectral accelerations at multiple periods) which is commonly used in reliability- and performance-based seismic design. In other words, a UHS does not provide any probabilistic knowledge about the simultaneous exceedance of spectral accelerations at multiple periods.

Furthermore, for the same probability level p_{M}, the controlling earthquakes in terms of magnitude and source-site distance extracted from a UHS at different vibration periods through scalar seismic hazard deaggregation (SHD) are often different (Halchuk and Adams, 2004). As a result, a UHS cannot be treated as a single design earthquake.

The seismic response spectral analysis (SRSA) of structures is based on seismic design spectra and modal superposition methods (Chopra, 2001). When a modal superposition method is applied to predict the peak response of a structure, the peak responses of the vibration modes of the structure are assumed to occur at the same time subjected to the same ground excitation. Since the spectral accelerations at different vibration periods on a UHS are generally induced by different earthquakes, it is inappropriate to obtain the peak first mode response from one earthquake, the peak second mode response from a different earthquake, and the peak third mode response from yet another earthquake, on the UHS (Ni *et al.*, 2011D).

3.1.2 Predicted Spectrum Based on GMPEs

In equation (2.3.13), the annual probability of exceedance λ_{s_j} is obtained by integrating over all possible occurrences of earthquakes surrounding a given site. To obtain an individual design earthquake based on scalar PSHA, λ_{s_j} can be disaggregated at predefined probability level p_{M}, and the most-likely combination (modal values) of magnitude m_β, source-site distance r_β, and ε_β, called "beta earthquake", can then be obtained, as discussed in Section 2.4.1.

If one seismic source is the dominant contributor for spectral accelerations at both 0.1 and 1 sec, one beta earthquake is used to represent the seismic hazard over the entire period range. If different seismic sources are the dominant contributors at 0.1 and 1 sec, two beta earthquakes are used to represent the hazards over the short period range and the long period range, respectively. In general, one small near-field earthquake and one large far-

field earthquake are regarded as sufficient to represent the short period range and the long period range of a UHS, respectively (McGuire, 1995, Atkinson and Beresnev, 1998).

Having obtained one beta earthquake (in terms of m_β, r_β, and ε_β) for the case of one dominant source, by substituting the beta earthquake into the GMPEs in equation (2.1.1) for spectral accelerations at different periods individually, the resulting design earthquake (in terms of seismic design spectrum), which closely matches the UHS over the entire period range, can be constructed.

For the case of different dominant sources, by substituting two resulting beta earthquakes into equations (2.1.1), respectively, two seismic design spectra, which closely match the short period range and the long period range of the UHS, respectively, can be generated. In this case, the resulting design spectrum is relatively narrow-band centered at the specified period in comparison with the UHS.

It is noted that if more than one GMPE is used, predefined weight should be assigned to each GMPE to obtain the weighted average design spectra.

A predicted design spectrum based on GMPEs can be interpreted as a single design earthquake in terms of the m_β-r_β pair. However, the primary advantage of the PSHA of integrating all possible earthquake occurrences surrounding the site of interest is not completely reflected in the predicted spectra, because the seismic hazard of the site is simply represented by the beta earthquakes. Since each point on a predicted spectrum is obtained independently through the beta earthquake and the prediction equation, the probabilistic knowledge about the simultaneous occurrence of these points on a spectrum is not provided.

3.1.3 Conditional Mean Spectrum Considering Epsilon

Similar to the predicted design spectra, to account for the relationship between spectral acceleration $S_a(T_1)$ at fundamental period T_1 and spectral accelerations $S_a(T_j)$ at other periods T_j ($j = 2, 3, \ldots, k$), Baker and Cornell (2006b) proposed the concept of conditional mean spectrum considering ε (CMS-ε) based on the assumption that spectral accelerations at two different periods are jointly lognormally distributed for a given scenario earthquake, which was verified later by Jayaram and Baker (2008).

Assume that the variance in conditional spectral accelerations $\ln S_a(T_j)$ is primarily due to ε rather than variations in magnitude and distance (Baker and Cornell, 2005). For a specified annual probability of exceedance p_M, the logarithmic mean and standard deviation of the CMS-ε conditional on the occurrence of $S_a(T_1)=s_1$ can be approximated by

$$\mu_{\ln S_a(T_j)\,|\,S_a(T_1)=s_1,\bar{m},\bar{r}} = \mu_{\ln S_a(T_j)\,|\,\bar{m},\bar{r}} + \rho_{\ln S_a(T_1),\,\ln S_a(T_j)}\,\bar{\varepsilon}_{S_a(T_1)}\,\sigma_{\ln S_a(T_j)\,|\,\bar{m}}, \tag{3.1.1a}$$

$$\sigma_{\ln S_a(T_j)\,|\,S_a(T_1)=s_1,\bar{m}} = \sigma_{\ln S_a(T_j)\,|\,\bar{m}}\sqrt{1-\rho^2_{\ln S_a(T_1),\,\ln S_a(T_j)}}, \tag{3.1.1b}$$

where s_1 is the spectral acceleration on a UHS at the structural fundamental period T_1 obtained using equation (2.3.13). $\bar{m}$, $\bar{r}$, and $\bar{\varepsilon}_{S_a(T_1)}$ are the mean values of the results of the scalar seismic hazard deaggregation (SHD) towards the occurrence of $S_a(T_1)=s_1$ (not $>s_1$), as presented in Section 2.4.1. The mean $\mu_{\ln S_a(T_j)\,|\,\bar{m},\bar{r}}$ and standard deviation $\sigma_{\ln S_a(T_j)\,|\,\bar{m}}$ of $\ln S_a(T_j)$ can be determined using GMPEs in equation (2.1.1), and $\rho_{\ln S_a(T_1),\,\ln S_a(T_j)}$ is the correlation coefficient between $\ln S_a(T_1)$ and $\ln S_a(T_j)$, as discussed in Section 2.1.2. Since the scenario earthquake is obtained from the spectral acceleration at the fundamental period, the CMS-ε is centered at this period with narrow-band spectral shape when compared to the corresponding UHS.

Based on the assumption of joint lognormal distribution, the probabilistic meaning of equation (3.1.1a) is that, given the occurrence of the causal earthquake in terms of $\bar{m}$, $\bar{r}$, and $\bar{\varepsilon}_{S_a(T_1)}$, and the spectral acceleration $S_a(T_1)=s_1$ at the fundamental period T_1, the annual probability of logarithmic spectral acceleration $\ln S_a(T_j)$ at vibration period T_j exceeding $\ln s_j = \mu_{\ln S_a(T_j)\,|\,S_a(T_1)=s_1,\bar{m},\bar{r}}$ is 50%. The vector $\{s_1, s_2, \ldots, s_k\}^T$ gives the CMS-ε for the specified marginal probability of exceedance p_M at fundamental period T_1. For the conditional probability of exceedance other than 50%, the randomness of $S_a(T_j)$ conditional on $S_a(T_1)=s_1$ can be characterized by the logarithmic standard deviation in equation (3.1.1b).

When $S_a(T_j)$ is the spectral acceleration at the fundamental period T_j ($j=1$), the correlation coefficient $\rho_{\ln S_a(T_1),\,\ln S_a(T_j)}$ is one and equation (3.1.1a) then reduces to the GMPE in equation (2.1.1). For spectral acceleration $S_a(T_j)$ at period T_j ($j\neq 1$), the difference between equations (3.1.1a) and (2.1.1) is characterized by $\rho_{\ln S_a(T_1),\,\ln S_a(T_j)}\,\bar{\varepsilon}_{S_a(T_1)}$ in equation

(3.1.1a), instead of $\varepsilon(T_j)$ in equation (2.1.1). $\rho_{\ln S_a(T_1),\,\ln S_a(T_j)}\,\bar{\varepsilon}_{S_a(T_1)}$ denotes the mean value of $\varepsilon(T_j)$ conditional on $\bar{\varepsilon}_{S_a(T_1)}$. With the decrease of the linear correlation between $\ln S_a(T_1)$ and $\ln S_a(T_j)$ in terms of the correlation coefficient, the deviation (second) term on the right-hand side of equation (3.1.1a) reduces. As a result, the hazard level of spectral acceleration $S_a(T_j)$ on a CMS-ε, controlled by the deviation term in equation (3.1.1a), depends on the statistical correlation between spectral accelerations at the fundamental period T_1 and period T_j.

For a CMS-ε, the marginal probability of exceedance p_M of spectral acceleration $S_a(T_1)$ at fundamental period T_1 is predefined, and the threshold value s_1 of this spectral acceleration and the causal earthquake in terms of $\bar{m}$, $\bar{r}$, and $\bar{\varepsilon}_{S_a(T_1)}$ can then be determined. Given $S_a(T_1)=s_1$ and the causal earthquake, the conditional probability of exceedance of any other spectral acceleration $S_a(T_j)$ ($j\neq 1$) on a CMS-ε is 50%. However, the probability of exceeding all the spectral accelerations on a CMS-ε simultaneously, based on the complete information available from the PSHA, remains unknown.

3.2 Generalized Approach for Generating Design Spectra

In Section 3.1, the primary properties and limitations of the existing PSHA-based seismic design spectra are discussed. These design spectra (UHS, predicted spectra, and CMS-ε) are unable to represent single design earthquakes or unable to provide the probability of simultaneous exceedance of spectral accelerations at vibration periods throughout the range of vibration period of engineering concern.

To not only overcome the deficiencies of these existing seismic design spectra but also preserve some advantages of these spectra, a generalized approach for the generation of seismic design spectra is developed based on both the scalar and vector-valued PSHA (Ni *et al.*, 2012).

The generalized approach to the generation of seismic design spectra based on PSHA is formulated using the following system of $k+1$ nonlinear equations:

- joint annual probability of exceedance from vector-valued PSHA governed by equation (2.3.17):

$$\begin{aligned}&\mathcal{P}\left\{S_a(T_1)>s_1,\ldots,S_a(T_k)>s_k\right\}\\&=\sum_{i=1}^{N_S}\nu_i\Big\{\int_r\int_m\mathcal{P}\left\{S_a(T_1)>s_1,\ldots,S_a(T_k)>s_k\,\middle|\,m,r\right\}f_M(m)f_R(r)\mathrm{d}m\,\mathrm{d}r\Big\}_i=p_{\mathrm{J}},\end{aligned}\quad(3.2.1a)$$

❧ marginal annual probability of exceedance from scalar PSHA governed by equation (2.3.13):

$$\mathcal{P}\left\{S_a(T_j)>s_j\right\}=\sum_{i=1}^{N_S}\nu_i\Big\{\int_r\int_m\mathcal{P}\left\{S_a(T_j)>s_j\,\middle|\,m,r\right\}f_M(m)f_R(r)\mathrm{d}m\,\mathrm{d}r\Big\}_i=\eta_j p_{\mathrm{M}},$$

$$j=\zeta,\zeta+1,\ldots,\xi-1,\xi,\quad 1\leqslant\zeta\leqslant\xi\leqslant k,\quad(3.2.1b)$$

❧ conditional probability of exceedance from scalar and vector-valued PSHA:

$$\begin{aligned}&\mathcal{P}\left\{S_a(T_j)>s_j\,\middle|\,S_a(T_\zeta)>s_\zeta,\ldots,S_a(T_\xi)>s_\xi\right\}\\&=\frac{\displaystyle\sum_{i=1}^{N_S}\nu_i\Big\{\int_r\int_m\mathcal{P}\left\{S_a(T_j)>s_j,S_a(T_\zeta)>s_\zeta,\ldots,S_a(T_\xi)>s_\xi\,\middle|\,m,r\right\}f_M(m)f_R(r)\mathrm{d}m\,\mathrm{d}r\Big\}_i}{\displaystyle\sum_{i=1}^{N_S}\nu_i\Big\{\int_r\int_m\mathcal{P}\left\{S_a(T_\zeta)>s_\zeta,\ldots,S_a(T_\xi)>s_\xi\,\middle|\,m,r\right\}f_M(m)f_R(r)\mathrm{d}m\,\mathrm{d}r\Big\}_i}\\&=p_{\mathrm{C}},\quad j=1,2,\ldots,\zeta-1,\xi+1,\ldots,k,\end{aligned}\quad(3.2.1c)$$

where p_{J}, p_{M}, and p_{C} are joint annual probability of exceedance, marginal annual probability of exceedance, and conditional probability of exceedance, respectively, and the subscripts "J", "M", and "C" stand for Joint, Marginal, and Conditional, respectively. In equations (3.2.1), k is the number of controlling periods defining spectral accelerations for the construction of design spectra, η_j is the seismic hazard weighting parameter, and parameters ζ and ξ are serial numbers of spectral accelerations.

In engineering practice, two characteristics of a seismic design spectrum are of primary importance: spectral shape, which characterizes frequency content, and amplitude, which is governed by seismic hazard (design) level. Traditionally, a conventional seismic design spectrum is the product of a standard design spectral shape and peak ground-motion parameter such as peak ground acceleration (PGA) for a given probability of exceedance. The standard spectral shape is obtained based on statistical analysis of normalized response

spectra from a large number of recorded ground motions, and the PGA is determined using scalar PSHA (Newmark *et al.*, 1973).

For the UHS, however, both spectral shape and amplitude are determined according to the marginal probability of exceedance p_M, as discussed in Section 3.1.1. In the proposed generalized approach, the spectral shape is determined via the marginal probability level governed by equation (3.2.1b), or the conditional probability level governed by equation (3.2.1c), or both. The amplitude of the design spectrum is controlled by the joint probability level governed by equation (3.2.1a).

As discussed previously, quantifying the probability of simultaneous exceedance of spectral accelerations at multiple vibration periods over the entire period range of engineering interest on a seismic design spectrum is crucial in the application of modal combination methods in structural dynamics, and reliability- and performance-based seismic design. The vector-valued PSHA governed by equation (3.2.1a) is used to achieve this vital requirement. Since the vector-valued PSHA provides the probability of exceeding all spectral accelerations on a design spectrum simultaneously, this joint annual probability of exceedance p_J is regarded as the probabilistic seismic hazard level for a design earthquake (design spectrum) as commonly used in reliability- and performance-based seismic design. The generated design spectrum can then be interpreted as a single design earthquake. Hence, when a design spectrum is generated using the proposed approach, p_J will be prespecified, such as 4×10^{-4} per annum (2% per 50 years), by decision-makers or design professionals.

The probability of exceeding spectral accelerations at all periods simultaneously needs to be calculated using the vector-valued PSHA governed by equation (3.2.1a) to provide quantitatively the seismic hazard level to the resulting design spectrum. In engineering practice, however, it may not be feasible to conduct a vector-valued PSHA with a very high dimension, say spectral accelerations at 200 vibration periods, i.e., $k = 200$ in equation (3.2.1a).

In this study, a set of eight ($k = 8$) critical controlling vibration periods of 0.01, 0.02, 0.05, 0.1, 0.3, 0.5, 1, and 5 sec is used by considering the past and present engineering practice for nuclear energy facilities (Newmark *et al.*, 1973, Atkinson and Elgohary, 2007). The

use of these controlling periods is based on the observation that considering additional intermediate periods between these controlling periods does not affect the resulting design spectra significantly, as will be discussed with numerical examples in Section 3.2.5.

In Sections 3.2.1-3.2.3, three types of seismic design spectra, named Vector-valued Uniform Hazard Spectra (VUHS), Vector-valued Non-Uniform Hazard Spectra (VNUHS), and Vector-valued Conditional Uniform Hazard Spectra (VCUHS), will be presented. They are generated by assigning specific values to parameters $p_{\mathrm{J}}, p_{\mathrm{C}}, \eta_j, \zeta$, and ξ in equations (3.2.1) and solving the system of equations (3.2.1) for unknowns $p_{\mathrm{M}}, s_1, s_2, \ldots, s_k$ using a suitable numerical method, such as the bisection method (Press *et al.*, 2007). $\mathbf{s} = \{s_1, s_2, \ldots, s_k\}^{\mathrm{T}}$ represents the spectral accelerations at the controlling periods on a resulting design spectrum corresponding to the target joint annual probability of exceedance p_{J}. The VUHS, VNUHS, or VCUHS can then be constructed by linearly connecting the spectral acceleration coordinates $\mathbf{s}$ at controlling periods in a linear-linear plot or a log-log plot (Humar and Rahgozar, 2000, Atkinson and Elgohary, 2007).

3.2.1 Vector-valued Uniform Hazard Spectrum

Detailed studies of spectral shapes of UHS at a number of sites throughout the United States have been conducted by computing the spectral accelerations at 12 periods ranging from 0.1 to 4.0 sec. It is concluded that, as the site-specific design spectra, UHS have shown distinctive and appropriate spectral shapes for different geographic areas, such as western and eastern North America regions (Algermissen and Letendecker, 1992). The spectral shape of UHS for eastern North America region has also been verified to properly reflect the characteristics of local seismic hazard environment (Atkinson and Elgohary, 2007).

On the other hand, as discussed in Sections 3.1.2 and 3.1.3, the predicted spectra and the CMS-ε possess relatively narrow-band spectral shapes. The narrow-band spectral shapes are suitable for structures, whose responses are mainly contributed by their first modes. In comparison with the predicted spectra and the CMS-ε, the relatively wide-band spectral shape of the UHS may be a more suitable design earthquake for structural responses with significant contributions from higher modes.

To not only preserve the essence (PSHA-based approach and spectral shape) of a uniform hazard spectrum (UHS) but also provide the probability of simultaneous exceedance of spectral accelerations on a design spectrum and be regarded as a single design earthquake, a *vector-valued uniform hazard spectrum* (VUHS) is developed (Ni *et al.*, 2011D).

In the generalized approach, when $\zeta = 1$ and $\xi = k$, equations (3.2.1) reduce to (3.2.1a) and (3.2.1b). By assigning 1 to η_j, equations (3.2.1a) and (3.2.1b) can be expressed as

$$\bar{P}\left\{S_a(T_1) > s_1, \ldots, S_a(T_k) > s_k\right\} = p_{\mathrm{J}}, \tag{3.2.2a}$$

$$\bar{P}\left\{S_a(T_j) > s_j\right\} = p_{\mathrm{M}}, \quad j = 1, 2, \ldots, k. \tag{3.2.2b}$$

The VUHS can then be generated by solving the system of equations (3.2.2). In equations (3.2.2), the joint probability of simultaneous exceedance p_{J} is provided, and the consistent marginal probability of exceedance p_{M}, i.e., the uniform hazard, preserves the spectral shape of a UHS.

It is noted that for a resulting VUHS, the corresponding joint annual probability of exceedance p_{J} is much smaller than the marginal probability of exceedance p_{M}, as will be seen in the numerical examples. A similar observation has also been made and explained by Baker and Cornell (2006A). Hence, the existing conventional UHS may be more conservative than intended due to the misuse of the marginal probability of exceedance as the joint probability of exceedance.

3.2.2 Vector-valued Non-Uniform Hazard Spectrum

In Section 3.2.1, the VUHS is generated by assigning consistent seismic hazard level for spectral accelerations at all controlling periods, i.e., the same p_{M} for all values of j in equation (3.2.2b). A relatively wide-band spectral shape is then obtained on a VUHS, since the seismic hazard from spectral acceleration at each individual controlling period is regarded equally important to the response of a structure. Hence, the VUHS may be a suitable design earthquake for structures having a wide range of structural modal periods, which contribute significantly to structural responses.

In engineering practice, structures with first-mode dominant or with the first a few closely-spaced modes dominant are not unusual. In equations (3.2.1), at the same joint

probability level p_J, a seismic design spectrum having a relatively narrow-band spectral shape, which is concentrated at a pre-specified period or a small range of periods, may be a more suitable design earthquake for these structures when compared to the wide-band VUHS.

To obtain a relatively narrow-band structure-specific seismic design spectrum based on PSHA, take $\zeta = 1$ and $\xi = k$, equations (3.2.1) can be expressed as

$$\bar{P}\left\{S_a(T_1) > s_1, \ldots, S_a(T_k) > s_k\right\} = p_J, \tag{3.2.3a}$$

$$\bar{P}\left\{S_a(T_j) > s_j\right\} = \eta_j p_M, \quad j = 1, 2, \ldots, k, \tag{3.2.3b}$$

where the seismic hazard weighting parameters η_j $(0 < \eta_j < 1)$ are used to reduce the marginal probabilities of exceedance and thus increase the spectral accelerations at these selected periods, which have significant contributions to structural responses. $\eta_j = 1$ is then taken for the rest of controlling periods.

In equation (3.2.3b), the parameters η_j are used to characterize the ratio of marginal probability levels of spectral accelerations at primary important periods and at secondary important periods. Seismic hazard design levels used in current engineering practice, i.e., annual probabilities of exceedance for spectral accelerations at individual periods, could be used to determine the values of η_j for spectral accelerations at selected dominant periods, as discussed below.

The selection of seismic hazard design level, which may also be called earthquake design level in SEAOC Report (SEAOC, 1995) or Seismic Design Category (SDC) in ASCE/SEI Standard 43-05 (ASCE, 2005), depends on mainly the importance level of the structure. For example, the seismic hazard design level of a rare earthquake is usually specified as 2×10^{-3} per annum (10% in 50 years) for ordinary civil structures, and the seismic hazard design level of an extremely rare earthquake (or maximum considered earthquake) is often set as 4×10^{-4} per annum (2% in 50 years) for critical structures (SEAOC, 1995, Ghobarah, 2001, ASCE, 2005). The ratio of 0.2 between these two seismic hazard design levels could be used to represent the difference between important and ordinary structures in terms of seismic design level (annual probability of exceedance for individual spectral acceleration).

In this study, the concept of the ratio of marginal probabilities of exceedance for distinguishing the importance levels of structures is extended to describe the relative importance levels of structural modes, i.e., the contributions to structural response from the structural modes. As a result, the seismic hazard weighting parameter η_j can be taken as the ratio of the selected seismic hazard design levels.

In equations (3.2.3), to maintain the same joint probability level p_J, with small values of parameters η_j assigned to selected dominant periods, the resulting spectral shape becomes narrower and more concentrated, with increased spectral amplitudes, at these dominant periods. However, if the dominant modal periods of a structure are generally determinate, i.e., little nonlinearity occurs or the level of nonlinearity is well estimated when subjected to an earthquake excitation, so that the spectral accelerations at the non-dominant periods have little effect on the structural response, very small values of η_j would introduce unnecessary conservatism to the design. Hence, the selection of seismic hazard design levels for determining η_j relies on engineering judgement and the frequency bandwidths of response spectra of local recorded ground motions.

However, regardless of the resulting spectral shape or the effect of spectral accelerations at non-dominant periods on structural responses, the spectral accelerations on a spectrum over the entire period range certainly occur at the same time when an earthquake occurs. Fortunately, the probability of this simultaneous occurrence can be quantified through the vector-valued PSHA governed by equation (3.2.3a). A single design earthquake associated with its seismic hazard level can then be provided.

Since the vector-valued PSHA governed by equation (3.2.3a) provides the seismic hazard level of a single design earthquake (the entire spectrum) and the scalar PSHA in equation (3.2.3b) produces a narrow-band spectral shape with inconsistent marginal probability levels through η_j, the name of *Vector-valued Non-Uniform Hazard Spectrum* (VNUHS) for the resulting spectrum is adopted.

3.2.3 Vector-valued Conditional Uniform Hazard Spectrum

In Section 3.2.2, a vector-valued non-uniform hazard spectrum (VNUHS) is generated based on the PSHA. A narrow-band spectral shape of the VNUHS is achieved by ma-

nipulating the marginal probabilities of exceedance for spectral accelerations at dominant periods individually, through the seismic hazard weighting parameters η_j. To not only obtain a relatively narrow-band spectral shape concentrated at selected dominant periods but also consider the spectral correlation between the dominant periods and non-dominant periods, an alternative seismic design spectrum, *Vector-valued Conditional Uniform Hazard Spectrum* (VCUHS) can be generated by specifying the parameters in equations (3.2.1) as follows.

Under the conditions that $\zeta = 1$ and $\xi = k$ are not satisfied simultaneously in equation (3.2.3b), the system of equations (3.2.3) for generating the VCUHS can be expressed as

$$\mathcal{P}\left\{S_a(T_1) > s_1, \ldots, S_a(T_k) > s_k\right\} = p_{\mathrm{J}}, \tag{3.2.4a}$$

$$\mathcal{P}\left\{S_a(T_j) > s_j\right\} = \eta_j p_{\mathrm{M}}, \quad j = \zeta, \zeta+1, \ldots, \xi-1, \xi, \quad 1 \leqslant \zeta \leqslant \xi \leqslant k, \tag{3.2.4b}$$

$$\mathcal{P}\left\{S_a(T_j) > s_j \,\middle|\, S_a(T_\zeta) > s_\zeta, \ldots, S_a(T_\xi) > s_\xi\right\} = p_{\mathrm{C}}, \quad j = 1, 2, \ldots, \zeta-1, \xi+1, \ldots, k. \tag{3.2.4c}$$

The joint probability of exceedance p_{J} is still maintained by equation (3.2.4a) to provide the seismic hazard level of a single design earthquake, while equations (3.2.4b) and (3.2.4c) control the spectral shape of the VCUHS. The properties of VCUHS are discussed using the following example.

As mentioned previously, by taking eight critical controlling periods ($k = 8$) in equations (3.2.4), the VCUHS can be satisfactorily represented by spectral accelerations at these eight periods. Suppose the dominant modal periods of a structure, which have dominant contributions to the structural response, are T_3 and T_4 (i.e., $\zeta = 3$ and $\xi = 4$), equation (3.2.4b) is used to characterize and emphasize the spectral accelerations at these two dominant periods; a value of 1 could be assigned to η_j ($j = 3, 4$) if these two dominant periods are regarded equally important.

While equation (3.2.4b) is used for spectral accelerations at dominant periods, spectral accelerations on a VCUHS at non-dominant periods are considered through equation (3.2.4c). The physical meaning of equation (3.2.4c) in this example is that, under the condition of the simultaneous exceedance of spectral accelerations at two dominant periods (i.e., $S_a(T_3) > s_3$ and $S_a(T_4) > s_4$), the probability that the spectral acceleration $S_a(T_j)$ at

any non-dominant period T_j (i.e., $j = 1, 2, 5, 6, 7, 8$) exceeds a threshold value s_j is p_C. The conditional probability of exceedance p_C can be taken as 50%, which means that the median values of spectral accelerations at non-dominant periods, conditional on the occurrence of the spectral accelerations at dominant periods ($S_a(T_3) > s_3$ and $S_a(T_4) > s_4$), are adopted for the VCUHS.

The conditional probability governed by equation (3.2.4c) accounts for the fact that the correlation of spectral accelerations decreases with the increasing separation of vibration periods, which is similar to the concept of the conditional mean spectrum considering ε (CMS-ε) as discussed in Section 3.1.3. To maintain the conditional probability of exceedance p_C in equation (3.2.4c), the marginal probability of exceedance of spectral acceleration $S_a(T_j)$ at non-dominant period T_j increases (i.e., its seismic hazard decreases) with the increasing separation between the non-dominant period T_j and the dominant periods T_3 and T_4. The consideration of spectral correlation could produce a spectral shape having more frequency contents concentrated around the dominant periods T_3 and T_4 and less frequency contents away from the dominant periods, when compared to the VNUHS presented in Section 3.2.2.

As mentioned in Section 3.1.3, the CMS-ε produces the conditional mean values of spectral accelerations at periods other than the fundamental period, given the occurrence of spectral acceleration $S_a(T_1) = s_1$ (not $> s_1$) at the fundamental period. From the point of view of seismic hazard level (probability of "exceedance") in this study, since "exceedance" is used for spectral accelerations at dominant periods in equation (3.2.4b), it is preferable to characterize the spectral accelerations at non-dominant periods under the condition that the spectral accelerations at dominant periods exceed (not equal to) certain thresholds as expressed by equation (3.2.4c).

In the generation of the CMS-ε, if spectral accelerations at multiple periods need to be considered, the mean value of spectral accelerations at these periods has to be calculated and regarded as a new ground-motion intensity measure to account for a combined effect of the occurrence of spectral accelerations at multiple periods (Baker and Cornell, 2006b). In generating the VCUHS, the spectral accelerations at multiple dominant periods can be characterized and emphasized directly via equation (3.2.4b), and the spectral accelerations at

non-dominant periods can be considered under the condition of simultaneous exceedance of spectral accelerations at dominant periods through equation (3.2.4c).

3.2.4 Approximation of Generalized Approach

In Sections 3.2.1-3.2.3, a generalized approach has been developed to generate site- and structure-specific seismic design spectra, vector-valued uniform hazard spectrum (VUHS), vector-valued non-uniform hazard spectrum (VNUHS), and vector-valued conditional uniform hazard spectrum (VCUHS), by performing scalar and vector-valued PSHA simultaneously. This approach is suitable for the design of critical structures and systems, such as nuclear energy facilities, in which detailed seismic hazard analysis is required (ASCE, 2005).

Due to the complexity and the specificity of conducting PSHA, however, the exact generalized approach may be performed only by experts in seismology. It is too expensive for the designers of ordinary civil structures to conduct the extensive seismic hazard analysis required in the exact approach to generate these structure-specific design spectra.

On the other hand, in the conceptual framework of performance-based seismic design (Bertero and Bertero, 2002), the first step is to select performance design objectives. These performance objectives are selected and expressed in terms of expected levels of damage resulting from expected levels of design earthquakes. The client is supposed to make this selection in consultation with the design professionals based on the expectations of the client, the seismic hazard exposure, economic analysis, and acceptable risk. Design earthquakes (seismic design spectra), which are easy to obtain and possess continuous levels of probability of exceedance, are desirable (Ni *et al.*, 2011D). Hence, an approximate method of the generalized approach is needed.

To simplify the procedure for generating the vector-valued uniform hazard spectra (VUHS), an approximate method has been proposed by Ni *et al.* (2011D). The vector-valued seismic hazard deaggregation (SHD) is performed for generating a controlling earthquake, in terms of magnitude m_C, source-site distance r_C, and the rate of occurrence ν_C, which contributes dominant seismic hazard over all sources to spectral accelerations throughout the entire period range at the site of interest, as presented in Section 2.4.2. The random variables M and R, and ν_i for all N_S seismic sources in equations (2.3.13) and (2.3.17) are then

replaced by three deterministic variables m_C, r_C, and ν_C to avoid cumbersome integrations in the PSHA. The succuss of this approximation depends on the fact that the controlling earthquake (m_C, r_C, and ν_C) generally possesses dominant hazard contributions to spectral accelerations on the entire design spectrum, i.e., to $\lambda_{s_1 \ldots s_k}$ in equation (2.3.17).

In the approximation of the VUHS (Ni *et al.*, 2011D), the controlling earthquake (m_C, r_C, and ν_C) from vector-valued SHD is used to simplify both the vector-valued and scalar PSHA governed by equations (2.3.13) and (2.3.17). However, the dominant hazard contributors (controlling earthquakes) to the scalar PSHA should be determined from the scalar SHD, which are always not identical to the controlling earthquake derived from the vector-valued SHD when multiple seismic sources dominate the hazard at a given site. As a result, using only the controlling earthquake from vector-valued SHD for simplifying the scalar PSHA could cause extra error in the approximation of the VUHS. This could be the primary reason that the error of the approximate VUHS for the case of multiple dominant sources is larger than that for single dominant source, as observed in Ni *et al.* (2011D).

To eliminate the extra error mentioned above, the controlling earthquake in terms of m_C, r_C, and ν_C for spectral accelerations at multiple periods from vector-valued SHD (in Section 2.4.2) is used for simplifying the vector-valued PSHA, while the controlling earthquakes in terms of $m_{C,j}$, $r_{C,j}$, and $\nu_{C,j}$ for spectral accelerations $S_a(T_j)$ at individual periods T_j from the scalar SHD (in Section 2.4.1) are used for approximating the scalar PSHA (Ni *et al.*, 2012). The approximation of the generalized approach governed by equations (3.2.1) is presented in detail in the following.

As discussed in Section 2.4, the controlling earthquake (Ni *et al.*, 2011D) is obtained for mean values and spectral accelerations exceeding (not equal to) thresholds. The use of the mean values and the exceedance of spectral accelerations for approximating equations (3.2.1) is due to the fact that (1) the mean values are globally evaluated for all the seismic sources around the site, and (2) all the probability distributions in equations (3.2.1) are for the exceedance of spectral accelerations.

To perform seismic hazard deaggregation (SHD) for determining controlling earthquakes, the probability levels need to be specified first and the corresponding threshold values of spectral accelerations can then be determined for the SHD.

In actual seismic hazard environments, for different probability levels p_M, the resulting controlling earthquakes (in terms of $m_{C,j}$, $r_{C,j}$, and $\nu_{C,j}$) from the scalar SHD vary in a small range for spectral accelerations at the same period. For simplicity in engineering practice, it is assumed that the controlling earthquakes, obtained from the scalar SHD for spectral accelerations at the same period but with different probability levels, are identical, and the variation of spectral acceleration is primarily due to ε (i.e., the conditional probability levels). This assumption is made because it is a common observation in the numerical results of the scalar SHD (Halchuk and Adams, 2004). A similar assumption is also made by Baker and Cornell (2005) for constructing the CMS-ε. Thus, the spectral accelerations on different probability levels at the same period can be induced approximately by the same earthquake (in terms of $m_{C,j}$, $r_{C,j}$, and $\nu_{C,j}$).

As can be seen in real scalar SHD cases (Halchuk and Adams, 2004), when the probability of exceedance p_M decreases for the same period, the resulting magnitude increases slightly and the resulting distance shortens slightly. In an average sense, the approximately median value of $p_M = 0.0045$ (20% per 50 years) among a small number of commonly used levels of annual probability of exceedance (2%, 5%, 10%, 20%, and 40% per 50 years) is then taken. In this study, based on the assumption discussed above, the controlling earthquake calculated at $p_M = 0.0045$ for a spectral acceleration via the scalar SHD is used as the controlling earthquake (in terms of $m_{C,j}$, $r_{C,j}$, and $\nu_{C,j}$) for all the probability levels of engineering interest.

For vector-valued SHD, it is also desirable to extract the controlling earthquake at a probability level, which is commonly used in practice. As can be seen in the numerical examples (Ni *et al.*, 2011D), the marginal probability levels p_M are close to 0.0045 if the commonly used joint probability level $p_J = 0.0004$ (2% per 50 years) is specified. To be approximately consistent with the scalar SHD in terms of the probability level, $p_J = 0.0004$ is then taken in the vector-valued SHD to determine the controlling earthquake.

As shown in equations (3.2.1), the effect of random variables M and R on the seismic hazard is considered by integrating their probability density functions with the probability distribution of spectral accelerations conditional on M and R. Incorporating with the

occurrence rate ν for each seismic source, the combined seismic hazard at the site of interest is then obtained.

Since the controlling earthquake is the dominant contributor to the seismic hazard over all possible earthquakes surrounding the site of interest, it is reasonable to use the deterministic values of magnitude and distance (controlling earthquakes) instead of the random variables M and R for simplicity and approximation. By substituting controlling earthquakes directly into the conditional probability distributions in equations (3.2.1), the numerical integrations in equations (3.2.1) can be avoided. After the substitutions, equations (2.1.24) and (2.1.26) represent the probabilities of spectral accelerations exceeding the threshold values when the controlling earthquake occurs. By multiplying the annual occurrence rate of the controlling earthquake to equations (2.1.24) and (2.1.26), the annual probabilities of exceedance of spectral accelerations are obtained.

The formulation of the generalized approach governed by equations (3.2.1) can thus be approximated as

- approximation of equation (3.2.1a):

$$\mathcal{P}\{S_a(T_1) > s_1, \ldots, S_a(T_k) > s_k\} = \nu_{\mathrm{C}}\, \mathcal{P}\{S_a(T_1) > s_1, \ldots, S_a(T_k) > s_k \,|\, m_{\mathrm{C}}, r_{\mathrm{C}}\} = p_{\mathrm{J}}, \tag{3.2.5a}$$

- approximation of equation (3.2.1b):

$$\mathcal{P}\{S_a(T_j) > s_j\} = \nu_{\mathrm{C},j}\, \mathcal{P}\{S_a(T_j) > s_j \,|\, m_{\mathrm{C},j}, r_{\mathrm{C},j}\} = \eta_j\, p_{\mathrm{M}},$$
$$j = \zeta, \zeta+1, \ldots, \xi-1, \xi, \quad 1 \leqslant \zeta \leqslant \xi \leqslant k, \tag{3.2.5b}$$

- approximation of equation (3.2.1c):

$$\mathcal{P}\{S_a(T_j) > s_j \,|\, S_a(T_\zeta) > s_\zeta, \ldots, S_a(T_\xi) > s_\xi\}$$
$$= \frac{\nu_{\mathrm{C}}\, \mathcal{P}\{S_a(T_j) > s_j, S_a(T_\zeta) > s_\zeta, \ldots, S_a(T_\xi) > s_\xi \,|\, m_{\mathrm{C}}, r_{\mathrm{C}}\}}{\nu_{\mathrm{C}}\, \mathcal{P}\{S_a(T_\zeta) > s_\zeta, \ldots, S_a(T_\xi) > s_\xi \,|\, m_{\mathrm{C}}, r_{\mathrm{C}}\}} = p_{\mathrm{C}},$$
$$j = 1, 2, \ldots, \zeta-1, \xi+1, \ldots, k. \tag{3.2.5c}$$

By using equations (3.2.5), all the integrations in equations (3.2.1) are avoided. Seismic design spectra can then be readily constructed for any specified probability level as long as

the controlling earthquakes and suitable ground-motion prediction equations (GMPEs) are provided by seismologists.

It is noted that, when spectral acceleration at only one dominant period is emphasized by equation (3.2.5b), i.e., $j=\zeta=\xi$ in equation (3.2.5b), the denominator of equation (3.2.5c) is a scalar PSHA; as a result, controlling earthquakes ($m_{C,\zeta}$, $r_{C,\zeta}$, and $\nu_{C,\zeta}$) from scalar SHD should be used for this denominator. Equation (3.2.5c) can then be expressed as

$$P\left\{S_a(T_j)>s_j \,\middle|\, S_a(T_\zeta)>s_\zeta\right\} = \frac{\nu_C\, P\left\{S_a(T_j)>s_j, S_a(T_\zeta)>s_\zeta \,\middle|\, m_C, r_C\right\}}{\nu_{C,\zeta}\, P\left\{S_a(T_\zeta)>s_\zeta \,\middle|\, m_{C,\zeta}, r_{C,\zeta}\right\}} = p_C,$$
$$j = 1, 2, \ldots, \zeta-1, \zeta+1, \ldots, k. \quad (3.2.6)$$

Since the controlling earthquake (m_C, r_C, and ν_C) from the vector-valued SHD contributes dominant seismic hazard to spectral accelerations over the entire period range, the controlling earthquake (m_C, r_C, and ν_C) is used for any vector-valued PSHA with more than one dimension in equations (3.2.5a) and (3.2.5c).

In seismic hazard deaggregation (SHD), the differences between the controlling earthquake from vector-valued SHD and those from scalar SHD, and the differences between the controlling earthquakes from scalar SHD for spectral accelerations at different periods depend on the relative seismic hazard contributions from the seismic sources surrounding the site of interest (Halchuk and Adams, 2004). When the seismic hazard at a given site is dominated by a single seismic source producing a single pair of magnitude and distance, which is the case for many coastal California sites, certain Central or Eastern U.S. sites near Charleston or New Madrid, and certain cities on western coast in Canada (Baker and Cornell, 2006b, Halchuk and Adams, 2004), the approximation of the generalized approach is very accurate.

3.2.5 Numerical Examples

In this section, the generalized approach and its approximation are demonstrated by several numerical examples based on a hypothetical configuration of seismic sources as shown in Figure 2.8. The effects of the selection of controlling vibration periods on the resulting seismic design spectra and seismic hazard deaggregation are also studied.

Exact generalized approach

For illustration purpose, magnitude M and distance R are assumed to be statistically independent, and the commonly used truncated exponential distribution for M and uniform distribution of seismic focus for R are employed in the exact generalized approach (3.2.1) to obtain the joint probability density function $f_M(m)f_R(r)$. The ground-motion prediction equations (GMPE) by Abrahamson and Silva (1997) and the most current matrix of spectral correlation by Baker and Jayaram (2008) are used for the conditional probability distributions of spectral accelerations. All the parameters in these distribution models are the same as used in Section 2.3.

As shown in Figure 3.2, vector-valued uniform hazard spectrum (VUHS), vector-valued non-uniform hazard spectrum (VNUHS), and vector-valued conditional uniform hazard spectrum (VCUHS) are generated at joint annual probability of exceedance of 4×10^{-4} when the fundamental period of a structure is assumed to be 0.1 sec. As discussed in Sections 3.2.1-3.2.3, the VNUHS and VCUHS have narrower spectral shapes and higher amplitudes at the period of 0.1 sec in comparison with the wide-band VUHS. Furthermore, the consideration of the spectral correlation results in the VCUHS having more frequency contents concentrated around the period of 0.1 sec when compared to the VNUHS. In this case, in comparison with the VUHS and VNUHS, the VCUHS could be a more suitable design earthquake for a structure with higher modes (modal periods smaller than 0.1 sec) contributing to the structural response, regardless the structure remains elastic (the fundamental period T_1 remains the same) or becomes inelastic (T_1 increases slightly) when subjected to earthquake excitation.

To account for the nonlinear behavior or the contributions of higher modes of a structure, the VNUHS and VCUHS can also be generated by emphasizing the spectral accelerations in a range of periods. As illustrated in Figure 3.3, the VUHS, VNUHS, and VCUHS are obtained at joint annual probability of exceedance of 4×10^{-4} for a structure having several dominant periods between 1 and 5 sec. Similar results as in Figure 3.2 are observed on the spectral shapes and amplitudes of the VUHS, VNUHS, and VCUHS.

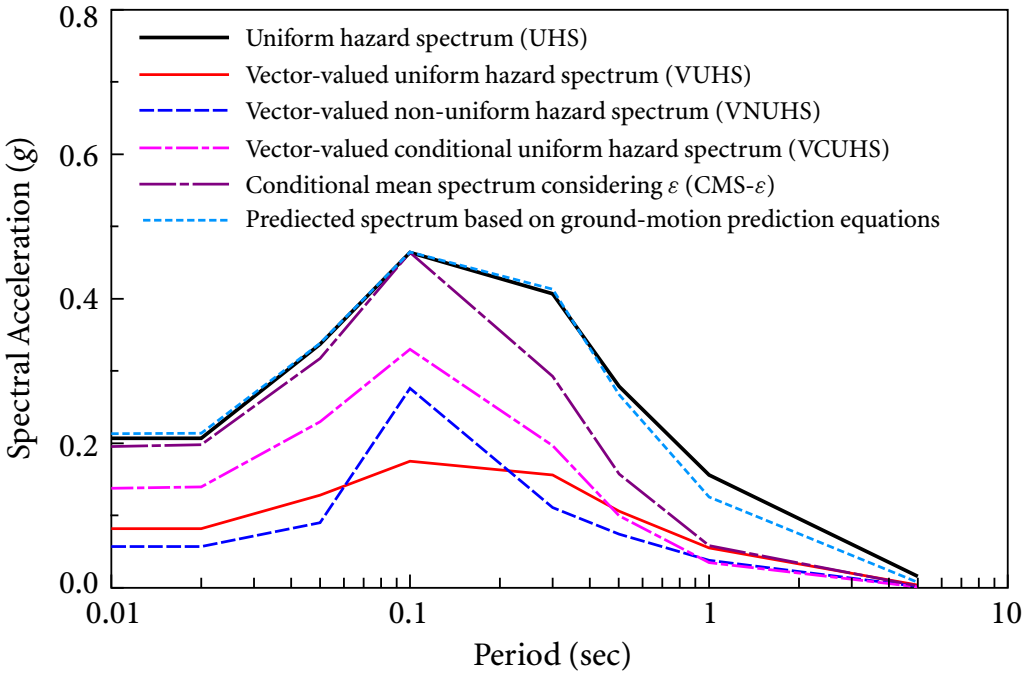

Figure 3.2 Seismic design spectra for dominant period of 0.1 sec at annual probability of exceedance of 4×10^{-4}

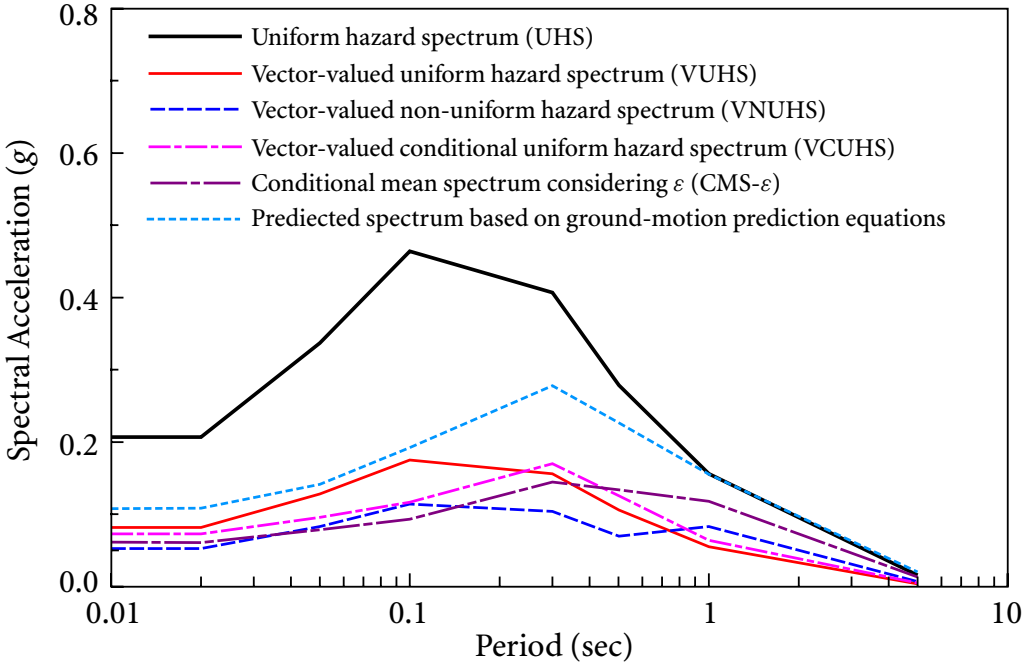

Figure 3.3 Seismic design spectra for dominant periods between 1 and 5 sec at annual probability of exceedance of 4×10^{-4}

It is noted that there are eight controlling periods used for generating the design spectra in this study; any intermediate periods can be added to the calculation of the spectra as required, which does not affect the resulting spectra significantly as will be discussed later.

For comparison, uniform hazard spectra (UHS), conditional mean spectra considering ε (CMS-ε), and predicted spectra based on ground-motion prediction equations (GMPEs) are also shown in Figures 3.2 and 3.3. These spectra are determined for marginal annual probability of exceedance of 4×10^{-4}. Due to the misuse of the marginal probability as the joint probability, these spectra are quite conservative in comparison with the proposed design spectra at specified periods (Ni *et al.*, 2011D).

Approximate generalized approach

To apply the approximate generalized approach governed by equations (3.2.5), controlling earthquakes need to be obtained first. By performing the vector-valued seismic hazard deaggregation (SHD) at joint annual probability of exceedance of 4×10^{-4}, as illustrated in Figure 2.14, the controlling earthquake, $m_C = 6.16$, $r_C = 54.00$ km, and $\nu_C = 0.052$, for spectral accelerations at eight controlling periods is determined. The controlling earthquakes in terms of $m_{C,j}$, $r_{C,j}$, and $\nu_{C,j}$ for spectral accelerations $S_a(T_j)$ at individual periods T_j are obtained from the scalar SHD at marginal annual probability of exceedance of 4.5×10^{-3}. The scalar SHD for spectral accelerations at 0.1 and 1 sec are shown in Figures 2.12 and 2.13, respectively. The controlling earthquakes from both scalar and vector-valued SHD are listed in Table 3.1.

By substituting the controlling earthquakes from the scalar and vector-valued SHD into equations (3.2.5), approximate VUHS, VNUHS, and VCUHS can be readily constructed for any joint annual probability of exceedance without cumbersome integrations required by the exact approach in equations (3.2.1). As shown in Figures 3.4-3.6, the approximate VUHS, VNUHS, and VCUHS agree very well with the accurate design spectra with an average relative error less than 10% for each spectrum.

Comparing with the approximate generalized approach proposed in Section 3.2, the approximate VUHS, VNUHS, and VCUHS generated using only the vector-valued SHD (Ni *et al.*, 2011D) have larger relative errors systematically as shown in Figures 3.4-3.6. As discussed in Section 3.2.4, this is primarily due to the difference between the resulting

controlling earthquake (m_C, r_C, and ν_C) for multiple periods from vector-valued SHD and those ($m_{C,j}$, $r_{C,j}$, and $\nu_{C,j}$) for individual periods from scalar SHD.

Table 3.1: Controlling earthquakes from seismic hazard deaggregation

Spectral acceleration (g)	Magnitude	Distance (km)	Rate of occurrence
Vector-valued $S_a(T_1), \ldots, S_a(T_8)$	$m_C = 6.16$	$r_C = 54.00$	$\nu_C = 0.052$
Scalar $S_a(T_1 = 0.01\text{sec}) = 0.079$	$m_{C,1} = 5.79$	$r_{C,1} = 42.60$	$\nu_{C,1} = 0.029$
Scalar $S_a(T_2 = 0.02\text{sec}) = 0.079$	$m_{C,2} = 5.81$	$r_{C,2} = 42.90$	$\nu_{C,2} = 0.029$
Scalar $S_a(T_3 = 0.05\text{sec}) = 0.126$	$m_{C,3} = 5.84$	$r_{C,3} = 42.99$	$\nu_{C,3} = 0.029$
Scalar $S_a(T_4 = 0.10\text{sec}) = 0.168$	$m_{C,4} = 6.00$	$r_{C,4} = 43.00$	$\nu_{C,4} = 0.029$
Scalar $S_a(T_5 = 0.30\text{sec}) = 0.152$	$m_{C,5} = 6.01$	$r_{C,5} = 56.30$	$\nu_{C,5} = 0.044$
Scalar $S_a(T_6 = 0.50\text{sec}) = 0.103$	$m_{C,6} = 6.14$	$r_{C,6} = 63.50$	$\nu_{C,6} = 0.053$
Scalar $S_a(T_7 = 1.00\text{sec}) = 0.053$	$m_{C,7} = 6.18$	$r_{C,7} = 80.44$	$\nu_{C,7} = 0.063$
Scalar $S_a(T_8 = 5.00\text{sec}) = 0.004$	$m_{C,8} = 6.21$	$r_{C,8} = 87.70$	$\nu_{C,8} = 0.072$

For example, when the approximate VUHS is generated as shown in Figure 3.4, an appropriate seismic hazard contributor to the scalar spectral acceleration $S_a(T_1 = 0.01\text{sec}) = 0.079$ in equation (3.2.5b) is the controlling earthquake represented by $m_{C,1} = 5.79$, $r_{C,1} = 42.60$ km, and $\nu_{C,1} = 0.029$, obtained from the scalar SHD. However, using the dominant hazard contributor ($m_C = 6.16$, $r_C = 54.00$ km, and $\nu_C = 0.052$) from the vector-valued SHD introduces the extra error in the approximate VUHS.

It is noted that the difference between the controlling earthquakes from scalar and vector-valued SHD depends much on the relative hazard contributions of the seismic sources and the relative separations of earthquake parameters, i.e., magnitudes, distances, and occurrence rates of the sources. Since the controlling earthquake (m_C, r_C, and ν_C) contributes seismic hazard to spectral accelerations over the entire period range of engineering interest in an average manner, it can be approximately interpreted as a weighted average of the controlling earthquakes ($m_{C,j}$, $r_{C,j}$, and $\nu_{C,j}$) from the scalar SHD. The difference between the controlling earthquakes from scalar and vector-valued SHD can be explained as statistical dispersion. This interpretation could help to understand the following conclusion.

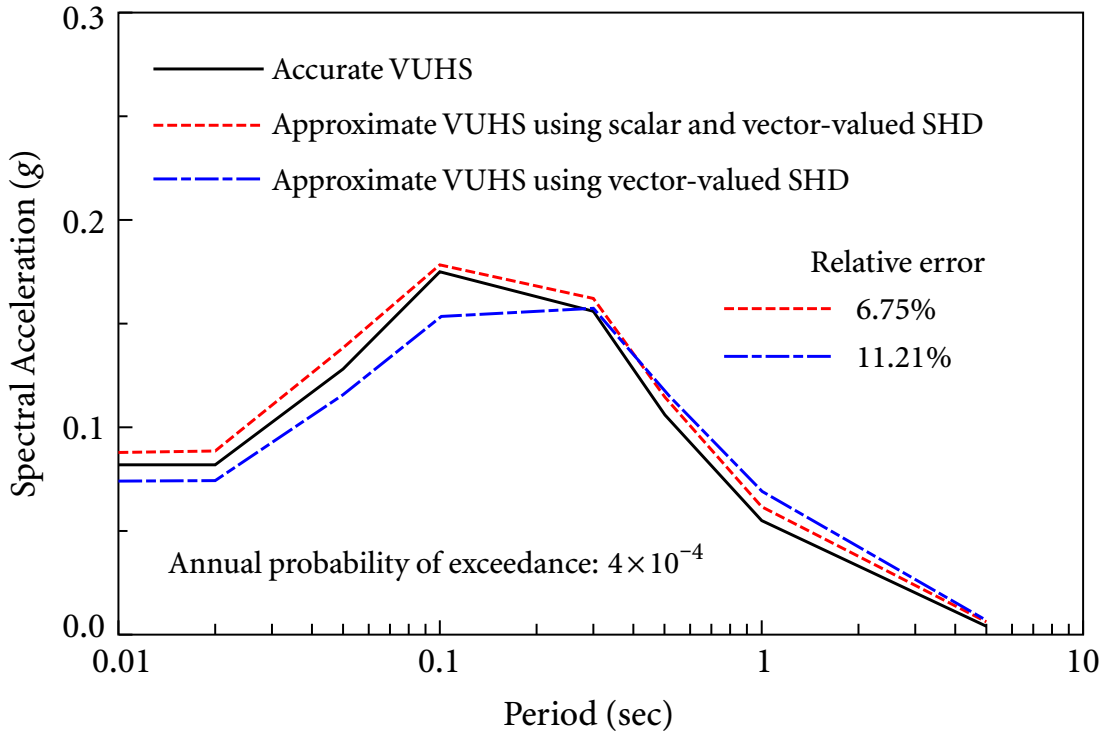

Figure 3.4 Vector-valued uniform hazard spectra using approximate generalized approach

When the seismic hazard tends to be dominated by a single source producing a single pair of magnitude and distance, all the controlling earthquakes from both scalar and vector-valued SHD approach this single earthquake, i.e., the difference (deviation) between the controlling earthquakes from scalar and vector-valued SHD is very small. In the other extreme case, when the seismic sources have nearly equal hazard contributions and their corresponding earthquake parameters are significantly different, the differences (deviations) between the controlling earthquake (m_{C}, r_{C}, and ν_{C}) from vector-valued SHD and those ($m_{\mathrm{C},j}$, $r_{\mathrm{C},j}$, and $\nu_{\mathrm{C},j}$) from scalar SHD are close to their upper-bounds (maximum values).

Since the hypothetical configuration of seismic sources shown in Figure 2.8 has two almost equal hazard contributors (sources) and wide relative separations of earthquake parameters, which covers the cases in many cities in Canada (Halchuk and Adams, 2004) and central and eastern United States (Harmsen *et al.*, 1999), the extra errors caused by

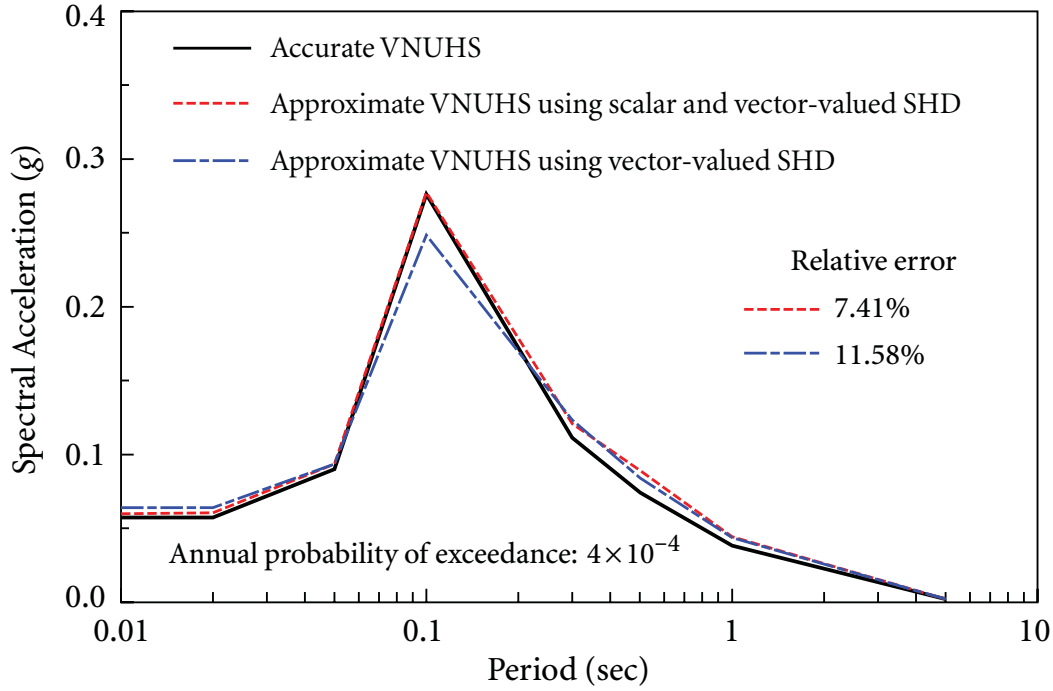

(a) VNUHS at dominant period of 0.1 sec

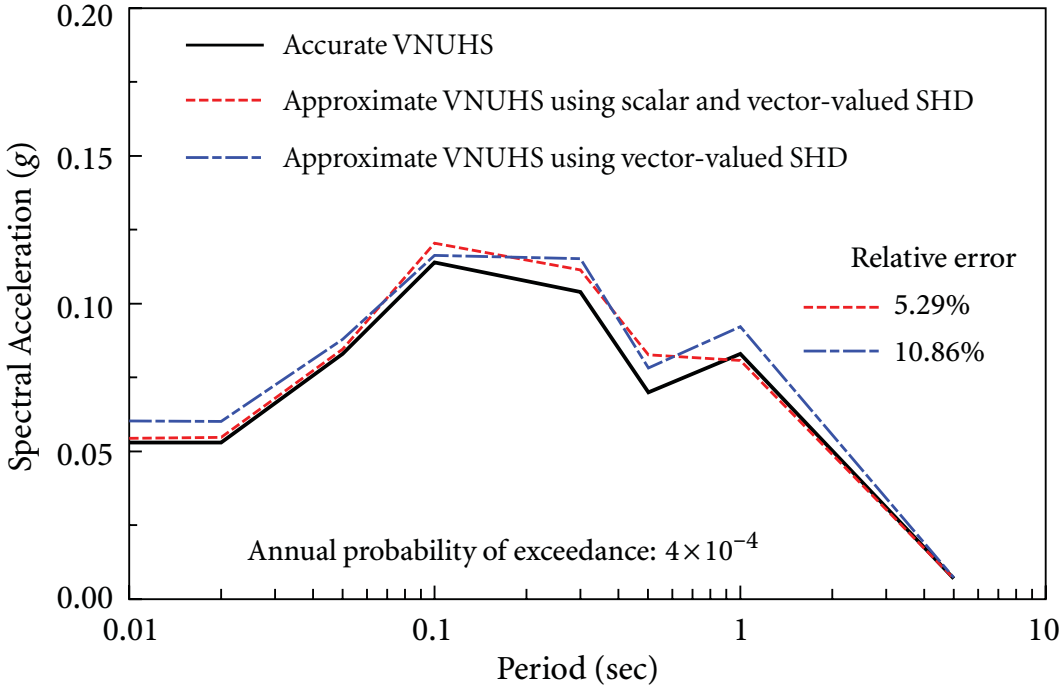

(b) VNUHS at dominant periods between 1 and 5 sec

Figure 3.5 Vector-valued non-uniform hazard spectra using approximate generalized approach

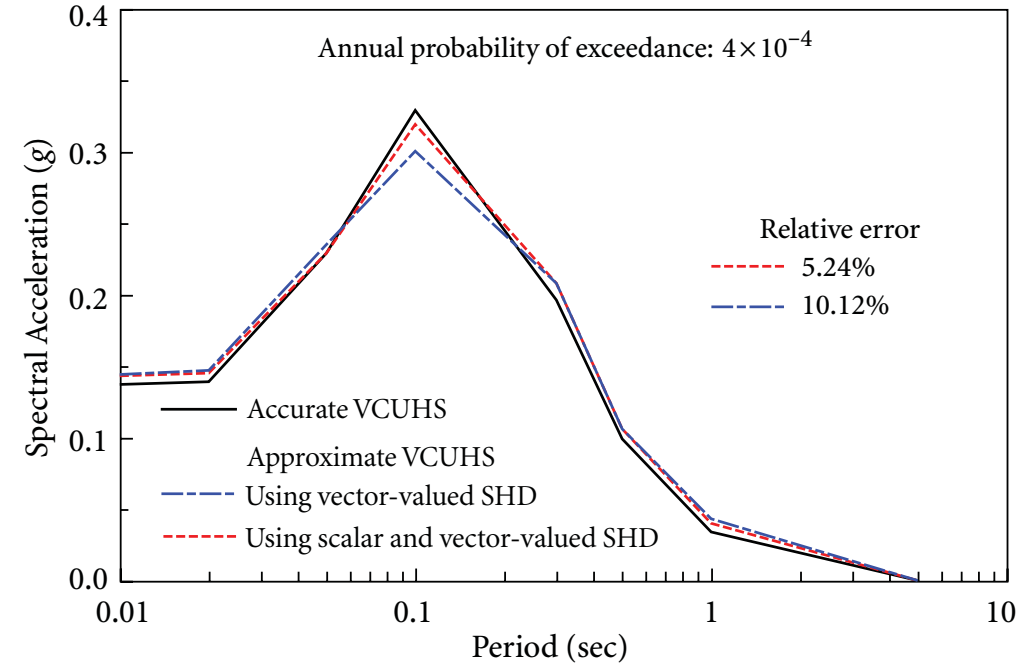

(a) VCUHS at dominant period of 0.1 sec

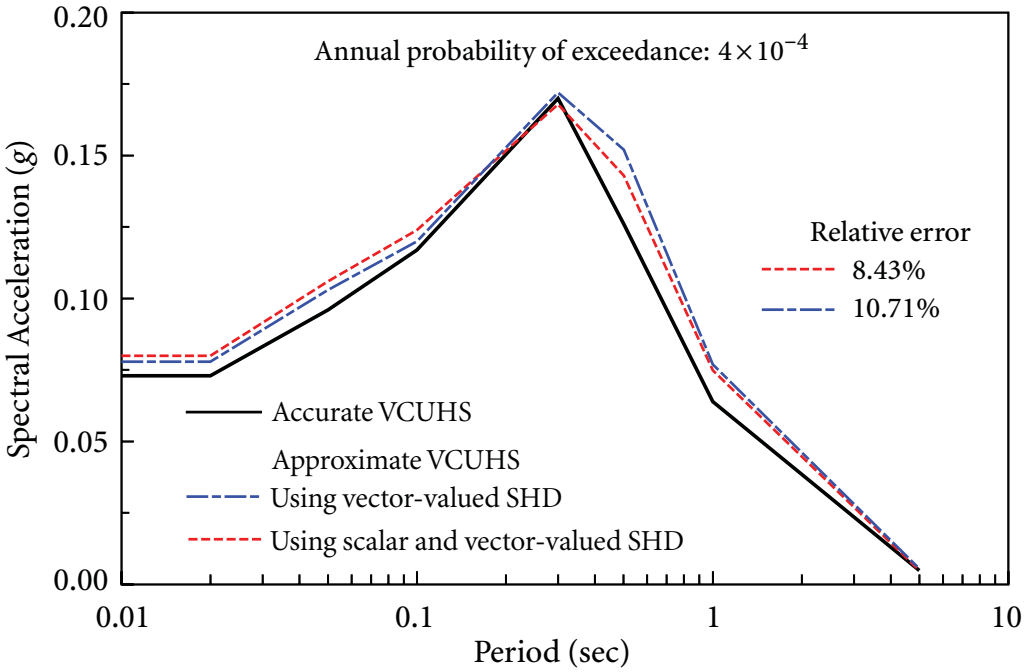

(b) VCUHS at dominant periods between 1 and 5 sec

Figure 3.6 Vector-valued conditional uniform hazard spectra using approximate generalized approach

using only the vector-valued SHD in the approximate approach could be the upper-bounds in many real cases. It should be emphasized that when the seismic hazard tends to be dominated by a single source producing a single pair of magnitude and distance, which is not an unusual case in reality, all the controlling earthquakes from both scalar and vector-valued SHD approach this single earthquake so that both approximations approach the exact solutions.

Selection of controlling vibration periods

In the proposed generalized approach presented in Section 3.2, eight critical controlling periods are used for generating the seismic design spectra based on both scalar and vector-valued PSHA. The controlling earthquake obtained from vector-valued SHD is also based on these eight controlling periods. It is important to study the effect of adding, shifting, or selecting different controlling periods on the resulting design spectra and the controlling earthquakes.

By applying the generalized approach governed by equations (3.2.1) for the hazard configuration in Figure 2.8, vector-valued uniform hazard spectra (VUHS) for the same joint annual probability of exceedance of 4×10^{-4} but different controlling periods are generated. As shown in Figure 3.7, in comparison with the VUHS at the eight critical controlling periods (0.01, 0.02, 0.05, 0.1, 0.3, 0.5, 1, 5 sec), the resulting VUHS are almost not affected by slightly shifting the periods, or adding several intermediate periods.

Based on the VUHS with different sets of controlling periods in Figure 3.7, the vector-valued SHD is also performed. The controlling earthquakes listed in Table 3.2 show that they are not sensitive to the change of the controlling periods. It is noted that since the controlling earthquake from vector-valued SHD is obtained by considering the simultaneous exceedance of spectral accelerations over the entire period range of engineering interest in an average sense, as long as the controlling periods spread over the entire period range roughly uniformly, the observation from Table 3.2 should be true for any number of controlling periods.

The above observations can be explained through the theory of probability. In the vector-valued PSHA, the selection of controlling periods affects only the first term in the integrand in equation (2.3.17), which is a multivariate normal distribution of the natural

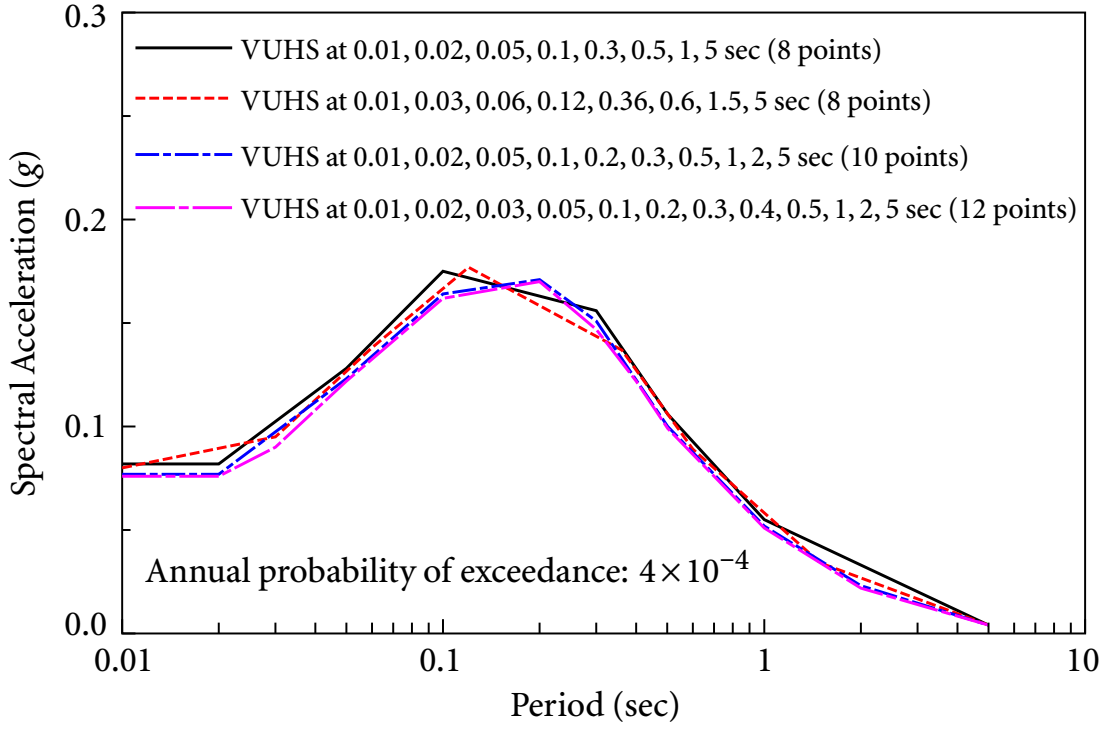

Figure 3.7 Vector-valued uniform hazard spectra with different controlling periods

logarithmic values of spectral accelerations, $\ln S_a(T_1), \ldots, \ln S_a(T_k)$, conditional on m and r, i.e., equation (2.1.26). The correlation coefficient between any two logarithmic spectral accelerations, in this multivariate normal distribution model, generally decreases with the increasing separation of their vibration periods, as discussed in Section 2.1.2.

Table 3.2: Controlling earthquakes from vector-valued SHD

Manipulation	# of periods	Magnitude m_C	Distance r_C (km)	Rate of occurrence ν_C
No	8	6.16	54.00	0.052
Shifting	8	6.16	57.70	0.054
Adding	10	6.15	57.53	0.053
Adding	12	6.15	59.00	0.052

On the other hand, when more spectral accelerations are considered in the multivariate normal distribution model in equation (2.1.26), i.e., k increases, the joint probability of exceeding these spectral accelerations simultaneously decreases. In other words, to maintain the joint probability level, the amplitudes of the design spectra decrease when k increases. Assuming an extreme case when one spectral acceleration $\ln S_a$, uncorrelated with any spectral accelerations used in the calculation (i.e., the correlation coefficient is zero), is added to the distribution model, the joint probability could decrease significantly; whereas in the other extreme case when $\ln S_a$ is perfectly correlated with one of the spectral accelerations used in the calculation (i.e., the correlation coefficient is one), the joint probability does not change.

Since the eight critical controlling periods selected cover the entire period range of engineering interest roughly uniformly, and the spectral accelerations at any intermediate periods are considerably correlated with their adjacent spectral accelerations, the resulting seismic design spectra and controlling earthquakes are not affected significantly by the change of the controlling periods. When more and more intermediate controlling periods are considered in equation (2.3.17), the rate of change in the resulting seismic design spectra will reduce dramatically, i.e., the change does not increase indefinitely, as shown in the following numerical examples.

To further investigate the effects of the selection of the controlling periods on the seismic design spectra, more controlling periods are used in the calculation. Since only the conditional multivariate normal distribution in equation (2.3.17) is affected by the selection of controlling periods and the controlling earthquake from vector-valued SHD is not sensitive to the change of the controlling periods, the approximate generalized approach based on only the controlling earthquake from vector-valued SHD ($m_{\mathrm{C}} = 6.16$, $r_{\mathrm{C}} = 54.00$ km, and $\nu_{\mathrm{C}} = 0.052$) is used to reduce computational effort.

In Figure 3.8, the approximate VUHS are generated using the ground-motion prediction equation (GMPEs) by Abrahamson and Silva (1997). The parameters in this GMPE are the same as in Section 2.3. Since a maximum of 28 controlling periods are allowed in this GMPE, to further increase the number of periods in a design spectrum, the GMPE by Boore and Atkinson (2008), which allows interpolation of periods, is used to generate the

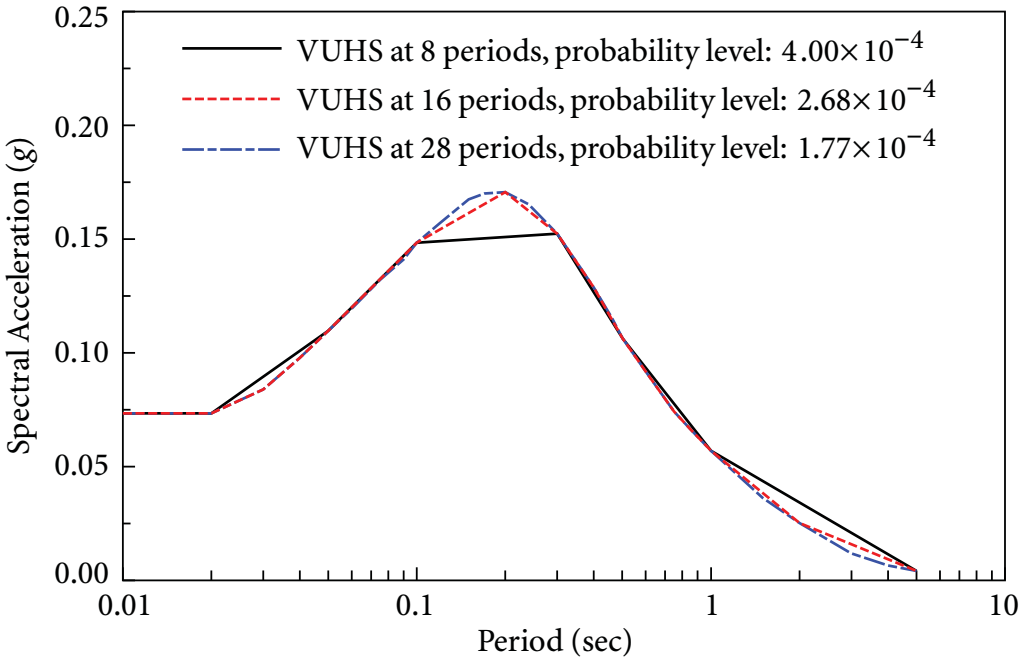

(a) VUHS for the same amplitude

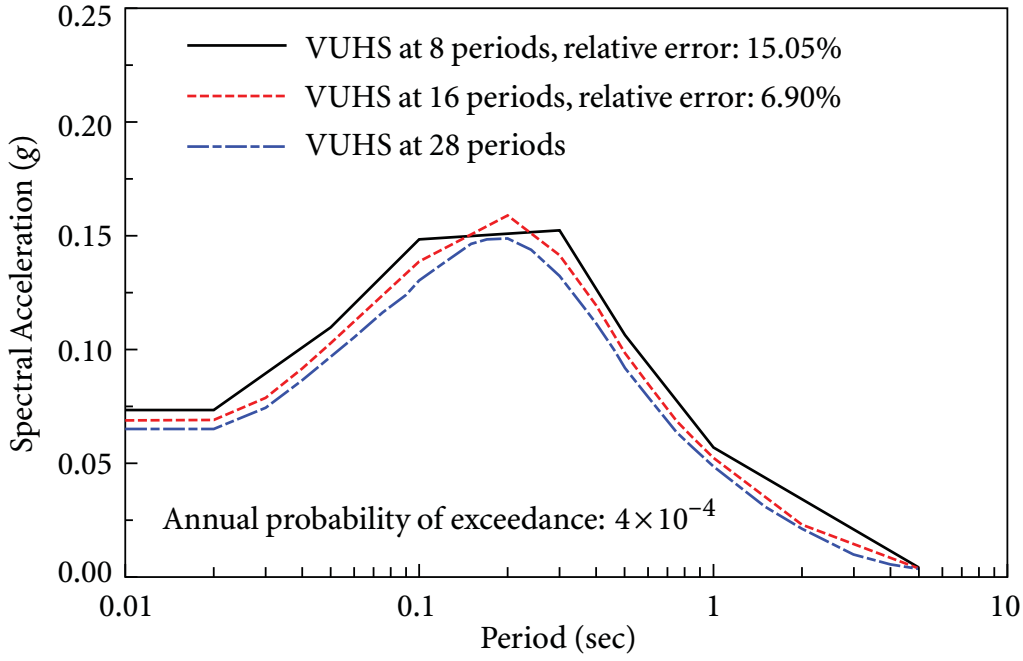

(b) VUHS for the same probability level

Figure 3.8 Approximate VUHS with different controlling periods using ground-motion prediction equation by Abrahamson and Silva (1997)

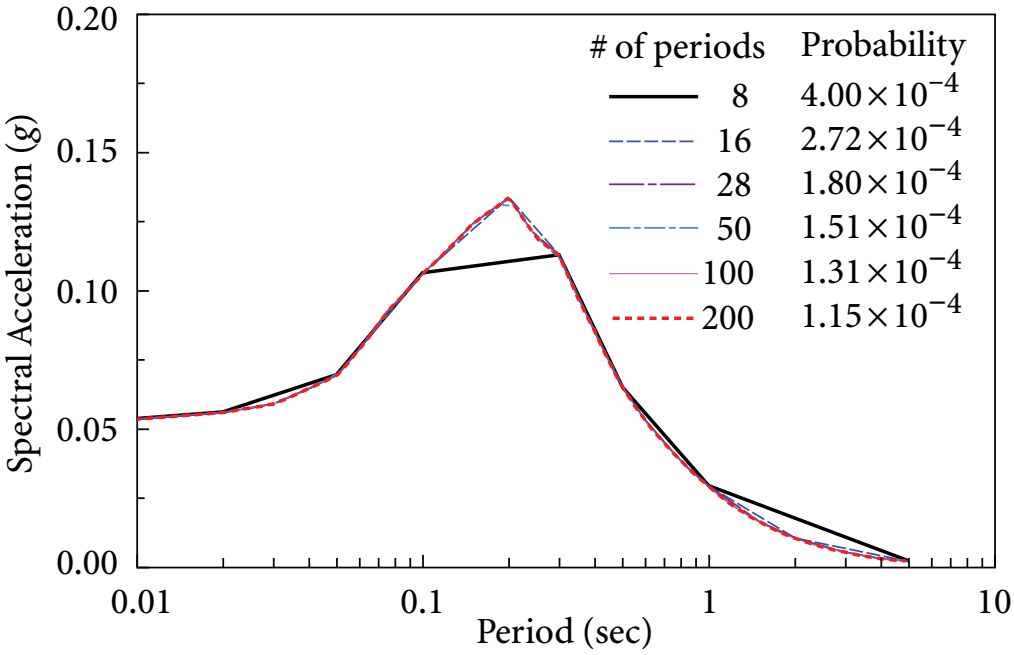

(a) VUHS for the same amplitude

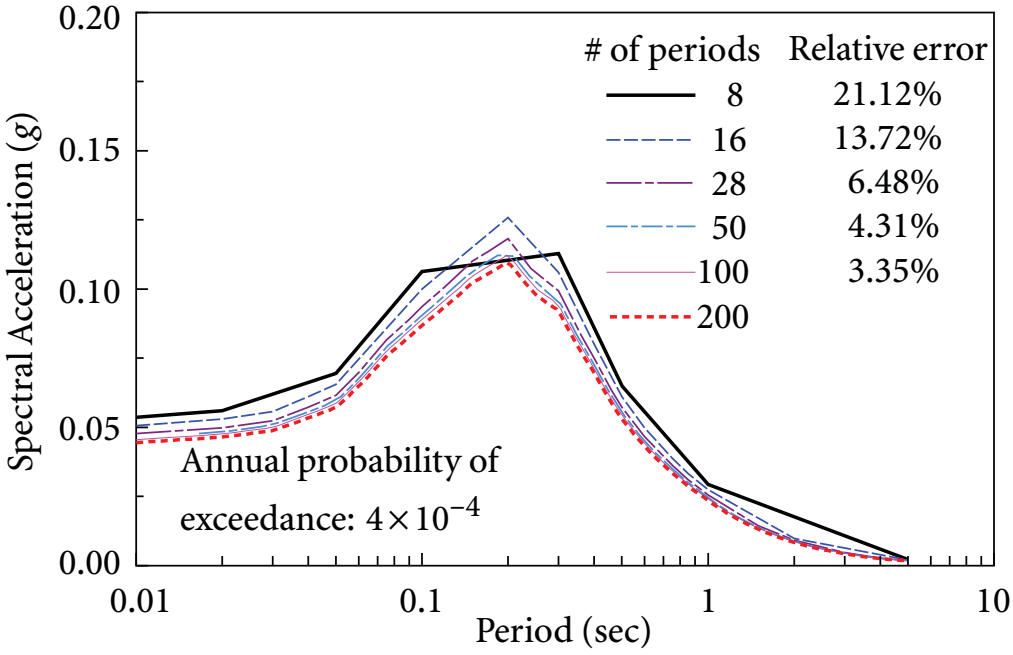

(b) VUHS for the same probability level

Figure 3.9 Approximate VUHS with different controlling periods using ground-motion prediction equation by Boore and Atkinson (2008)

approximate VUHS in Figure 3.9. In this GMPE, the fault type is specified as reverse fault and the shear wave velocity averaged over top 30 m of soil is 1300 m/sec for rock sites.

As can be seen in Figures 3.8(a) and 3.9(a), when the amplitudes of the VUHS are fixed for different controlling periods, i.e., the marginal probability of exceedance remains a constant for each of these two cases, the annual probability of exceedance decreases with the increase of the number of controlling periods. However, the probability level decreases more and more slowly even when the number of controlling periods grows more and more rapidly.

This result can also be observed in Figure 3.9(b), in which the VUHS are generated for the same probability of exceedance at different sets of controlling periods. If 200 controlling periods are deemed sufficient for plotting a smooth design spectrum, the VUHS computed at these 200 controlling periods can be regarded as numerically exact in comparison with those plotted at fewer than 200 controlling periods in Figure 3.9(b).The average error of the VUHS relative to the one using 200 periods decreases more and more slowly when the number of controlling periods grows more and more rapidly. This observation is consistent with the theoretical explanation discussed previously.

The errors of the VUHS at 8 and 16 periods, relative to the one using 28 periods, are 13.76% and 6.80%, respectively, based on the GMPE by Boore and Atkinson (2008). Using the GMPE by Abrahamson and Silva (1997), the errors of the VUHS at 8 and 16 periods are 15.05% and 6.90%, respectively, as shown in Figure 3.8(b).

The effect of the selection of the controlling periods in the spectrum generation using the GMPE by Boore and Atkinson (2008) is thus slightly smaller than that using the GMPE by Abrahamson and Silva (1997). This is mainly due to the fact that the standard deviations for average component in the GMPE by Boore and Atkinson (2008) are slightly smaller than those for an arbitrary component in the GMPE by Abrahamson and Silva (1997). For the same change in probability (the area under the probability density function between two thresholds), the difference between these two thresholds decreases with the decrease of the standard deviation.

For example, in Figure 3.8(a), the probability levels for 8 and 28 periods are 4×10^{-4} and 1.77×10^{-4}, respectively, for the same VUHS amplitude. To achieve the probability level of 4×10^{-4}, the VUHS at 28 periods is reduced by 13.04%. In Figure 3.9(a), however, the

VUHS at 28 periods is reduced by 12.08% to reach the probability level of 4×10^{-4}. Results similar to Figures 3.7-3.9 are also observed for VNUHS and VCUHS.

With the increase of the number of recorded ground motions and the advancement of techniques for determining the GMPEs in the future, the epistemic uncertainty part in the standard deviations could be further reduced so that the effect of the selection of the controlling periods on the design spectra could be neglected.

In this study, the eight controlling periods are selected following engineering practice for nuclear energy facilities. To potentially implement the proposed generalized approach into seismic design codes and standards, the controlling periods should be selected by considering all possible spectral peaks and valleys, corner frequencies, and the number of controlling periods, based on local seismic hazard environments (e.g., western or eastern North America), and social and economic factors (i.e., fewer controlling periods may yield larger conservatism for the design).

3.3 Summary

In this chapter, a novel generalized approach is developed to generate seismic design spectra using both scalar and vector-valued probabilistic seismic hazard analysis (PSHA). The annual probability of exceeding spectral accelerations over the entire period range of engineering interest on a design spectrum is provided so that it can be interpreted as a single design earthquake. The primary properties of the seismic design spectra are summarized as follows.

- Vector-valued uniform hazard spectrum (VUHS)
    1. The spectral shape of the conventional UHS, i.e., consistent seismic hazard at each spectral acceleration, is preserved on a VUHS.
    2. The VUHS is a suitable design earthquake for structures having a wide range of structural modal periods, having significant contributions to structural responses.
- Vector-valued non-uniform hazard spectrum (VNUHS)
    1. A relatively narrow-band spectral shape, which is concentrated at a pre-specified period or a range of periods, is achieved through the VNUHS.

2. The VNUHS is suitable for structures with known dominant modes, and little nonlinear behavior or well-estimated nonlinear behavior.

❧ Vector-valued conditional uniform hazard spectrum (VCUHS)

1. A relatively narrow-band spectral shape concentrated at specified dominant periods is achieved, in which the spectral correlation between the dominant periods and non-dominant periods is considered.
2. It is suitable for structures with known first mode, but unknown higher-mode effects and nonlinear behavior.

An approximation of the generalized approach is also proposed so that the seismic design spectra can be readily incorporated into structural design and performance-based seismic design. This approximate approach is based on a set of controlling earthquakes derived from both scalar and vector-valued seismic hazard deaggregation (SHD).

It is demonstrated that the selection of the controlling vibration periods does not significantly affect the resulting design spectra and controlling earthquakes, as long as the selected periods cover the entire period range of engineering interest roughly uniformly.

C H A P T E R 4

Spectrum-Compatible Ground Motions

Seismic Response History Analysis (SRHA) (see Appendix A.2.2) is a major seismic response analysis method for seismic design verification of ordinary civil structures (NBCC, 2005, NBCC, 2010, UBC, 1997) and seismic qualification of critical structures, such as nuclear power plants (CSA, 1981, ASCE, 1998, ASCE, 2009). The SRHA procedure is concerned with the determination of structural response as a function of time when the structural system is subjected to a given ground acceleration (Chopra, 2001). Hence, representative (design) input earthquake ground motions are required for this analysis method.

There are three types of earthquake ground motions for SRHA procedure: recorded earthquake ground motions, spectrum-compatible artificial/synthetic earthquake ground motions, and spectrum-compatible ground motions based on recorded ground motions. An earthquake ground motion, whose response spectrum closely matches or envelopes a seismic design spectrum over a range of vibration periods of engineering concern, is usually called a spectrum-compatible earthquake ground motion. The use of spectrum-compatible ground motions instead of recorded ground motions is attractive for multiple reasons: (1) they are able to produce structural responses that present relatively lower dispersion; (2) there are only a small number of recorded ground motions available for many regions in the world (Carballo, 2000). NIST (2011) states that the use of spectrum-compatible earthquake ground motions provides more accurate estimates of the mean or average structural response.

In this chapter, the existing approaches for generating spectral-compatible earthquake ground motions are reviewed in Section 4.1. Hilbert-Huang Transform (HHT) is described in Section 4.2. Based on the HHT, three methodologies are developed for generating single, multiple, and tri-directional spectrum-compatible earthquake ground motions in Sections 4.3-4.5, respectively. Some conclusions are summarized in Section 4.6.

4.1 Existing Spectral Matching Algorithms

Several studies have been done for generating spectrum-compatible artificial/synthetic earthquake ground motions. One of the most classical attempts is to use a Fourier series representation for the ground motion to be generated based on the random vibration theory. The sinusoidal motions are then summed and a subsequent iterative process refines the result to match the response spectrum of the generated ground motion with the target seismic response spectrum. In these studies, various envelope or shape functions are used to characterize approximately the nonstationary properties of real recorded ground motions (Scanlan and Sachs, 1974, Levy and Wilkinson, 1976, Vanmarcke and Gasparini, 1977, King and Chen, 1977, Preumont, 1980, Preumont, 1984, Spanos and Loli, 1985).

Synthetic earthquake ground motions can be generated from seismological source models by accounting for path and site effects. Atkinson and Boore (1998) and Atkinson (2009) simulated earthquake ground motions consistent with the earthquake magnitudes and distances that contribute relatively most strongly to hazard at the selected sites and probability level. These simulated motions match the short- and long-period ranges of the target uniform hazard spectrum (UHS), respectively. These simulations for local and regional crustal, in-slab, and interface earthquakes are based on point-source stochastic simulation procedure (Boore, 1983) or stochastic finite-fault method (Motazedian and Atkinson, 2005).

Iyengar and Rao (1979) attempted to generate spectrum-compatible artificial earthquake ground motions from a random process without resorting to the power spectral density function. This approach with random phases, amplitudes, and signs ensures that the generated response spectra are at least greater than the target velocity response spectra. Giaralis and Spanos (2009) used a stochastic dynamics solution based on wavelet technique

to obtain a family of simulated nonstationary earthquake motions, whose response spectra are on the average in good agreement with the target displacement response spectrum.

However, real recorded earthquake ground motions are complicated; they are influenced by, and consequently reflect, characteristics of the seismic source, the rupture process, the source-site travel path, and local site conditions. Although it is convenient to characterize them with a small number of parameters, such characterizations can never be complete. Artificial/synthetic ground motions that match a small number of target parameters are not unique; many different motions can produce the same target parameters. If such a set of motions are used to analyze structures for which response of the structures correlates little to the target parameters, the predicted response is going to be inconsistent (Kramer, 1996). Moreover, artificial/synthetic earthquake ground motion cannot be used for nonlinear seismic analysis as required in ASCE/SEI Standard 43-05 (ASCE, 2005).

Recorded earthquake ground motions contain a wealth of information about the nature of the earthquake and carry all the ground-motion characteristics (amplitude, frequency, energy content, duration, and phase characteristics), and reflect all the factors that influence earthquake motions (characteristics of the source, path, and site). With the increase of available recorded strong motions, using and scaling the recorded ground motions become one of the most popular research topics in this field.

Tsai (1972) selected an existing recorded ground motion whose spectrum matches closely with the target seismic design spectrum. The recorded motion was then passed successively through certain frequency-suppressing filters to reduce the spectrum wherever necessary. Similarly, sinusoidal motions were superposed over the selected motion to increase the spectrum as required. Several researchers used a very similar technique. However, they found it convenient to work in the frequency domain rather than with the time-histories in the time domain. The technique is to scale the Fourier amplitudes or phases of the recorded motion such that the resulting response spectrum is compatible with the target design spectrum (Rizzo *et al.*, 1975, Kost *et al.*, 1978, Silva and Lee, 1987).

However, Fourier-based techniques do not account for the instantaneous variations in the frequency contents of an earthquake ground motion, which arise due to the arrivals of different types of seismic waves at different time-instants and due to the phenomenon

of dispersion in these waves. In order to simulate the nonstationary characteristics of earthquake ground motions, a wavelet-based procedure has been used. It decomposes an recorded earthquake ground motion into a desired number of time-history components with non-overlapping frequency contents; each of the time-history components is then suitably scaled to match the response spectrum of the modified recorded motion with a target seismic design spectrum (Mukherjee and Gupta, 2002). The wavelet-based technique, however, is still not good enough for characterizing the instantaneous variations in the frequency contents of an earthquake motion, since it is unable to locate the frequency distribution of the signal accurately (Huang *et al.*, 1998).

An alternative method in preserving the nonstationary characteristics of earthquake ground motions is to adjust recorded ground motions by adding wavelet functions in the time domain to match the target design spectra. This method is based on the assumption that the time at which the spectral response of a time-history occurs is not perturbed by a small adjustment of the time-history (Kaul, 1978, Lilhanand and Tseng, 1988, Lee and Kim, 1999, Choi and Lee, 2003, Hancock *et al.*, 2006, Atik and Abrahamson, 2010). The method, however, cannot generate spectrum-compatible ground motions based on multiple recorded ground motions. Furthermore, the effectiveness of the spectral matching may highly depend on the seed recorded ground motion.

To consider a large number of recorded ground motions simultaneously, a neural-network-based technique has been proposed. It uses the decomposing capabilities of Fourier or wavelet packet transform on recorded ground motions, and the learning abilities of stochastic neural network to expand the knowledge of the inverse mapping from target response spectrum to generated earthquake ground motion (Ghaboussi and Lin, 1998, Lin and Ghaboussi, 2001, Lin *et al.*, 2006, Amiri *et al.*, 2009). This method, however, is still based on Fourier technique or wavelet technique and the generated ground motions may not be able to meet the strict requirements in the code (ASCE, 1998, ASCE, 2005, ASCE, 2009).

4.2 Hilbert-Huang Transform

In Section 4.1, the existing approaches for generating spectral-compatible earthquake ground motions are discussed. To overcome some deficiencies of the existing spectral matching algorithm, the Hilbert-Huang transform (HHT) has been applied in generating spectrum-compatible earthquake ground motions (Ni *et al*., 2010, Ni *et al*., 2011A, Ni *et al*., 2011C, Ni *et al*., 2011B).

The Hilbert-Huang Transform (HHT), developed by Huang *et al.* (1998), can represent nonstationary and nonlinear data such as earthquake ground motions by decomposing the data into several components and transforming the data from time domain to frequency domain.

The HHT has been applied to a wide range of areas. Current major applications of the HHT include image processing, meteorology and atmospherology, ocean engineering, health monitoring, system identification, and earthquake engineering.

In the past decade, some researchers applied the HHT in processing and analyzing recorded earthquake ground motions (Huang *et al*., 2001, Loh *et al*., 2001, Zhang *et al*., 2003A, Zhang *et al*., 2003B). They concluded that the Hilbert-Huang spectral analysis gave the most detailed information in a time–frequency–energy presentation compared to traditional data processing techniques. The HHT was also used in simulating a large number of earthquake ground motions by randomly shifting the instantaneous frequencies of the recorded earthquake ground motions (Wen and Gu, 2004, Gu and Wen, 2007).

Compared to Fourier transform and wavelet transform, the HHT can meet the necessary conditions for the basis to represent a nonstationary and nonlinear time series: complete, local, and adaptive. The condition of completeness guarantees the degree of precision of the expansion. The requirement for locality is the most crucial for nonstationarity, which means all events have to be identified by the time of their occurrence. Consequently, it is required that both the amplitude (or energy) and the frequency be functions of time. The requirement for adaptivity is also crucial for both nonstationary and nonlinear data. It is impossible to expect a predetermined basis to fit all the phenomena in the data. An easy

way to generate the necessary adaptive basis is to derive the basis from the data themselves. This is the substantial advantage of the HHT over other transform techniques.

The Hilbert-Huang transform (HHT) is the result of the Empirical Mode Decomposition (EMD) and the Hilbert Spectral Analysis (HSA). The HHT uses the EMD method to decompose a signal into a number of so-called Intrinsic Mode Functions (IMF), and uses the HSA method to obtain instantaneous frequency data. The EMD and HSA are introduced in Sections 4.2.1 and 4.2.2, respectively.

4.2.1 Empirical Mode Decomposition

The empirical mode decomposition (EMD) is based on the assumption that any time series (earthquake ground motion in this study) consists of different, simple, and intrinsic modes of oscillation, derived from the earthquake motion (Huang *et al.*, 1998). Each of these oscillatory modes, called an intrinsic mode function (IMF), is defined by the following conditions:

1. Over the entire time-history, the number of extrema and the number of zero-crossings must be equal or differ at most by one;
2. At any point, the mean value of the envelope defined by the local maxima and the envelope defined by the local minima is zero.

An IMF represents a simple oscillatory mode similar to a component in the Fourier-based simple harmonic function, but more general. A systematic way to decompose an earthquake ground motion $X(t)$, called the Sifting Process (SP) of the EMD, is described as follows.

First, identify all the local extrema of the earthquake ground motion. Connect all the local maxima by a cubic spline to produce the upper envelope of the data. Repeat the procedure for the local minima to produce the lower envelope of the data. The upper and lower envelopes should encompass all the data between them. The mean of these two envelopes is designated as $m_1(t)$, and the difference between the ground motion $X(t)$ and $m_1(t)$ is the first component $h_1(t)$, i.e.,

$$h_1(t) = X(t) - m_1(t). \tag{4.2.1}$$

In the subsequent process, $h_1(t)$ is treated as the data, then

$$h_{11}(t) = h_1(t) - m_{11}(t), \tag{4.2.2}$$

where $m_{11}(t)$ is the mean of the upper and lower envelopes of $h_1(t)$.

Repeat the previous process until all the conditions in the definition of an IMF is achieved. After repeated sifting, $h_{1i}(t)$ is given by

$$h_{1i}(t) = h_{1(i-1)}(t) - m_{1i}(t), \tag{4.2.3}$$

where $m_{1i}(t)$ is the mean of the upper and lower envelopes of $h_{1(i-1)}(t)$. $h_{1i}(t)$ is designated as the first IMF $c_1(t)$ from the earthquake ground motion $X(t)$, i.e.,

$$c_1(t) = h_{1i}(t). \tag{4.2.4}$$

It is noted that the standard deviation SD, which is computed from two consecutive sifting results, is used as the criterion for terminating the sifting process for each IMF. SD is defined as

$$\mathrm{SD} = \sum_{t=0}^{T} \frac{\left[h_{1(i-1)}(t) - h_{1i}(t)\right]^2}{h_{1(i-1)}^2(t)}, \tag{4.2.5}$$

where T is the total time length of the discrete time series data. When $\mathrm{SD} \leqslant 0.2$, the sifting process for each IMF is terminated (Huang *et al.*, 1998).

Typically, $c_1(t)$ contains the shortest-period component of the original ground motion $X(t)$. $c_1(t)$ is then removed from the original data $X(t)$ to obtain the residue

$$r_1(t) = X(t) - c_1(t). \tag{4.2.6}$$

The residue $r_1(t)$, which contains longer-period components, is treated as a new data and subjected to the same sifting process as described above. This procedure can be repeated to obtain all the subsequent r_k functions as follows:

$$r_{k-1}(t) - c_k(t) = r_k(t), \quad k = 2, 3, \ldots, n. \tag{4.2.7}$$

The sifting process (SP) can be terminated by either of the following predetermined criteria:

1. Either the component $c_n(t)$ or the residue $r_n(t)$ becomes so small that it is less than a predetermined value;
2. The residue $r_n(t)$ becomes a monotonic function.

The original earthquake ground motion is then the sum of the IMF $c_k(t)$ plus the final residue $r_n(t)$

$$X(t) = \sum_{k=1}^{n} c_k(t) + r_n(t). \tag{4.2.8}$$

Thus, the earthquake ground motion is decomposed into n IMF $c_1(t), c_2(t), \ldots, c_n(t)$ and a residue $r_n(t)$ that can be either the mean trend or a constant.

Figure 4.2 shows all eight IMF of the El-Centro earthquake ground motion, recorded in 1940 Imperial Valley Earthquake as shown in Figure 4.1. It is seen that each component emphasizes a different oscillation mode with different amplitude and frequency content. The first IMF has the highest-frequency content, and the frequency content decreases with the increase in IMF until the 8th IMF.

The final residue $r_8(t)$ of the El-Centro ground motion through EMD procedure is shown in Figure 4.3. This final residue is smaller than a predetermined value, from which no more IMF can be extracted. Figure 4.4 shows the difference between the original El-Centro ground motion and the reconstructed one given by equation (4.2.8). This small error indicates the completeness of the expansion, and the reconstructed data is numerically identical to the original one.

4.2.2 Hilbert Spectral Analysis

For given data $C(t)$, the Hilbert transform $Y(t)$ is define as

$$Y(t) = \frac{1}{\pi}\,\mathbb{P}\int_{-\infty}^{\infty} \frac{C(t')}{t - t'}\mathrm{d}t', \tag{4.2.9}$$

where $\mathbb{P}$ denotes the Cauchy principal value. With this definition, $C(t)$ and $Y(t)$ can be combined to form the analytic signal $Z(t)$, given by

$$Z(t) = C(t) + \mathrm{i}\,Y(t) = a(t)\mathrm{e}^{\mathrm{i}\theta(t)}, \tag{4.2.10}$$

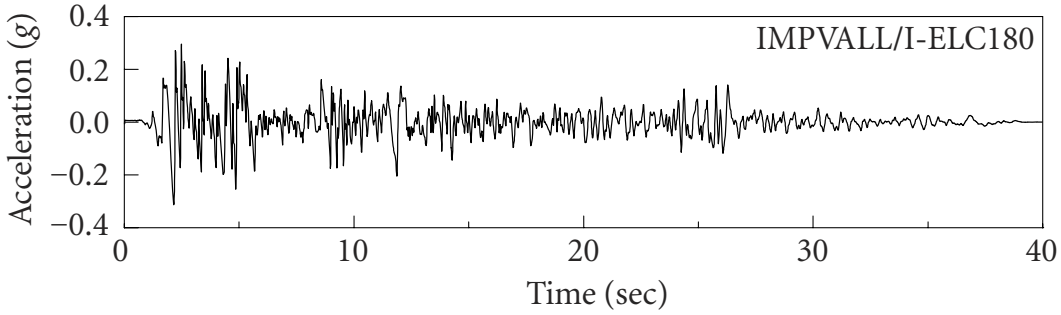

Figure 4.1 Earthquake ground motion recorded in Imperial Valley Earthquake, 1940

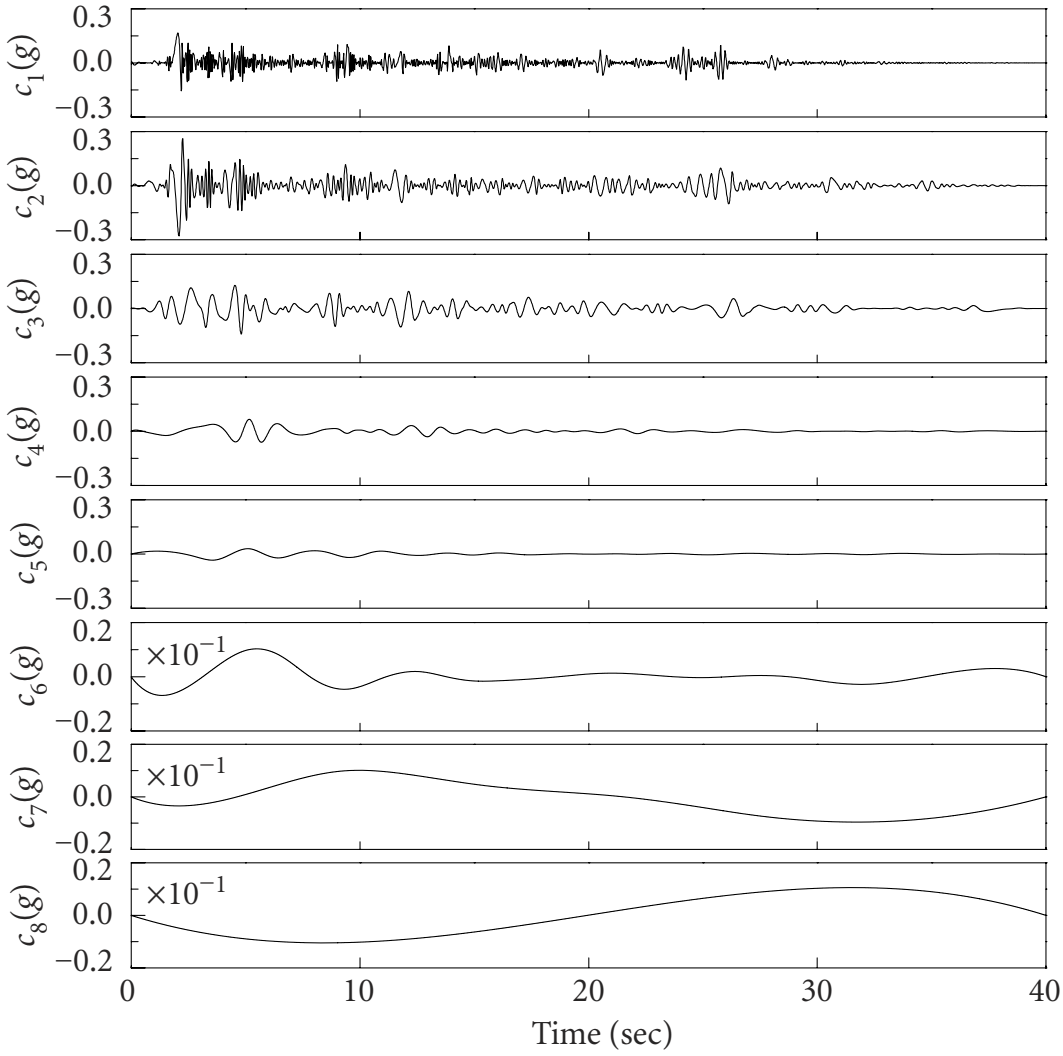

Figure 4.2 Eight intrinsic mode functions of El-Centro ground motion through empirical mode decomposition

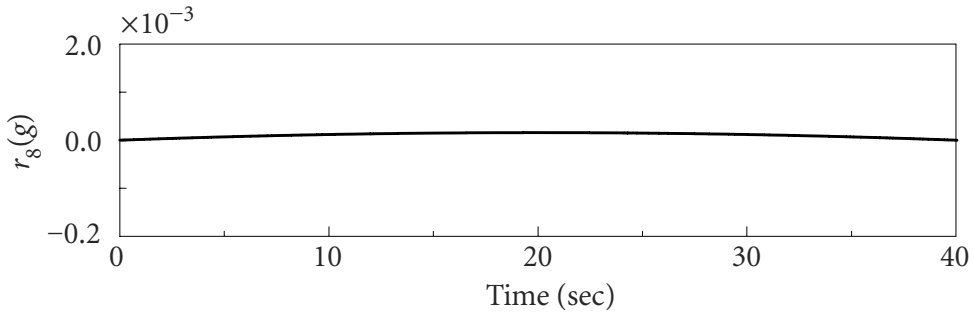

Figure 4.3 Final residue of El-Centro ground motion through empirical mode decomposition

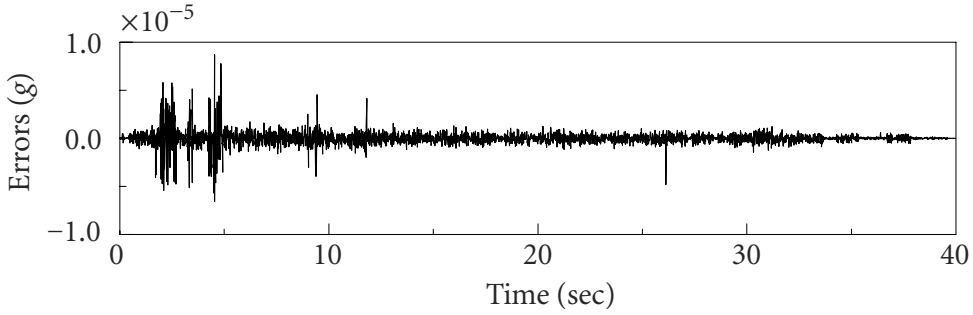

Figure 4.4 Difference between original and reconstructed El-Centro ground motion

where time-dependent amplitude $a(t)$ and phase $\theta(t)$ are expressed as

$$a(t) = \sqrt{C^2(t) + Y^2(t)}, \quad \theta(t) = \tan^{-1} \frac{Y(t)}{C(t)}. \tag{4.2.11}$$

From the polar coordinate expression of equation (4.2.10), the instantaneous frequency can be defined as

$$\omega(t) = \frac{\mathrm{d}\theta(t)}{\mathrm{d}t}. \tag{4.2.12}$$

Applying the Hilbert transform to the n intrinsic mode functions (IMF) of $X(t)$ in equation (4.2.8), the earthquake ground motion $X(t)$ can be written as

$$X(t) = \Re \sum_{k=1}^{n} a_k(t) \mathrm{e}^{\mathrm{i} \int \omega_k(t) \mathrm{d}t}, \tag{4.2.13}$$

where $\Re$ denotes the real part, $a_k(t)$ and $\omega_k(t)$ are the time-dependent amplitude and instantaneous frequency associated with the kth IMF, respectively. The residue $r_n(t)$ is not included because of its monotonic property.

Figures 4.5 and 4.6 show all eight time-dependent amplitudes and instantaneous frequencies of IMF of the El-Centro ground motion, respectively, which are generated through the Hilbert-Huang transform (HHT). Eight acceleration response spectra of IMF of the El-Centro ground motion are shown in Figure 4.7. For ease of comparison, the response spectrum of each IMF is normalized by its peak ground acceleration (PGA). Corresponding to the IMF changing from high frequency to low frequency, the characteristic periods of the response spectra, on which the peak values of the spectral accelerations occur, move from short period to long period as shown in Figure 4.7.

Based on equation (4.2.13), the time-dependent amplitude and the instantaneous frequency can be represented as functions of time in a three-dimensional plot, in which the amplitude can be contoured or color-mapped on the frequency-time plane. This frequency-time distribution of the amplitude $H(\omega, t)$ is called the Hilbert Amplitude Spectrum (HAS) or simply Hilbert spectrum. The Hilbert Energy Spectrum (HES) can be produced by replacing the amplitude with its squared values. The HES is widely recognized as the most detailed presentation of a time series in time–frequency–energy manner. The color-mapped HES of the El-Centro earthquake ground motion is shown in Figure 4.8. In the HES, the energy increases with the color changing from light grey to black.

It is noted that the Hilbert transform described in equations (4.2.9)-(4.2.13) is not new. However, the incorporation of the Hilbert transform into the empirical mode decomposition (EMD) and thus the HHT representation of data in equation (4.2.13) are entirely novel (Huang *et al.*, 1998). Huang *et al.* (1998) show that the instantaneous frequency has physical meaning only through its definition on each intrinsic mode function (IMF); by contrast, the instantaneous frequency defined through the Hilbert transform of original data might be less directly related to frequency content because of the violation of the mono-component condition on the Hilbert transform.

In order to generate earthquake ground motions compatible with the target seismic design spectra based on recorded earthquake ground motions, the characteristics of the recorded ground motions should be determined; that is, the amplitudes or energy distributions and the frequency contents of the motions need to be analyzed.

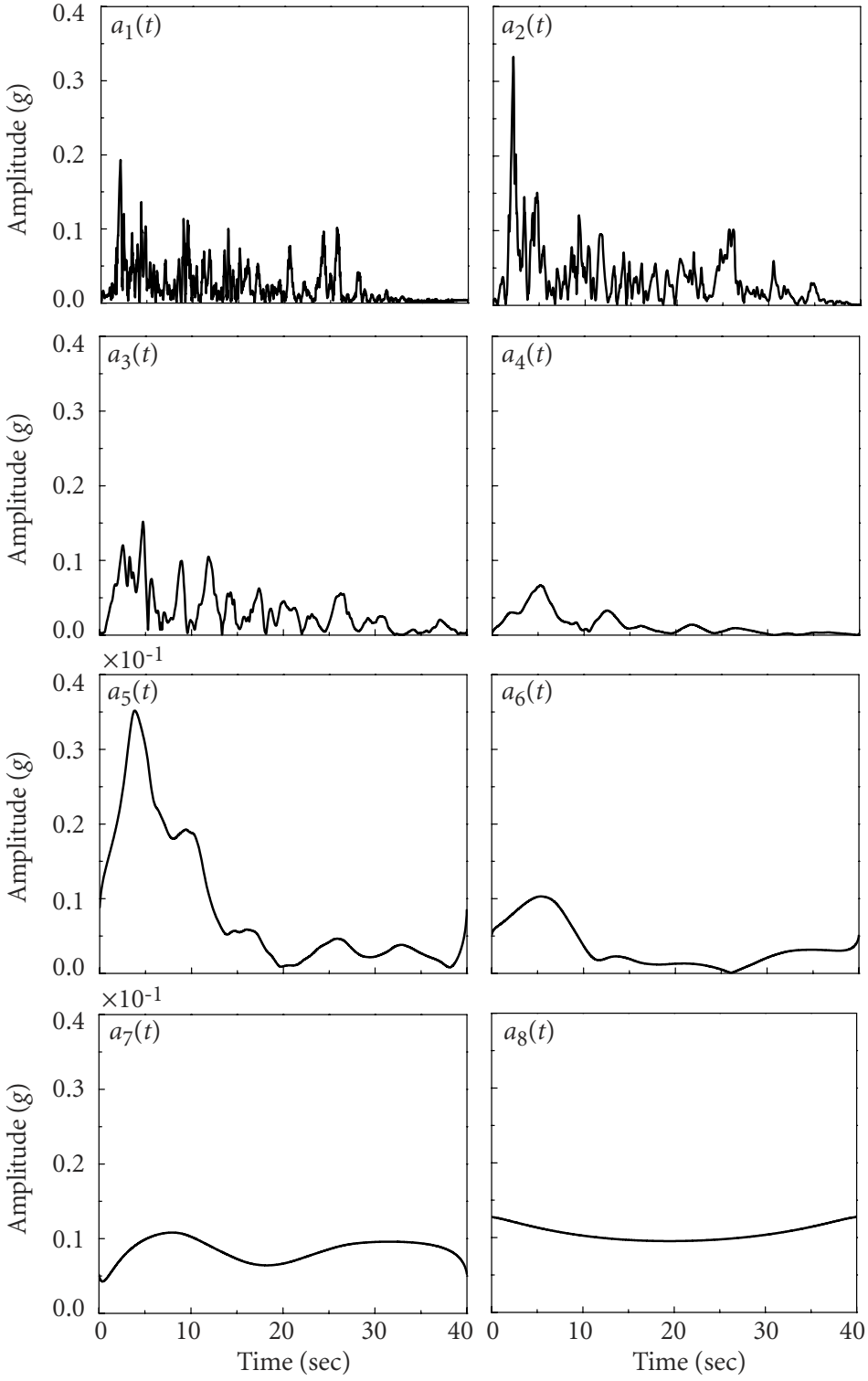

Figure 4.5 Eight time-dependent amplitudes of intrinsic mode functions of the El-Centro motion

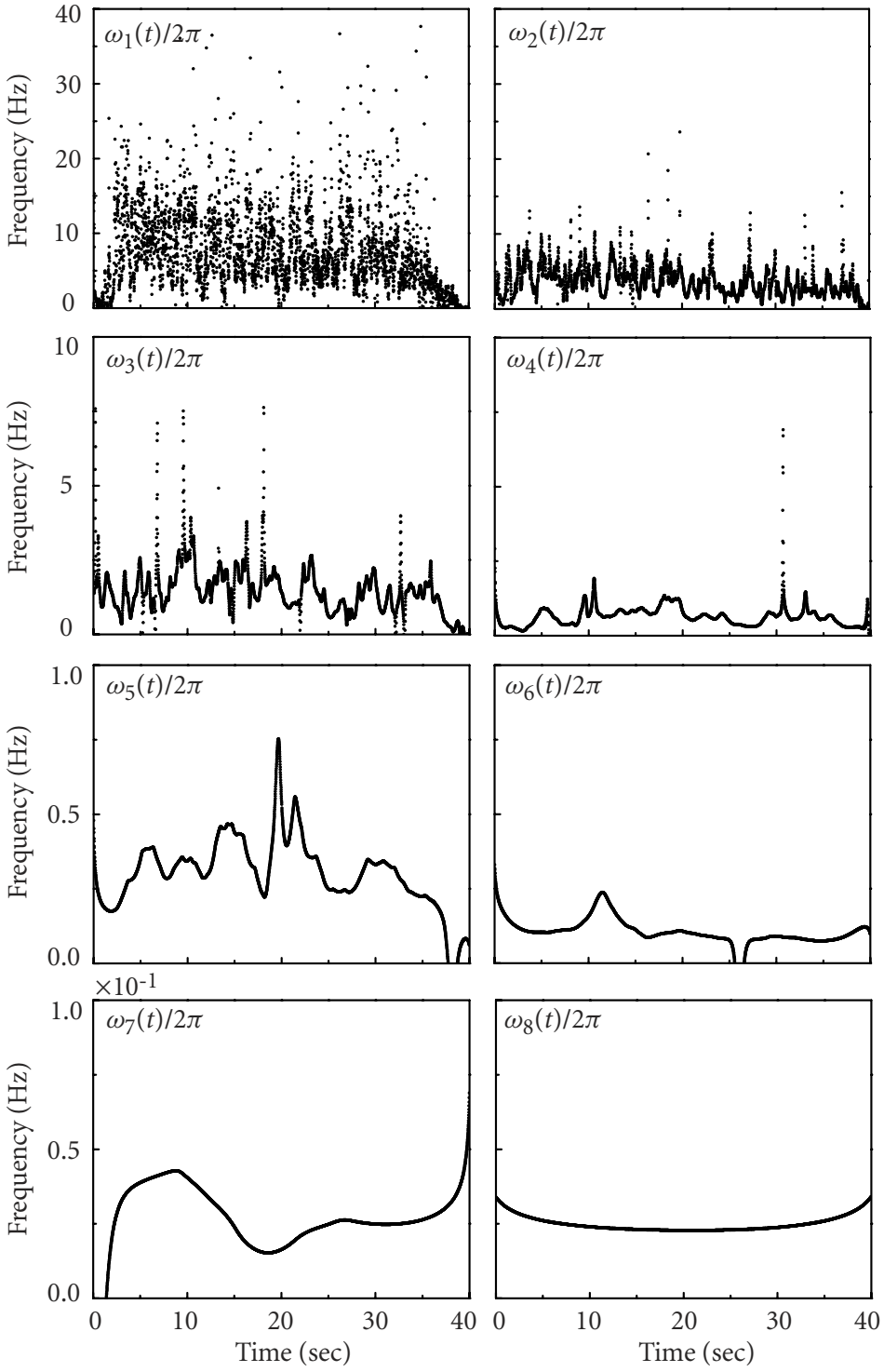

Figure 4.6 Eight instantaneous frequencies of intrinsic mode functions of the El-Centro motion

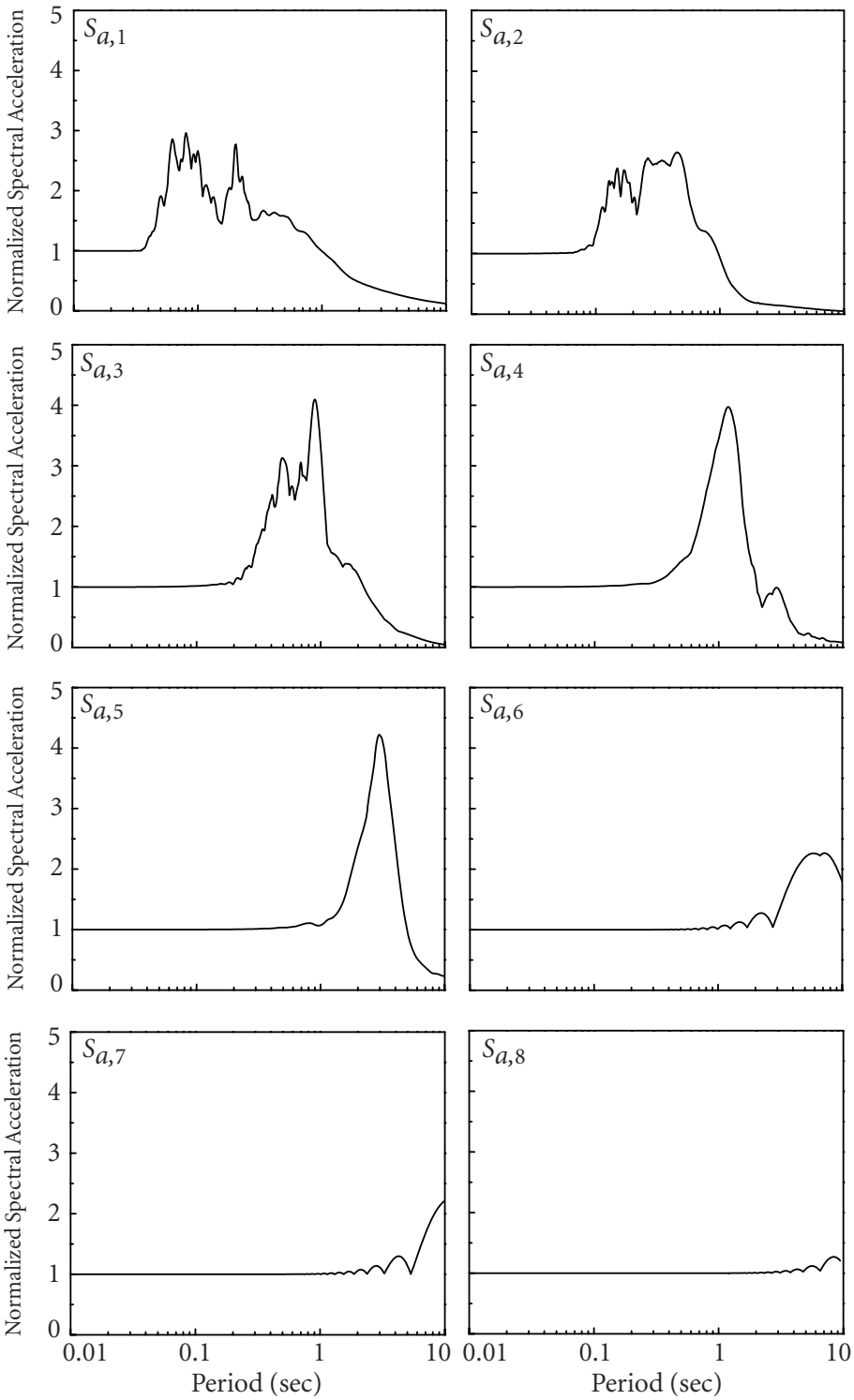

Figure 4.7 Eight normalized response spectra of intrinsic mode functions of the El-Centro ground motion

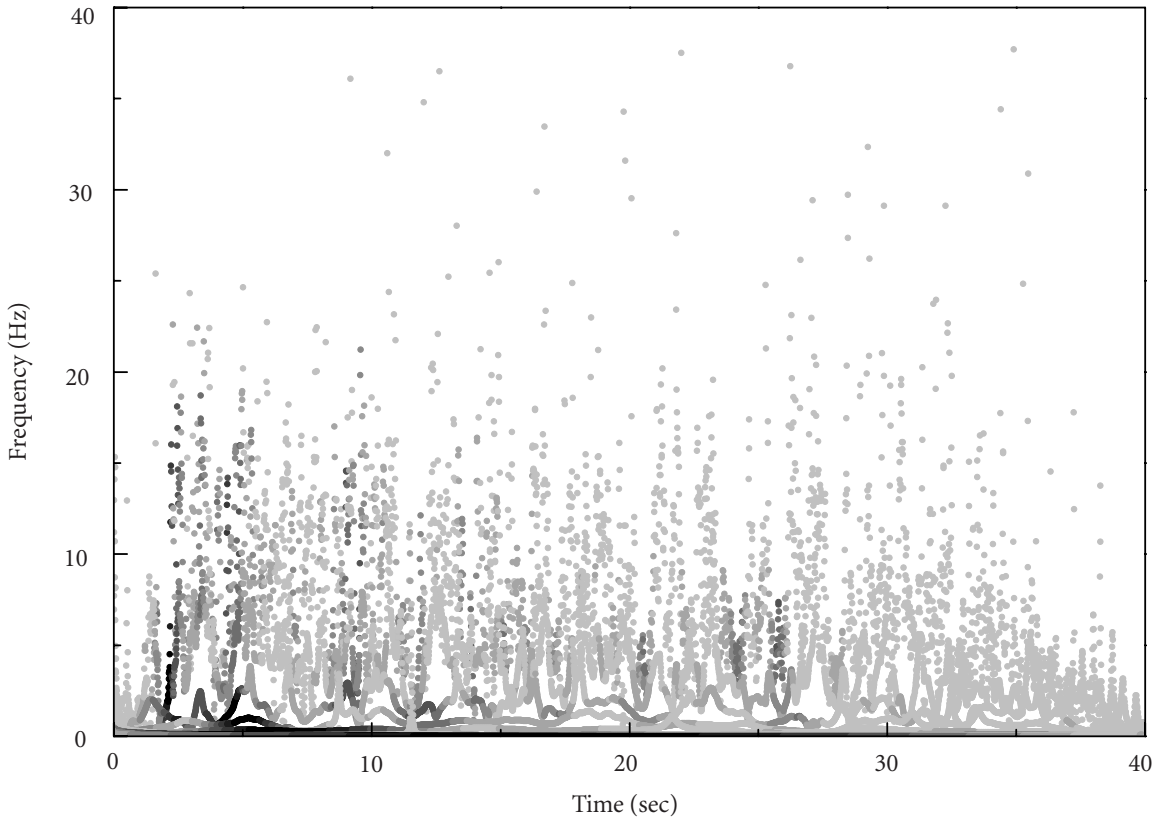

Figure 4.8 Hilbert energy spectrum of El-Centro ground motion

Historically, frequency-related characteristics of data are usually revealed by analyzing the data in transformed domains using the Fourier Transform (FT) technique. This approach can reveal the amplitude or energy distribution and frequency content of the ground motion.

Equation (4.2.13) gives both the amplitude and the frequency of each component as functions of time. The same data if expanded in Fourier representation would be

$$X(t) = \Re \sum_{k=1}^{n} a_k e^{\mathrm{i}\,\omega_k t}, \tag{4.2.14}$$

with both a_k and ω_k being constants. The contrast between equations (4.2.13) and (4.2.14) is clear: the HHT represents a generalized Fourier expansion. The time-dependent amplitude and the instantaneous frequency have not only greatly improved the efficiency of the expansion, but also enabled the expansion to accommodate nonstationary data such as earthquake ground motions.

Because Fourier transform expresses data in terms of a superposition of trigonometric functions, it typically needs many harmonic components to simulate non-sinusoidal wave-trains, which causes low efficiency of the expansion. For the HHT, a small number of components, usually around 10, are generated. The adaptivity is then achieved, because the information contained in the data is preserved as the basis of each component derived from the data themselves.

Fourier Spectral Analysis (FSA) (see Appendix A.3) is meaningful only for stationary data. The FSA defines harmonic components globally. It yields average characteristics over the duration of the data window, even if those detailed characteristics, e.g., dominant frequencies, may change significantly over different portions of the window. For the HHT, the amplitude and the instantaneous frequency of each component change with time, which achieves the locality for nonstationary data.

The Hilbert-Huang transform (HHT) is therefore an adaptive and highly efficient decomposition method to generate the time-dependent amplitudes and instantaneous frequencies of the nonstationary earthquake ground motions without distorting the information contained in the data.

4.3 Spectral Matching for Single Motions

To generate a spectrum-compatible earthquake ground motion, the target seismic design spectrum needs to be determined first. The seed recorded earthquake ground motions are then selected according to the type of the selected target design spectra.

As discussed in Chapter 3, from the statistical analysis of a large number of worldwide recorded ground motions or probabilistic seismic hazard analysis (PSHA), various types of target seismic design spectra have been proposed. They mainly include: Conventional Design Spectrum (CDS) (Newmark *et al.*, 1973, NRC, 1973, CSA, 1981, UBC, 1997), predicted spectrum based on ground-motion prediction equations (GMPEs) (McGuire, 1995), uniform hazard spectrum (UHS) (NBCC, 2005, ASCE, 2006, Atkinson and Boore, 2007, NBCC, 2010), conditional mean spectrum considering ε (CMS-ε) (Baker and Cornell, 2006b), vector-valued uniform hazard spectrum (VUHS) (Ni *et al.*, 2011d), vector-valued

non-uniform hazard spectrum (VNUHS), and vector-valued conditional uniform hazard spectrum (VCUHS) (Ni *et al.*, 2012).

Conceptually, each seismic design spectrum is determined by combining the seismic hazard contributions from a large number of recorded ground motions to account for large uncertainties of earthquake ground motions. To generate representative (spectrum-compatible) earthquake ground motions, it is desirable to properly characterize and use the valuable information contained in multiple selected seed recorded ground motions. In the generation procedure presented in this section, the HHT is applied to analyze and identify the useful information contained in multiple recorded ground motions, based on which a spectrum-compatible ground motion is generated.

For the selection of recorded ground motions, scalar seismic hazard deaggregation (SHD), as discussed in Section 2.4.1, has been widely used as a useful tool. It provides a representative earthquake in terms of earthquake magnitude and source-site distance, which contributes dominant seismic hazard to spectral acceleration at a specified vibration period at the site of interest. Since the existing seismic design spectra are derived from various methodologies or techniques, their intrinsic physical meanings are different. The use of the scalar SHD for the selection of seed recorded ground motions to various types of seismic design spectra is discussed in the following.

A CDS is the statistical result of processing a large number of ground motions recorded from different earthquakes with different magnitudes and distances. The UHS or VUHS possesses a relatively wide-band spectral shape, which is also contributed from earthquakes with different magnitudes and distances. According to the theory of wave propagation, strong motions of small near-field earthquakes arrive earlier and contribute more hazard to spectral accelerations at short vibration periods, while strong motions of large far-field earthquakes arrive later and contribute more hazard to spectral accelerations at long vibration periods. Hence, using scalar SHD, a representative earthquake with small magnitude and short distance is calculated towards spectral acceleration at a specified short period, and another earthquake represented by large magnitude and long distance is obtained towards spectral acceleration at a specified long period. These two representative earthquakes from the scalar SHD are then used for the selection of seed recorded ground motions.

As discussed in Chapter 3, predicted spectra based on GMPEs, CMS-ε, VNUHS, or VCUHS possess relatively narrow-band spectral shapes, concentrated at a specified vibration period or a range of vibration periods. The seed recorded earthquake ground motions can then be selected according to the magnitude-distance pairs determined towards spectral accelerations at the specified vibration periods using the scalar SHD.

It is noted that the number of selected recorded ground motion sets depends much on the compatibility level required. In principle, the more sets of earthquake ground motions are used, the higher level of compatibility can be achieved. In this Chapter, three sets (two horizontal and/or one vertical components for each set) of recorded ground motions are generally selected for a target design spectrum, as it has been demonstrated that they are enough to achieve a high level of compatibility (Ni *et al.*, 2011A). It has been shown that an acceptable level of compatibility can be achieved using even a single recorded ground motion (Ni *et al.*, 2010).

In the seismic design practice, once a target seismic design spectrum is selected, the entire spectrum is treated as a single design earthquake regardless of the way in which the spectrum is established. The generated spectrum-compatible earthquake ground motions are regarded as from this single scenario earthquake (i.e., the target spectrum), although the target spectrum is an idealized model of the surrounding seismic hazard and each of the generated spectrum-compatible ground motions contains a combined effect of different earthquakes from small near-field earthquakes to large far-field earthquakes. The generated ground motions then contain the characteristics of multiple recorded ground motions, which is consistent with the physical meanings of the target design spectra. In the proposed generation procedure, any seismic design spectrum can be selected as a target design spectrum based on engineering practice.

As discussed above, multiple recorded ground motions will be combined to generate a spectrum-compatible ground motion. In practice, most recorded ground motions have different motion durations. To maintain the consistency of the time axis across the ground motions, the seed recorded ground motions can be truncated at their ends under the premise that the portions of strong motion are preserved. The strong motion portion can

be determined as the duration in which the cumulative energy in an accelerogram moves from 5% to 75% of the total cumulative energy (ASCE, 2005).

The recorded earthquake accelerograms used in this chapter are searched from strong motion databases of the Pacific Earthquake Engineering Research (PEER) center and the Natural Resources Canada (NRCAN). All the selected recorded ground motions are recorded by free-field instruments or instrument shelters at firm ground. The magnitude-distance pairs of the selected recorded earthquake ground motions are approximately consistent with the results of the SHD and, as a result, generally contribute the dominant seismic hazard to the corresponding sites of interest.

4.3.1 Generation of Single Ground Motions

Having determined the target seismic design spectrum and the seed recorded earthquake ground motions, a spectrum-compatible ground motion can be generated using the HHT and optimization technique (Ni *et al.*, 2011A).

To obtain the time series basis for the ground-motion generation, each selected recorded earthquake ground motion is decomposed into several intrinsic mode functions (IMF) via empirical mode decomposition (EMD). The n generated IMF from the selected recorded ground motions are treated as the basis for representing a nonstationary earthquake ground motion time-history. Compared to Fourier transform and wavelet transform, the basis to represent a time-series are derived from the recorded ground motions themselves by the HHT. Hence, these IMF preserve the information of the nature of the selected ground motions, which is consistent with the seismic hazard circumstances at the site of interest.

Each IMF is then transferred from time domain to frequency domain through Hilbert spectral analysis (HSA). The time-dependent amplitude and the instantaneous frequency of each IMF are generated. The HHT amplitudes and the instantaneous frequencies of the recorded ground motions are thus scaled to obtain the modified earthquake ground motion

$$\mathrm{TH}(\mathbf{x}, t) = \Re \sum_{k=1}^{n} \left[x_k \, a_k(t) \right] \mathrm{e}^{\mathrm{i}\, x_{n+k} \int \omega_k(t) \mathrm{d}t}, \tag{4.3.1}$$

where $x_1, x_2, \ldots, x_n$ are the amplitude scaling parameters, and $x_{n+1}, x_{n+2}, \ldots, x_{2n}$ are the frequency scaling parameters. $\mathbf{x} = \{x_1, x_2, \ldots, x_{2n}\}^T$ is the vector of scaling parameters.

The purpose of generating spectrum-compatible earthquake ground motion is to make the ground motion time-history rich in all frequencies and covering a stated period range without "peaks and troughs" that may bias structural responses. By scaling the amplitudes of the IMF, the frequency contents over corresponding frequency ranges can be changed to enrich the time-history in all frequencies as required. Since each IMF contains a range of frequencies, adjacent IMF of each recorded ground motion may overlap or separate in the frequency domain. Slightly adjusting the instantaneous frequencies of the IMF can ensure that there are no significant gaps in the frequency contents of the IMF.

An optimization model is then constructed:

$$\begin{aligned} &\text{minimize:} \quad V = \sum_{p=1}^{P} f_p(\mathbf{x}), \quad f_p(\mathbf{x}) = \frac{\left| S[\mathrm{TH}(\mathbf{x}, t), T_p] - S_{\mathrm{T}}(T_p) \right|}{S_{\mathrm{T}}(T_p)}, \\ &\text{subjected to constraints:} \quad x_k > 0, \quad k = 1, 2, \ldots, n, \end{aligned} \tag{4.3.2}$$

where $S[\mathrm{TH}(\mathbf{x}, t), T_p]$ is the spectral acceleration of the earthquake ground motion $\mathrm{TH}(\mathbf{x}, t)$ at a specific period T_p, $S_{\mathrm{T}}(T_p)$ is the spectral acceleration of the target design spectrum at T_p (the subscript "T" standing for Target), P is the total number of period points at which the response spectra are calculated, and V is called the objective function.

There are a great number of optimization techniques, such as the Quasi-Newton method and the Nelder-Mead method (Nocedal and Wright, 1999), which can be used to achieve the minimization of the objective function V to make the response spectrum of the modified earthquake ground motion as close to the target design spectrum as possible. For the optimization problems in this chapter, the nonlinear Quasi-Newton algorithm (constrained nonlinear multi-variable line-search) is applied. A detailed description of the Quasi-Newton algorithm can be found in Nocedal and Wright (1999).

By solving the optimization problem in equation (4.3.2) using a suitable optimization algorithm, a spectrum-compatible earthquake ground motion, whose response spectrum closely matches the target design spectrum, can be obtained. It contains the desired characteristics of ground motions from actual earthquakes that contribute relatively the dominant seismic hazard to the site of interest. The generated spectrum-compatible earthquake

ground motion also preserves the nonstationary characteristics of the seed recorded ground motions through the HHT.

It is noted that the earthquake ground motion time-histories generated by the proposed method may need appropriate baseline corrections to eliminate unrealistic long period components so that the corresponding velocity and displacement time-histories do not become unrealistic and have non-zero residuals. However, the acceleration time-histories and their response spectra at vibration periods of most engineering interest usually are not sensitive to the specific baseline correction (Boore *et al.*, 2002). Hence, the baseline correction, based on linear polynomial equation and Butterworth filter from 0.05 Hz to 100 Hz with the order of 4, is applied to each generated spectrum-compatible earthquake ground motion at the end of the generation procedure.

4.3.2 Numerical Examples

For illustration purpose, four numerical examples are presented in this section. The uniform hazard spectra (UHS) for Quebec City and La Malbaie, respectively, are used as the target seismic design spectra. The UHS at Quebec City and La Malbaie were derived for ordinary building structures by the Geological Survey of Canada (GSC) (Humar and Rahgozar, 2000).

The conventional design spectra (CDS) for nuclear energy facilities in New York City and Chicago, respectively, are also used as the target seismic design spectra. The CDS at New York City and Chicago are from the U.S. Geological Survey (USGS) and Regulatory Guide 1.60 (NRC, 1973).

In general, structures of nuclear energy facilities (existing plants and new designs) are very stiff with fundamental frequencies in the range of 3-15 Hz (EPRI, 2007). It is adequate for the frequency range of the CDS for nuclear energy facilities to include from 0.1 Hz to 25 Hz. The selected UHS for non-nuclear building structures also stop at frequency 25 Hz, since these structures are usually more flexible than nuclear structures (NBCC, 2005, NBCC, 2010).

Information of the selected target seismic design spectra is listed in Table 4.1. All four seismic design spectra are for firm ground conditions (average shear wave velocity to a depth of 30 m greater than 750 m/sec) and for 5% critical damping.

The seed recorded ground motions for each site are selected based on the results of the seismic hazard deaggregation (SHD) (Halchuk and Adams, 2004, Harmsen *et al*., 1999). The results of the SHD and the selected recorded earthquake ground motions for all sites are listed in Tables 4.2 and 4.3, respectively.

Table 4.1: Target seismic design spectra

Location	Type	Probability of exceedence	Resource
Quebec City	UHS	0.0004 per annum	GSC
La Malbaie	UHS	0.0004 per annum	GSC
New York City	CDS	0.0004 per annum	RG 1.60 and USGS
Chicago	CDS	0.0004 per annum	RG 1.60 and USGS

Table 4.2: Mean values of seismic hazard deaggregation

Location	Vibration period	Seismicity	Hypocentral distance	Moment magnitude
Quebec City	s(0.2 sec)*	0.56 g	41 km	6.1
	s(1.0 sec)*	0.14 g	100 km	7.1
La Malbaie	s(0.2 sec)*	2.30 g	20 km	6.9
	s(1.0 sec)*	0.57 g	22 km	7.1
New York City	s(0.2 sec)*	0.423 g	37.7 km	5.79
	s(1.0 sec)*	0.093 g	102.4 km	6.39
Chicago	s(0.2 sec)*	0.184 g	85.1 km	5.60
	s(1.0 sec)*	0.065 g	357.6 km	7.11

$*$ $s(T)$ is the uniform hazard spectral acceleration at vibration period T.

Table 4.3: Selected recorded earthquake ground motions

Location	EQ*	TP§	D† (km)	M‡	Hor-1⋆	Hor-2⋆
Quebec City	WN	SN	21.2	6.0	A-MTW000	A-MTW090
	NPS	SN	25.8	6.0	SIL000	SIL090
	LP	LF	79.7	6.9	RIN000	RIN090
La Malbaie	LP	SN	11.2	6.9	G01000	G01090
	NOR	SN	22.7	6.7	WON095	WON185
	DUZ	LF	30.2	7.1	1060-N	1060-E
New York City	WN	SN	21.2	6.0	A-MTW000	A-MTW090
	SA	SN	52.2	5.9	S16-214	S16-124
	LP	LF	79.7	6.9	RIN000	RIN090
Chicago	SA	SN	96.9	5.9	S08-063	S08-333
	SA	SN	116.4	5.9	S10-000	S10-270
	AQ	LF	412.1	7.1	HAD-EW	HAD-NS

∗ Earthquake names: WN, Whittier Narrows Earthquake, 1987/10/01 14:42; NPS, N. Palm Springs Earthquake, 1986/07/08 09:20; LP, Loma Prieta Earthquake, 1989/10/18 00:05; NOR, Northridge Earthquake, 1994/01/17 12:31; DUZ, Duzce Earthquake, Turkey, 1999/11/12 18:57; SA, Saguenay Earthquake, 1988/11/25 23:46; AQ, Aqaba Earthquake, 1995/11/22 04:18.

§ Earthquake types: SN, Small Near-field Earthquake; LF, Large Far-field Earthquake.

† D is the closest distance to fault rupture, which is generally the hypocentral distance.

‡ M is the moment magnitude.

⋆ Names of the horizontal components of the records, which can be searched from PEER and NRCAN databases.

Compared to the target design spectra, the short period portion of the response spectrum of an recorded ground motion is highly non-smooth. For Quebec City, La Malbaie, New York City, and Chicago, three sets of recorded ground motions (two orthogonal horizontal ground motions in one set) are selected for each of these four sites. To make the resulting response spectrum closely match the target design spectrum, two sets of ground motions recorded from small near-field earthquakes are used to characterize the short period plateau portion of the target design spectrum, and one set of ground motions recorded from a large far-field earthquake is used to describe the long period portion of the target design spectrum.

The response spectra of the generated earthquake ground motions and the selected seed recorded ground motions for each site are shown in Figures 4.9-4.12, respectively. The resulting response spectra closely match the target design spectra. The generated spectrum-compatible earthquake ground motions and their corresponding seed recorded ground motions for each site are shown in Figures 4.13, 4.15, 4.16, 4.17, 4.19, 4.20, 4.21, 4.23, 4.24, 4.25, 4.27, and 4.28, respectively. The generated spectrum-compatible earthquake ground motions generally preserve the temporal characteristics of the seed recorded ground motions. For example, as shown in Figure 4.13, both the early arrival small near-field strong motions and the late arrival large far-field strong motions are merged into the generated motion, which is consist with the UHS physical meaning that both small near-field and large far-field earthquakes contribute the seismic hazard to the design earthquake.

In matching the short period portion of the response spectrum of the generated ground motion to the target spectrum, the short period intrinsic mode functions (IMF), i.e., the first one or two components, are the main contributors. However, because these short period IMF cover a relatively wide range of period, it is very difficult to just match the short period portion of the generated and target spectra without significantly affecting the match in the mid and long period ranges. Since the optimization model in equation (4.3.2) can be regarded as a comprise in selecting the scaling parameters to reach a minimal overall relative difference between the generated and the target spectra, it is not hard to see that the optimization model tends to sacrifice the match in the short period portion.

As shown in Figure 4.9, the difference between the resulting spectrum and the target spectrum is relatively large over the period range from 0.04 sec to 0.1 sec. Further studies may be needed to improve the empirical mode decomposition (EMD) and to decompose the signal into more components in the short period range. The results will also be improved if more earthquake ground motions with higher frequency contents are recorded.

The color-mapped Hilbert energy spectrum of the generated spectrum-compatible earthquake ground motion for each numerical example is shown in Figures 4.14, 4.18, 4.22, and 4.26, respectively. It can be seen that the generated ground motions have sufficient energy over the entire period range. More energy can also be observed at the beginning of the ground motion time-histories in the frequency-time distribution of energy, which is consistent with the nonstationary characteristics of the generated ground motions.

In the numerical examples, the seed earthquake ground motions are decomposed into approximate 50 intrinsic mode functions (IMF) as the basis for generating a spectrum-compatible earthquake ground motion. However, there are overlaps between many response spectra of these IMF, i.e., some IMF occupy similar frequency contents. These overlapping IMF may be redundant for the purpose of generating spectrum-compatible earthquake ground motions.

The purpose of generating spectrum-compatible earthquake ground motion is to make the ground motion time-history rich in all frequencies and covering a stated period range without "peaks and troughs" that may bias structural responses. Hence, a small number of IMF, whose narrow-band response spectra cover from short period to long period without significant gaps between each other, can be selected as the basis for the ground motion generation. To include the crucial information of all seed recorded ground motions, at least one short period IMF is selected from each seed recorded ground motion, induced by small near-field earthquake, as the short period basis, and at least one long period IMF is chosen from each seed recorded motion, induced by large far-field earthquake, as the long period basis.

Figure 4.29 shows 21 narrow-band normalized response spectra of the IMF, which are selected from a pool of 59 IMF for Quebec City following the criteria described in the previous paragraph. As shown in Figure 4.30, a satisfactory resulting spectrum is achieved

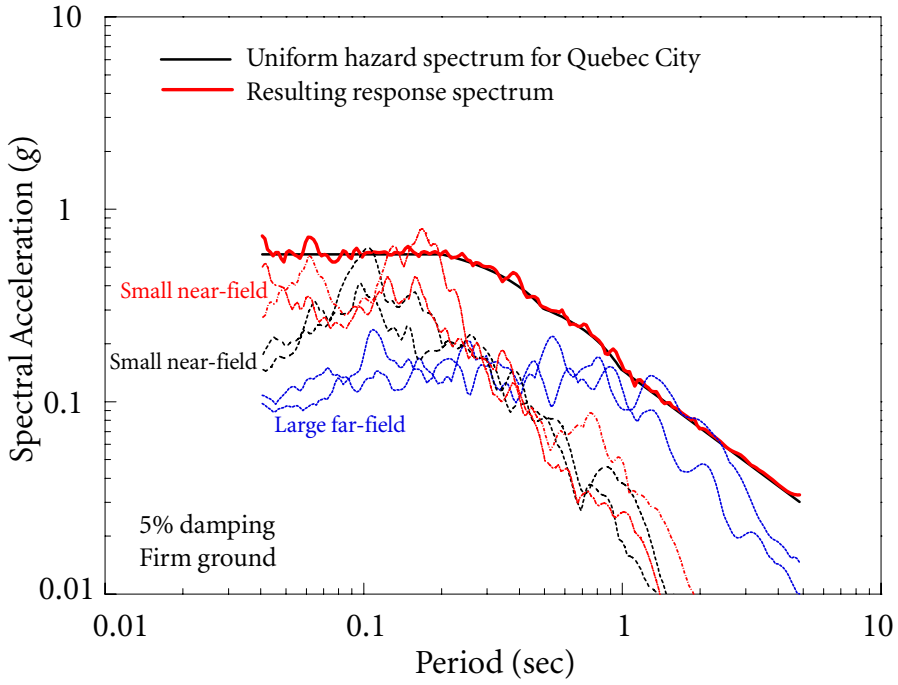

Figure 4.9 Quebec City: target uniform hazard spectrum, response spectrum of generated earthquake ground motion, and response spectra of seed recorded earthquake ground motions

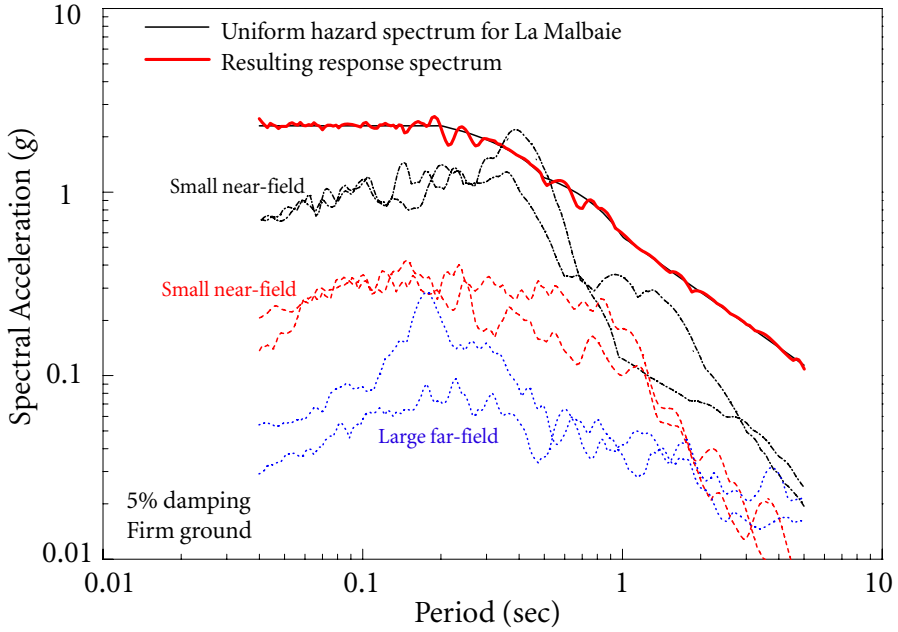

Figure 4.10 La Malbaie: target uniform hazard spectrum, response spectrum of generated earthquake ground motion, and response spectra of seed recorded earthquake ground motions

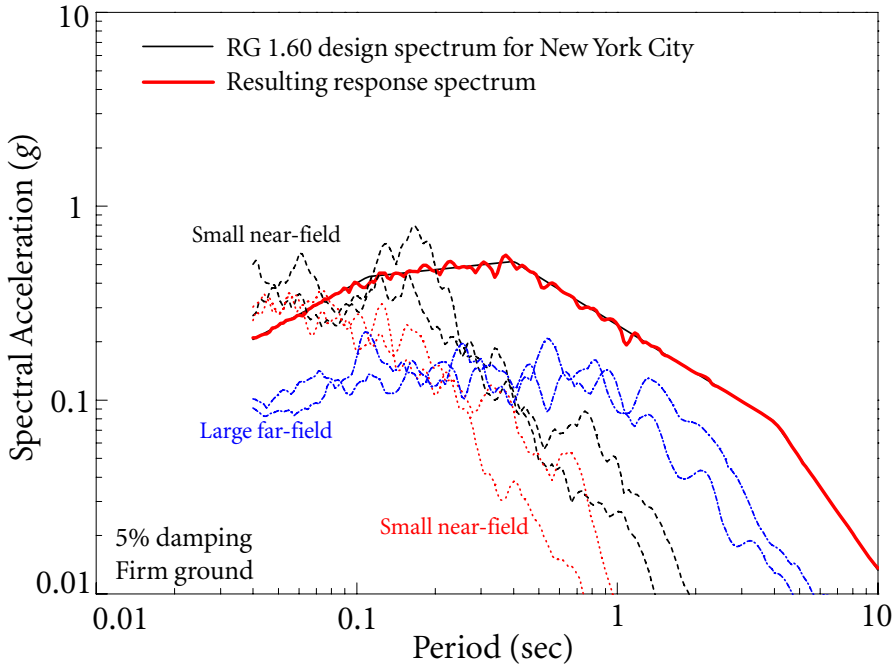

Figure 4.11 New York City: target RG 1.60 design spectrum, response spectrum of generated earthquake ground motion, and response spectra of seed recorded earthquake ground motions

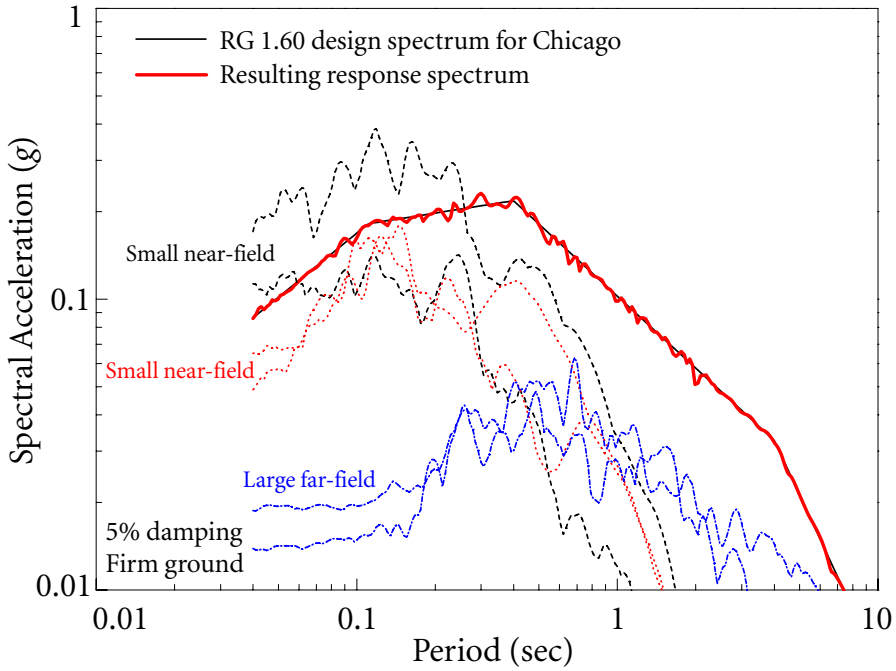

Figure 4.12 Chicago: target RG 1.60 design spectrum, response spectrum of generated earthquake ground motion, and response spectra of seed recorded earthquake ground motions

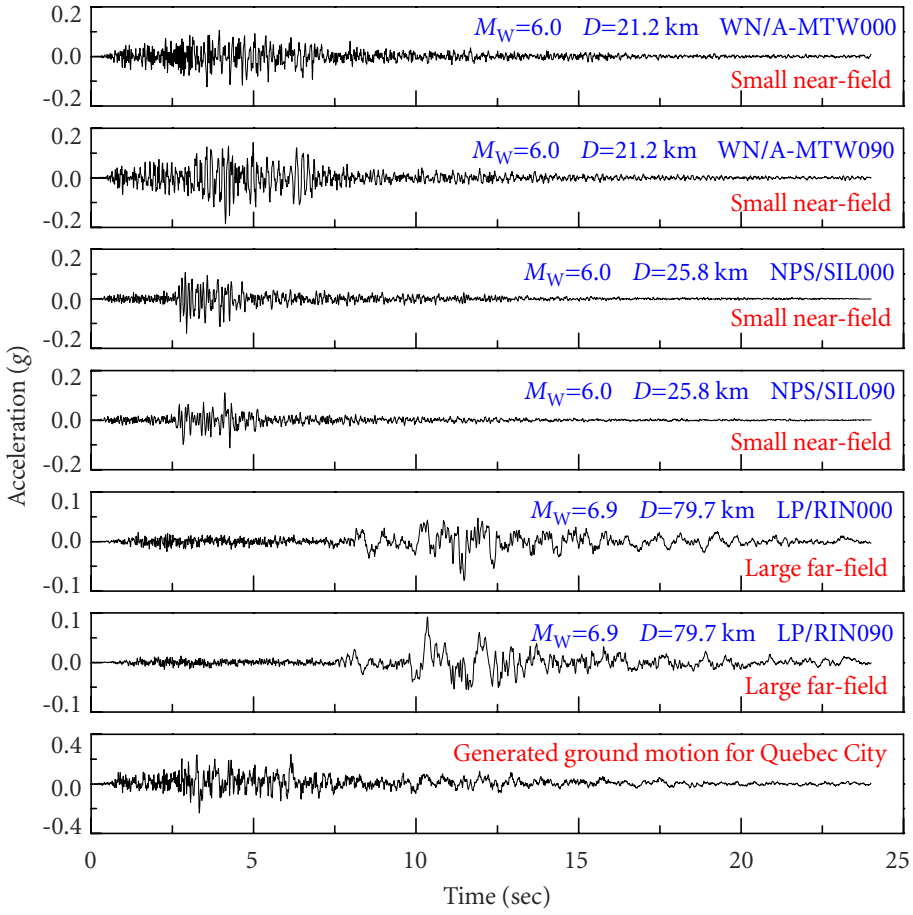

Figure 4.13 Seed and generated earthquake ground motions for UHS at Quebec City

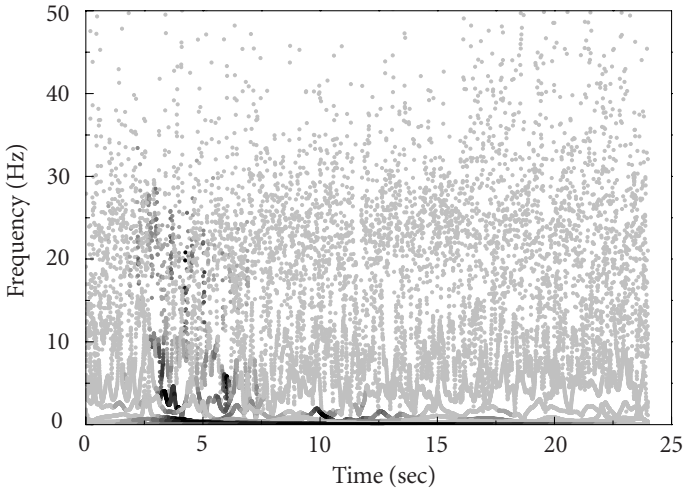

Figure 4.14 Hilbert energy spectrum of generated earthquake ground motion for UHS at Quebec City

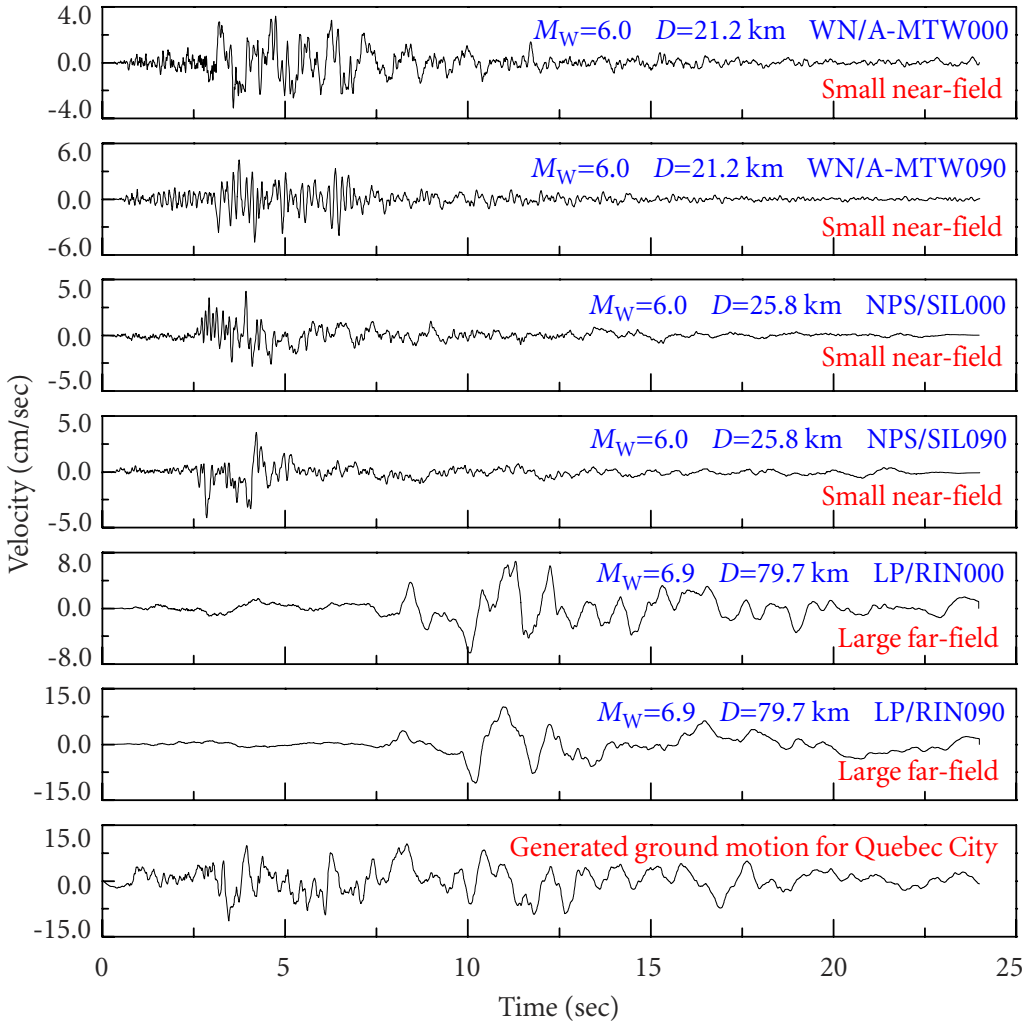

Figure 4.15 Seed and generated earthquake ground motions for UHS at Quebec City

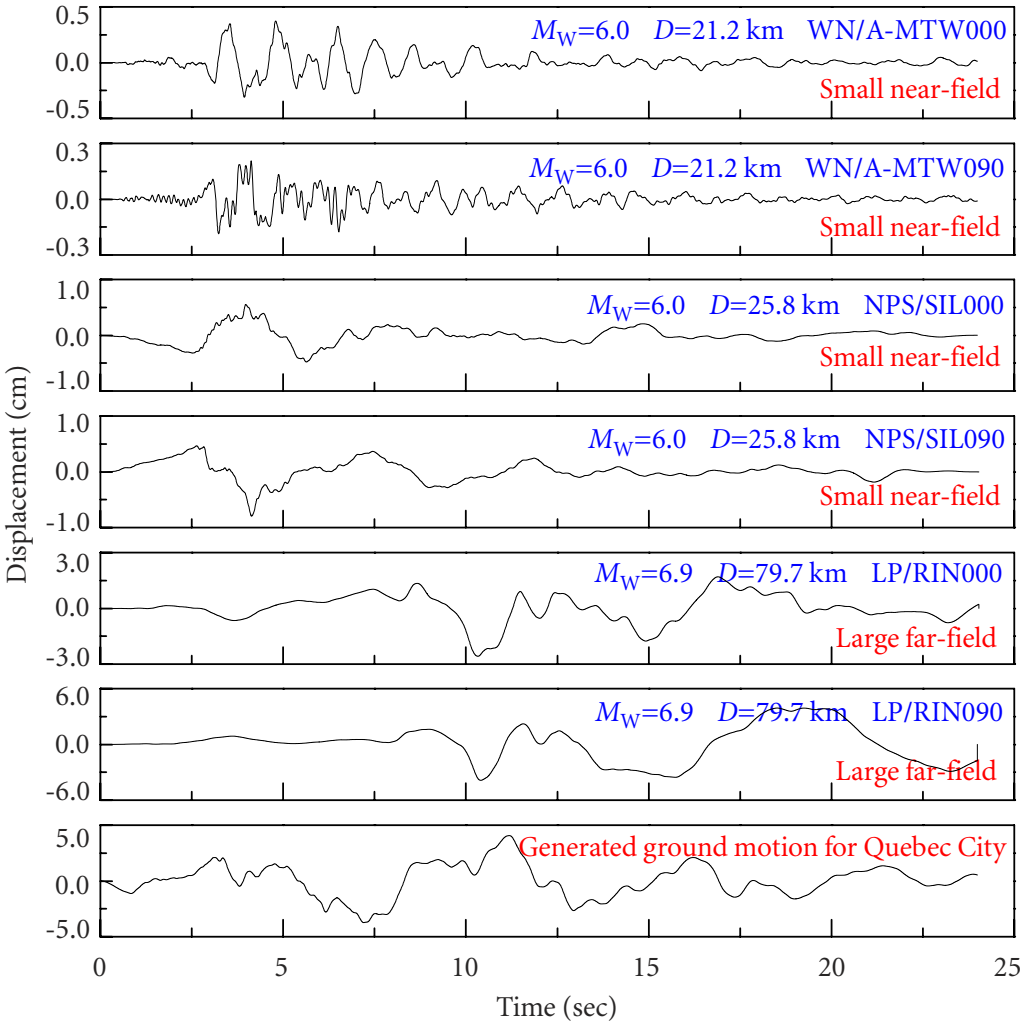

Figure 4.16 Seed and generated earthquake ground motions for UHS at Quebec City

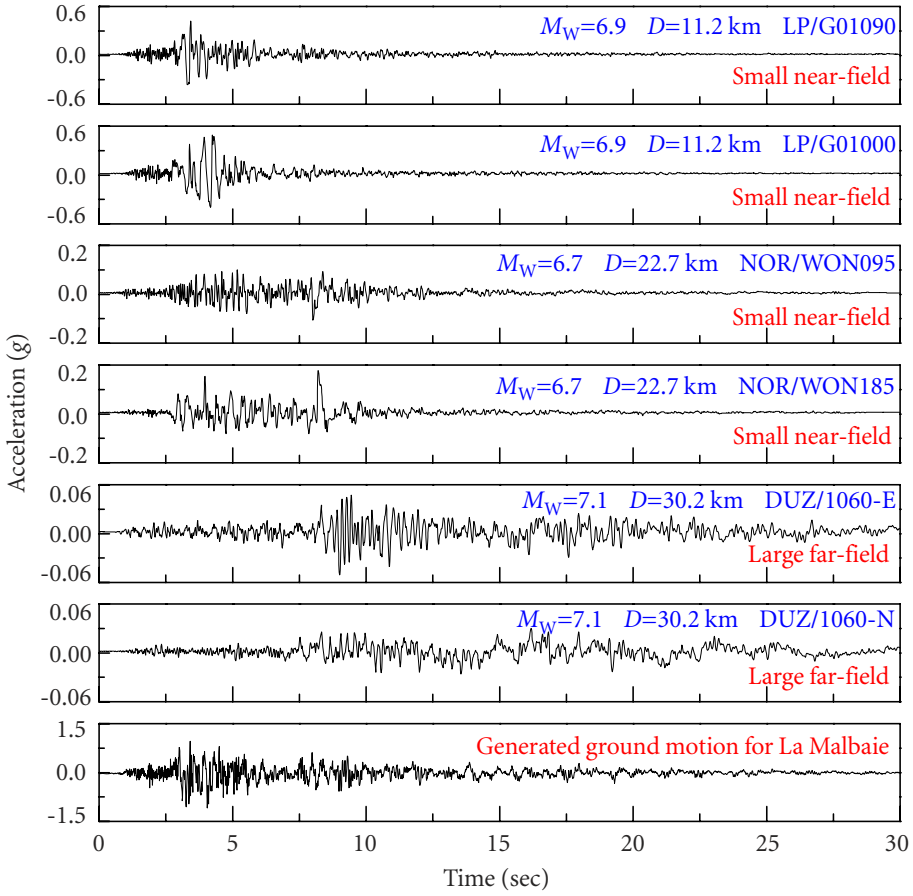

Figure 4.17 Seed and generated earthquake ground motions for UHS at La Malbaie

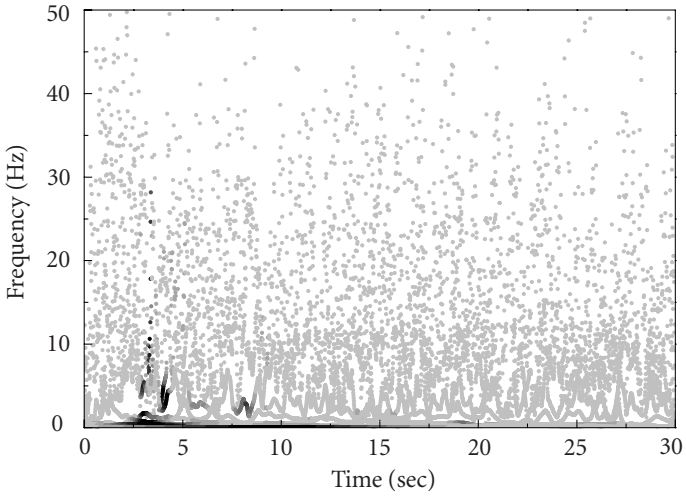

Figure 4.18 Hilbert energy spectrum of generated ground motion for UHS at La Malbaie

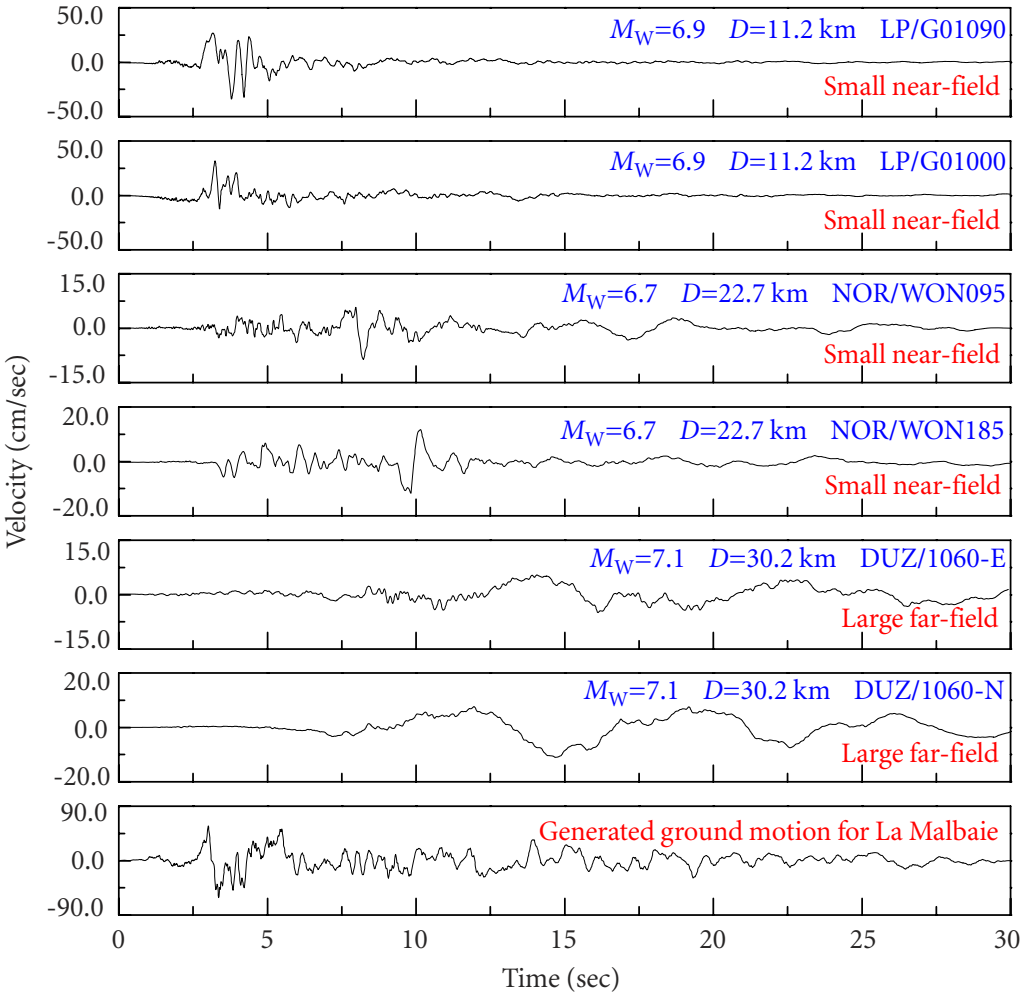

Figure 4.19 Seed and generated earthquake ground motions for UHS at La Malbaie

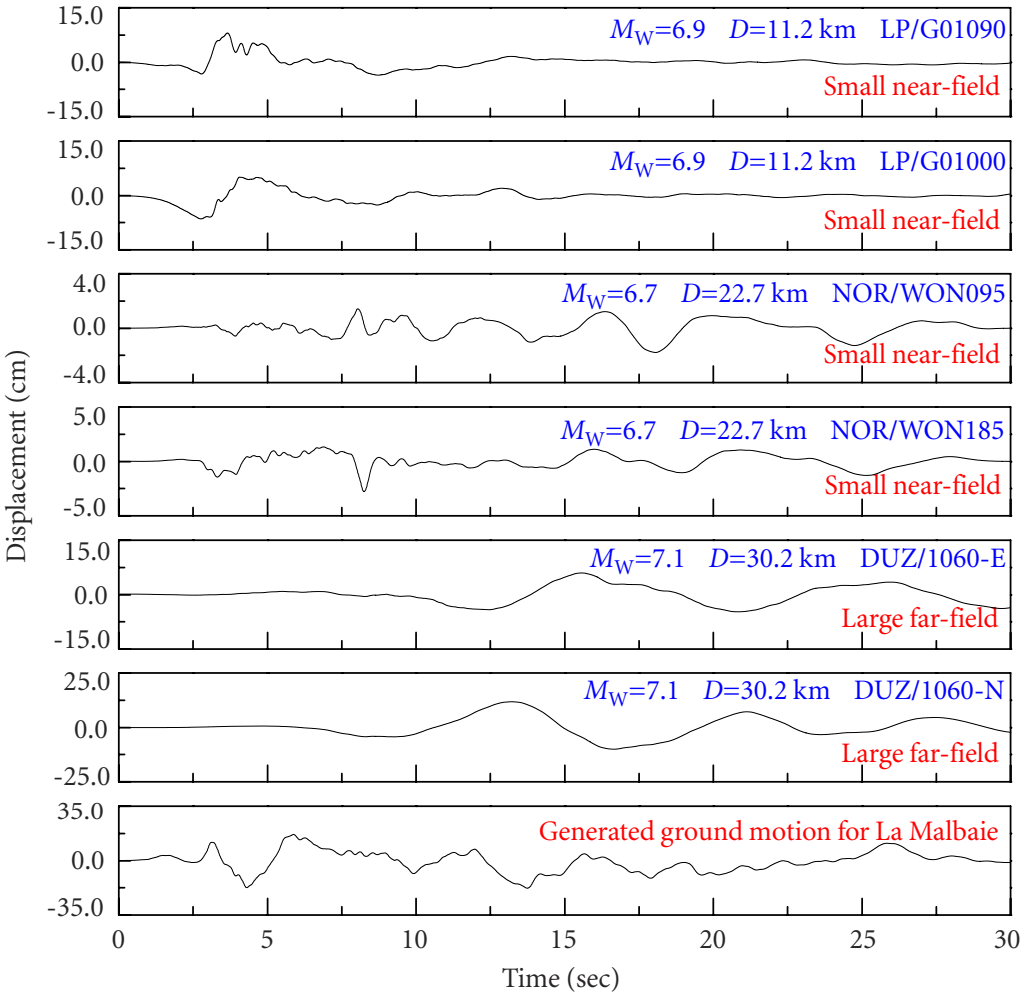

Figure 4.20 Seed and generated earthquake ground motions for UHS at La Malbaie

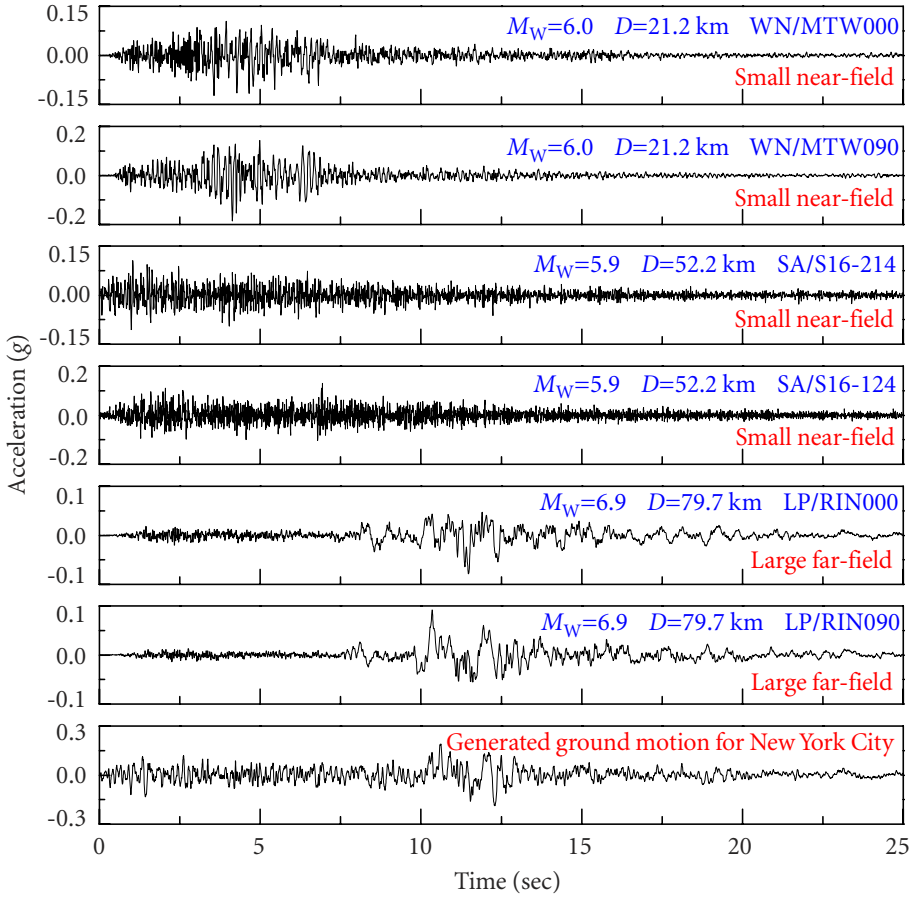

Figure 4.21 Seed and generated earthquake ground motions for CDS at New York City

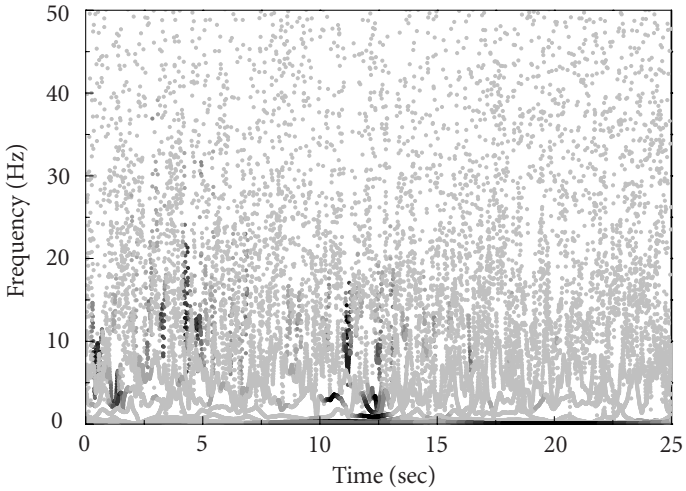

Figure 4.22 Hilbert energy spectrum of generated ground motion for CDS at New York City

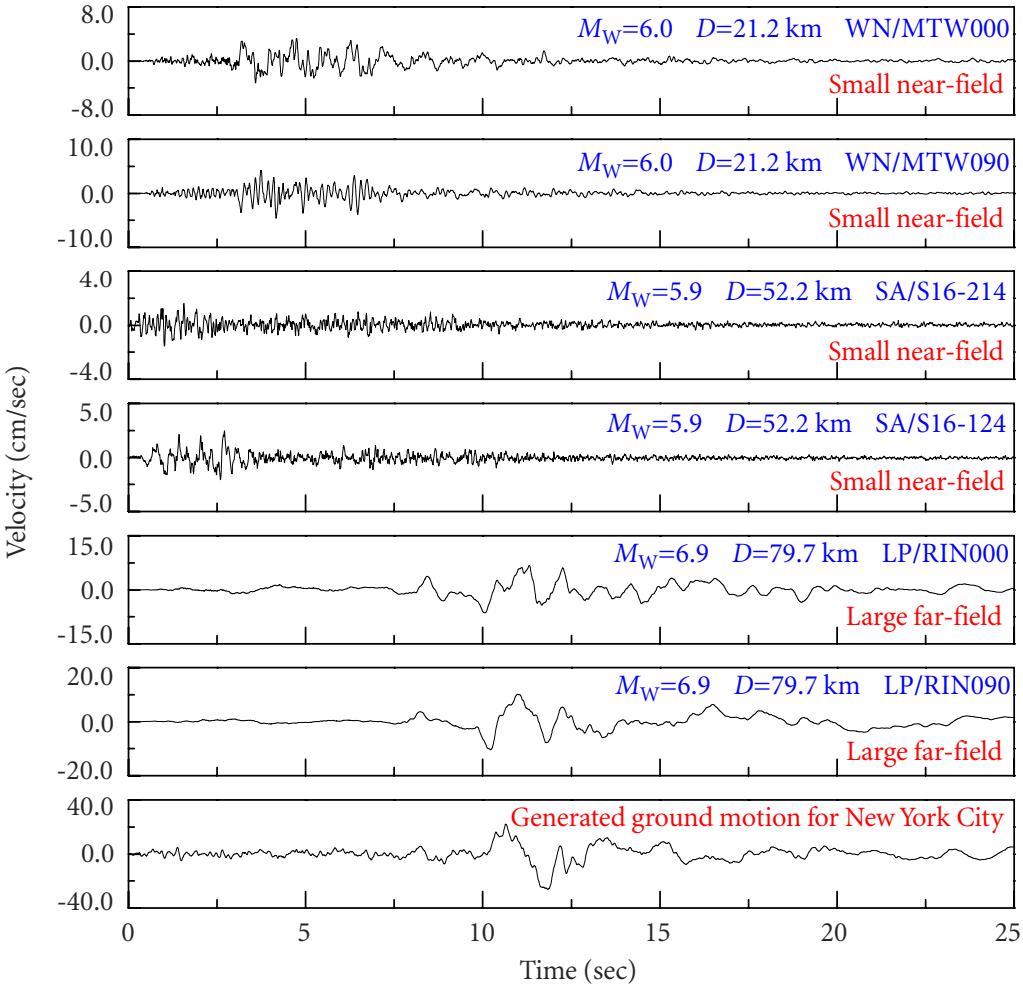

Figure 4.23 Seed and generated earthquake ground motions for CDS at New York City

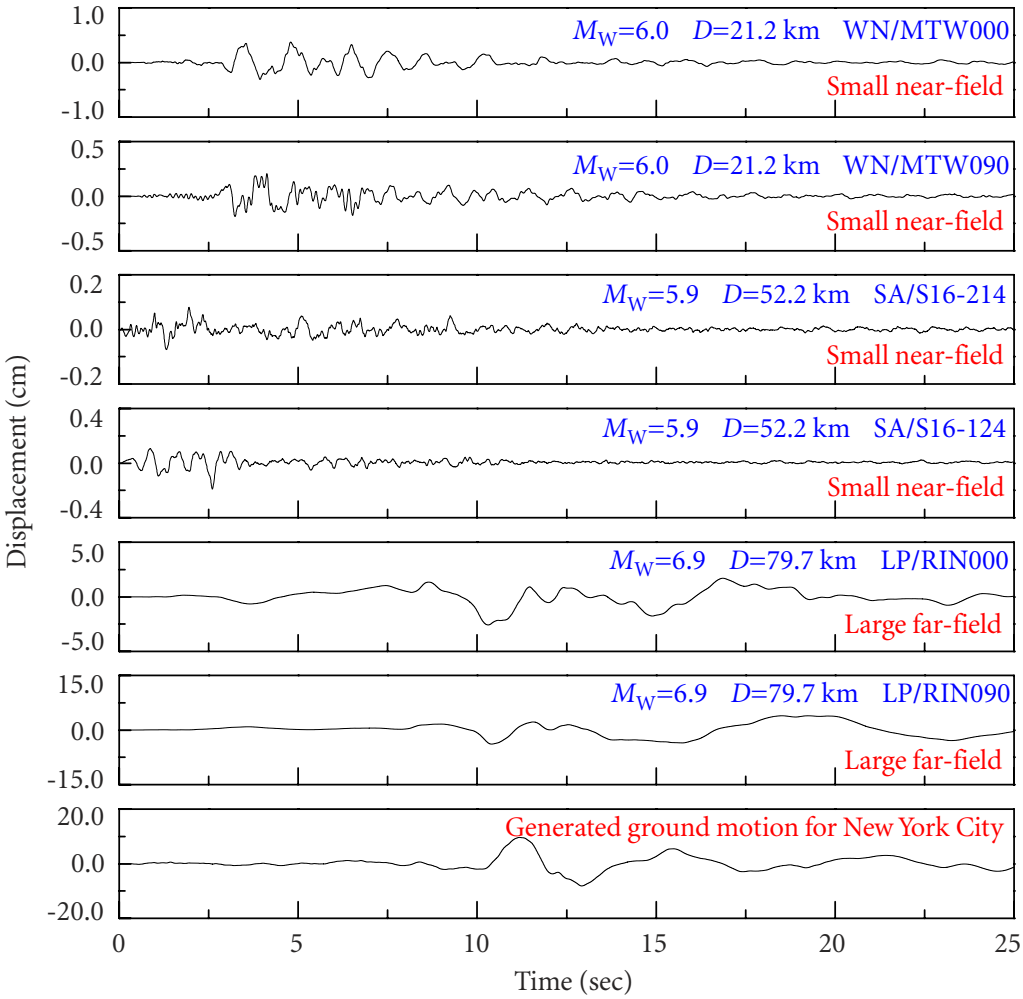

Figure 4.24 Seed and generated earthquake ground motions for CDS at New York City

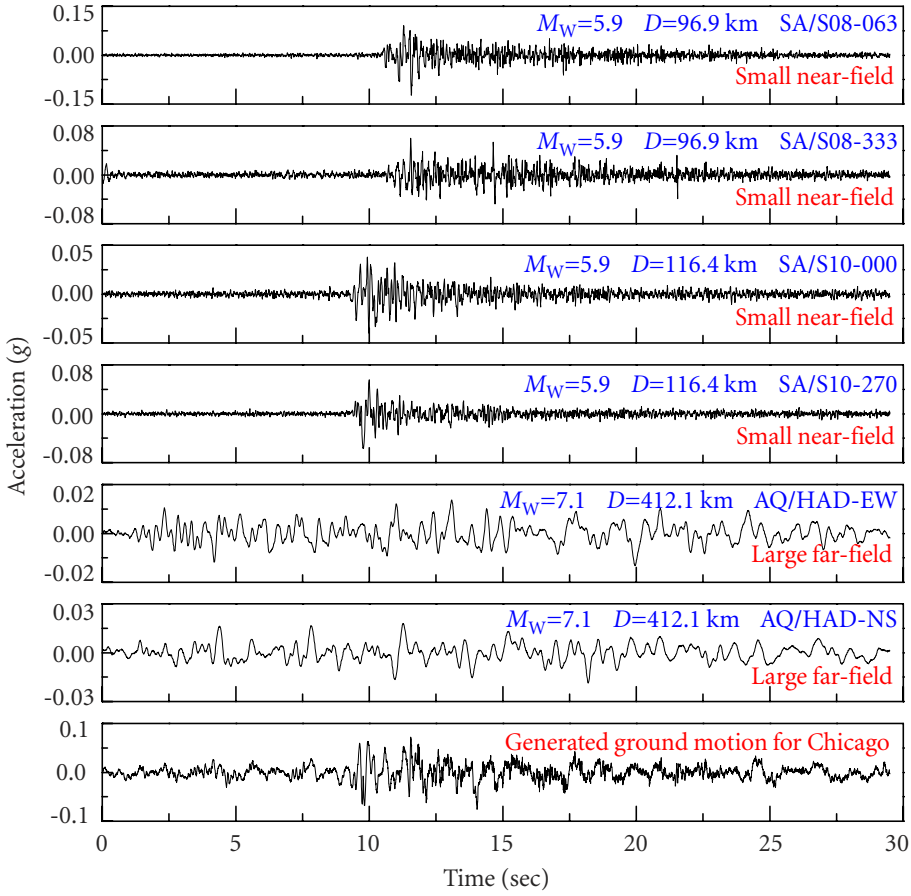

Figure 4.25 Seed and generated earthquake ground motions for CDS at Chicago

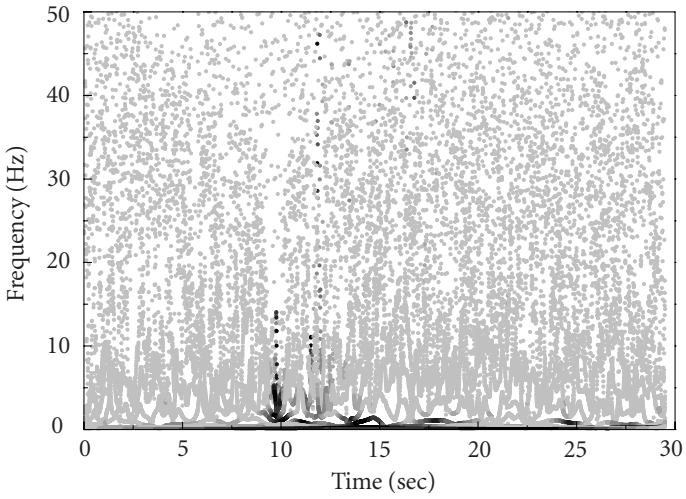

Figure 4.26 Hilbert energy spectrum of generated ground motion for CDS at Chicago

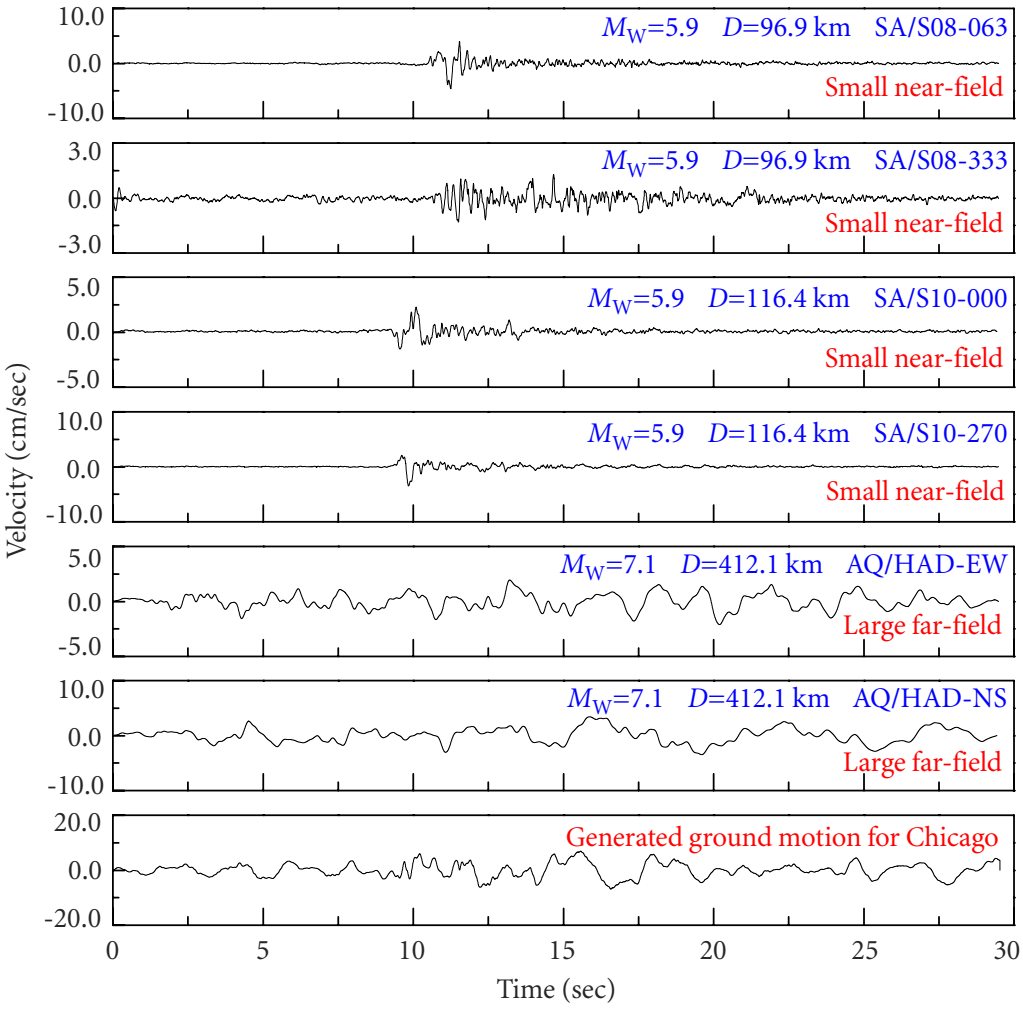

Figure 4.27 Seed and generated earthquake ground motions for CDS at Chicago

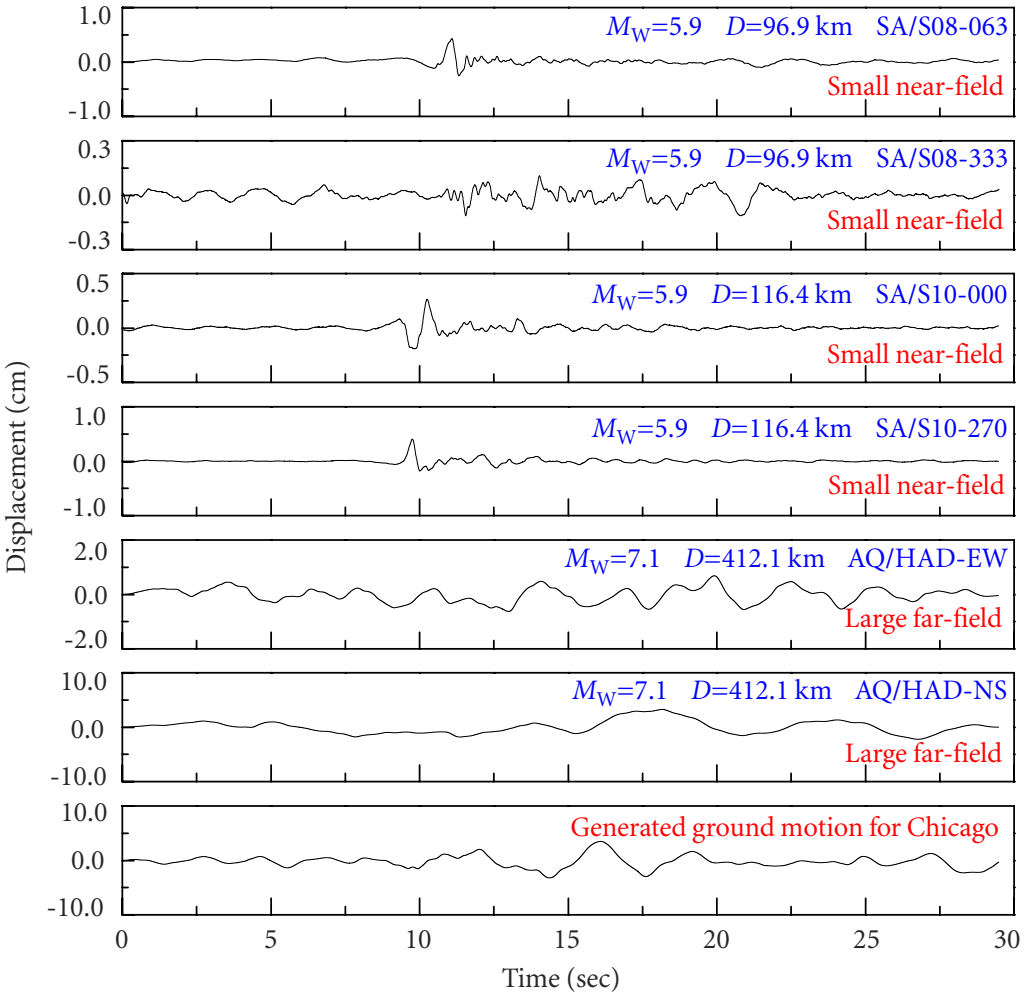

Figure 4.28 Seed and generated earthquake ground motions for CDS at Chicago

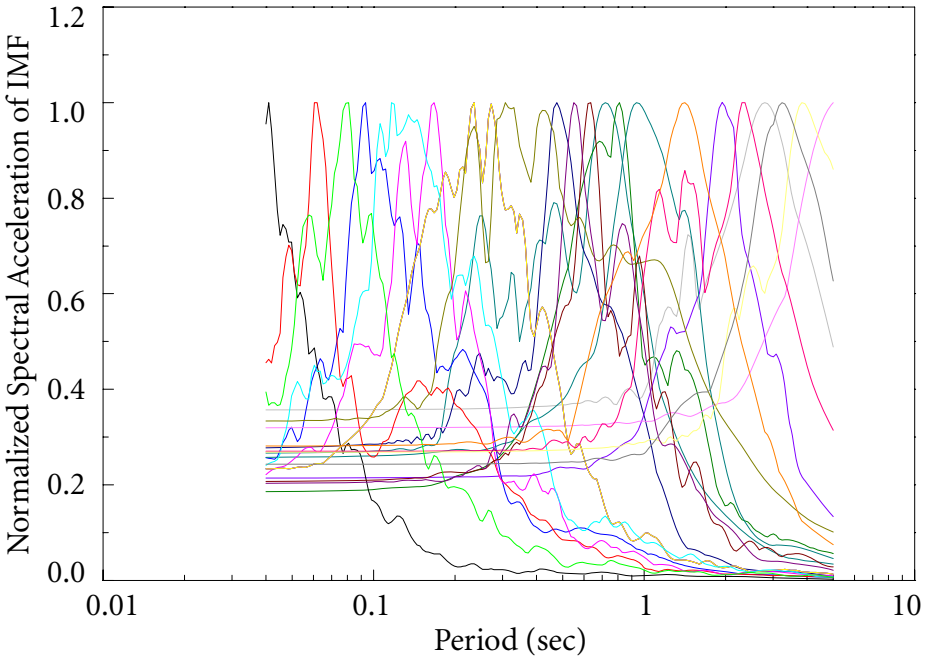

Figure 4.29 21 normalized response spectra of intrinsic mode functions for Quebec City

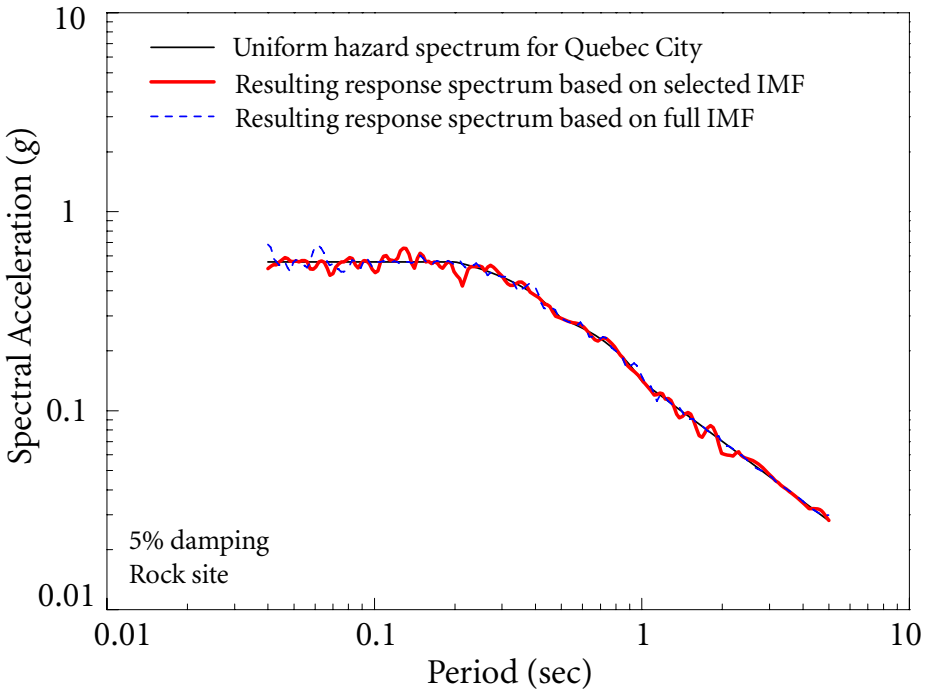

Figure 4.30 Comparison of response spectra based on full intrinsic mode functions and selected intrinsic mode functions

based on the selected 21 IMF. This procedure can significantly reduce the number of IMF with overlapping frequencies, hence the dimension of the optimization problem, and speed up the convergence of the computation.

From the numerical examples, the following observations can be made:

1. The success of the generation procedure in any practical situation depends much on the availability and the selection of recorded strong ground motions. Although the results of seismic hazard deaggregation (SHD) in terms of magnitude-distance pairs provide much useful information for the selection of recorded ground motions, strong ground motions, which are recorded around the sites of interest and reflect the most realistic seismic hazard of the sites, are still desired. This difficulty will be alleviated with the increase of the number of the available recorded ground motions over time.

2. A classical optimization algorithm, Quasi-Newton method, is used to minimize the objective function in the generation procedure. Since the objective function of the proposed method may be highly non-linear or non-smooth, it is challenging to find global minima by the classical optimization algorithms. The initial values of the optimization parameters may also influence the results of the computation. Further studies may be needed to find the most suitable optimization algorithm for this generation method.

4.4 Spectral Matching for Multiple Motions

To obtain realistic dispersion of structural responses due to the natural aleatory uncertainty arising from the physical variability of earthquake ground motions, many building code provisions require multiple input earthquake ground motions for the analysis. In most building codes (e.g., FEMA, 2001, CNE, 2004, ASCE, 2006), the maximum structural response from all input earthquake ground motions has to be considered for design if 3 to 6 ground motions are used. If at least 7 earthquake ground motions are used for the analysis, the average of the responses from those ground motions can be taken as the design value.

In any practical situation, the success of spectrum-compatible generation methods based on modifying recorded ground motions, as discussed in Section 4.3.2, depends much on

the availability and selection of recorded strong ground motions. In practice, a number of spectrum-compatible earthquake ground motions can be generated record-by-record based on the same number of recorded ground motions. However, such actual earthquake ground motions, which are recorded near the sites of interest and reflect the most realistic seismic hazard of the sites, may not be available, for example in most areas of eastern North America. Hence, an approach that can generate a desired number of spectrum-compatible earthquake ground motions based on a small number of recorded ground motions is needed.

In this section, an approach for generating a desired number of earthquake ground motions based on a small number of recorded earthquake ground motions is presented, which has been published in Ni *et al.* (2011B). It is a direct extension of the HHT-based method (Ni *et al.*, 2011A), presented in Section 4.3. The mean value of the response spectra of the generated ground motions closely matches the target seismic design spectrum. The matrix of correlation coefficients of spectral accelerations of the generated earthquake ground motions closely matches the target spectral correlation matrix, discussed in Section 2.1.2. The generation procedure not only preserves the nonstationary characteristics of seed recorded ground but also accounts for the intrinsic aleatory variability of real recorded ground motions for a given scenario earthquake.

4.4.1 Generation of Multiple Ground Motions

To generate a desired number of spectrum-compatible earthquake ground motions, the target seismic design spectrum and spectral correlation matrix are determined first. The seed recorded ground motions are then selected according to the type of the target design spectrum using the SHD, as discussed in Section 2.1.2. Using the HHT and an appropriate optimization algorithm, a set of spectrum-compatible earthquake ground motions can be generated.

According to the seismic design codes for building structures (UBC, 1997, NBCC, 2005, ASCE, 2006, NBCC, 2010), spectrum-compatible earthquake ground motions may be obtained by scaling and/or modifying recorded ground motions (selected from records of earthquake events having magnitudes, distances, and source mechanisms that are consistent with the seismic hazard at the sites of interest). Response spectra of the modified

earthquake ground motions, either individually or in combination, shall equal or exceed the target seismic design spectrum throughout the range of period of interest, i.e., the periods of the modes contributing to the response of the particular structure (Naeim and Lew, 1995). These code requirements characterize only the consistency of earthquake ground motions.

However, as pointed out by Baker and Cornell (2006A), a set of ground motions having only extremely consistent spectral shapes cannot be an accurate representation of realistic seismic hazard. The natural aleatory uncertainty arising from the physical variability of earthquake ground motions will not be properly characterized if a set of ground motions having extremely consistent spectral shapes are used for a given scenario earthquake. Since there are no provisions in the design codes describing the intrinsic aleatory variability of a set of selected ground motions and the internal relations between each other, the spectral correlation matrix, derived by the Next Generation Attenuation (NGA) Project (Baker and Jayaram, 2008) and discussed in Section 2.1.2, is employed as one of the measures of the variability of generated ground motions for a given scenario earthquake.

The correlation between spectral acceleration values of a set of earthquake ground motions from a given scenario earthquake (with the same magnitude and source-site distance) at different vibration periods has been recognized as one of the most important properties in quantifying the intrinsic aleatory variability of ground motions for a given scenario earthquake (Baker and Cornell, 2006A, Baker and Jayaram, 2008). It is noted that the same scenario earthquake in terms of magnitude and distance is required only as an abstract concept; the actual values of the magnitude and distance are not needed for the spectral correlations.

For the extreme case when all the response spectra have the same spectral shapes but different amplitudes, as shown in Figure 11(b) in Baker and Cornell (2006A), the correlation coefficients of spectral accelerations given by equation (2.1.21) are all 1; whereas, for the other extreme case when the response spectra are uncorrelated, as shown in Figure 11(a) in Baker and Cornell (2006A), the correlation coefficients of spectral accelerations are all 0. However, because of the natural intrinsic aleatory variability of ground motions for a given scenario earthquake, the values of the spectral correlation coefficients of a set of recorded ground motions should be between 0 and 1. The spectral correlation matrix, obtained

empirically by Baker and Jayaram (2008) based on regression analysis of a large strong motion database, is shown in Figure 2.2.

Wang (2010, 2011) used the spectral correlation matrix as one of the targets for selecting recorded ground motions from a large ground-motion database. The response history analysis of a 20-story reinforced concrete frame structure using the selected ground motions demonstrated excellent capacity of the ground motion selection algorithm, based on the spectral correlation matrix, in the study of distribution of nonlinear structural responses. Jayaram *et al.* (2011) developed a ground-motion selection algorithm for matching a target response spectrum mean and variance by considering the spectral correlation.

Baker and Cornell (2006a) pointed out that the spectral correlation should be considered when multiple synthetic ground motions or spectra are simulated. While the code requirements of magnitude, source-site distance, and spectrum-compatibility guarantee the consistency of a set of earthquake ground motions for a given design earthquake (i.e., the target seismic design spectrum is regarded as a single design earthquake), the empirical matrix of correlation coefficients of spectral accelerations can be used as an extra generation target to quantify the intrinsic aleatory variability of a set of ground motions for this design earthquake.

Hence, while the commonly-used coefficients of variation (COV) or standard deviations of spectral accelerations at individual periods account for the variability of spectral amplitudes at single points, the spectral correlation coefficients guarantee the natural intrinsic aleatory variability of ground motions between different spectral accelerations. Both the coefficients of variation at individual spectral accelerations and the correlation coefficients between different spectral accelerations will be considered in the generation algorithm.

To simulate multiple spectrum-compatible earthquake ground motions, a representative seed earthquake ground motion (either generated or recorded) is needed. When a target design spectrum is selected as a scenario design earthquake, an earthquake ground motion, compatible with this target spectrum, is believed to represent the scenario design earthquake in terms of frequency content. Hence, a seed spectrum-compatible earthquake ground motion will be generated or selected to simulate more spectrum-compatible ground motions.

To preserve the nonstationary characteristics of seed recorded ground motions, the seed spectrum-compatible earthquake ground motion, denoted as $\mathrm{TH}_{\mathrm{S}}(t)$, can be generated using the method presented in Section 4.3. The subscript "S" stands for seed spectrum-compatible earthquake ground motion.

From the point of view of frequency content, the predicted spectrum based on GMPEs, CMS-ε, VNUHS, or VCUHS possesses a relatively narrow-band spectral shape and can be interpreted as a single design earthquake in terms of magnitude-distance pairs. If the response spectrum of an recorded ground motion is compatible with one of these target design spectra, it can be used as the seed spectrum-compatible earthquake ground motion $\mathrm{TH}_{\mathrm{S}}(t)$. The step for generating the seed spectrum-compatible earthquake ground motion can be skipped.

Having obtained the (generated or actual) seed spectrum-compatible earthquake ground motion $\mathrm{TH}_{\mathrm{S}}(t)$, a desired number of spectrum-compatible earthquake ground motions, possessing the natural intrinsic variability of earthquake ground motions, can be generated as follows.

The seed earthquake ground motion $\mathrm{TH}_{\mathrm{S}}(t)$ is decomposed via empirical mode decomposition (EMD) into n intrinsic mode functions (IMF) in the Hilbert-Huang transform (HHT) as the basis for representing generated earthquake ground motions. The time-dependent amplitudes $a_k(t)$ and the instantaneous frequencies $\omega_k(t)$ of the seed spectrum-compatible ground motion are then obtained through the Hilbert spectral analysis (HSA).

The ith earthquake ground motion can then be obtained by linearly scaling the amplitude and shifting the phase of each IMF of the seed ground motion simultaneously:

$$\mathrm{TH}_i(\mathbf{x}_i, t) = \Re \sum_{k=1}^{n} x_{i,k}\, a_k(t)\, \mathrm{e}^{\mathrm{i}\left[\int \omega_k(t)\mathrm{d}t + x_{i,n+k}\right]}, \quad i = 1, 2, \ldots, N, \tag{4.4.1}$$

where $\mathrm{TH}_i(\mathbf{x}_i, t)$ is the ith spectrum-compatible earthquake ground motion generated, N is the desired number of generated earthquake ground motions, $x_{i,1}, x_{i,2}, \ldots, x_{i,n}$ are amplitude scaling parameters, and $x_{i,n+1}, x_{i,n+2}, \ldots, x_{i,2n}$ are the phase shifting parameters between 0 and 2π. By linearly scaling the amplitude and shifting the phase of each IMF of the seed spectrum-compatible ground motion, each earthquake ground motion gener-

ated contains the same frequencies as represented by the IMF basis derived from the seed spectrum-compatible ground motion.

Various optimization models can then be established as required,

$$\begin{aligned} &\text{minimize:} \quad V = \alpha_1 V_1 + \alpha_2 V_2, \\ &\text{subjected to constraints:} \quad x_{i,k} > 0,\ 0 \leqslant x_{i,n+k} \leqslant 2\pi, \ \text{ and } \ \mathrm{COV}(\mathbf{x}, T_p) \leqslant c_1, \end{aligned} \tag{4.4.2}$$

or

$$\begin{aligned} &\text{minimize:} \quad V = \alpha_1 V_1 + \alpha_2 V_2, \\ &\text{subjected to constraints:} \quad c_2 \leqslant x_{i,k} \leqslant c_3 \ \text{ and } \ 0 \leqslant x_{i,n+k} \leqslant 2\pi, \end{aligned} \tag{4.4.3}$$

where

$$\begin{aligned} V_1 &= \sum_{p=1}^{P} w_p \frac{\left|\overline{S[\mathbf{x}, T_p]} - S_{\mathrm{T}}(T_p)\right|}{S_{\mathrm{T}}(T_p)}, \quad \overline{S[\mathbf{x}, T_p]} = \frac{1}{N}\sum_{i=1}^{N} S[\mathrm{TH}_i(\mathbf{x}_i, t), T_p], \\ V_2 &= \sum_{u=1}^{r}\sum_{v=1}^{r} w_{u,v} \frac{\left|\rho_{\ln S_a(T_u),\ln S_a(T_v)} - \rho^{\mathrm{T}}_{\ln S_a(T_u),\ln S_a(T_v)}\right|}{\rho^{\mathrm{T}}_{\ln S_a(T_u),\ln S_a(T_v)}}. \end{aligned} \tag{4.4.4}$$

The objective function V_1 in equation (4.4.4) is the relative error of the spectral accelerations. $S[\mathrm{TH}_i(\mathbf{x}_i, t), T_p]$ is the spectral acceleration of the ith generated earthquake ground motion $\mathrm{TH}_i(\mathbf{x}_i, t)$ at a specific period T_p, $\overline{S[\mathbf{x}, T_p]}$ is the mean value of the resulting spectral accelerations at T_p, $S_{\mathrm{T}}(T_p)$ is spectral acceleration of the target seismic design spectrum at T_p, and P is the total number of period points at which the response spectra are calculated.

The objective function V_2 in equation (4.4.4) is the relative error for the spectral correlation coefficients. $\rho_{\ln S_a(T_u),\ln S_a(T_v)}$ is the correlation coefficient between spectral accelerations of the generated ground motions at periods T_u and T_v as defined in equation (2.1.21); $\rho^{\mathrm{T}}_{\ln S_a(T_u),\ln S_a(T_v)}$ is the corresponding target correlation coefficient derived from statistical analysis of a large strong motion database. This spectral correlation matrix reflects satisfactorily the inherent natural aleatory uncertainty arising from the physical variability of ground motions for a given earthquake. To ensure that the generated earthquake ground motions exhibit the required natural aleatory uncertainty, the empirical matrix of spectral correlations is thus incorporated in the objective function V_2. r is the total number of key periods for matching spectral correlations. In equation (4.4.4), w_p and $w_{u,v}$ are pre-

scribed weights, through which matches of spectral parameters at certain periods can be emphasized as required.

In optimization model (4.4.2), the variability of spectral accelerations of the generated ground motions at individual periods is described and constrained through the Coefficients of Variation COV($\mathbf{x}$, T_p) of the resulting spectral accelerations at individual periods T_p. Constant c_1 is the prescribed coefficient of variation for the spectral acceleration. The dispersion of the resulting spectral accelerations can also be controlled by constraining the global amplitude scaling parameters $x_{i,k}$ through the prescribed positive constants c_2 and c_3 in optimization model (4.4.3). α_1 and α_2 in optimization models (4.4.2) and (4.4.3) are prescribed weights, which can usually be assigned as 1 since the matchings of the spectra and the spectral correlations are regarded as equally important.

By minimizing the objective function V in optimization model (4.4.2) or (4.4.3), a total of N earthquake ground motions, the mean value of whose response spectra closely matches the target design spectrum, can be generated. This set of generated earthquake ground motions can thus not only meet the requirement of consistency but also exhibit the natural aleatory variability of real recorded ground motions from a single scenario earthquake.

It is noted that the optimization models are not limited to equations (4.4.2) and (4.4.3), which are the total weighted errors between the results and the targets subjected to certain constraints. Any proper objective functions and constraints can be established according to the codes and practical requirements.

4.4.2 Numerical Examples

To illustrate the generation procedure of a set of spectrum-compatible earthquake ground motions for a given scenario earthquake, several numerical examples are presented and discussed in this section.

The uniform hazard spectrum (UHS) in 2005 National Building Code of Canada (NBCC, 2005) for the City of Toronto is used as the target seismic design spectrum. The probability of exceedance of the Toronto UHS is 0.0004 per annum (2% per 50 years). The Toronto UHS is for firm ground (average shear wave velocity to a depth of 30 m between 360 and 750 m/sec) and for 5% critical damping.

The latest results of the correlation coefficients of spectral accelerations derived by the Next Generation Attenuation (NGA) Project (Baker and Jayaram, 2008), as described in Section 2.1.2, are used as the target spectral correlation matrix in the objective function V_2 in equation (4.4.4), as shown in Figure 2.2. For illustration purpose, 0.5, 0.5 and 1.5 are assigned to c_1, c_2, and c_3 in the optimization problems (4.4.2) and (4.4.3), respectively, in the numerical examples.

The seed recorded ground motions for the City of Toronto are selected based on the results of scalar seismic hazard deaggregation (SHD) for spectral accelerations at individual periods (Halchuk and Adams, 2004). The SHD results and the recorded earthquake ground motions selected accordingly for Toronto are listed in Tables 4.4 and 4.5, respectively.

It should also be mentioned that the ground motions of two selected small near-field earthquakes are recorded in eastern North America region. Since there are no large far-field earthquakes, having such magnitude-distance pairs as indicated by the scalar SHD, recorded in eastern North America region (Cramer *et al.*, 2010), the ground motions of large far-field earthquake recorded in Southern California are selected. This difficulty will be alleviated with the increase of the number of available earthquake records over time.

To ensure that the response spectra of the generated earthquake ground motions are calculated accurately, the spectral accelerations at 5% damping are computed at 210 frequency points ($P=210$), which are uniformly spaced over the logarithmic frequency scale with 100 points per decade from 0.2 Hz to 25 Hz. For the spectral correlation matrix, 21 key frequency points ($r=21$), uniformly spaced over the logarithmic frequency scale with 10 points per decade from 0.2 Hz to 25 Hz, are adopted. To achieve spectral matching over the entire frequency range of interest, equal weights are assigned to all spectral accelerations, i.e., $w_p=1$ and $w_{u,v}=1$ in equation (4.4.4).

The response spectra of the seed recorded ground motions and the generated seed spectrum-compatible earthquake ground motion accordingly are shown in Figures 4.31-4.34. The response spectrum of the seed ground motion generated closely matches the target UHS for the City of Toronto. Furthermore, as shown in Figure 4.32, the generated seed spectrum-compatible ground motion preserves the temporal characteristics of the seed recorded ground motions in the time domain, since the generation basis are obtained

from the seed recorded ground motions themselves. Hence, this generated spectrum-compatible ground motion is regarded as a representative ground motion of the target scenario earthquake (the UHS for Toronto in this case), which will be used as the basis for the multiple ground-motion generation.

Table 4.4: Mean values of seismic hazard deaggregation

Location	Vibration period	Seismicity	Hypocentral distance	Moment magnitude
Toronto	s(0.2 sec)*	0.28 g	51 km	6.2
	s(1.0 sec)*	0.06 g	240 km	6.7

$*$ $s(T)$ is the uniform hazard spectral acceleration at vibration period T.

Table 4.5: Selected seed recorded ground motions

Location	EQ*	TP§	$D^{\dagger}$ (km)	$M^{\ddagger}$	Comp-1*	Comp-2*
Toronto	SA	SN	52.2	5.9	S16-214	S16-124
	SA	SN	70.5	5.9	S17-000	S17-270
	SF	LF	224.1	6.6	SDC000	SDC090

$*$ SA, Saguenay Earthquake, 1988/11/25 23:46; SF, San Fernando Earthquake, 1971/02/09 14:00.

§ Earthquake types: SN, Small Near-field Earthquake; LF, Large Far-field Earthquake.

† D is the closest distance to fault rupture, which is generally the hypocentral distance.

‡ M is the moment magnitude.

$\star$ Names of two horizontal components of earthquake records, which are searched from the Pacific Earthquake Engineering Research Center (PEER) and the Natural Resources Canada (NRCAN) databases.

By manipulating this seed spectrum-compatible earthquake ground motion using equation (4.4.1), two sets of 10 and 15 ground motions are generated by constraining the

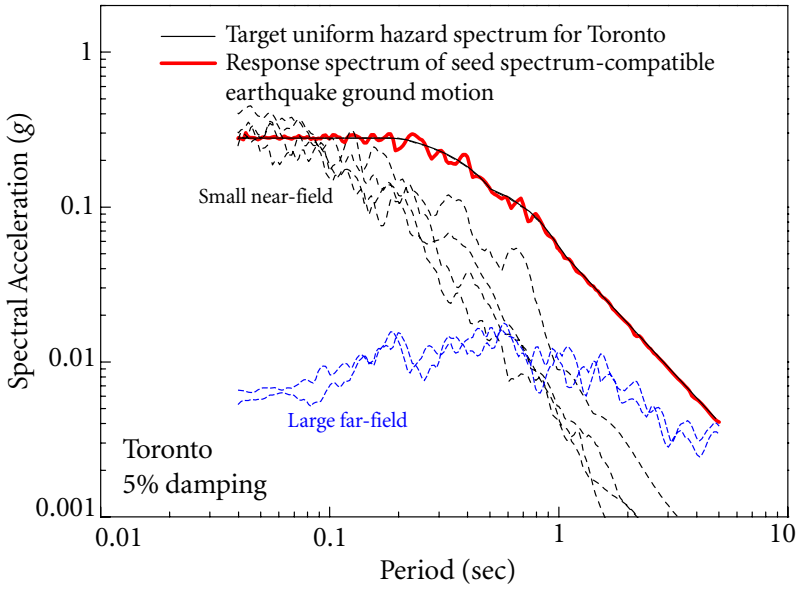

Figure 4.31 Response spectra of recorded ground motions and seed spectrum-compatible earthquake ground motion

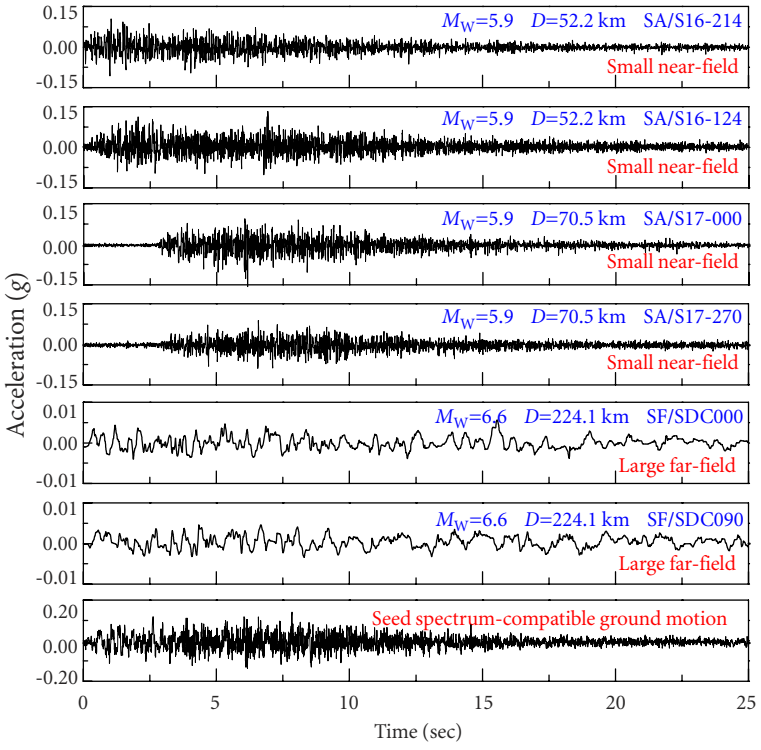

Figure 4.32 Seed recorded ground motions and seed spectrum-compatible earthquake ground motion

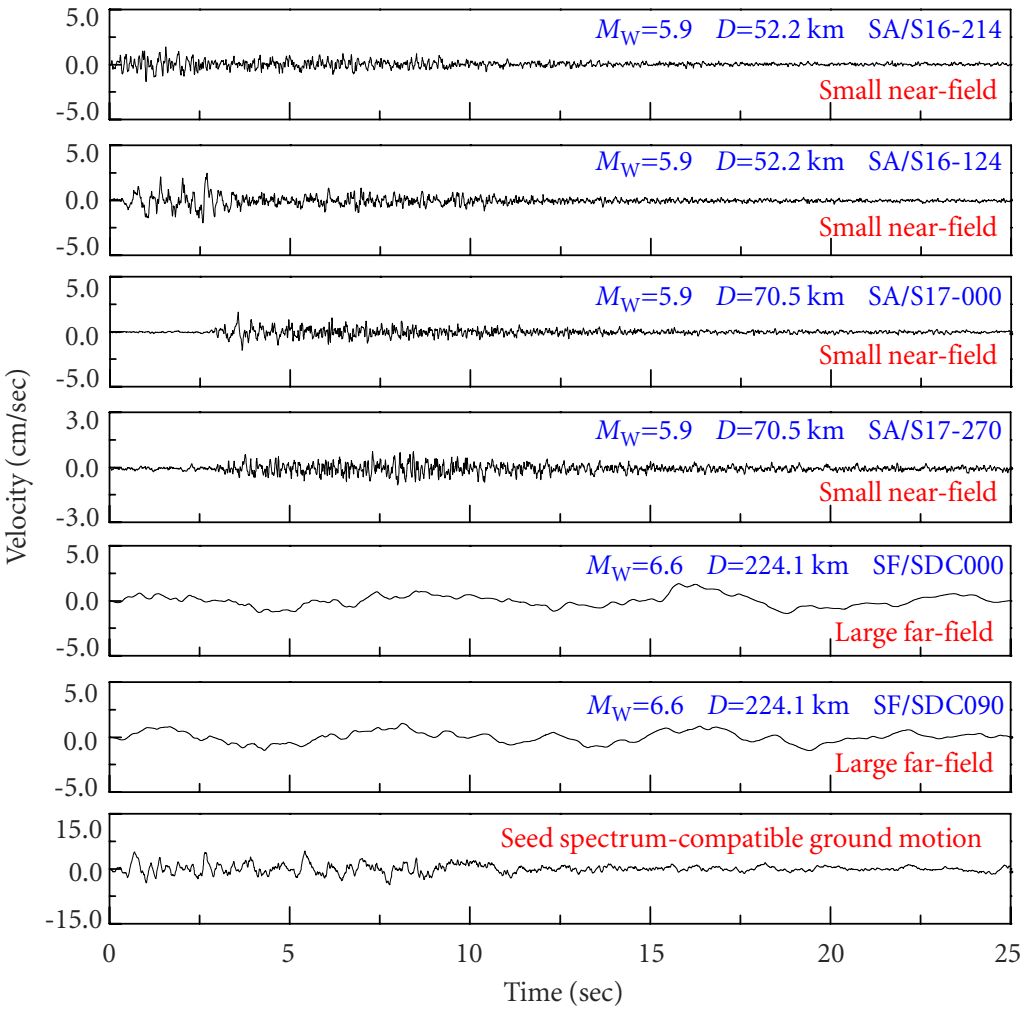

Figure 4.33 Seed recorded ground motions and seed spectrum-compatible earthquake ground motion

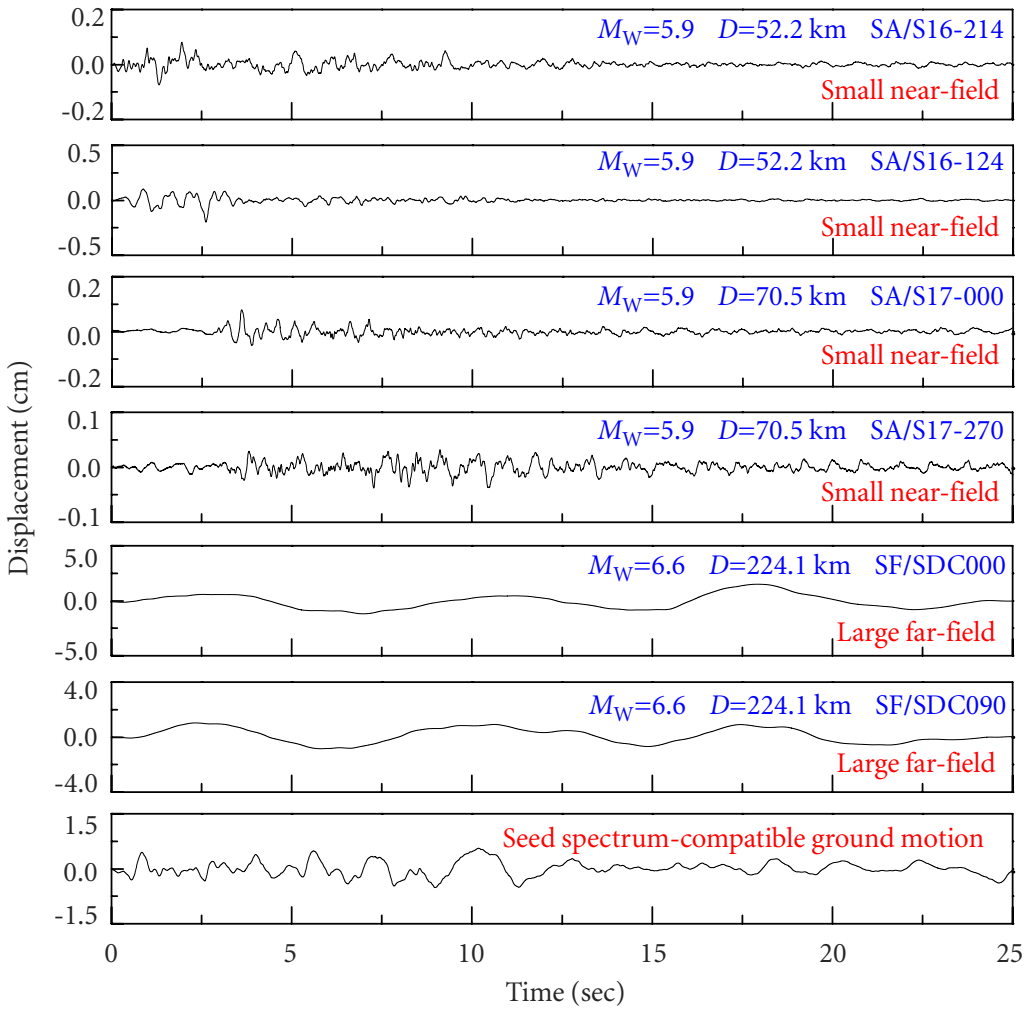

Figure 4.34 Seed recorded ground motions and seed spectrum-compatible earthquake ground motion

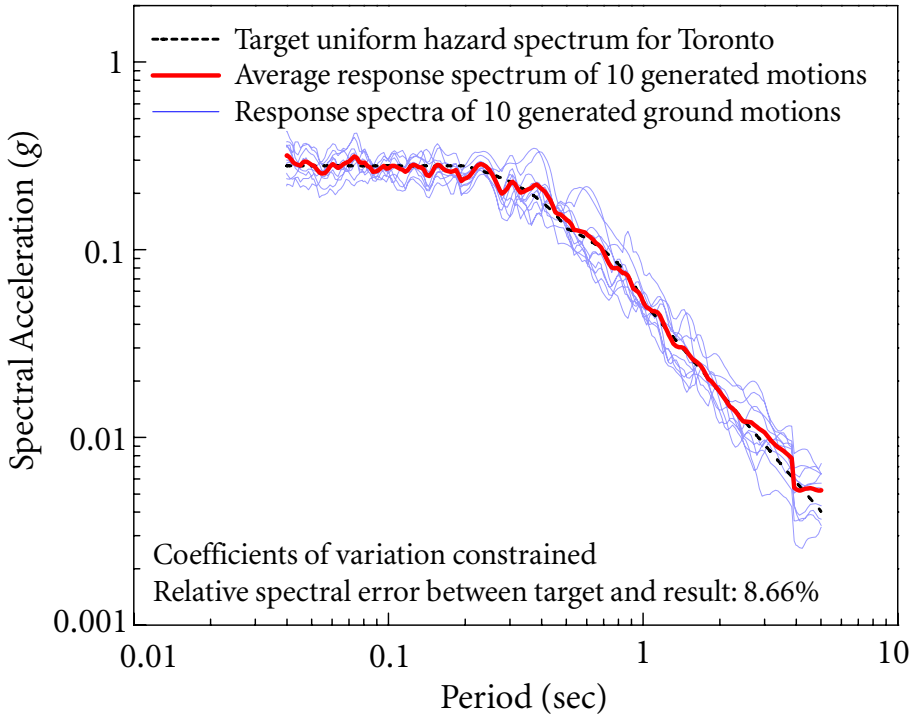

Figure 4.35 10 resulting response spectra with coefficients of variation constrained

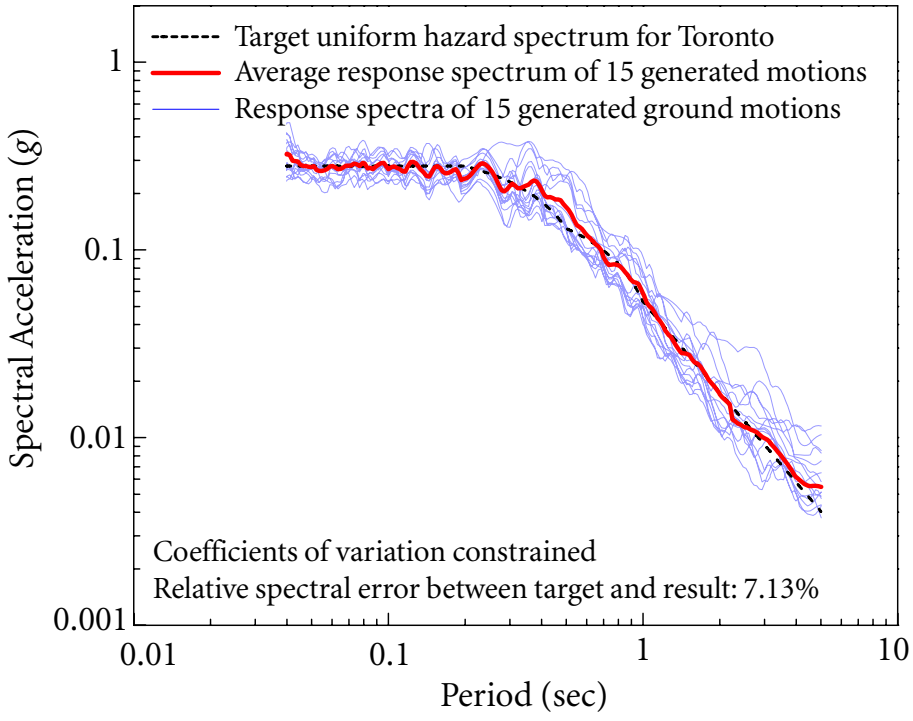

Figure 4.36 15 resulting response spectra with coefficients of variation constrained

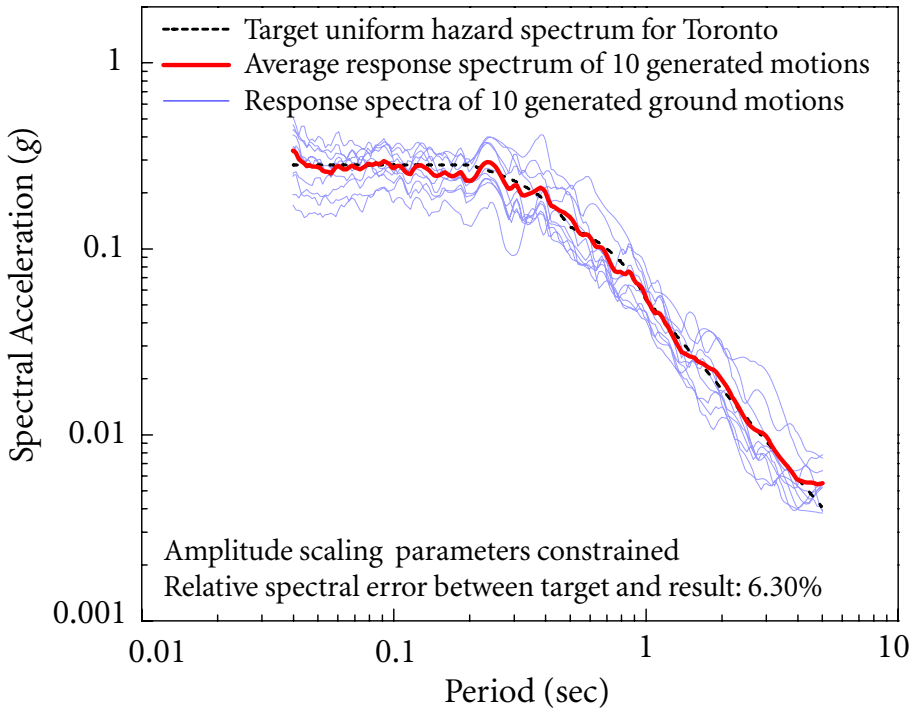

Figure 4.37 10 resulting response spectra with amplitude scaling parameters constrained

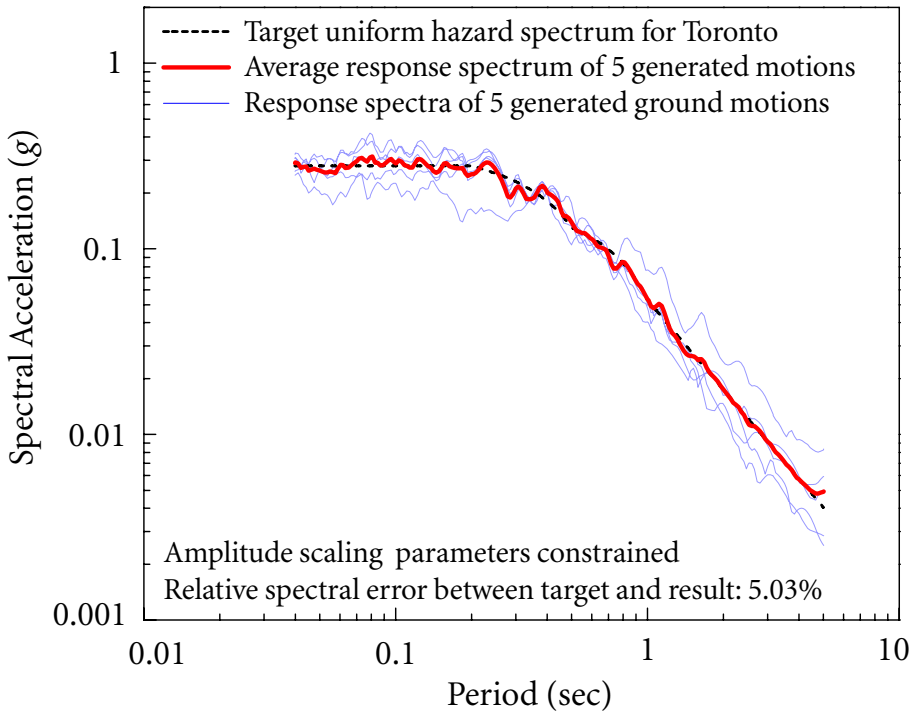

Figure 4.38 5 resulting response spectra with amplitude scaling parameters constrained

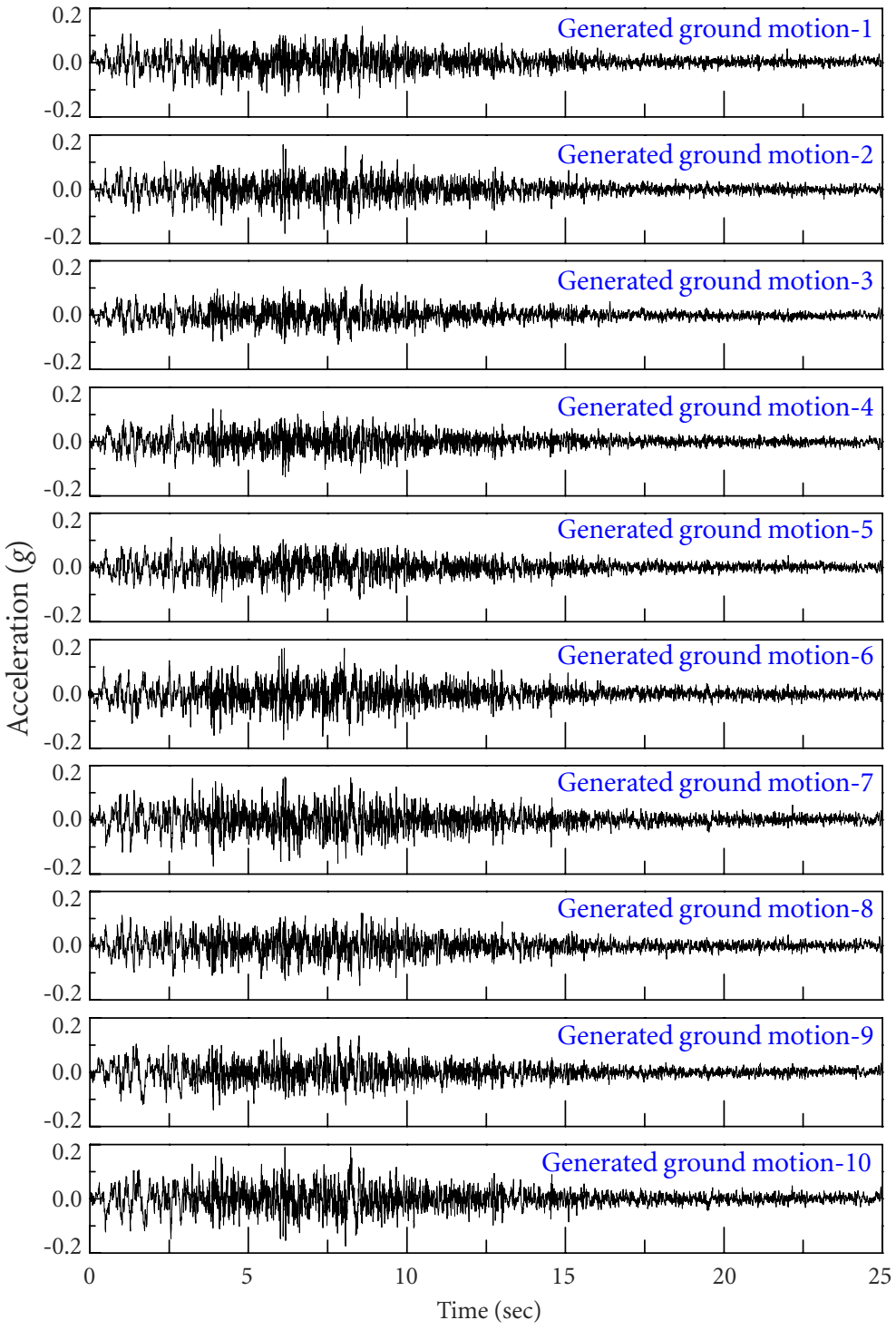

Figure 4.39 10 generated spectrum-compatible earthquake ground motions (COV constrained)

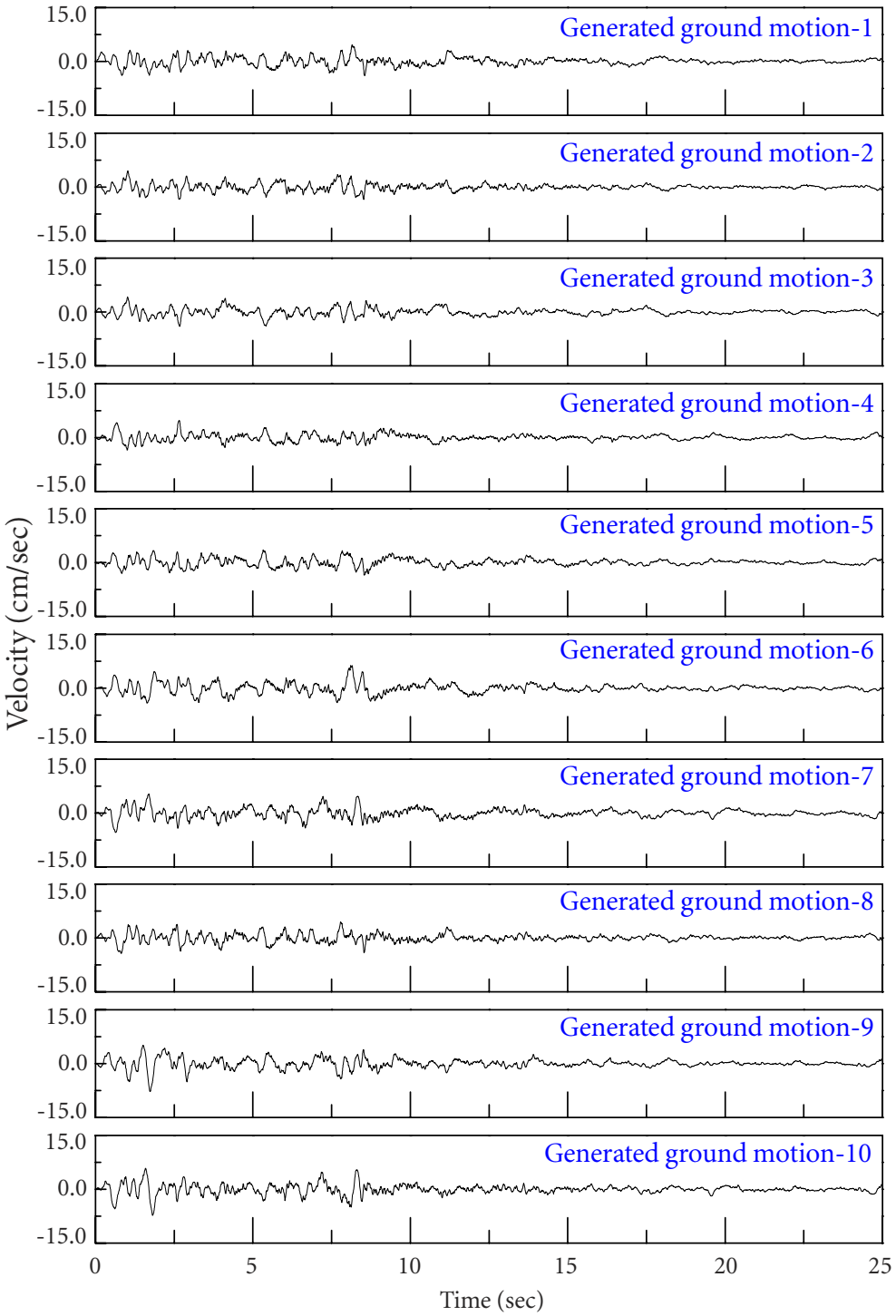

Figure 4.40 10 generated spectrum-compatible earthquake ground motions (COV constrained)

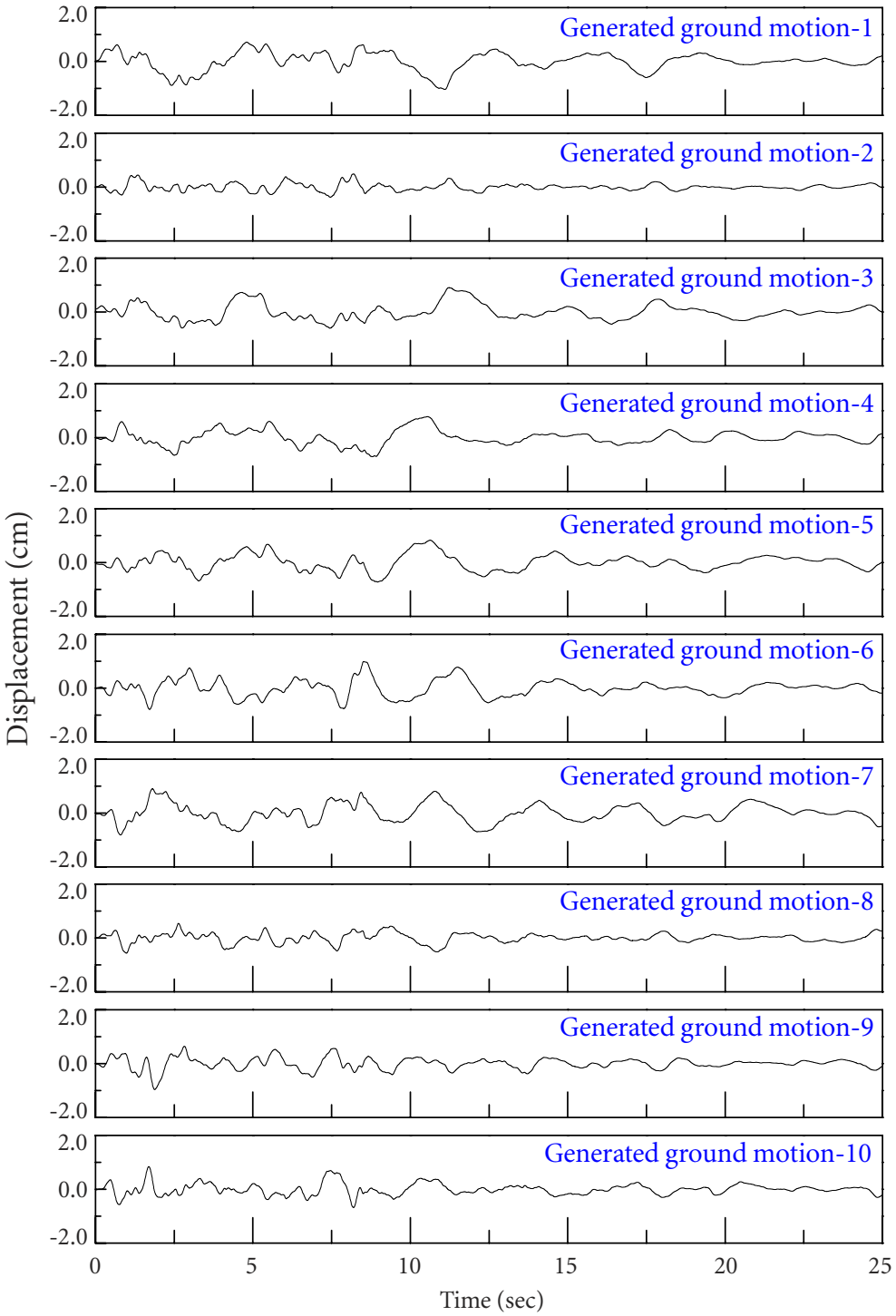

Figure 4.41 10 generated spectrum-compatible earthquake ground motions (COV constrained)

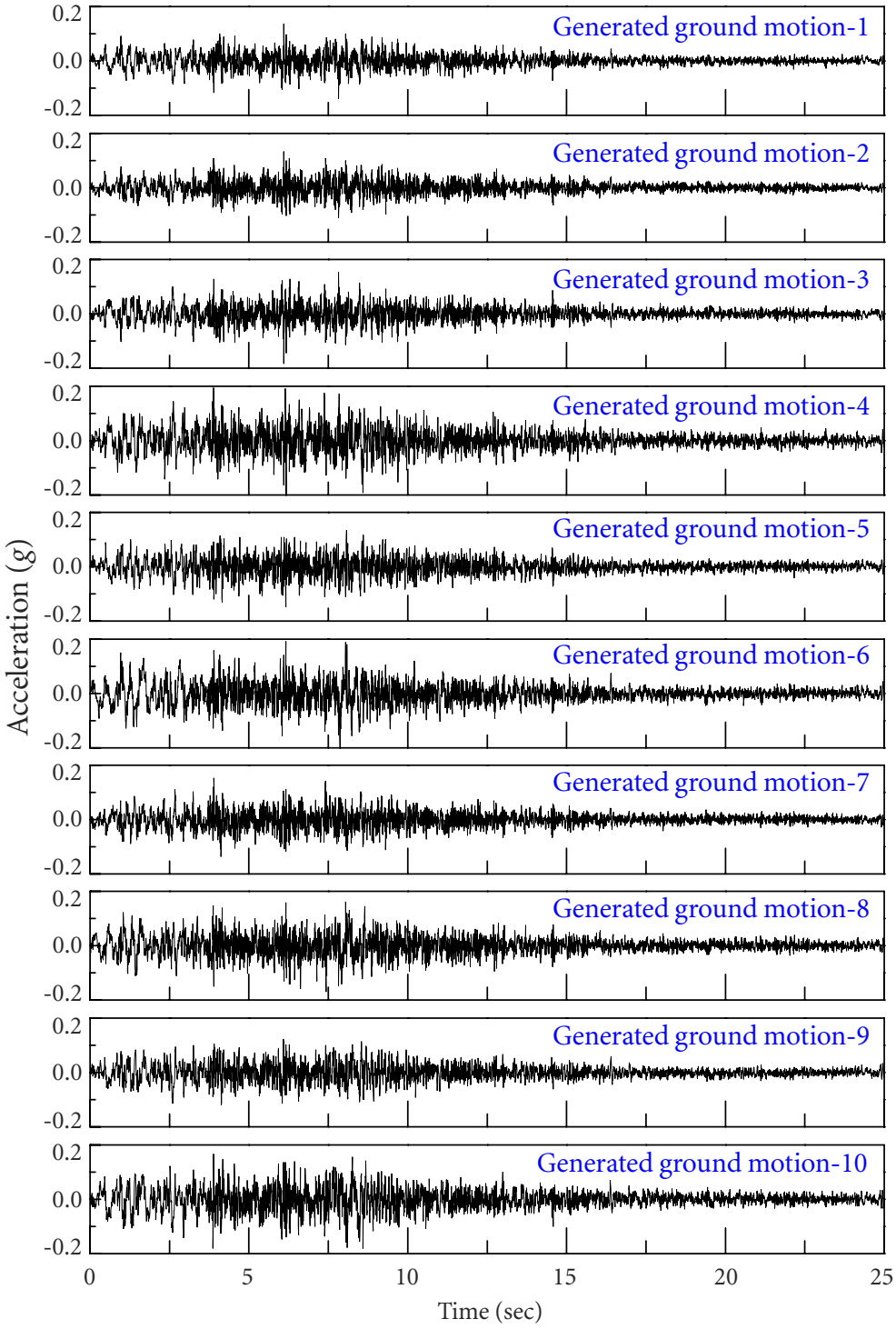

Figure 4.42 10 generated spectrum-compatible earthquake ground motions (Amplitude constrained)

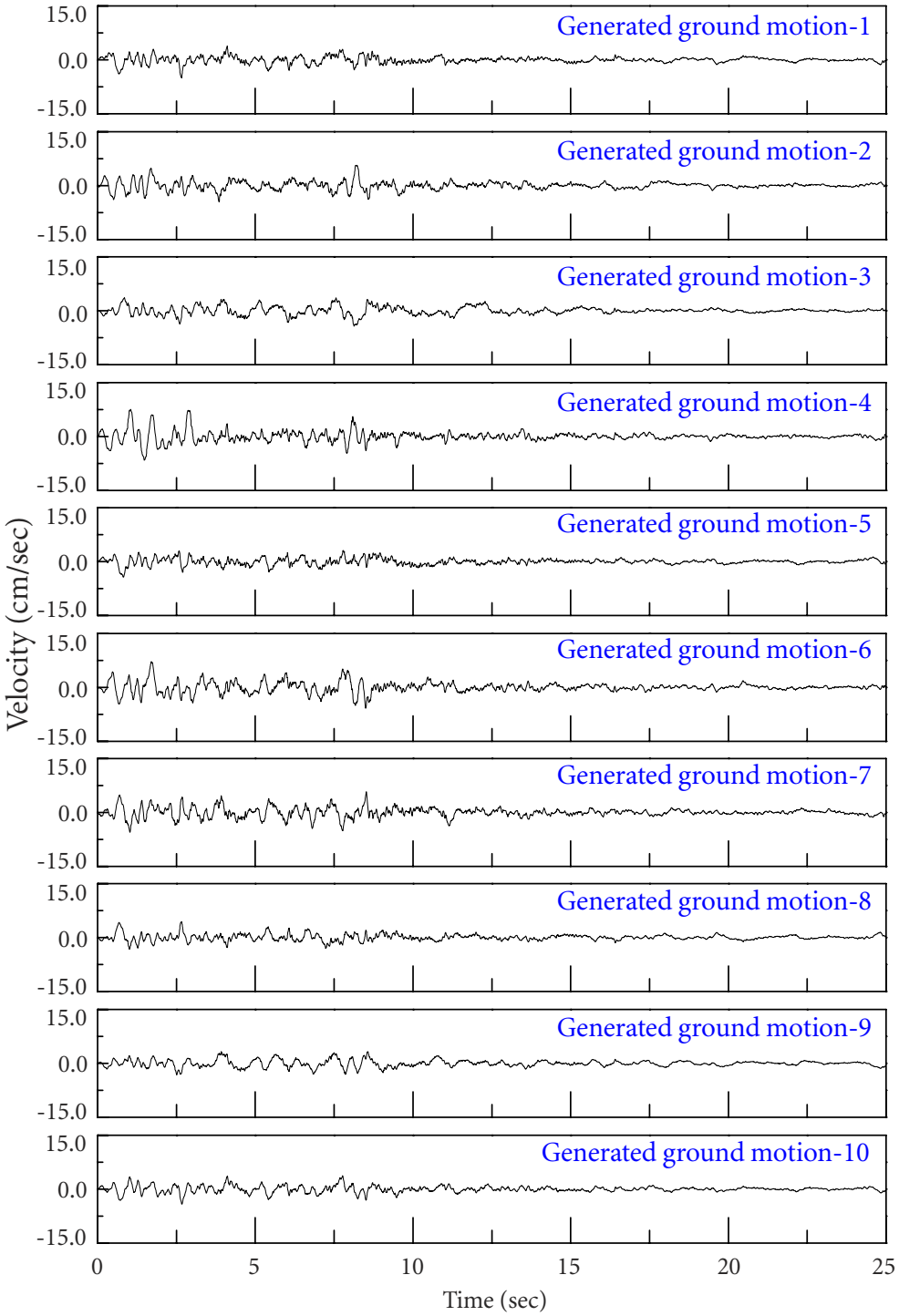

Figure 4.43 10 generated spectrum-compatible earthquake ground motions (Amplitude constrained)

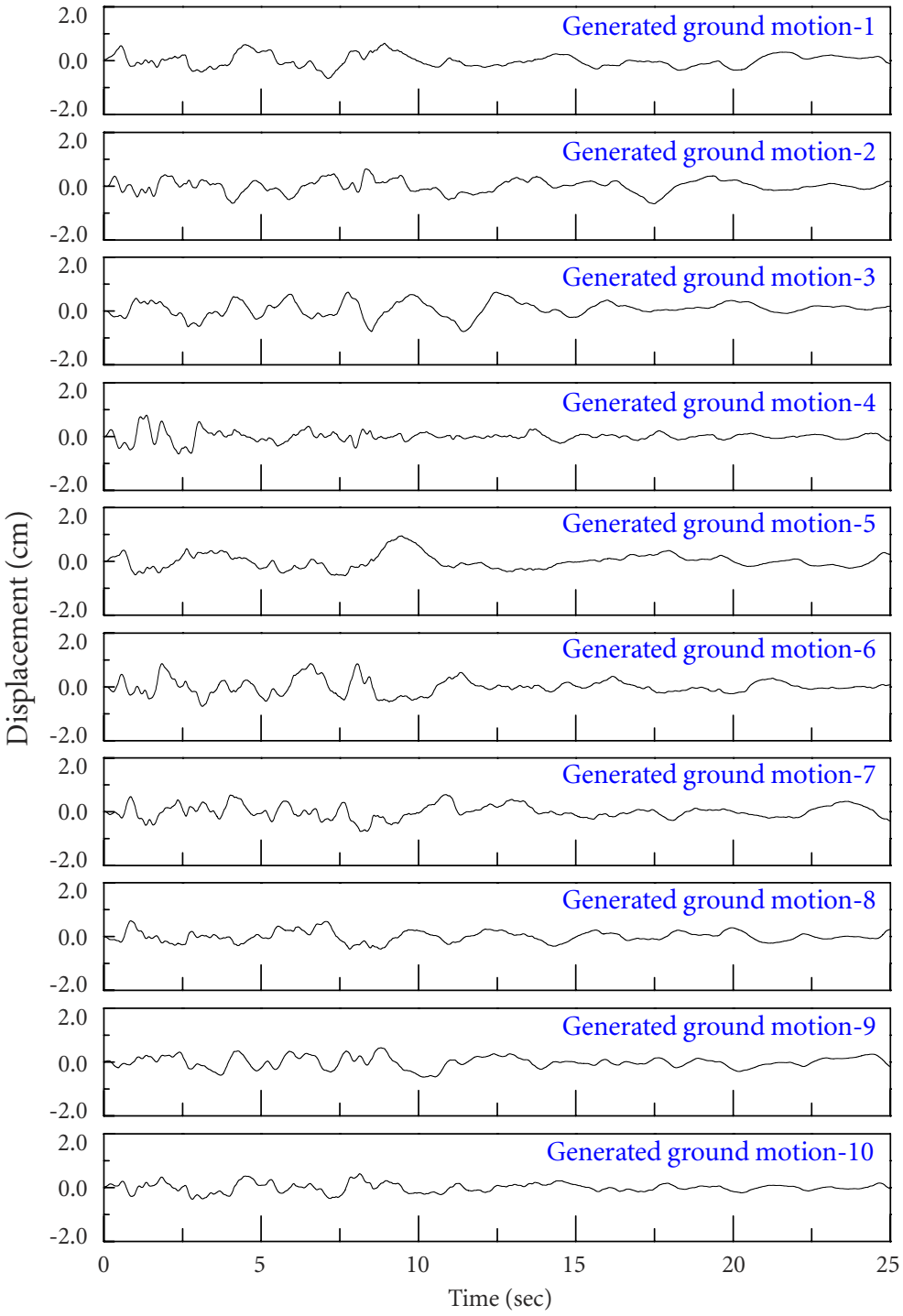

Figure 4.44 10 generated spectrum-compatible earthquake ground motions (Amplitude constrained)

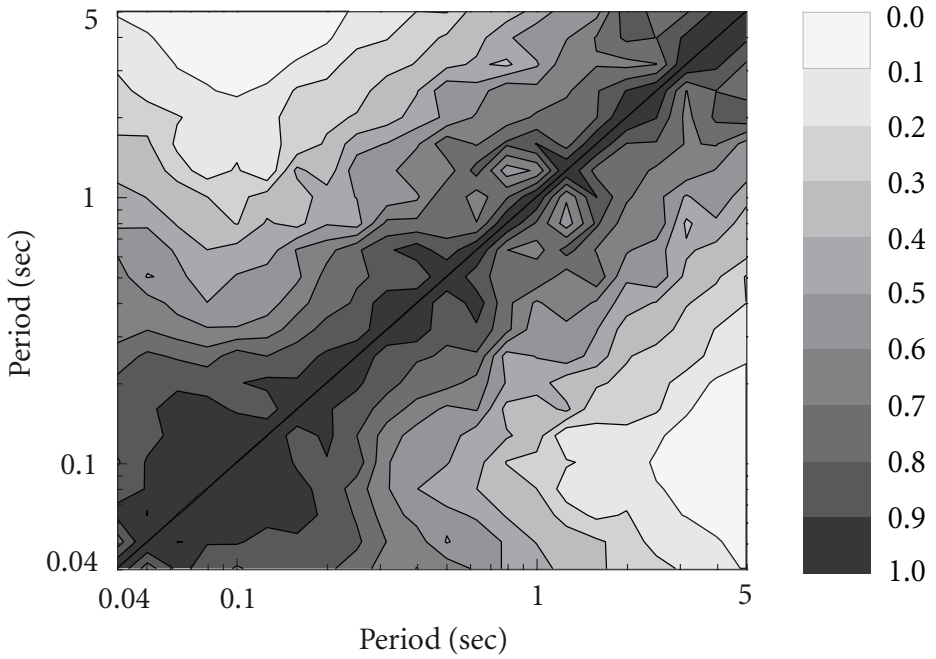

(a) COV constrained, 10 motions, relative error 8.70%

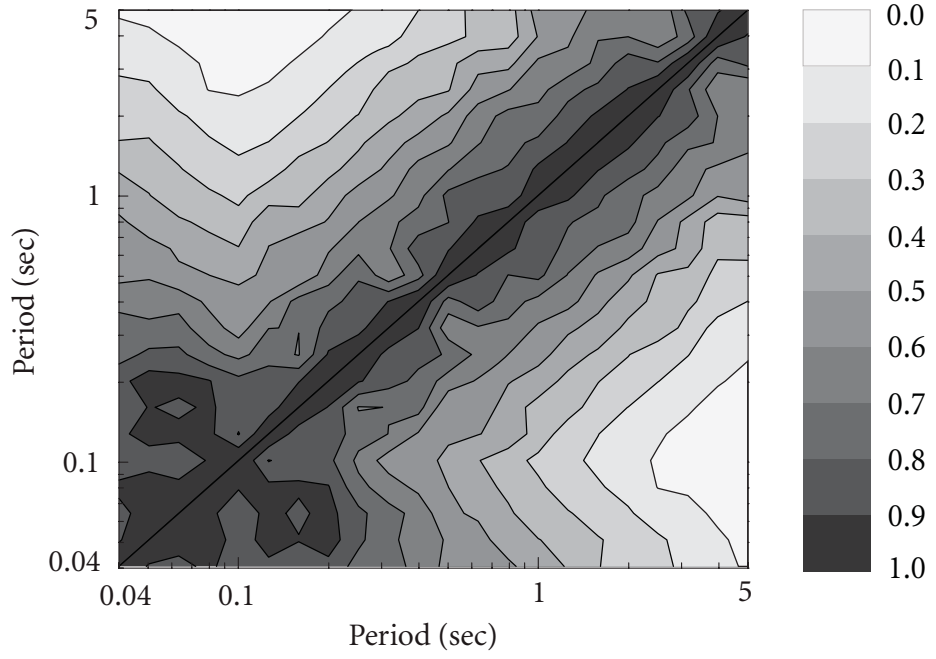

(b) COV constrained, 15 motions, relative error 4.11%

Figure 4.45 Resulting spectral correlation matrices with COV constrained

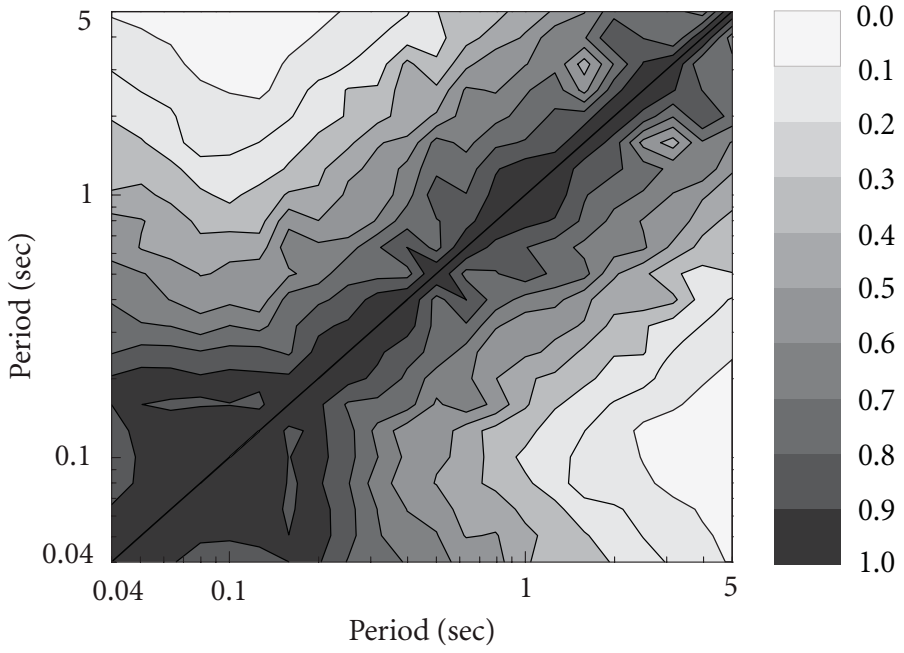

(a) Amplitude constrained, 10 motions, relative error 5.50%

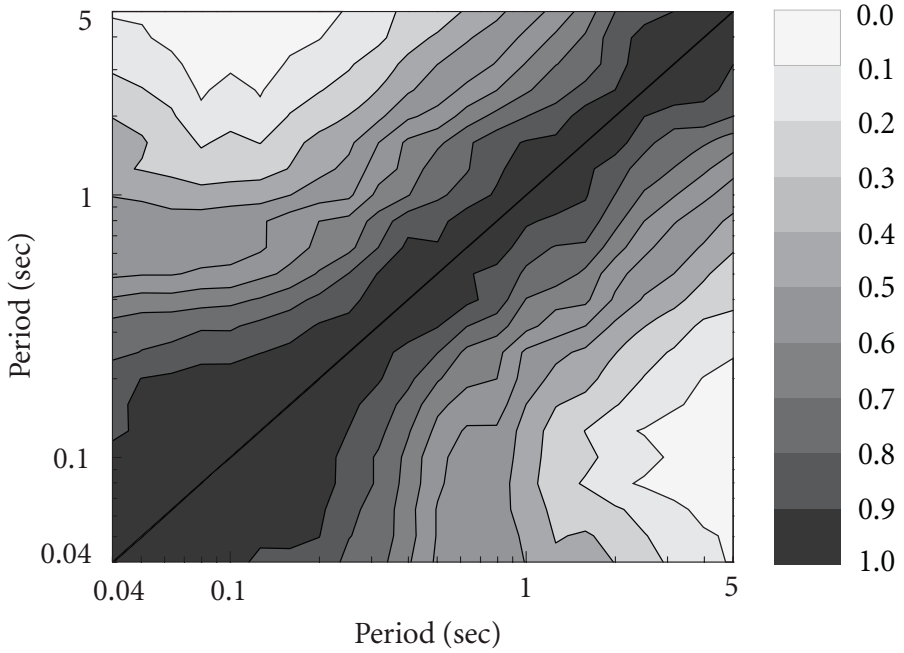

(b) Amplitude constrained, 5 motions, relative error 8.65%

Figure 4.46 Resulting spectral correlation matrices with amplitude constrained

coefficient of variation (COV) of spectral accelerations at each vibration period of interest, and two sets of 10 and 5 ground motions are generated by controlling the amplitude scaling parameters globally, by solving optimization problems (4.4.2) and (4.4.3), respectively. The response spectra of the generated earthquake ground motions for these four cases are shown in Figures 4.35-4.38. Since the spectral amplitude variability (COV or amplitude scaling parameters) is considered in the optimization constraints, the resulting response spectra in each set demonstrate generally similar spectral shapes and a bounded variability of spectral accelerations at individual periods as required. As shown in Figures 4.35-4.38, the mean value of the response spectra of the generated earthquake ground motions in each set closely matches the target UHS for Toronto with average relative error less than 10%.

Two sets of 10 earthquake ground motions generated by constraining the COV and the amplitude scaling parameters are shown in Figures 4.39-4.41 and 4.42-4.43, respectively. Since these earthquake ground motions are simulated based on the same nonstationary basis (IMF components) derived via EMD from the seed spectrum-compatible earthquake ground motion, and only the amplitudes and the phases of the IMF components are manipulated for the generation, each earthquake ground motion generated contains the same frequencies as represented by the IMF component basis. Hence, the generated earthquake ground motions are similar to the seed spectrum-compatible earthquake ground motion in the time-domain and generally preserve the temporal characteristics of the seed recorded ground motions.

The generated earthquake ground motions demonstrate consistent characteristics in both spectral shape (as shown in Figures 4.35-4.38) and time-domain (as shown in Figures 4.39 and 4.42), associated with the bounded variability of spectral accelerations at individual periods as required. On the other hand, the small discrepancy (average relative error of less than 10% for each case) between the target spectral correlation matrix (Figure 2.2) and the resulting spectral correlation matrix (Figures 4.45 and 4.46) guarantees the intrinsic aleatory variability of the generated ground motions for a scenario earthquake.

For solving the constrained nonlinear optimization problem (4.4.2) or (4.4.3), a basic optimization strategy, constrained nonlinear multi-variable line-search algorithm (Nocedal and Wright, 1999), is applied. To illustrate the robustness of the method, four examples for

different numbers of generated ground motions under different optimization constraints are presented in this study. For each example, the average relative errors of the spectral matching and the correlation matrix matching are all less than 10% after 300 iterations in the optimization.

It is also observed in these examples that, under the same constraint condition, the total relative errors for the case with more generated ground motions are all smaller than those with fewer generated ground motions. This is because, when more earthquake ground motions are generated, more samples for describing the statistical characteristics (including mean, coefficients of variation, and coefficients of correlation) and more optimization parameters for minimizing the objective functions jointly improve the optimization convergence.

4.5 Spectral Matching for Tri-directional Motions

Several researchers have studied the characteristics of tri-directional earthquake ground motions. Chen (1975) defined the correlation coefficient of two earthquake ground motion time-histories in orthogonal directions as an index of statistical independence of these two ground motions. Based on statistical analysis of 104 sets of recorded ground motions, it is recommended that the statistically independent artificial ground motions should be those with absolute correlation coefficients less than or equal to 0.16. Penzien and Watabe (1975) and Hadjian (1981) conducted similar research and concluded that the absolute correlation coefficients of two orthogonal ground motions are from 0.14 to 0.5.

Levy and Wilkinson (1976) attempted to generate two orthogonal spectrum-compatible artificial earthquake ground motions, which are statistically independent. The first spectrum-compatible earthquake ground motion is represented by Fourier series. The median values of the adjacent Fourier amplitudes and frequencies of the first ground motion are then used to construct another earthquake ground motion. These two ground motions, whose correlation coefficient is small, are thought to be statistically independent. However, this approach is unable to preset the value of the correlation coefficient of the two earthquake

ground motions, and hence unable to guarantee two generated ground motions to be statistically independent.

According to the codes for seismic design and analysis of nuclear energy facilities (ASCE, 1998, ASCE, 2005, ASCE, 2009), tri-directional earthquake ground motions are needed for seismic design and analysis of nuclear energy facilities unless the uncoupled response of the structure is expected. Time-history for each direction of motion shall be compatible with the corresponding target seismic design spectrum. Three orthogonal ground motions of the design earthquake shall be statistically independent of each other.

The target seismic design spectra for safety-related nuclear structures shall be defined for ground motions in two orthogonal horizontal and one vertical directions. Except for unusual circumstances of geology or location of seismic sources, the target spectra in two horizontal directions shall be assumed equal. The vertical component of the target design spectra can be obtained by scaling the corresponding coordinates of the horizontal target spectra using specified factors throughout the frequency range.

For generating tri-directional spectrum-compatible earthquake ground motions, the quantitative acceptance criteria of earthquake ground motions in the codes (ASCE, 1998, ASCE, 2005, ASCE, 2009) are summarized:

1. Spectral accelerations at 5% damping shall be computed at 100 points per frequency decade, uniformly spaced over the logarithmic frequency scale.
2. The peak ground acceleration (PGA) shall equal or exceed the PGA of the target seismic design spectrum.
3. The 5% damped response spectrum of the ground motion shall not fall more than 10% below the target spectrum at any one frequency and not exceed the target spectrum more than 30% in the frequency range between 0.2 Hz and 25 Hz.
4. No more than 9 adjacent frequency points are allowed to fall below the target spectrum.
5. The average of the ratios of response spectrum of the ground motion to the target spectrum frequency by frequency shall be equal to or greater than 1.
6. To be considered statistically independent, the correlation coefficients between three orthogonal components of one set of ground motions shall not exceed 0.3.

In this section, the generation method presented in Section 4.3 is extended to generate a set of tri-directional orthogonal earthquake ground motions compatible with the target seismic design spectra for nuclear energy facilities (Ni *et al.*, 2011c). Three orthogonal components of generated earthquake ground motion are statistically independent from the point of view of practical engineering. Two horizontal components of the generated ground motion have the same frequency-time-energy distribution. The generated ground motion time-histories can preserve the nonstationary characteristics of the seed recorded ground motions and can also meet the stringent code requirements (ASCE, 1998, ASCE, 2005, ASCE, 2009) for nuclear energy facilities.

4.5.1 Generation of Tri-directional Ground Motions

To generate a set of tri-directional spectrum-compatible earthquake ground motions, the target seismic design spectra for three orthogonal directions are first determined, according to the code requirements. The seed recorded ground motions are then selected according to the type of the selected target design spectra using the SHD, as discussed in Section 2.1.2. Using the HHT and an appropriate optimization algorithm, a set of tri-directional spectrum-compatible earthquake ground motions can be generated.

Generation of the first horizontal spectrum-compatible ground motion

Each of the selected horizontal recorded ground motions is decomposed into several intrinsic mode functions (IMF) via empirical mode decomposition (EMD). The l generated IMF from the selected horizontal recorded ground motions are treated as the basis to represent a nonstationary earthquake ground motion.

The time-dependent amplitude and the instantaneous frequency of each IMF are then generated through HSA. The HHT amplitudes $a_{1,i}(t)$ and the instantaneous frequencies $\omega_{1,i}(t)$ of the horizontal recorded ground motions are thus scaled to obtain the first horizontal earthquake ground motion

$$\mathrm{TH}_{\mathrm{H1}}(\mathbf{x},t) = \Re \sum_{i=1}^{l} \left[x_i a_{1,i}(t)\right] \mathrm{e}^{\mathrm{i}\, x_{l+i} \int \omega_{1,i}(t)\mathrm{d}t}, \tag{4.5.1}$$

where $x_1, x_2, \ldots, x_l$ are the amplitude scaling parameters, $x_{l+1}, x_{l+2}, \ldots, x_{2l}$ are the frequency scaling parameters, and $\mathbf{x} = \{x_1, x_2, \ldots, x_{2l}\}^T$ is the vector of scaling parameters.

An optimization model is then constructed:

$$\begin{aligned} &\text{minimize:} \quad V = \sum_{p=1}^{P} f_p(\mathbf{x}), \quad f_p(\mathbf{x}) = \frac{\left| S[\mathrm{TH}_{\mathrm{H1}}(\mathbf{x}, t), T_p] - S_{\mathrm{T,H}}(T_p) \right|}{S_{\mathrm{T,H}}(T_p)}, \\ &\text{subjected to constraints:} \quad x_r > 0, \quad r = 1, 2, \ldots, 2l, \end{aligned} \tag{4.5.2}$$

where $S[\mathrm{TH}_{\mathrm{H1}}(\mathbf{x}, t), T_p]$ is the spectral acceleration of the first generated horizontal earthquake ground motion $\mathrm{TH}_{\mathrm{H1}}(\mathbf{x}, t)$ at a specific period T_p, and $S_{\mathrm{T,H}}(T_p)$ is the spectral acceleration of the target design spectrum for horizontal component at T_p.

By solving the optimization problem (4.5.2) with a suitable optimization algorithm, the first horizontal earthquake ground motion, whose response spectrum closely matches the target design spectrum, is generated. The first horizontal spectrum-compatible earthquake ground motion can then be obtained by scaling the generated motion linearly to meet the acceptance criteria in the codes (ASCE, 1998, ASCE, 2005, ASCE, 2009).

Generation of the second horizontal spectrum-compatible ground motion

Having obtained the first horizontal spectrum-compatible earthquake ground motion $\mathrm{TH}_{\mathrm{H1}}(t)$, it is treated as a new seed earthquake ground motion and decomposed into m IMF components as the basis to represent the second horizontal ground motion via EMD.

The time-dependent amplitudes $a_{2,j}(t)$ and the instantaneous frequencies $\omega_{2,j}(t)$ of the first horizontal ground motion are then generated through HSA. The phase of each IMF of the first horizontal ground motion are thus shifted to obtain the second horizontal earthquake ground motion

$$\mathrm{TH}_{\mathrm{H2}}(\mathbf{x}, t) = \Re \sum_{j=1}^{m} a_{2,j}(t)\, \mathrm{e}^{\mathrm{i}\left[\int \omega_{2,j}(t)\mathrm{d}t + x_j\right]}, \tag{4.5.3}$$

where $x_1, x_2, \ldots, x_m$ are the phase shifting parameters in the range from 0 to 2π. By merely shifting the phase of each IMF, the second generated horizontal ground motion has the same frequency-time-energy distribution, i.e., Hilbert energy spectrum, as the first generated horizontal earthquake ground motion $\mathrm{TH}_{\mathrm{H1}}(t)$ (Wen and Gu, 2004).

A constrained optimization model is then used:

$$\begin{aligned} &\text{minimize:} \quad V = \sum_{p=1}^{P} f_p(\mathbf{x}), \quad f_p(\mathbf{x}) = \frac{\left|S[\mathrm{TH}_{\mathrm{H2}}(\mathbf{x},t),T_p] - S_{\mathrm{T,H}}(T_p)\right|}{S_{\mathrm{T,H}}(T_p)}, \\ &\text{subjected to constraints:} \quad \left|\rho[\mathrm{TH}_{\mathrm{H1}}(t),\mathrm{TH}_{\mathrm{H2}}(\mathbf{x},t)]\right| \leqslant c, \end{aligned} \tag{4.5.4}$$

where c is a small prescribed value to ensure that these two generated earthquake ground motions are statistically independent in engineering sense. The correlation coefficient between the first and second generated horizontal ground motions $\mathrm{TH}_{\mathrm{H1}}(t)$ and $\mathrm{TH}_{\mathrm{H2}}(t)$ is defined as

$$\rho[\mathrm{TH}_{\mathrm{H1}}(t),\mathrm{TH}_{\mathrm{H2}}(t)] = \frac{\mathrm{E}\left[\{\mathrm{TH}_{\mathrm{H1}}(t)-\mu_{\mathrm{H1}}\}\{\mathrm{TH}_{\mathrm{H2}}(t)-\mu_{\mathrm{H2}}\}\right]}{\sigma_{\mathrm{H1}}\cdot\sigma_{\mathrm{H2}}}, \tag{4.5.5}$$

where $\mathrm{E}[\cdot]$ is the mathematical expectation, μ_{H1} and μ_{H2} are the mean values, and σ_{H1} and σ_{H2} are the standard deviations of $\mathrm{TH}_{\mathrm{H1}}(t)$ and $\mathrm{TH}_{\mathrm{H2}}(t)$, respectively (Chen, 1975, ASCE, 2005).

By solving the optimization problem (4.5.4), the second horizontal earthquake ground motion, which is statistically independent of the first horizontal earthquake ground motion and closely matches the target design spectrum, is generated.

For generating the second horizontal spectrum-compatible earthquake ground motion, the Hilbert energy spectrum (HES) is considered to be a further quantitative generation target in this study. While the seismic design spectrum characterizes the ground motion and effects on structures, the HES represents the time–frequency–energy distribution of the ground motion. Since the target seismic design spectra for two horizontal directions are the same, equal Hilbert energy spectra of the two generated horizontal earthquake ground motions is desirable to represent the seismic hazard environment at the same location.

Having the second horizontal earthquake ground motion, which closely matches the target design spectrum, the second horizontal spectrum-compatible earthquake ground motion can then be obtained by scaling the second generated ground motion linearly, with the same scaling factor as used for the first generated ground motion, to achieve the same HES as the first ground motion and meet the acceptance criteria in the codes (ASCE, 1998, ASCE, 2005, ASCE, 2009). It is noted that linearly scaling two time-histories does not change the correlation coefficient between them.

Generation of vertical spectrum-compatible ground motion

The last step is to generate vertical spectrum-compatible earthquake ground motion. Each of the selected vertical recorded ground motion is decomposed into a number of IMF components via EMD. The n generated IMF components from the selected vertical recorded ground motions are treated as the basis to represent a nonstationary vertical earthquake ground motion.

The time-dependent amplitude and the instantaneous frequency of each IMF are then generated through HSA. The HHT amplitudes $a_{\mathrm{V},k}(t)$ and the instantaneous frequencies $\omega_{\mathrm{V},k}(t)$ of the vertical recorded ground motions are thus scaled to obtain the vertical earthquake ground motion

$$\mathrm{TH_V}(\mathbf{x},t) = \Re \sum_{k=1}^{n} \left[x_k\, a_{\mathrm{V},k}(t)\right] \mathrm{e}^{\mathrm{i}\, x_{n+k} \int \omega_{\mathrm{V},k}(t)\mathrm{d}t}, \tag{4.5.6}$$

where $x_1, x_2, \ldots, x_n$ are the amplitude scaling parameters, $x_{n+1}, x_{n+2}, \ldots, x_{2n}$ are the frequency scaling parameters, and $\mathbf{x} = \{x_1, x_2, \ldots, x_{2n}\}^T$ is the vector of scaling parameters.

A constrained optimization model is then used:

$$\begin{aligned} &\text{minimize:} \quad V = \sum_{p=1}^{P} f_p(\mathbf{x}), \quad f_p(\mathbf{x}) = \frac{\left|S[\mathrm{TH_V}(\mathbf{x},t), T_p] - S_{\mathrm{T,V}}(T_p)\right|}{S_{\mathrm{T,V}}(T_p)}, \\ &\text{subjected to constraints:} \quad \left|\rho[\mathrm{TH_V}(\mathbf{x},t), \mathrm{TH_{H1}}(t)]\right| \leqslant c, \\ &\qquad\qquad\qquad\qquad\quad \left|\rho[\mathrm{TH_V}(\mathbf{x},t), \mathrm{TH_{H2}}(t)]\right| \leqslant c, \end{aligned} \tag{4.5.7}$$

where $S_{\mathrm{T,V}}(T_p)$ is the spectral acceleration of the target design spectrum for vertical component at period T_p.

By solving optimization problem (4.5.7), the earthquake ground motion in the vertical direction, whose response spectrum closely matches the target design spectrum for vertical component, is generated. The vertical spectrum-compatible earthquake ground motion can then be obtained by scaling the generated ground motion linearly to meet the acceptance criteria in the codes (ASCE, 1998, ASCE, 2005, ASCE, 2009). The generated spectrum-compatible earthquake ground motion in the vertical direction is thus statistically independent of each of the two generated spectrum-compatible earthquake ground motions in the horizontal directions.

4.5.2 Numerical Examples

The conventional design spectra (CDS) for nuclear energy facilities at Quebec City are used as the horizontal target design spectrum. The standard spectral shape of the CDS is from Standard CAN3-N289.3-M81 (CSA, 1981). The peak ground acceleration (PGA) for Quebec City is derived by the Geological Survey of Canada (GSC), which has the probability of exceedence of 0.0004 per annum (2% in 50 years). The CDS for Quebec City is then obtained by scaling the standard spectral shape using the PGA for Quebec City.

As the second example, the uniform hazard spectra (UHS) for nuclear energy facilities in eastern North America (ENA) region is used as the horizontal target design spectrum. The ENA UHS is derived for nuclear energy facilities in ENA region with low probability of exceedence level from 0.001 to 0.00001 per annum (Atkinson and Elgohary, 2007). The ENA UHS for nuclear power plants stops at high frequency of 100 Hz because its spectral shape has much larger amplitudes at frequencies between 20 Hz and 100 Hz compared to the CDS for nuclear energy facilities. It is widely recognized that the ENA UHS is consistent with the seismic hazard circumstances in eastern North America region and this high-frequency ground motion may cause damaging response stresses in high-frequency sensitive equipments of nuclear power plants (EPRI, 2007).

These two selected target design spectra are for firm ground conditions (average shear wave velocity to a depth of 30 m greater than 750 m/sec) and for 5% critical damping.

According to the seismic design codes (CSA, 1981, ASCE, 1998), the vertical target design spectra for Quebec City and ENA region are obtained by scaling the corresponding coordinates of the horizontal design spectra for these two sites by two-thirds throughout the entire frequency range.

The seed recorded ground motions for each site are selected based on the results of the seismic hazard deaggregation (SHD) (Halchuk and Adams, 2004, Atkinson and Elgohary, 2007). The results of the SHD and the selected earthquake ground motions for these two sites are listed in Tables 4.6 and 4.7, respectively.

Table 4.6: Mean values of seismic hazard deaggregation

Location	Vibration period	Seismicity	Hypocentral distance	Moment magnitude
Quebec City	s(0.2 sec)*	0.56 g	41 km	6.4
	s(1.0 sec)*	0.14 g	100 km	7.1
ENA Sites	Short	Moderate	0–50 km	5.5–6.5
	Long	Moderate	20–150 km	6.5–7.5

$*$ $s(T)$ is the uniform hazard spectral acceleration at vibration period T.

To characterize the large-amplitude high frequency portion of the Eastern North America (ENA) UHS, three small near-field earthquakes are selected. One large far-field earthquake is used for the low frequency portion of the ENA UHS.

The response spectra of the generated horizontal and vertical earthquake ground motions and the selected seed recorded earthquake ground motions for each site are shown in Figures 4.47, 4.53, 4.59, and 4.65, respectively. The ratios of response spectra of generated spectrum-compatible earthquake ground motions to the target design spectra frequency by frequency, as shown in Figures 4.48, 4.54, 4.60, and 4.66, are within the range from 0.9 to 1.3.

As shown in Table 4.8, the PGA of each generated earthquake ground motion is greater than that of the corresponding target seismic design spectrum. The average of the ratios of each resulting response spectrum to the target design spectrum frequency by frequency is greater than 1. The correlation coefficients between the components of each set of tri-directional ground motion are less than 0.3. The generated tri-directional spectrum-compatible earthquake ground motions thus meet all the acceptance criteria in the codes (ASCE, 1998, ASCE, 2005, ASCE, 2009).

The generated horizontal and vertical spectrum-compatible earthquake ground motions and their corresponding seed recorded earthquake ground motions for each site are shown in Figures 4.49-4.51, 4.55, 4.57, 4.58, 4.61-4.63, 4.67, 4.69, and 4.70. Although the two gener-

Table 4.7: Selected actual earthquake records

Location	EQ*	TP§	D† (km)	M‡	Hor-1⋆,-2⋆	Ver⋆
Quebec City	WN	SN	21.2	6.0	A-MTW-000,-090	A-MTW-UP
	NPS	SN	25.8	6.0	SIL-000,-090	SIL-UP
	LP	LF	79.7	6.9	RIN-000,-090	RIN-UP
ENA Sites	CL	SN	16.3	6.2	G01-230,-320	G01-UP
	SA	SN	51.7	5.9	S16-214,-124	S16-UP
	SA	SN	70.5	5.9	S17-000,-270	S17-UP
	LP	LF	78.3	6.9	PJH-045,-315	PJH-UP

∗ Earthquake names: WN, Whittier Narrows Earthquake, 1987/10/01 14:42; NPS, N. Palm Springs Earthquake, 1986/07/08 09:20; LP, Loma Prieta Earthquake, 1989/10/18 00:05; CL, Coyote Lake Earthquake, 1979/08/06 17:05; SA, Saguenay Earthquake, 1988/11/25 23:46.

§ Earthquake types: SN, Small Near-field Earthquake; LF, Large Far-field Earthquake.

† D is the closest distance to fault rupture, which is generally the hypocentral distance.

‡ M is the moment magnitude.

⋆ Names of two horizontal components and one vertical component of earthquake records, which can be searched from PEER and NRCAN databases.

ated horizontal components of each set of the ground motion appear to be similar, they are statistically independent. The generated spectrum-compatible earthquake ground motions generally preserve the temporal characteristics of the seed recorded ground motions.

Table 4.8: Information of generated earthquake ground motions

Location	PGA-DS* (g)	PGA-TH§ (g)	AR†	ρ‡
Quebec City	H1⋆ = 0.367 H2⋆ = 0.367 V⋆ = 0.245	H1 = 0.429 H2 = 0.425 V = 0.271	H1 = 1.09 H2 = 1.36 V = 1.32	ρ[H1, H2] = 0.058 ρ[H1, V] = 0.026 ρ[H2, V] = 0.025
ENA Sites	H1 = 0.300 H2 = 0.300 V = 0.200	H1 = 0.367 H2 = 0.388 V = 0.208	H1 = 1.16 H2 = 1.11 V = 1.02	ρ[H1, H2] = 0.275 ρ[H1, V] = 0.018 ρ[H2, V] = 0.013

∗ Peak ground acceleration of target seismic design spectrum.

§ Peak ground acceleration of generated earthquake ground motion.

† Average of ratios of resulting response spectrum to target seismic design spectrum.

‡ Correlation coefficient between two ground motion components.

⋆ H1, H2, and V are two horizontal components and one vertical component of a set of tri-directional ground motions, respectively.

The color-mapped Hilbert energy spectrum (HES) of the generated tri-directional spectrum-compatible earthquake ground motion for each numerical example is shown in Figures 4.52, 4.56, 4.64, and 4.68, respectively. Two horizontal generated earthquake ground motions of each set of the ground motion have the same HES. It can be seen that the generated earthquake ground motions have sufficient energy over the entire frequency range.

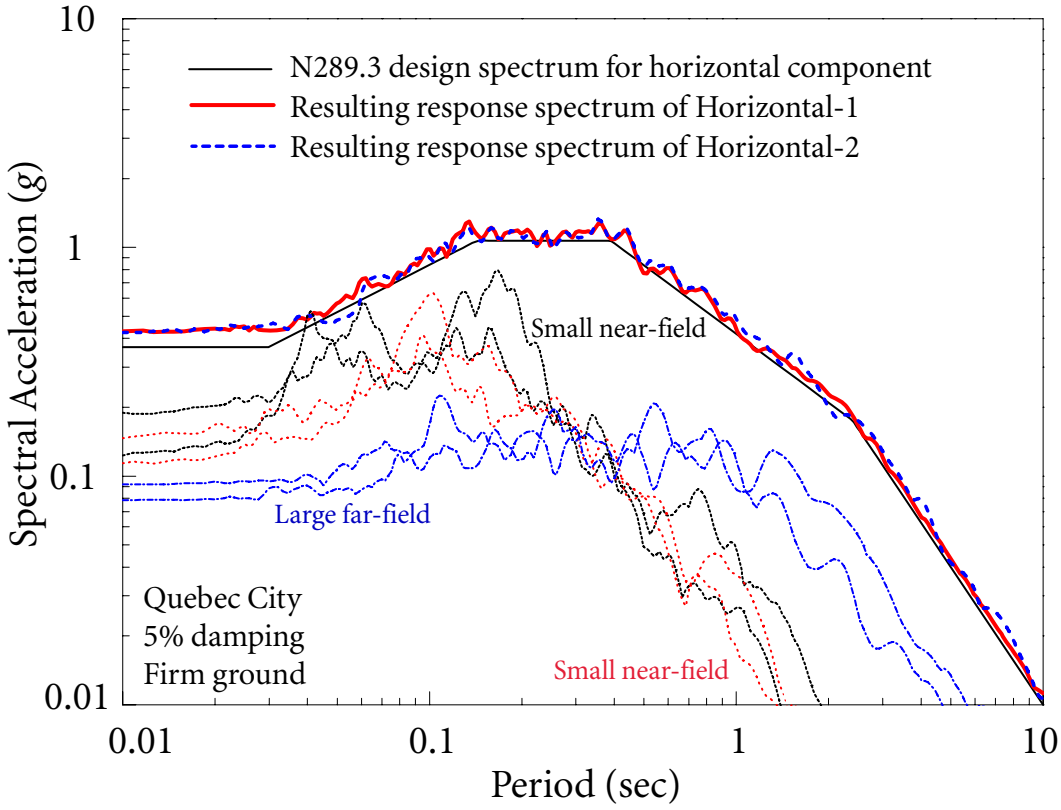

Figure 4.47 Horizontal response spectra for Quebec City

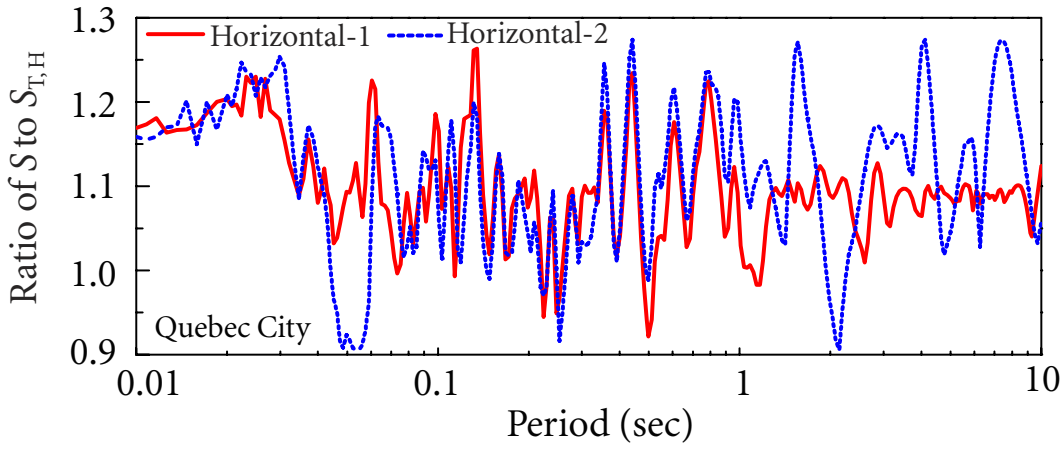

Figure 4.48 Ratio of resulting horizontal response spectra to target horizontal design spectrum for Quebec City

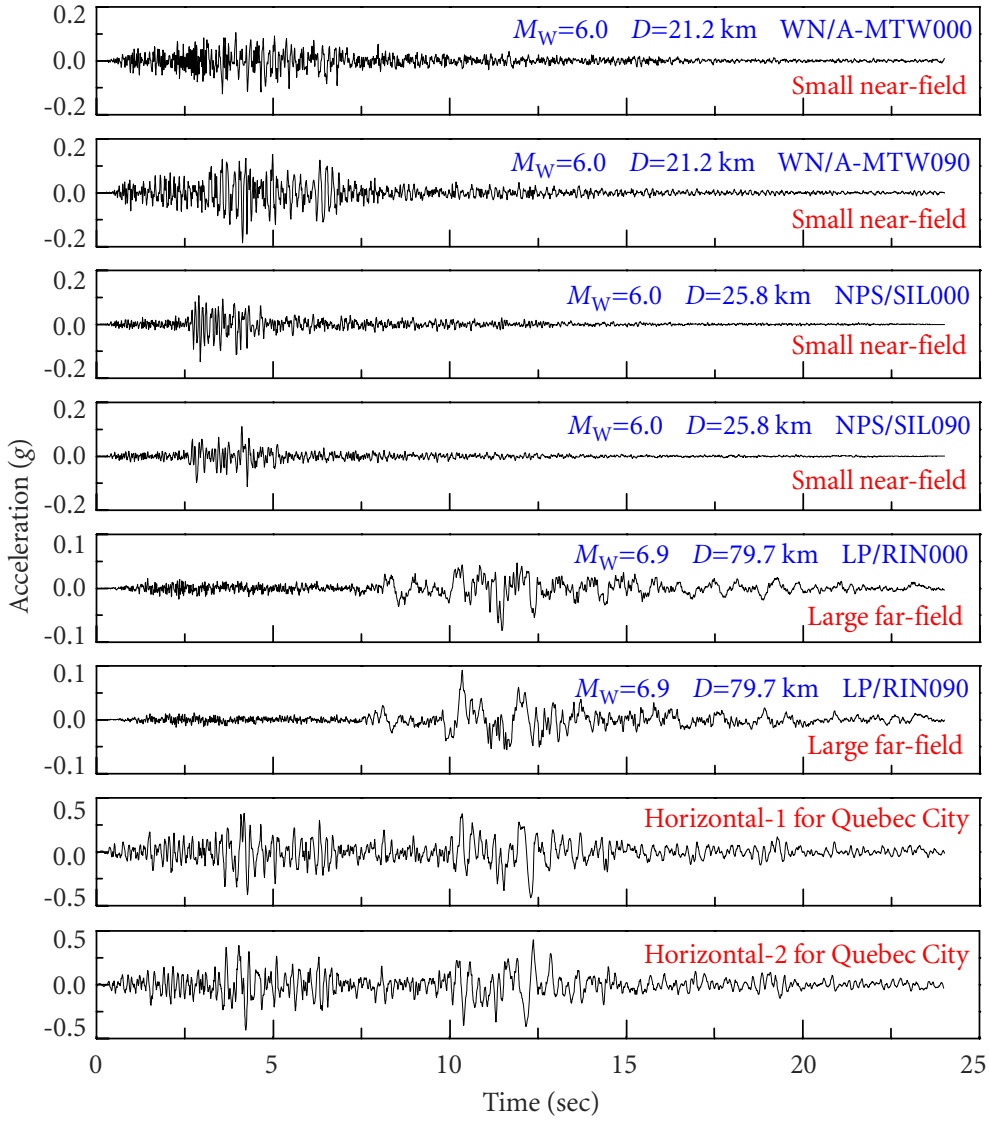

Figure 4.49 Horizontal earthquake ground motions for Quebec City

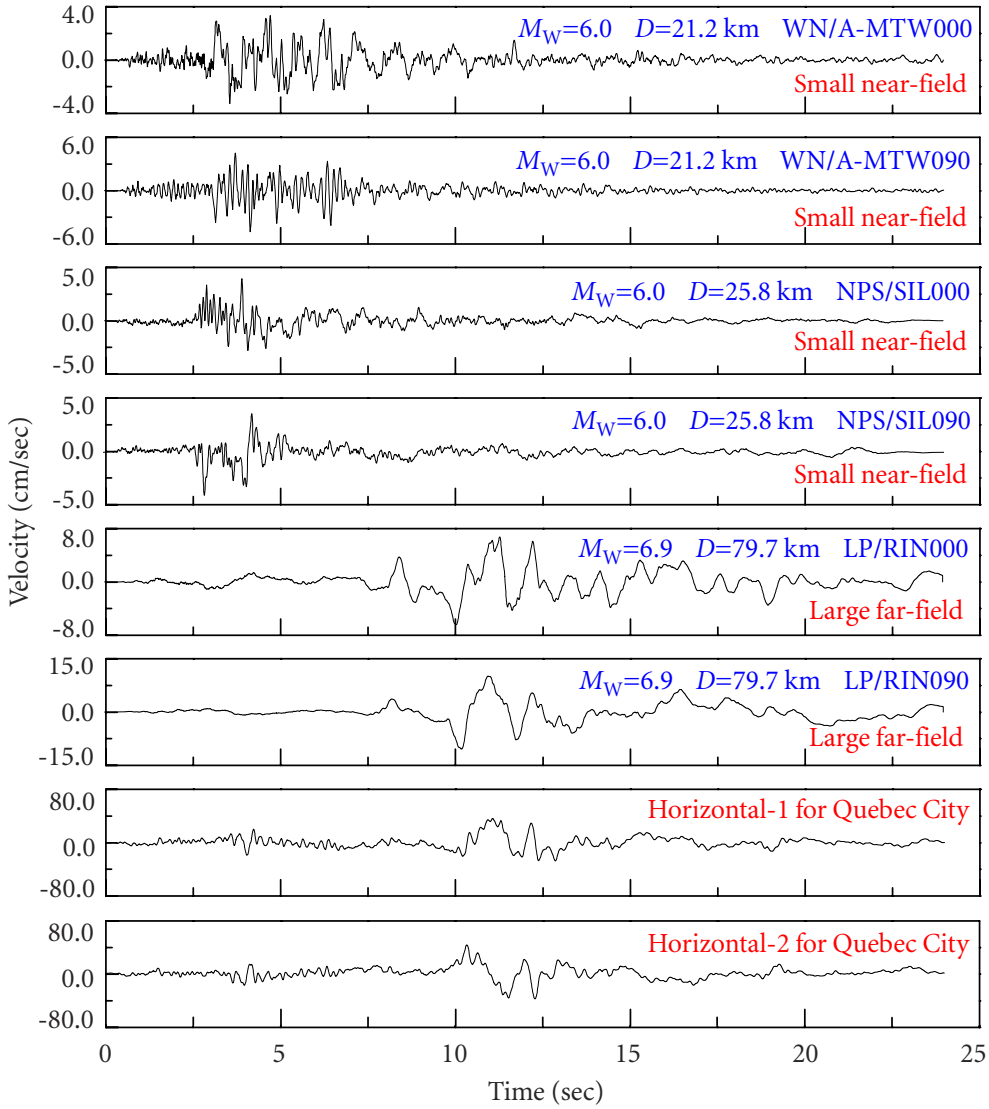

Figure 4.50 Horizontal earthquake ground motions for Quebec City

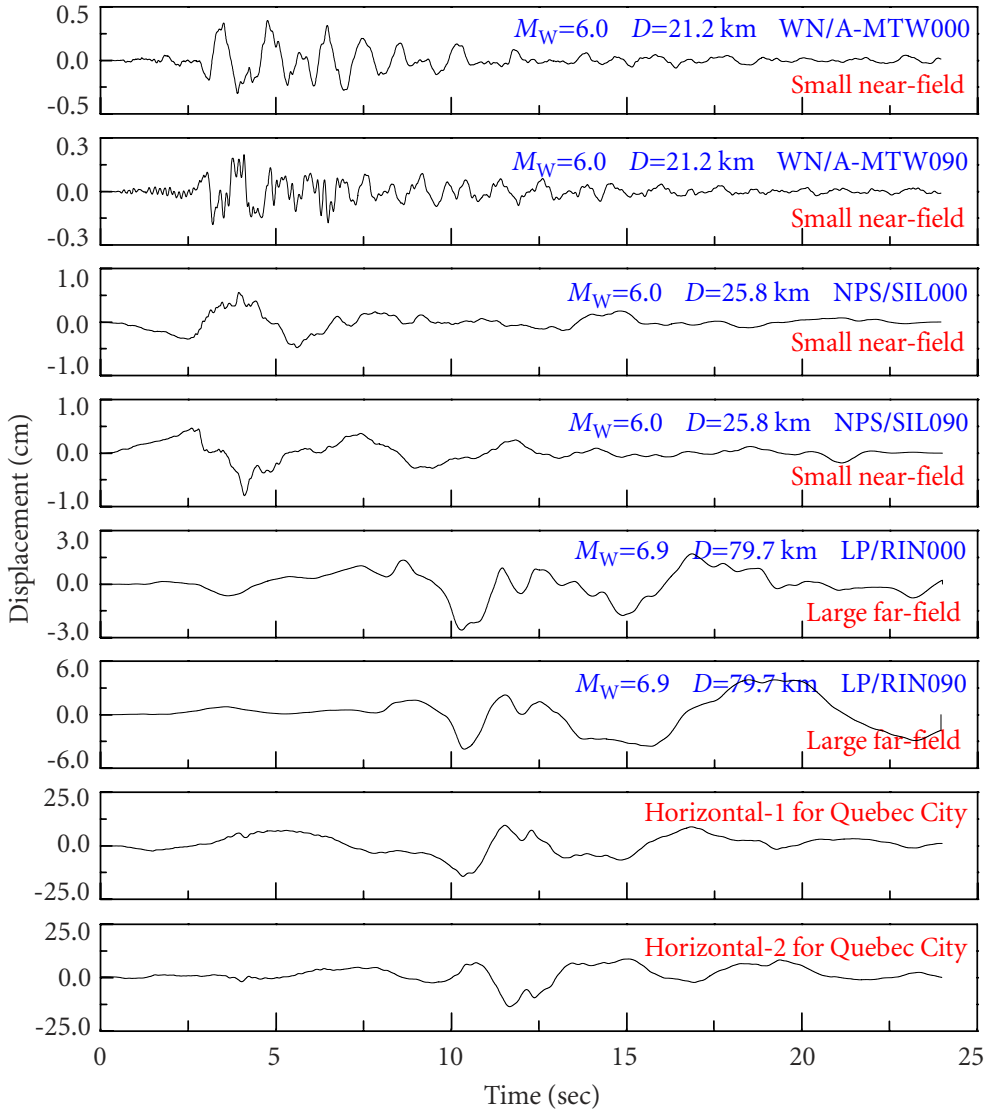

Figure 4.51 Horizontal earthquake ground motions for Quebec City

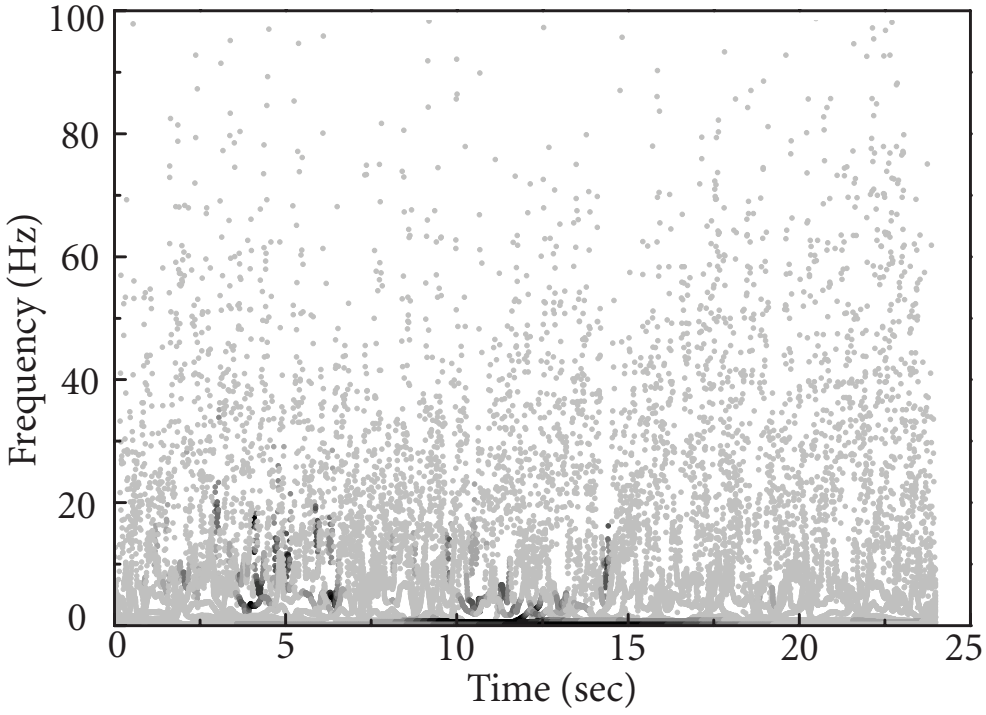

Figure 4.52 Hilbert energy spectrum of generated horizontal ground motions for Quebec City

4.6 Summary

In this chapter, the properties and limitations of the existing spectral matching algorithms are discussed. To overcome some deficiencies of the existing method, the Hilbert-Huang transform (HHT) is applied to generate spectrum-compatible earthquake ground motions based on recorded ground motions. The primary advantage of using the HHT in compatibility algorithms is that the basis functions of the HHT transformation are empirically derived from the ground motion data themselves, which guarantees the adaptivity of the transformation method and thus preserves the nonstationary characteristics of seed recorded ground motions. Strategies for selecting recorded ground motions based on the PSHA are also provided, which are compatible with the physical meanings of the PSHA-based seismic design spectra. The spectral matching algorithms proposed in this chapter are summarized as follows:

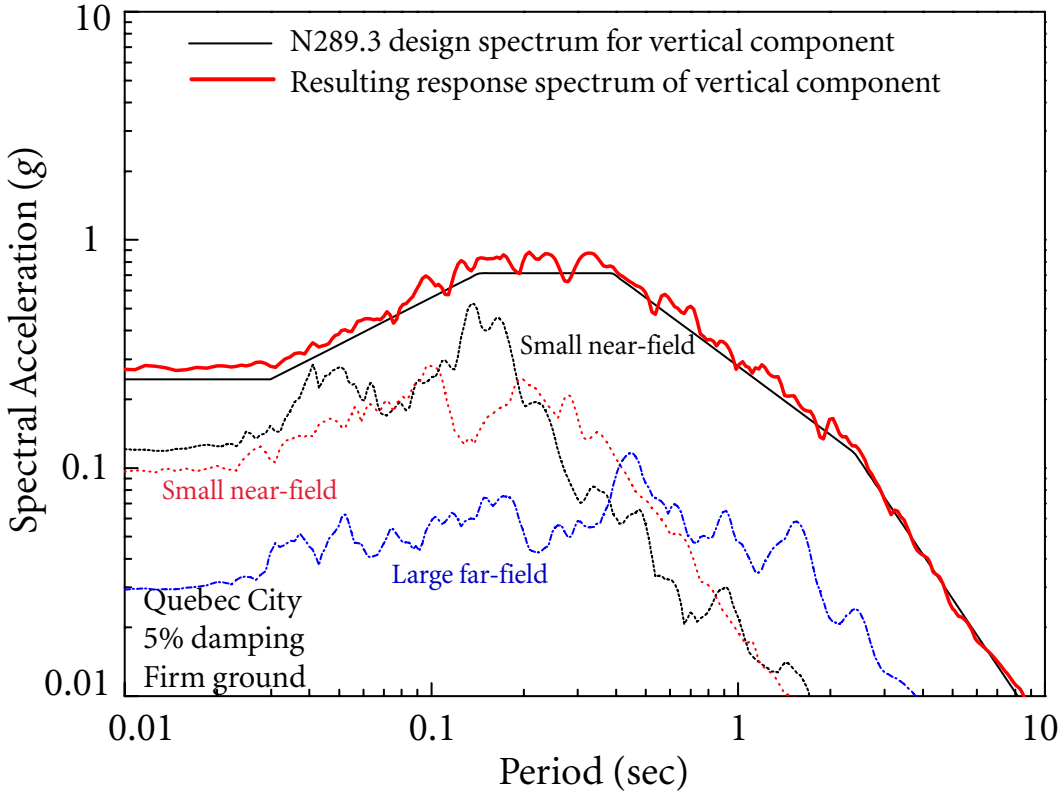

Figure 4.53 Vertical response spectra for Quebec City

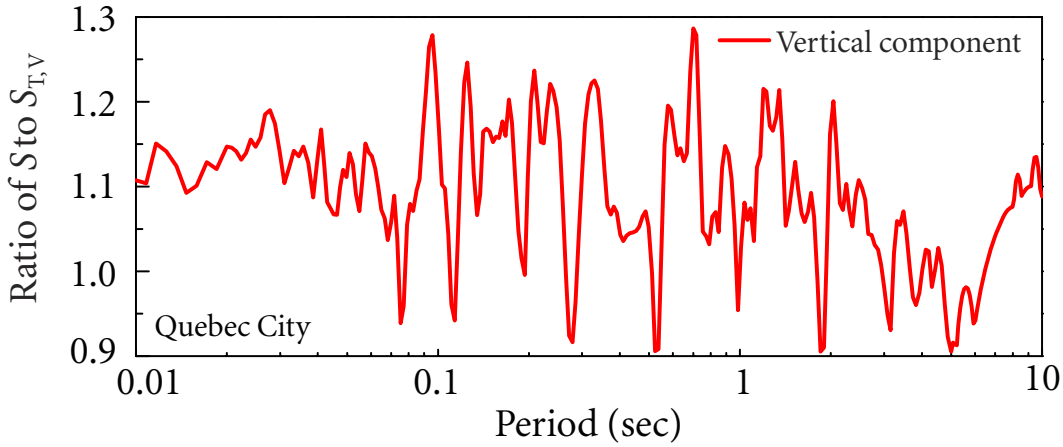

Figure 4.54 Ratio of resulting vertical response spectrum to target vertical design spectrum for Quebec City

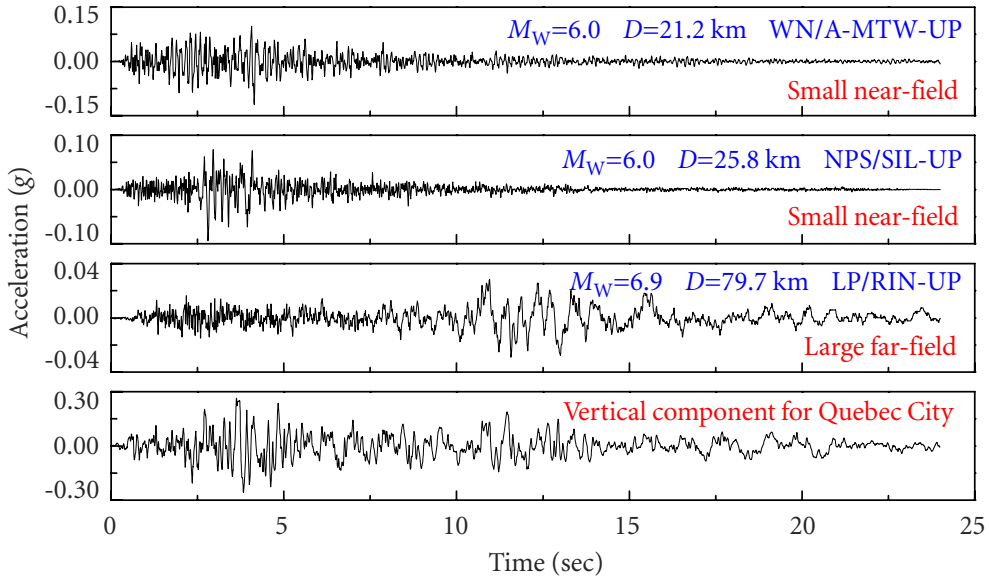

Figure 4.55 Vertical earthquake ground motions for Quebec City

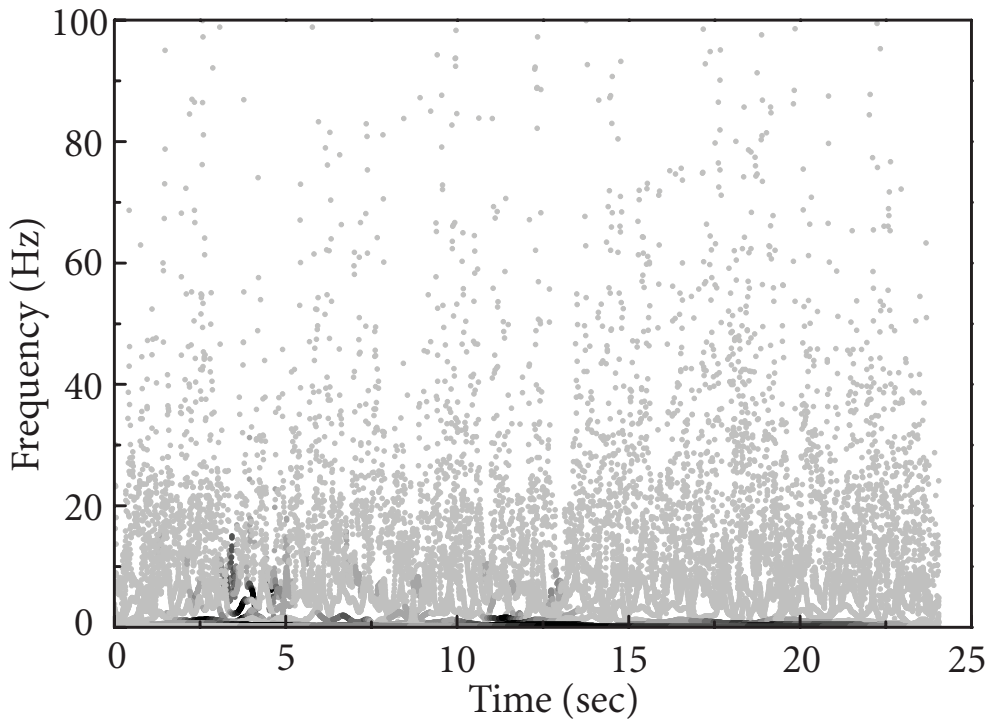

Figure 4.56 Hilbert energy spectrum of generated vertical ground motion for Quebec City

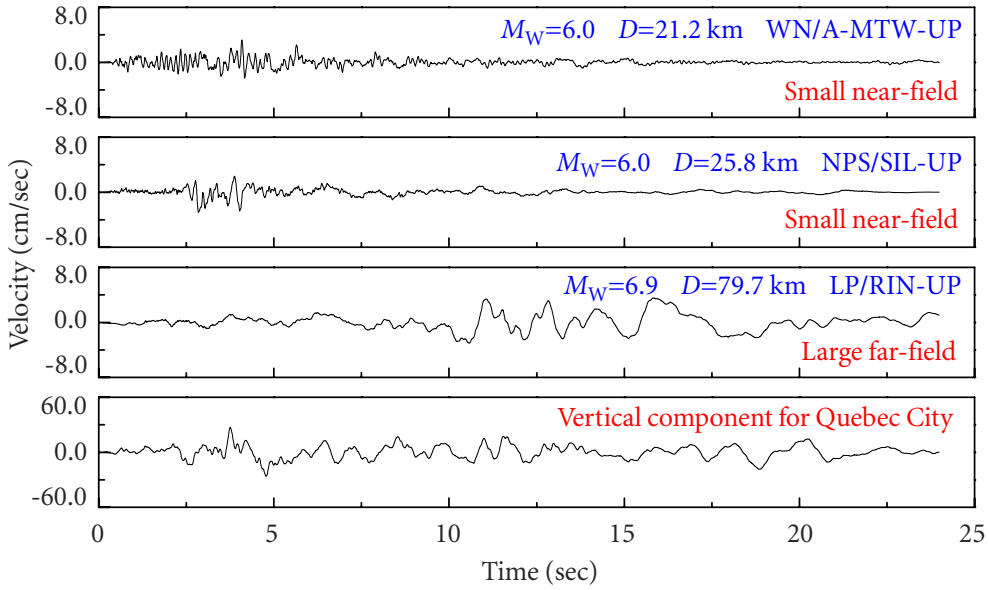

Figure 4.57 Vertical earthquake ground motions for Quebec City

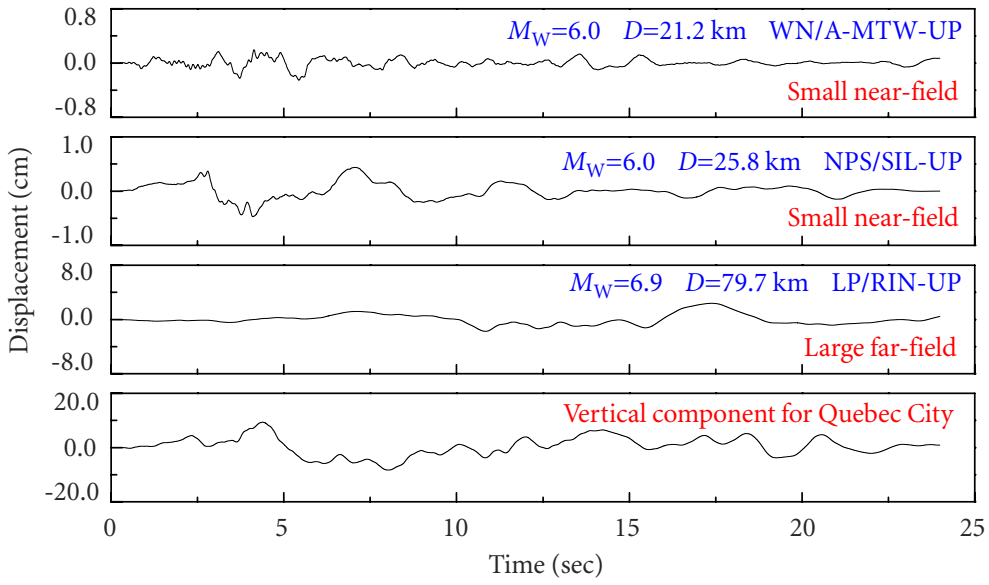

Figure 4.58 Vertical earthquake ground motions for Quebec City

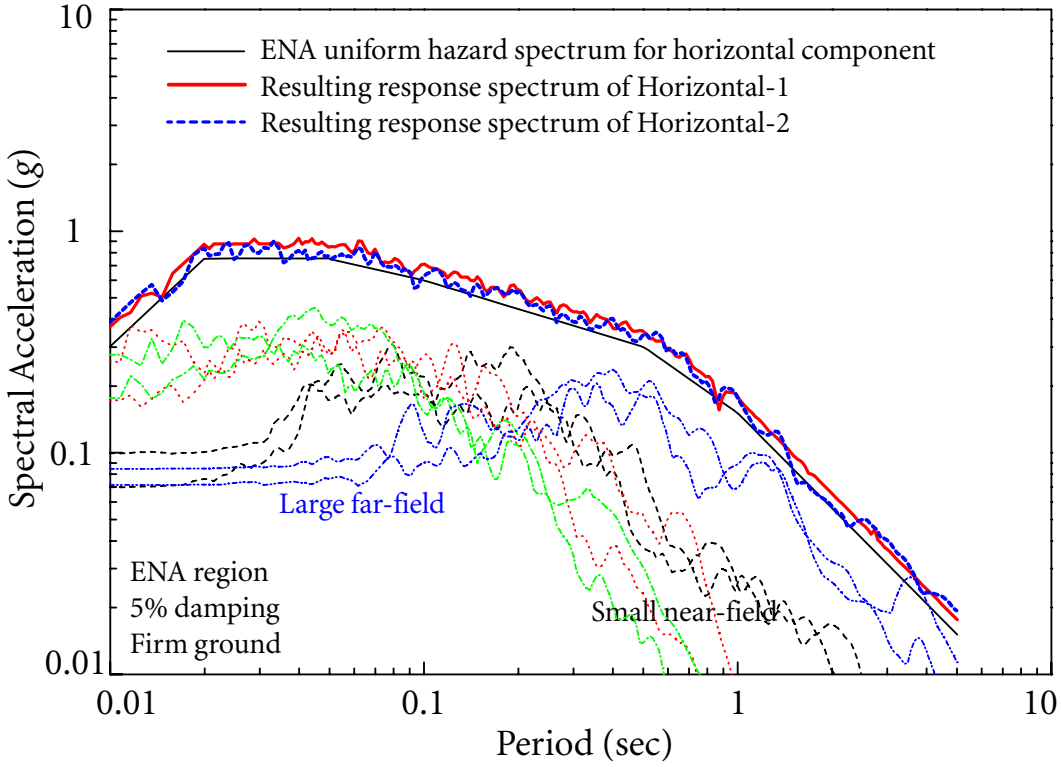

Figure 4.59 Horizontal response spectra for eastern North America

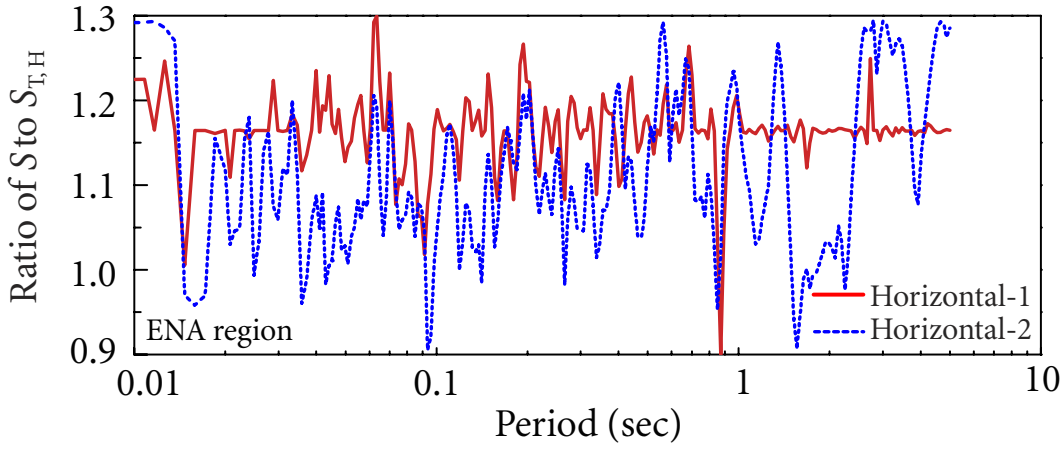

Figure 4.60 Ratio of resulting horizontal response spectra to target horizontal UHS for ENA

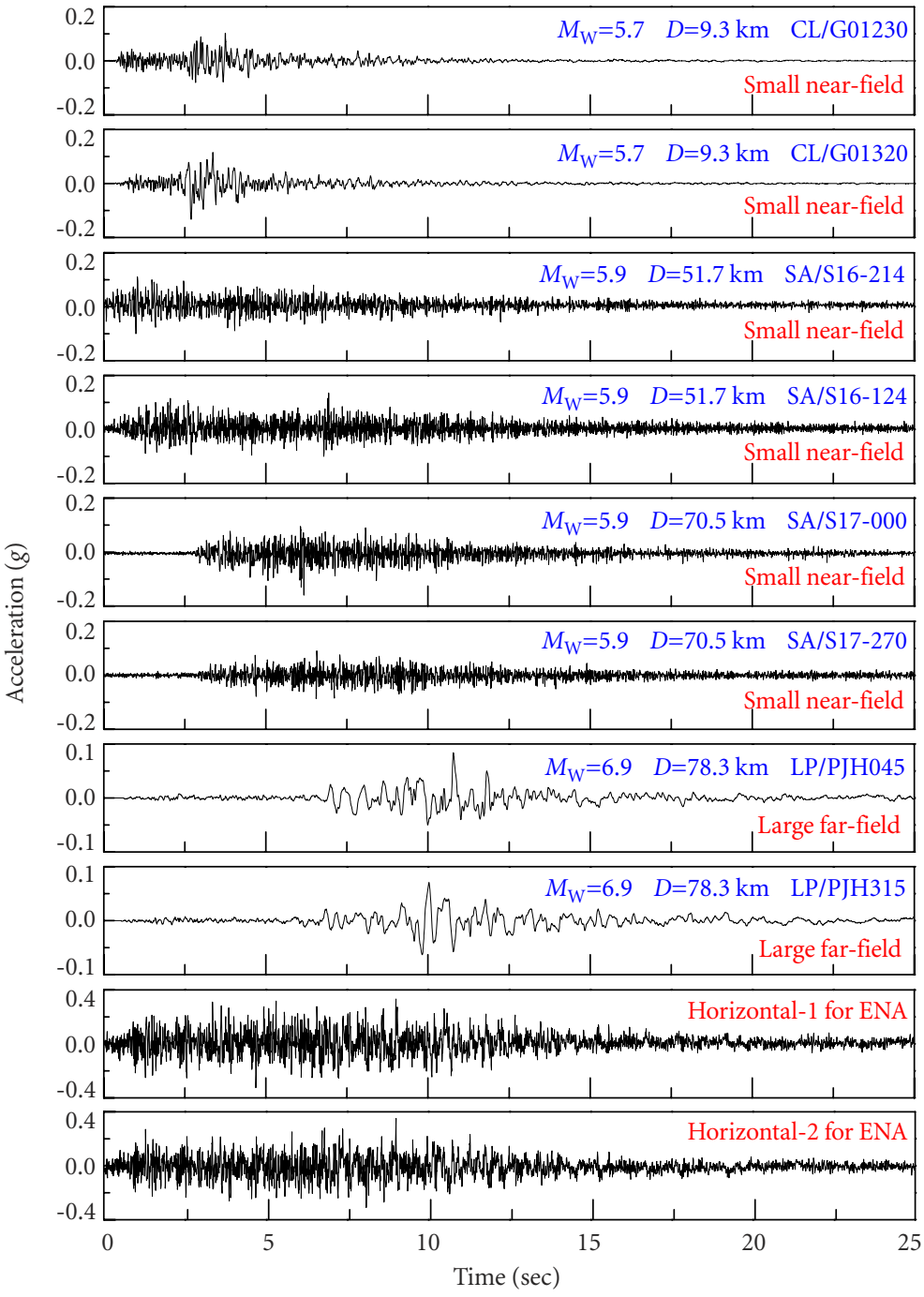

Figure 4.61 Horizontal earthquake ground motions for ENA

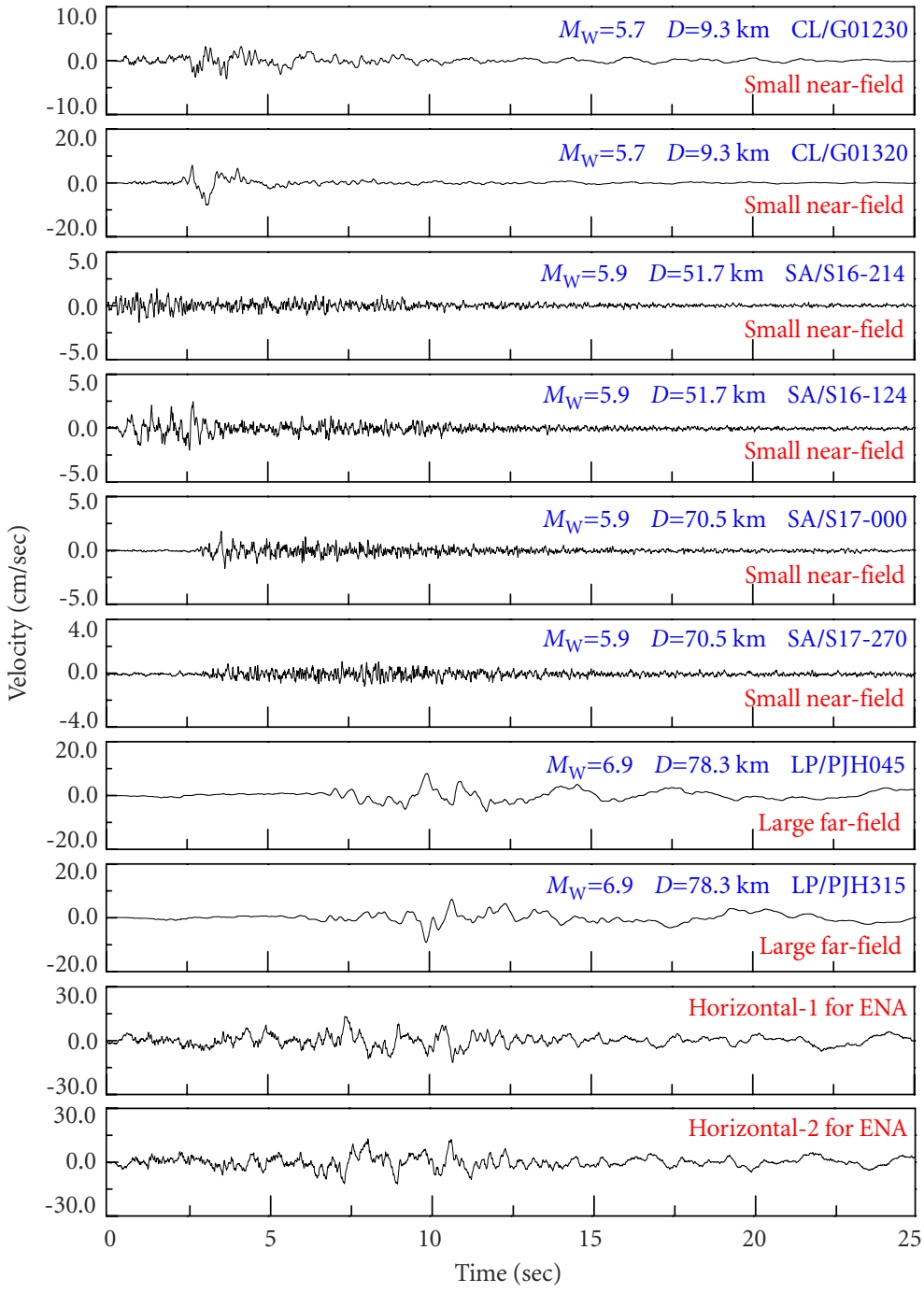

Figure 4.62 Horizontal earthquake ground motions for ENA

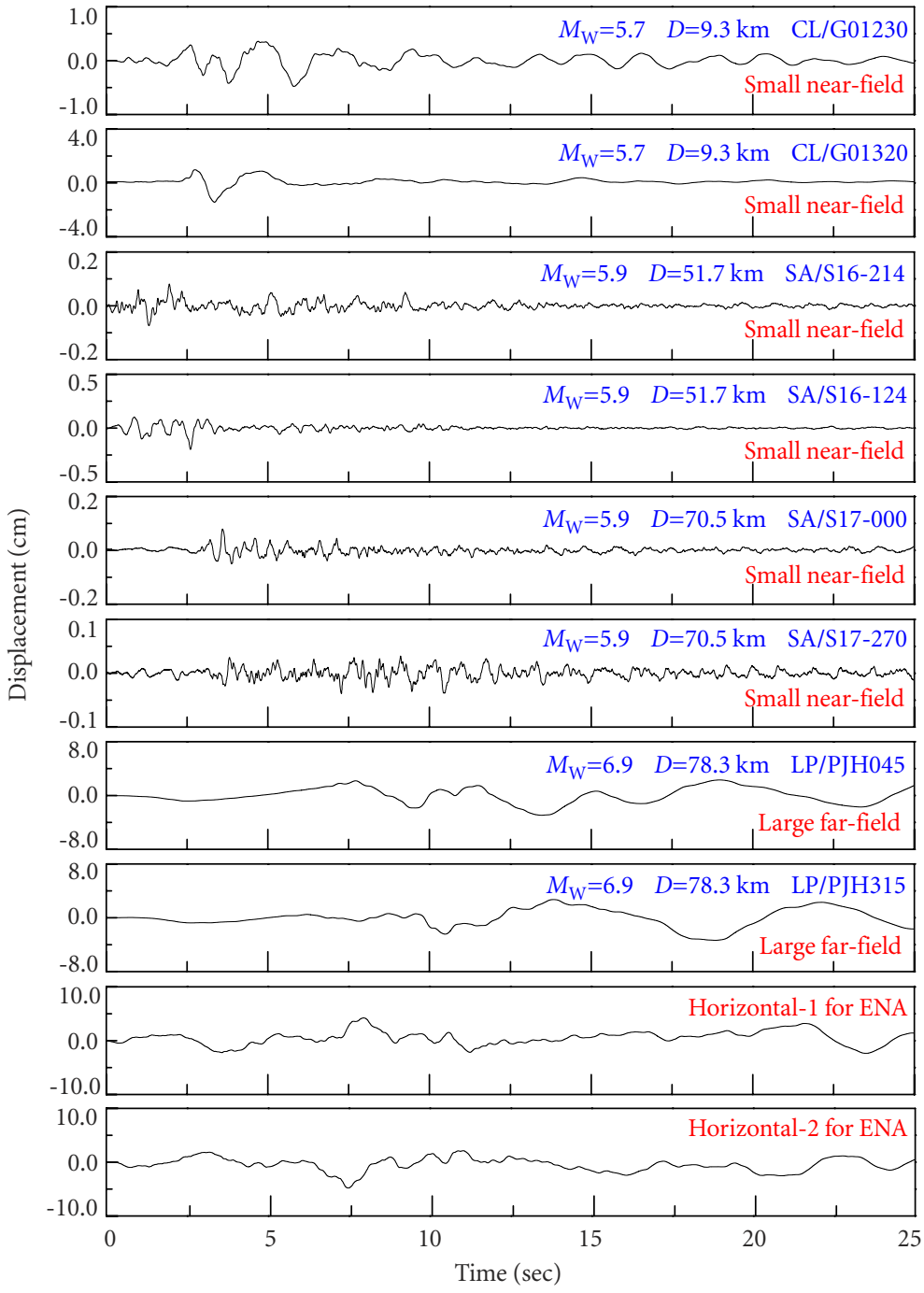

Figure 4.63 Horizontal earthquake ground motions for ENA

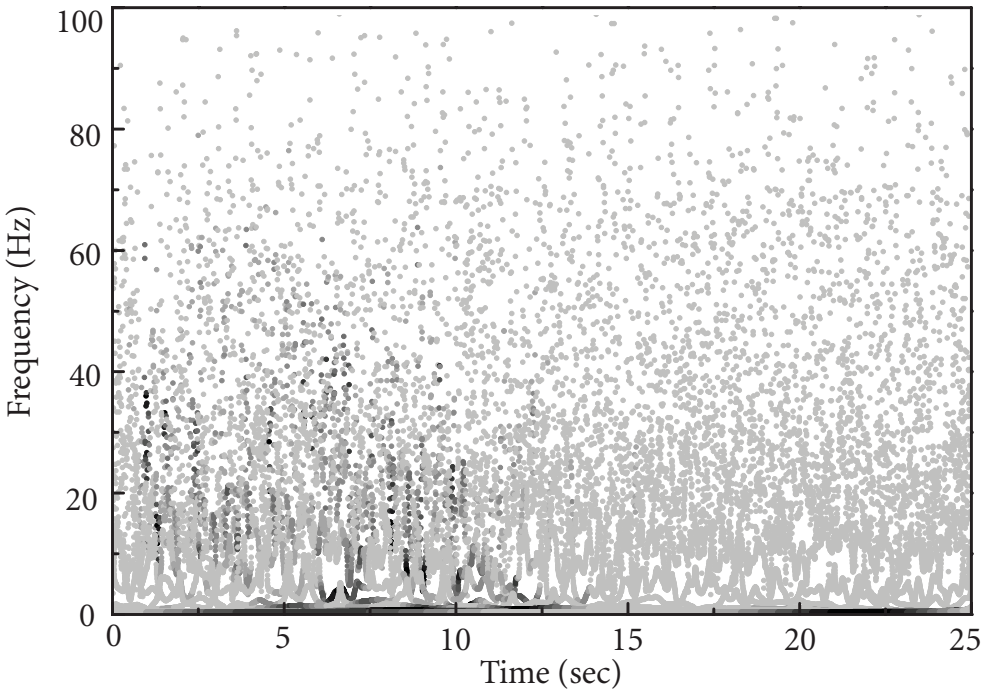

Figure 4.64 Hilbert energy spectrum of generated horizontal ground motions for ENA

1. A method for generating a single earthquake ground motion compatible with the target seismic design spectrum, based on the HHT of multiple recorded ground motions and optimization technique, is proposed. The generation procedure is suitable for any type of seismic design spectra. The generated earthquake ground motions preserve the nonstationary characteristics of the seed recorded ground motions.

2. Based on the first proposed method, an approach is presented for generating a desired number of earthquake ground motions compatible with a target seismic design spectrum for building structural design based on a small number of recorded ground motions. This set of spectrum-compatible earthquake ground motions is generated by using the HHT and solving related optimization problems. The variabilities of the resulting spectral accelerations at individual vibration periods and between any two periods are considered. The generation procedure not only preserves the nonstationary characteristics of the seed recorded ground motions but also ensures the intrinsic aleatory variability of the generated ground motions for a scenario earthquake.

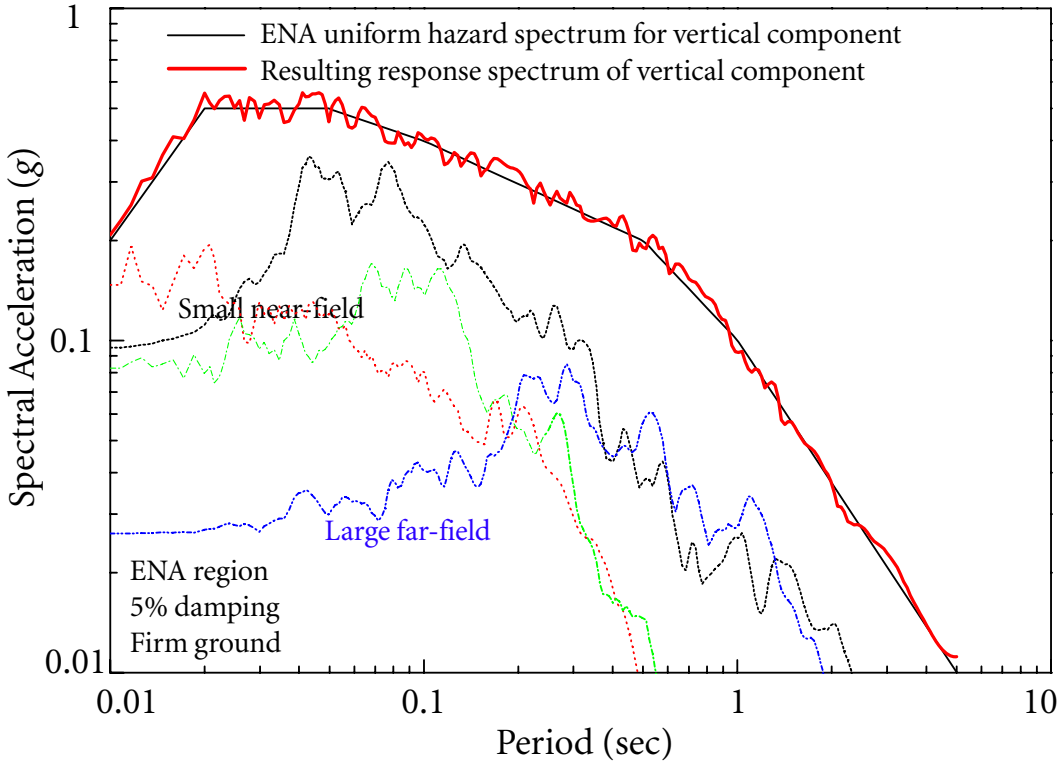

Figure 4.65 Vertical response spectra for ENA

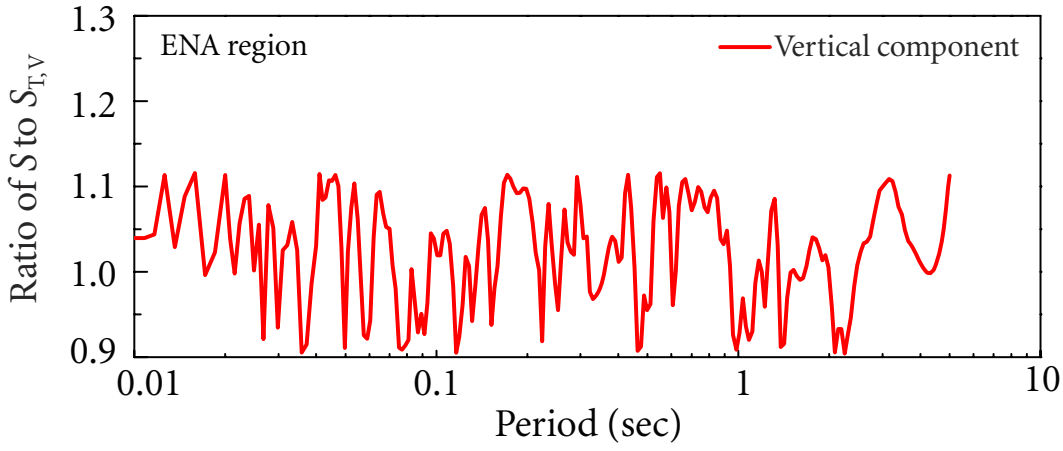

Figure 4.66 Ratio of resulting vertical response spectrum to target vertical UHS for ENA

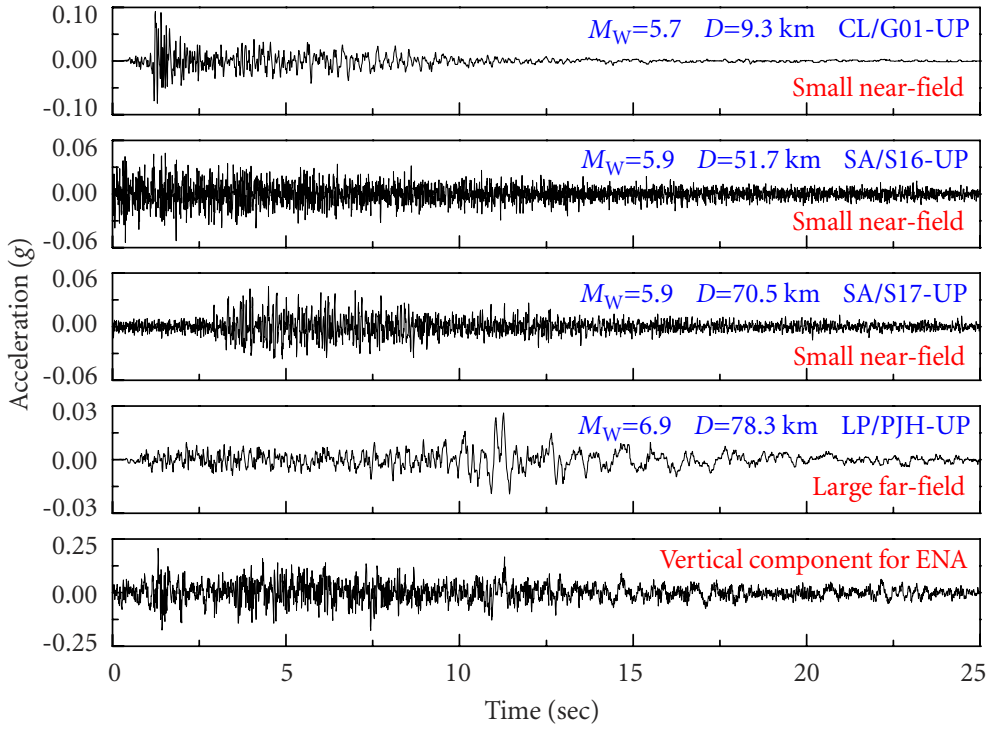

Figure 4.67 Vertical earthquake ground motions for ENA

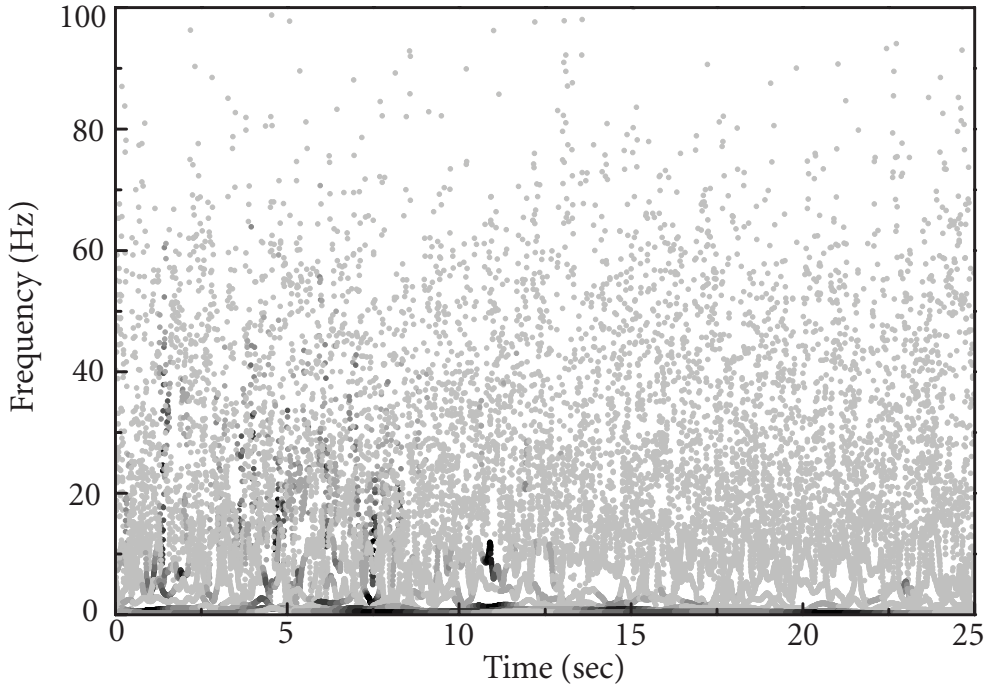

Figure 4.68 Hilbert energy spectrum of generated vertical ground motion for ENA

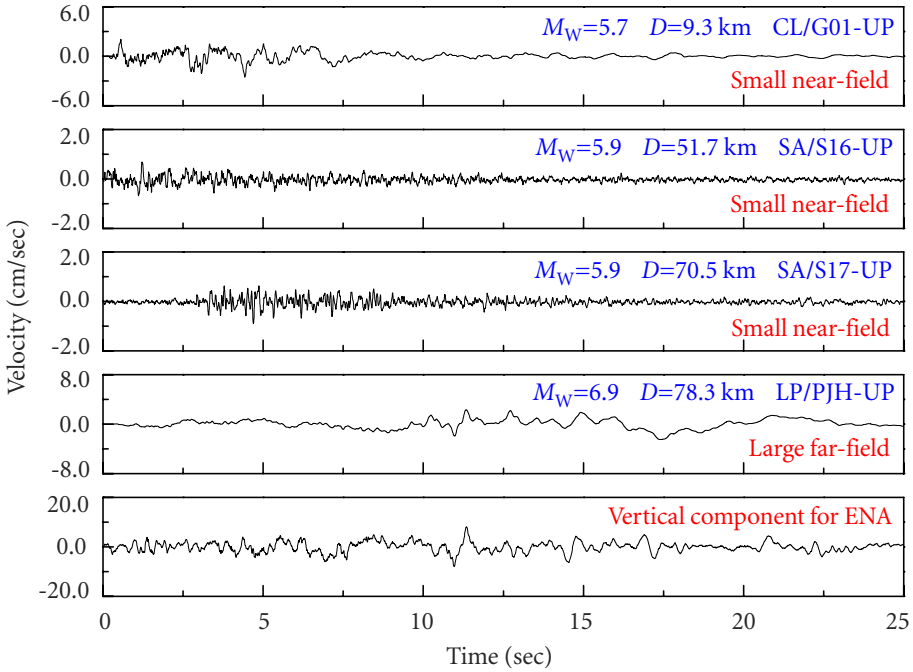

Figure 4.69 Vertical earthquake ground motions for ENA

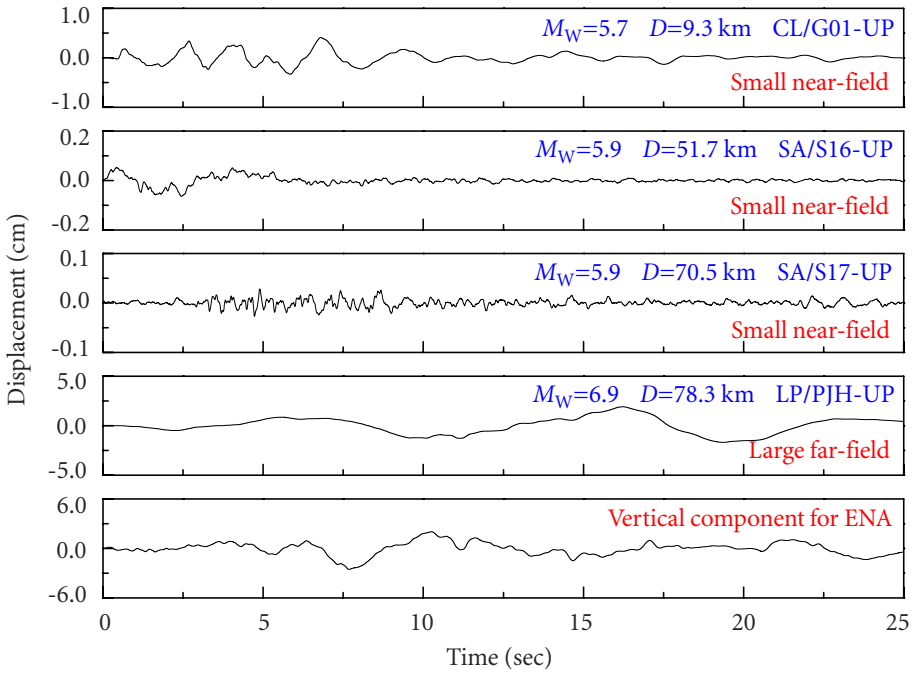

Figure 4.70 Vertical earthquake ground motions for ENA

3. Based on the first proposed method, a method for generating a set of tri-directional earthquake ground motions compatible with the target seismic design spectra, for nuclear energy facilities and based on multiple sets of recorded ground motions and optimization techniques, is presented. Three orthogonal components of generated earthquake ground motion are statistically independent in an engineering sense. Two horizontal components have the same frequency-time-energy distribution. The generation procedure preserves the nonstationary characteristics of the seed recorded ground motions and also meets the stringent requirements in current seismic design codes.

The spectral matching algorithms presented in this chapter are all programmed using MATLAB codes. A built-in optimization algorithm, constrained nonlinear multi-variable line-search, is applied to minimize all the objective functions. In order to popularize the proposed approaches, these spectral matching algorithms in MATLAB codes may be organized and be available to the public for download in the near future as part of a future study.

C H A P T E R 5

Conclusions and Future Research

Probabilistic seismic hazard analysis (PSHA) is a crucial tool for the determination of design earthquakes including seismic design spectra and seismic design ground motions. The purpose of this study is to bridge the gap between seismological analyses and engineering applications, i.e., to find suitable representations of design earthquakes from the PSHA. Several contributions for this purpose have been made in this study as summarized in the following.

5.1 Vector-valued Seismic Hazard Deaggregation

The scalar seismic hazard deaggregation (SHD) has been widely used for obtaining the contributing parameters (such as earthquake magnitude, source-site distance, epsilon, and the rate of occurrence) of earthquake scenarios to the seismic hazard at a given site. However, the scalar SHD does not consider the simultaneous exceedance of spectral accelerations at multiple vibration periods, i.e., the representative earthquakes are extracted for spectral accelerations at individual periods separately. In this study, the scalar SHD procedure is extended to vector-valued SHD for determining the controlling earthquake that contributes seismic hazard to spectral accelerations at multiple periods simultaneously.

5.2 Generalized Approach for Generating Design Spectra

In this study, a generalized approach is developed to generate seismic design spectra using both scalar and vector-valued probabilistic seismic hazard analysis (PSHA). The annual probability of exceeding spectral accelerations over the entire period range of engineering interest on a design spectrum is provided so that it can be interpreted as a single design earthquake. The primary properties of the seismic design spectra are summarized as follows.

- Vector-valued uniform hazard spectrum (VUHS)

    1. The spectral shape of the conventional UHS, i.e., consistent seismic hazard at each spectral acceleration, is preserved on a VUHS.
    2. The VUHS is a suitable design earthquake for structures having a wide range of structural modal periods, which have significant contributions to structural responses.

- Vector-valued non-uniform hazard spectrum (VNUHS)

    1. A relatively narrow-band spectral shape, which is concentrated at a pre-specified period or a range of periods, is achieved through the VNUHS.
    2. The VNUHS is suitable for structures with known dominant modes, and little nonlinear behavior or well-estimated nonlinear behavior.

- Vector-valued conditional uniform hazard spectrum (VCUHS)

    1. A relatively narrow-band spectral shape concentrated at specified dominant periods and the consideration of spectral correlation between the dominant periods and non-dominant periods are achieved.
    2. It is suitable for structures with known first mode but unknown higher modes effects and nonlinear behavior.

An approximation of the generalized approach is also proposed so that the seismic design spectra can be readily incorporated into ordinary structural design and performance-based

seismic design. This approximate approach is based on a set of controlling earthquakes derived from both scalar and vector-valued seismic hazard deaggregation (SHD). It is demonstrated that the selection of the controlling vibration periods does not affect the resulting design spectra and controlling earthquakes significantly, as long as the selected periods cover the entire period range of engineering interest roughly uniformly.

5.3 Spectral Matching Algorithms Based on HHT

To overcome some deficiencies of the existing method, the Hilbert-Huang transform (HHT) is applied to generate spectrum-compatible earthquake ground motions based on recorded ground motions. The primary advantage of using the HHT in the compatibility algorithm is that the basis functions of the HHT transformation are empirically derived from the ground motion data themselves, which guarantees the adaptivity of the transformation method and thus preserves the nonstationary characteristics of seed recorded ground motions. Strategies for the selection of the recorded ground motions based on the PSHA are also provided, which are compatible with the physical meanings of the PSHA-based seismic design spectra. The spectral matching algorithms proposed in this chapter are summarized as follows:

1. A method for generating a single earthquake ground motion compatible with the target seismic design spectrum, based on the HHT of multiple recorded ground motions and optimization technique, is proposed. The generation procedure is suitable for any type of seismic design spectra. The generated earthquake ground motions preserve the nonstationary characteristics of the seed recorded ground motions.

2. Based on the first proposed method, an approach is presented for generating a desired number of earthquake ground motions compatible with a target seismic design spectrum for building structural design based on a small number of recorded ground motions. This set of spectrum-compatible earthquake ground motions is generated by using the HHT and solving related optimization problems. The variabilities of the resulting spectral accelerations at individual vibration periods and between any two periods are considered. The generation procedure not only preserves the nonstation-

ary characteristics of the seed recorded ground motions but also assures the intrinsic aleatory variability of the generated ground motions for a scenario earthquake.

3. Based on the first proposed method, a method for generating a set of tri-directional earthquake ground motions compatible with the target seismic design spectra for nuclear energy facilities, based on multiple sets of recorded ground motions and optimization techniques, is presented. Three orthogonal components of generated earthquake ground motion are statistically independent in an engineering sense. Two horizontal components have the same frequency-time-energy distribution. The generation procedure preserves the nonstationary characteristics of the seed recorded ground motions and also meets the strict requirements in current seismic design codes.

5.4 Future Research

In Chapter 3, a generalized approach is developed to generate seismic design spectra using both scalar and vector-valued probabilistic seismic hazard analysis (PSHA). The spectral amplitude is quantified using vector-valued PSHA to provide the probability of simultaneous exceedance of spectral accelerations at multiple vibration periods over the entire period range of engineering interest on the design spectrum. The spectral shape is determined based on only the marginal probability or conditional probability level provided by the PSHA. However, the spectral shape of a seismic design spectrum characterizes the intrinsic frequency contents of a scenario design earthquake based on real recorded ground motions. If the characteristics of spectral shape of recorded ground motions can be incorporated into the determination of seismic design spectra based on PSHA, it would be of great help for the design spectra to properly reflect the local seismic hazard environment. Further investigations are needed on this issue.

In Chapter 4, three methodologies are developed for generating single, multiple, and tri-directional spectrum-compatible earthquake ground motions based on the Hilbert-Huang transform (HHT). The primary advantage of using the HHT in the compatibility algorithm is that the basis functions of the HHT transformation are empirically derived

from the recorded ground motions themselves, which guarantees the adaptivity of the transformation method and thus preserves the nonstationary characteristics of the seed recorded ground motions. However, the lack of a completely analytical expression in the HHT and the rigorous orthogonality of the HHT basis functions prevents it from being incorporated into random vibration theory, through which the calculations of structural and soil response in the frequency domain, e.g., for generating floor response spectra and design ground motions considering incoherency effects, are conducted. Further studies on this issue are also desirable.

Bibliography

Abrahamson, N.A. and Silva, W.J., 1997. Empirical response spectral attenuation relations for shallow crustal earthquakes. *Seismological Research Letters*, **68**(1), 94–127.

Abrahamson, N.A. and Silva, W.J., 2008. Summary of the Abrahamson & Silva NGA ground-motion relations. *Earthquake Spectra*, **24**(1), 67–97.

Algermissen, S.T. and Letendecker, E.V., 1992. A technique for uniform hazard spectra estimation in the US. In *Proceedings of* 10*th World Conference on Earthquake Engineering*, Balkema, Rotterdam.

Amiri, G.G., Bagheri, A., and Razaghi, S.A.S., 2009. Generation of multiple earthquake accelerograms compatible with spectrum via the wavelet packet transform and stochastic neural networks. *Journal of Earthquake Engineering*, **13**(7), 899–915.

ASCE, 1998. *Seismic Analysis of Safety-Related Nuclear Structures and Commentary, ASCE Standard* 4-98. American Society of Civil Engineers (ASCE).

ASCE, 2005. *Seismic Design Criteria for Structures, Systems, and Components in Nuclear Facilities, ASCE/SEI Standard* 43-05. Structural Engineering Institute, American Society of Civil Engineers (ASCE).

ASCE, 2006. *Minimum Design Loads for Buildings and Other Structures, ASCE Standard* 7-2005. American Society of Civil Engineers (ASCE).

ASCE, 2009. *Seismic Analysis of Safety-Related Nuclear Structures and Commentary, ASCE Standard* 4-09 *(Draft)*. American Society of Civil Engineers (ASCE).

Atik, L.A. and Abrahamson, N., 2010. An improved method for nonstationary spectral matching. *Earthquake Spectra*, **26**(3), 601–617.

Atkinson, G.M. and Beresnev, L.A., 1998. Compatible ground-motion time histories for new national seismic hazard maps. *Canadian Journal of Civil Engineering*, **25**(2), 305–318.

Atkinson, G.M. and Boore, D.M., 1998. Evaluation of models for earthquake source spectra in eastern North America. *Bulletin of the Seismological Society of America*, **88**(4), 917–934.

Atkinson, G.M. and Boore, D.M., 2006. Earthquake ground-motion prediction equations for eastern North America. *Bulletin of the Seismological Society of America*, **96**(6), 2181–2205.

Atkinson, G.M. and Boore, D.M., 2007. Erratum: Earthquake ground-motion prediction equations for eastern North America. *Bulletin of the Seismological Society of America*, **97**(3), 1032.

Atkinson, G.M. and Elgohary, M., 2007. Typical uniform hazard spectra for eastern North American sites at low probability levels. *Canadian Journal of Civil Engineering*, **34**(1), 12–18.

Atkinson, G.M., 2009. Earthquake time histories compatible with the 2005 National Building Code of Canada uniform hazard spectrum. *Canadian Journal of Civil Engineering*, **36**, 991–1000.

Baker, J.W. and Cornell, C.A., 2005. *Vector-valued Ground Motion Intensity Measures for Probabilistic Seismic Demand Analysis*. The John A. Blume Earthquake Engineering Center, Report No. 150.

Baker, J.W. and Cornell, C.A., 2006A. Correlation of response spectral values for multicomponent ground motions. *Bulletin of the Seismological Society of America*, **96**(1), 215–227.

Baker, J.W. and Cornell, C.A., 2006B. Spectral shape, epsilon and record selection. *Earthquake Engineering and Structural Dynamics*, **35**(9), 1077–1095.

Baker, J.W. and Cornell, C.A., 2006C. Which spectral acceleration are you using. *Earthquake Spectra*, **22**(2), 293–312.

Baker, J.W. and Jayaram, N., 2008. Correlation of spectral acceleration values from NGA ground motion models. *Earthquake Spectra*, **24**(1), 299–317.

Bazzurro, P. and Cornell, C.A., 1999. Disaggregation of seismic hazard. *Bulletin of the Seismological Society of America*, **89**(2), 501–520.

Bazzurro, P. and Cornell, C.A., 2002. Vector-valued probabilistic seismic hazard analysis. In *Proceedings of 7th U.S. National Conference on Earthquake Engineering*, Boston, Massachusetts.

Bertero, R.D. and Bertero, V.V., 2002. Performance-based seismic engineering: the need for a reliable conceptual comprehensive approach. *Earthquake Engineering and Structural Dynamics*, **31**(3), 627–652.

Boore, D.M. and Atkinson, G.M., 2008. Ground-motion prediction equations for the average horizontal component of PGA, PGV, and 5%-damped PSA at spectral periods between 0.01 s and 10.0 s. *Earthquake Spectra*, **24**(1), 99–138.

Boore, D.M., Stephens, C.D., and Joyner, W.B., 2002. Comments on baseline correction of digital strong-motion data: Examples from the 1999 Hector Mine, California, earthquake. *Bulletin of the Seismological Society of America*, **92**(4), 1543–1560.

Boore, D.M., Watson-Lamprey, J., and Abrahamson, N.A., 2006. Orientation-independent measures of ground motion. *Bulletin of the Seismological Society of America*, **96**(4A), 1502–1511.

Boore, D.M., 1983. Stochastic simulation of high-frequency ground motions based on seismological models of the radiated spectra. *Bulletin of the Seismological Society of America*, **73**(6A), 1865–1894.

Campbell, K.W. and Bozorgnia, Y., 2008. NGA ground motion model for the geometric mean horizontal component of PGA, PGV, PGD and 5% damped linear elastic response spectra for periods ranging from 0.01 to 10 s. *Earthquake Spectra*, **24**(1), 139–171.

Carballo, J.E., 2000. *Probabilistic Seismic Demand Analysis: Spectrum Matching and Design*. Doctoral Dissertation, Stanford University, California.

Chen, C., 1975. Definition of statistically independent time histories. *Journal of the Structural Division, ASCE*, **101**(2), 449–451.

Chiou, B. S.-J. and Youngs, R.R., 2008. An NGA model for the average horizontal component of peak ground motion and response spectra. *Earthquake Spectra*, **24**(1), 173–215.

Choi, D-H. and Lee, S-H., 2003. Multi-damping earthquake design spectra-compatible motion histories. *Nuclear Engineering and Design*, **226**(3), 221–230.

Chopra, A.K., 2001. *Dynamics of Structures: Theory and Applications to Earthquake Engineering*. Prentice-Hall, New Jersey, second edition.

CNE, 2004. *Eurocode 8: Design of Structures for Earthquake Resistance, Part 1: General Rules, Seismic Actions and Rules for Buildings*. European Committee for Standardization, Brussels.

Cornell, C.A., 1968. Engineering seismic risk analysis. *Bulletin of the Seismological Society of America*, **58**(5), 1583–1606.

Cramer, C.H., Kutliroff, J.R., and Dangkua, D.T., 2010. A database of eastern North America ground motions for the Next Generation Attenuation East Project. In *Proceedings of the 9th U.S. National and 10th Canadian Conference on Earthquake Engineering*, Toronto, Canada. Paper No. 0697.

CSA, 1981. *Design Procedures for Seismic Qualification of CANDU Nuclear Power Plants, Standard* CSA/CAN3-N289.3. Canadian Standard Association (CSA), Mississauga, Ontario.

Der-Kiureghian, A., 1979. *On Response of Structures to Stationary Excitations*. Report No. UCB/EERC-79/32, Earthquake Engineering Research Center, University of California at Berkeley, California.

Der-Kiureghian, A., 1980. *A Response Spectrum Method for Random Vibrations*. Report No. UCB/EERC-80/15, Earthquake Engineering Research Center, University of California at Berkeley, California.

Douglas, J., 2011. *Ground-Motion Prediction Equations 1964–2010*. BRGM/RP-59356-FR.

EPRI, 2007. *Program on Technology Innovation: The Effects of High Frequency Ground Motion on Structures, Components, and Equipment in Nuclear Power Plants*, volume 1015108. Electric Power Research Institute, California.

FEMA, 2001. *NEHRP Recommended Provisions for Seismic Regulations for New Buildings and Other Structures, 2000 Edition, Part 1: Provisions (FEMA 368)*. Building Seismic

Safety Council for the Federal Emergency Management Agency, Washington D.C.

Frankel, A., 1995. Mapping seismic hazard in the central and eastern United States. *Seismological Research Letters*, **66**(4), 8–21.

Ghaboussi, J. and Lin, C.-C.J., 1998. New method of generating spectrum compatible accelerograms using neural networks. *Earthquake Engineering and Structural Dynamics*, **27**(4), 377–396.

Ghobarah, A., 2001. Performance-based design in earthquake engineering: State of development. *Engineering Structures*, **23**(8), 878–884.

Giaralis, A. and Spanos, P.D., 2009. Wavelet-based response spectrum compatible synthesis of accelerograms-Eurocode application (EC8). *Soil Dynamics and Earthquake Engineering*, **29**(1), 219–235.

Gutenberg, B. and Richter, C.F., 1944. Frequency of earthquakes in california. *Bulletin of the Seismological Society of America*, **34**(4), 185–188.

Gu, P. and Wen, Y.K., 2007. A record-based method for the generation of tridirectional uniform hazard-response spectra and ground motions using the Hilbert-Huang transform. *Bulletin of the Seismological Society of America*, **97**(5), 1539–1556.

Hadjian, A.H., 1981. On the correlation of the components of strong ground motion–Part 2. *Bulletin of the Seismological Society of America*, **71**(4), 1323–1331.

Halchuk, S. and Adams, J., 2004. Deaggregation of seismic hazard for selected canadian cities. In *Proceedings of 13th World Conference on Earthquake Engineering*, Vancouver, Canada. Paper No. 2470.

Hancock, J., Watson-Lamprey, J., Abrahamson, N.A., Bommer, J.J., Markatis, A., McCoy, E., and Mendis, R., 2006. An improved method of matching response spectra of recorded earthquake ground motion using wavelets. *Journal of Earthquake Engineering*, **10**(Supplement 001), 67–89.

Harmsen, S., Perkins, D., and Frankel, A., 1999. Deaggregation of probabilistic ground motions in the central and eastern United States. *Bulletin of the Seismological Society of America*, **89**(1), 1–13.

Huang, N.E., Chern, C.C., Huang, K., Salvino, L.W., Long, S.R., and Fan, K.L., 2001. A new spectral representation of earthquake data: Hilbert spectral analysis of station TUC129, Chi-Chi, Taiwan, September 21, 1999. *Bulletin of the Seismological Society of America*, **91**(5), 1310–1338.

Huang, N.E., Shen, Z., Long, S.R., Wu, M.C., Shih, H.H., Zheng, Q., Yen, N.C., Tung, C.C., and Liu, H.H., 1998. The empirical mode decomposition and the Hilbert spectrum for nonlinear and non-stationary time series analysis. *The Royal Society London A: Mathematical, Physical and Engineering Sciences*, **454**(1971), 903–995.

Humar, J.L. and Rahgozar, M.A., 2000. Application of uniform hazard spectra in seismic design of multistory buildings. *Canadian Journal of Civil Engineering*, **27**(3), 563–580.

Inoue, T. and Cornell, C.A., 1990. *Seismic Hazard Analysis of Multi-Degree-of-Freedom Structures*. Department of Civil and Environmental Engineering, Reliability of Marine Structures Program, Stanford University.

Iyengar, R.N. and Rao, P.N., 1979. Generation of spectrum compatible accelerograms. *Earthquake Engineering and Structural Dynamics*, **7**(3), 253–263.

Jayaram, N. and Baker, J.W., 2008. Statistical tests of the joint distribution of spectral acceleration values. *Bulletin of the Seismological Society of America*, **98**(5), 2231–2243.

Jayaram, N., Lin, T., and Baker, J.W., 2011. A computationally efficient ground-motion selection algorithm for matching a target response spectrum mean and variance. *Earthquake Spectra*, **27**(3), 797–815.

Kaul, M.K., 1978. Spectrum-consistent time-history generation. *Journal of the Engineering Mechanics Division, ASCE*, **104**(4), 781–788.

King, A.C.Y. and Chen, C., 1977. Artificial earthquake generation for nuclear power plant design. In *Proceedings of the 6th World Conference on Earthquake Engineering*, 2609–2613, New Delhi, India.

Kost, G., Tellkamp, T., Kamil, H., Gantayat, A., and Weber, F., 1978. Automated generation of spectrum compatible artificial time histories. *Nuclear Engineering and Design*, **45**(1), 243–249.

Kramer, S.L., 1996. *Geotechnical Earthquake Engineering*. Prentice-Hall, New Jersey.

Lee, S-H. and Kim, J-S., 1999. Generation of an improved artificial time history matching multiple-damping design response spectra. In *Transactions of 15th International Conferences on Structural Mechanics in Reactor Technology (SMiRT-15)*, Seoul, Korea. Paper K14/4.

Levy, S. and Wilkinson, J.P.D., 1976. Generation of artificial time-histories rich in all frequencies, from given response spectra. *Nuclear Engineering and Design*, **38**(2), 241–251.

Lilhanand, K. and Tseng, W.S., 1988. Development and application of realistic earthquake time histories compatible with multiple-damping design spectra. In *Proceedings of the 9th World Conference on Earthquake Engineering*, 819–824, Tokyo, Japan.

Lin, C.-C.J. and Ghaboussi, J., 2001. Generating multiple spectrum compatible accelerograms using stochastic neural networks. *Earthquake Engineering and Structural Dynamics*, **30**(7), 1021–1042.

Lin, C.-C.J., Liu, Z.-M., and Lin, Y.-C., 2006. New methodology of generating multiple spectrum compatible earthquake accelerogram for Taiwan area using neural networks. In *Proceedings of the 4th International Conference on Earthquake Engineering*, Taipei, Taiwan. Paper No. 264.

Loh, C-H., Wu, T-C., and Huang, N.E., 2001. Application of the empirical mode decomposition-Hilbert spectrum method to identify near-fault ground-motion characteristics and structural responses. *Bulletin of the Seismological Society of America*, **91**(5), 1339–1357.

Maison, B.F., Neuss, C.F., and Kasai, K., 1983. The comparative performance of seismic response spectrum combination rules in building analysis. *Earthquake Engineering and Structural Dynamics*, **11**(5), 623–647.

McGuire, R., 1995. Probabilistic seismic hazard analysis and design earthquakes: Closing the loop. *Bulletin of the Seismological Society of America*, **85**(5), 1275–1284.

McGuire, R., 2004. *Seismic Hazard and Risk Analysis*. Earthquake Engineering Research Institute, Oakland.

Motazedian, D. and Atkinson, G., 2005. Stochastic finite-fault model based on dynamic corner frequency. *Bulletin of the Seismological Society of America*, **95**(3), 995–1010.

Mukherjee, S. and Gupta, V.K., 2002. Wavelet-based generation of spectrum-compatible time-histories. *Soil Dynamics and Earthquake Engineering*, **22**(9-12), 799–804.

Naeim, F. and Lew, M., 1995. On the use of design spectrum compatible time histories. *Earthquake Spectra*, **11**(1), 111–127.

NBCC, 2005. *National Building Code of Canada* 2005. National Research Council of Canada, Ottawa, Ontario.

NBCC, 2010. *National Building Code of Canada* 2010. National Research Council of Canada, Ottawa, Ontario.

Newmark, N.M., Blume, J.A., and Kapur, K.K., 1973. Seismic design spectra for nuclear power plants. *Journal of the Power Division*, **99**(2), 287–303.

Newmark, N.M. and Rosenblueth, E., 1971. *Fundamentals of Earthquake Engineering*. Prentice-Hall, New Jersey.

NIST, 2011. *Selecting and Scaling Earthquake Ground Motions for Performing Response-History Analyses*. U.S. Department of Commerce, National Institute of Standards and Technology Engineering Laboratory, NIST GCR 11-917-15, Gaithersburg, Maryland.

Ni, S.-H., Xie, W.-C., and Pandey, M.D., 2010. Generation of modified earthquake time-histories using Hilbert-Huang transform. In *Proceedings of the 5th International Conference on Bridge Maintenance, Safety and Management*, 2211–2215, Philadelphia, Pennsylvania.

Ni, S.-H., Xie, W.-C., and Pandey, M.D., 2011A. Application of Hilbert-Huang transform in generating spectrum-compatible earthquake time histories. *ISRN Signal Processing*, **2011**, ARTICLE ID 563678.

Ni, S.-H., Xie, W.-C., and Pandey, M.D., 2011B. Generation of multiple spectrum-compatible earthquake ground motions using Hilbert-Huang transform. *Structural Safety*, (SUBMITTED).

Ni, S.-H., Xie, W.-C., and Pandey, M.D., 2011c. Tri-directional spectrum-compatible earthquake time-histories for nuclear energy facilities. *Nuclear Engineering and Design*, **241**(8), 2732–2743.

Ni, S.-H., Xie, W.-C., and Pandey, M.D., 2012. Seismic design spectra based on probabilistic seismic hazard analysis. *Earthquake Spectra*, (SUBMITTED).

Ni, S.-H., Zhang, D.-Y., Xie, W.-C., and Pandey, M.D., 2011d. Vector-valued uniform hazard spectra. *Earthquake Spectra*, (ACCEPTED).

Nocedal, J. and Wright, S.J., 1999. *Numerical Optimization*. Springer, New York.

NRC, U.S, 1973. *Design Response Spectra for Seismic Design of Nuclear Power Plants, Regulatory Guide* 1.60. U.S. Nuclear Regulatory Commission.

Penzien, J. and Watabe, M., 1975. Characteristics of 3-dimensional earthquake ground motions. *Earthquake Engineering and Structural Dynamics*, **3**(4), 365–373.

Press, W.H., Teukolsky, S.A., Vetterling, W.T., and Flannery, B.P., 2007. *Numerical Recipes: The Art of Scientific Computing*. Cambridge University Press, San Francisco, third edition.

Preumont, A., 1980. A method for the generation of artificial earthquake accelerograms. *Nuclear Engineering and Design*, **59**(2), 357–368.

Preumont, A., 1984. The generation of spectrum compatible accelerograms for the design of nuclear power plants. *Earthquake Engineering and Structural Dynamics*, **12**(4), 481–497.

Reiter, L., 1990. *Earthquake Hazard Analysis: Issues and Insights*. Columbia University Press, New York.

Rizzo, P.C., Shaw, D.E., and Jarecki, S.J., 1975. Development of real/synthetic time histories to match smooth design spectra. *Nuclear Engineering and Design*, **32**(1), 148–155.

Rosenblueth, E., 1951. *A Basis for Aseismic Design of Structures*. Ph. D. thesis, University of Illinois at Urbana-Champaign.

Scanlan, R.H. and Sachs, K., 1974. Earthquake time histories and response spectra. *Journal of the Engineering Mechanics Division, ASCE*, **100**(4), 635–655.

SEAOC, 1995. *Vision* 2000, *Performance Based Seismic Engineering of Buildings, Vols. I and II: Conceptual Framework*. Structural Engineers Association of California, California.

Silva, W.J. and Lee, K., 1987. WES RASCAL code for synthesizing earthquake ground motions. In *State-of-the-Art for Assessing Earthquake Hazards in the United States*, US Army Corps of Engineers, Vicksburg, Mississippi. Report 24, Miscellaneous Paper S-73-1.

Spanos, P.D. and Loli, L.M. Vargas, 1985. A statistical approach to generation of design spectrum compatible earthquake time histories. *Soil Dynamics and Earthquake Engineering*, **4**(1), 2–8.

Tsai, N.C., 1972. Spectrum-compatible motions for design purposes. *Journal of the Engineering Mechanics Division, ASCE*, **98**(2), 345–356.

UBC, 1997. *1997 Uniform Building Code*. The International Conference of Building Officials (ICBO), California.

Vanmarcke, E.H. and Gasparini, D.A., 1977. Simulated earthquake ground motions. In *Transactions of 4th International Conferences on Structural Mechanics in Reactor Technology (SMiRT-4)*, San Francisco. Paper K1/9.

Wang, G., 2010. A ground motion selection and modification method preserving characteristics and aleatory variability of scenario earthquakes. In *Proceedings of the 9th U.S. National and 10th Canadian Conference on Earthquake Engineering*, Toronto, Canada. Paper No. 1270.

Wang, G., 2011. A ground motion selection and modification method capturing response spectrum characteristics and variability of scenario earthquakes. *Soil Dynamics and Earthquake Engineering*, **31**(1), 611–625.

Wen, Y.K. and Gu, P., 2004. Description and simulation of nonstationary processes based on Hilbert spectra. *ASCE Journal of Engineering Mechanics*, **130**(8), 942–951.

Zhang, R.R., Ma, S., and Hartzell, S., 2003A. Signatures of the seismic source in EMD-based characterization of the 1994 Northridge, California, earthquake recordings. *Bulletin of the Seismological Society of America*, **93**(1), 501–518.

Zhang, R.R., Ma, S., Safak, E., and Hartzell, S., 2003B. Hilbert-Huang transform analysis of dynamic and earthquake motion recordings. *Journal of Engineering Mechanics*, **129**(8), 861–875.

APPENDIX A

A.1 Earthquake Response Spectrum

G.W. Housner was instrumental in the widespread acceptance of the concept of the earthquake response spectrum, introduced by M.A. Biot in 1932, as a practical means of characterizing ground motions and their effects on structures. Now a central concept in earthquake engineering, the earthquake response spectrum provides a convenient means to summarize the peak response of all possible linear single degree-of-freedom (SDOF) systems to a particular component of ground motion. It also provides a practical approach to apply the knowledge of structural dynamics to the design of structures and development of lateral force requirements in building codes.

For a fixed damping ratio ζ, a plot of the peak value of a response quantity as a function of the natural vibration period T_n of the system or a related parameter, such as circular frequency ω_n or cyclic frequency f_n, is called the *earthquake response spectrum* for that quantity. Several such plots for different values of ζ are included to cover the range of damping values encountered in actual structures. Whether the peak response is plotted against f_n or T_n is a matter of personal preference. The latter has been chosen because engineers prefer to use natural period rather than natural frequency as the period of vibration is a more familiar concept and one that is intuitively appealing. Earthquake response spectra can be established mathematically as follows.

The equation of motion of a linear single DOF system as shown in Figure A.1 subjected to ground acceleration $\ddot{u}_g(t)$ is given by

$$\ddot{u} + 2\zeta\omega_n\dot{u} + \omega_n^2 u = -\ddot{u}_g(t). \tag{A.1.1}$$

It is clear that, for given $\ddot{u}_g(t)$, the relative displacement response $u \equiv u(t, T_n, \zeta)$, with respect to the ground, of the system depends only on the natural frequency ω_n or natural period T_n of the system and its damping ratio ζ.

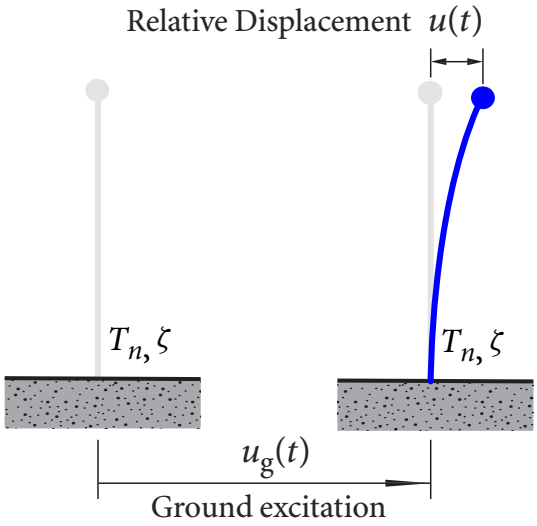

Figure A.1 Single degree-of-freedom (SDOF) system

The displacement response of the linear single DOF system in equation (A.1.1) to an arbitrary ground motion with zero initial conditions can be solved by Duhamel's integral as

$$u(t) = -\frac{1}{\omega_d}\int_0^t \ddot{u}_g(\tau)\mathrm{e}^{-\zeta\omega_n(t-\tau)}\sin[\omega_d(t-\tau)]\mathrm{d}\tau, \tag{A.1.2}$$

where $\omega_d = \omega_n\sqrt{1-\zeta^2}$.

Differentiating equation (A.1.2) with respect to t leads to

$$\dot{u}(t) = -\zeta\omega_n u(t) - \int_0^t \ddot{u}_g(\tau)\mathrm{e}^{-\zeta\omega_n(t-\tau)}\cos[\omega_d(t-\tau)]\mathrm{d}\tau. \tag{A.1.3}$$

Using equation (A.1.1), the absolute acceleration $\ddot{u}^{\mathrm{a}}(t)$ of the mass is given by

$$\ddot{u}^{\mathrm{a}}(t) = \ddot{u}_g(t) + \ddot{u}(t) = -2\zeta\omega_n\dot{u}(t) - \omega_n^2 u(t). \tag{A.1.4}$$

A variety of earthquake response spectra can be defined depending on the response quantity that is plotted. Consider the following peak responses:

$$S_d(T_n, \zeta) \equiv \max\left|u(t, T_n, \zeta)\right|_t, \tag{A.1.5}$$

$$S_v(T_n, \zeta) \equiv \max\left|\dot{u}(t, T_n, \zeta)\right|_t, \tag{A.1.6}$$

$$S_a(T_n, \zeta) \equiv \max\left|\ddot{u}^{\mathrm{a}}(t, T_n, \zeta)\right|_t. \tag{A.1.7}$$

The *relative displacement response spectrum* is a plot of $S_d(T_n, \zeta)$ against T_n for fixed ζ. A similar plot for $S_v(T_n, \zeta)$ is the *relative velocity response spectrum*. A plot for $S_a(T_n, \zeta)$ is the *absolute acceleration response spectrum*, the vertical coordinate of which is also called spectral acceleration (Chopra, 2001). Figure A.2 shows the concept of the earthquake response spectrum.

A.2 Seismic Analysis of Linear Systems

In this section, the *Seismic Response History Analysis* (SRHA) and the *Seismic Response Spectrum Analysis* (SRSA) are presented for earthquake analysis of structures idealized as lumped-mass linear systems.

A.2.1 Modal Analysis

The system of equations of motion for a linear n degrees-of-freedom (DOF) system as shown in Figure A.3 subjected to earthquake-induced ground motion $\ddot{u}_{\mathrm{g}}(t)$ is given by

$$\mathbf{m}\ddot{\mathbf{x}} + \mathbf{c}\dot{\mathbf{x}} + \mathbf{k}\mathbf{x} = -\mathbf{m}\boldsymbol{\nu}\ddot{u}_{\mathrm{g}}(t), \tag{A.2.1}$$

where $\mathbf{x} = \{x_1, x_2, \ldots, x_n\}^T$ is the relative displacement vector with respect to the ground, $\boldsymbol{\nu}$ is an n-dimensional column vector with all element being 1, and $\mathbf{m}$, $\mathbf{c}$, and $\mathbf{k}$ are the mass matrix, damping matrix, and stiffness matrix of the system, respectively.

To solve equations (A.2.1), modal analysis can be applied to determine the dynamic response of linear systems with classical damping, which is a reasonable model for many structures.

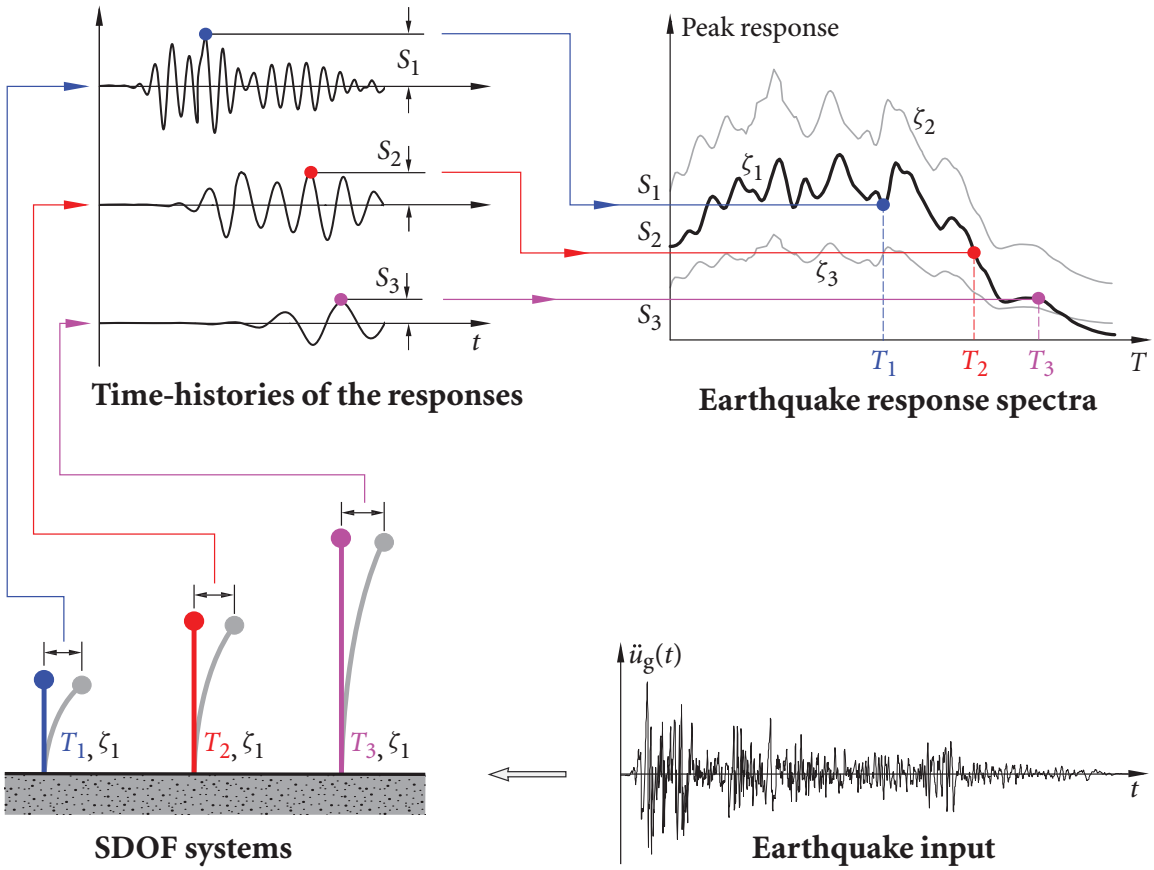

Figure A.2 Concept of the earthquake response spectrum

In modal analysis of earthquake response, undamped free vibrations are considered first. The equations of motion (A.2.1) are then reduced to

$$\mathbf{m}\ddot{\mathbf{x}} + \mathbf{k}\mathbf{x} = \mathbf{0}. \tag{A.2.2}$$

Seeking a solution of the form

$$\mathbf{x}(t) = \boldsymbol{\phi} \sin(\omega t + \theta) \tag{A.2.3}$$

and substituting into equation (A.2.2) yield

$$\left[\mathbf{k} - \omega^2 \mathbf{m}\right]\boldsymbol{\phi} \sin(\omega t + \theta) = \mathbf{0}. \tag{A.2.4}$$

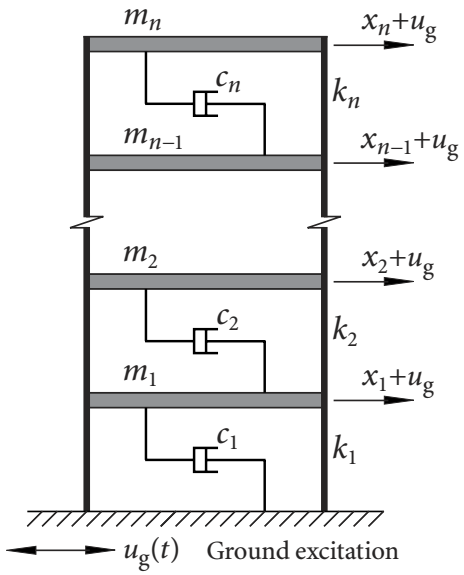

Figure A.3 An n-storey shear building modelled as an n degrees-of-freedom system

Since $\sin(\omega t+\theta)$ is not identically zero, one must have

$$\big[\mathbf{k}-\omega^2\mathbf{m}\big]\boldsymbol{\phi}=\mathbf{0}. \tag{A.2.5}$$

Equation (A.2.5) is a system of n homogeneous linear *algebraic* equations. To have non-zero solutions for $\boldsymbol{\phi}$, the determinant of the coefficient matrix must be zero:

$$\det\big[\mathbf{k}-\omega^2\mathbf{m}\big]=0, \tag{A.2.6}$$

which leads to the *characteristic equation*, a polynomial equation in ω^2 of degree n. Equation (A.2.6) is also called the *frequency equation*. Since the mass and stiffness matrices $\mathbf{m}$ and $\mathbf{k}$ are symmetric and positive definite, it can be shown that all roots ω^2 of the frequency equation are real and positive. The jth root ω_j, which is called the jth eigenvalue ($\omega_1<\omega_2<\ldots<\omega_n$), is the natural circular frequency of the jth mode of the system or the jth *modal frequency*.

Corresponding to the jth eigenvalue ω_j, a non-zero solution $\boldsymbol{\phi}_j$ of system (A.2.5),

$$\big[\mathbf{k}-\omega_j^2\mathbf{m}\big]\boldsymbol{\phi}_j=\mathbf{0}, \tag{A.2.7}$$

is the jth eigenvector or the jth *mode shape*.

The natural mode shapes corresponding to different natural frequencies can be shown to satisfy the following orthogonality conditions. When $j \neq r$,

$$\boldsymbol{\phi}_j^T \mathbf{k} \boldsymbol{\phi}_r = 0, \quad \boldsymbol{\phi}_j^T \mathbf{m} \boldsymbol{\phi}_r = 0, \tag{A.2.8}$$

which are important properties for solving equations (A.2.1).

Any set of n independent vectors can be used as a basis for representing any other vector of dimension n. The natural modes are used as such a basis. Thus, the displacement vector $\mathbf{x}$ of the n-DOF system can be expanded in terms of modal contributions:

$$\mathbf{x}(t) = \sum_{r=1}^{n} \boldsymbol{\phi}_r q_r(t). \tag{A.2.9}$$

Substituting equation (A.2.9) into equation (A.2.1) gives

$$\sum_{r=1}^{n} \mathbf{m} \boldsymbol{\phi}_r \ddot{q}_r(t) + \sum_{r=1}^{n} \mathbf{c} \boldsymbol{\phi}_r \dot{q}_r(t) + \sum_{r=1}^{n} \mathbf{k} \boldsymbol{\phi}_r q_r(t) = -\mathbf{m} \boldsymbol{\nu} \ddot{u}_{\mathrm{g}}(t). \tag{A.2.10}$$

Pre-multiplying each term in equation (A.2.10) by $\boldsymbol{\phi}_j^T$ gives

$$\sum_{r=1}^{n} \boldsymbol{\phi}_j^T \mathbf{m} \boldsymbol{\phi}_r \ddot{q}_r(t) + \sum_{r=1}^{n} \boldsymbol{\phi}_j^T \mathbf{c} \boldsymbol{\phi}_r \dot{q}_r(t) + \sum_{r=1}^{n} \boldsymbol{\phi}_j^T \mathbf{k} \boldsymbol{\phi}_r q_r(t) = -\boldsymbol{\phi}_j^T \mathbf{m} \boldsymbol{\nu} \ddot{u}_{\mathrm{g}}(t). \tag{A.2.11}$$

Assuming that the orthogonality condition applies to the damping matrix

$$\boldsymbol{\phi}_j^T \mathbf{c} \boldsymbol{\phi}_r = \begin{cases} 0, & j \neq r, \\ C_j, & j = r, \end{cases} \tag{A.2.12}$$

equation (A.2.11) becomes

$$M_j \ddot{q}_j(t) + C_j \dot{q}_j(t) + K_j q_j(t) = -L_j \ddot{u}_{\mathrm{g}}(t), \quad j = 1, 2, \ldots, n, \tag{A.2.13}$$

where

$$M_j = \boldsymbol{\phi}_j^T \mathbf{m} \boldsymbol{\phi}_j, \quad C_j = \boldsymbol{\phi}_j^T \mathbf{c} \boldsymbol{\phi}_j, \quad K_j = \boldsymbol{\phi}_j^T \mathbf{k} \boldsymbol{\phi}_j, \quad L_j = \boldsymbol{\phi}_j^T \mathbf{m} \boldsymbol{\nu}. \tag{A.2.14}$$

Dividing equation (A.2.13) by M_j gives

$$\ddot{q}_j(t) + 2\zeta_j \omega_j \dot{q}_j(t) + \omega_j^2 q_j(t) = -\gamma_j \ddot{u}_{\mathrm{g}}(t), \quad j = 1, 2, \ldots, n, \tag{A.2.15}$$

where ζ_j is the damping ratio for the jth mode. The modal participation factor γ_j is given by

$$\gamma_j = \frac{L_j}{M_j} = \frac{\boldsymbol{\phi}_j^T \mathbf{m} \boldsymbol{\nu}}{\boldsymbol{\phi}_j^T \mathbf{m} \boldsymbol{\phi}_j}. \tag{A.2.16}$$

Replacing $q_j(t)$ by $u_j(t)$ in equation (A.2.15) to emphasize the motion of an single degree-of-freedom system subjected to ground acceleration $\ddot{u}_g(t)$ for the jth mode of the system:

$$\ddot{u}_j(t) + 2\zeta_j \omega_j \dot{u}_j(t) + \omega_j^2 u_j(t) = -\ddot{u}_g(t), \quad j = 1, 2, \ldots, n, \tag{A.2.17}$$

and comparing equation (A.2.15) to (A.2.17) gives

$$q_j(t) = \gamma_j u_j(t). \tag{A.2.18}$$

Thus, the set of n coupled differential equations (A.2.1) in nodal displacements $x_j(t)$ is transformed to the set of n uncoupled differential equations (A.2.13) in modal coordinates $q_j(t)$. Equation (A.2.17) governs the equation of motion of the jth mode (a single DOF system) of the structural system with damping ratio ζ_j and natural frequency ω_j subjected to ground acceleration $\ddot{u}_g(t)$. $u_j(t)$ in equation (A.2.17) can be determined using equation (A.1.2). The response of the linear n degrees-of-freedom system as shown in Figure A.3 subjected to earthquake-induced ground motion $\ddot{u}_g(t)$ then can be obtained using equations (A.2.9) and (A.2.18).

A.2.2 Seismic Response History Analysis

The *Seismic Response History Analysis* (SRHA) procedure is concerned with the calculation of structural response as a function of time when the system is subjected to a given ground acceleration $\ddot{u}_g(t)$.

For illustration purpose, the nodal inertia forces of the n-DOF system are computed using SRHA. From equations (A.2.9) and (A.2.18), the acceleration vector of modal masses (degrees-of-freedom) of the system relative to the ground is given by

$$\ddot{\mathbf{x}}(t) = \sum_{j=1}^{n} \boldsymbol{\phi}_j \gamma_j \ddot{u}_j(t), \tag{A.2.19}$$

where $\ddot{u}_j(t)$ is the acceleration of the jth mode of the system relative to the ground.

The vector of the earthquake-induced ground motion can be written as

$$\ddot{\mathbf{u}}_{\mathrm{g}}(t) = \sum_{j=1}^{n} \boldsymbol{\phi}_j \gamma_j \ddot{u}_{\mathrm{g}}(t), \tag{A.2.20}$$

since

$$\boldsymbol{v} = \sum_{j=1}^{n} \boldsymbol{\phi}_j \gamma_j, \tag{A.2.21}$$

according to equation (A.2.18), which implies that the modal participation factor γ_j is equal to the modal coordinate $q_j(t)$, when the displacement of each degree-of-freedom of the system is unit.

The nodal inertia forces of the n-DOF system is given by

$$\mathbf{F}(t) = -\mathbf{m}\big[\ddot{\mathbf{u}}_{\mathrm{g}}(t) + \ddot{\mathbf{x}}(t)\big], \tag{A.2.22}$$

where $\big[\ddot{\mathbf{u}}_{\mathrm{g}}(t) + \ddot{\mathbf{x}}(t)\big]$ is the vector of the nodal absolute acceleration of the system. Substituting equations (A.2.19) and (A.2.20) into equation (A.2.22) gives

$$\mathbf{F}(t) = -\mathbf{m} \sum_{j=1}^{n} \boldsymbol{\phi}_j \gamma_j \big[\ddot{u}_{\mathrm{g}}(t) + \ddot{u}_j(t)\big], \tag{A.2.23}$$

which is a function of time.

A.2.3 Seismic Response Spectrum Analysis

The *Seismic Response Spectrum Analysis* (SRSA) is concerned with procedures to compute the peak response of a structure during an earthquake directly from the earthquake response (or design) spectrum without the need for seismic response history analysis of the structure. This procedure is not an exact predictor of peak response, but it provides an estimate that is sufficiently accurate for structural design applications.

From equation (A.2.23), the inertia forces on the modal masses of the jth mode of the n degrees-of-freedom system subjected to the ground acceleration is given by

$$\mathbf{F}_j(t) = -\mathbf{m}\boldsymbol{\phi}_j \gamma_j \big[\ddot{u}_{\mathrm{g}}(t) + \ddot{u}_j(t)\big], \quad j = 1, 2, \ldots, n. \tag{A.2.24}$$

Based on the assumption that the peak response (inertia force) of each mode of the system occurs at the same time, the absolute peak response of the jth mode of the system can be

expressed as

$$\mathbf{F}_{j,\max}(t) = -\mathbf{m}\boldsymbol{\phi}_j\gamma_j\left|\ddot{u}_g(t)+\ddot{u}_j(t)\right|_{\max}, \tag{A.2.25}$$

where $\left|\ddot{u}_g(t)+\ddot{u}_j(t)\right|_{\max}$ is the peak absolute acceleration of the jth mode of the system, which can be obtained from the *earthquake response spectrum* for the jth mode with modal period T_j and modal damping ratio ζ_j as discussed in Appendix A.1, i.e.,

$$\left|\ddot{u}_g(t)+\ddot{u}_j(t)\right|_{\max} = S_a(T_j,\zeta_j), \tag{A.2.26}$$

in which $S_a(T_j,\zeta_j)$ is the spectral acceleration for period T_j and damping ratio ζ_j as indicated in equation (A.1.7). The peak response of the n-DOF system can then be obtained by combining the peak response of each mode using a modal combination rule as presented in Appendix A.3.

A.3 Combination Rules for Modal Superposition Method

A suitable combination rule is required to conduct the SRSA. In this section, various existing combination rules of modal superposition method for SRSA are presented. The assumptions for using modal superposition method to predict approximate seismic demands of structures are discussed.

The modal superposition method in SRSA is to transform the coupled multiple degrees-of-freedom equations of motion to a set of uncoupled equations in normal coordinates. Because no time information is available when the peak modal values occur, approximations must be introduced in combining these peak modal responses determined from the earthquake response spectrum. Based on the assumption that all modal peaks occur at the same time when subjected to a single ground excitation, combination rules can be used to obtain approximate peak response of the structure.

The *square-root-of-sum-of-squares* (SRSS) rule for modal combination, developed in E. Rosenblueth's Ph.D. thesis (Rosenblueth, 1951), is given by

$$R_{\max} = \left(\sum_{j=1}^{n} R_j^2\right)^{\frac{1}{2}}, \tag{A.3.1}$$

where $R_{\max}$ is an estimated maximum response for quantity R (e.g., nodal inertia force), R_j is the maximum response of quantity R in mode j, and n is the number of modes

considered. The SRSS rule provides excellent response estimates for structures with well-separated natural frequencies. This limitation has not always been recognized in applying this rule to practical problems, and at times it has been misapplied to systems with closely spaced natural frequencies, such as piping systems in nuclear power plants and multi-story buildings with non-symmetric plan (Chopra, 2001).

The *complete quadratic combination* (CQC) rule for modal combination is applicable to a wider class of structures as it overcomes the limitations of the SRSS rule. The CQC rule (Der-Kiureghian, 1979, Der-Kiureghian, 1980) is given by

$$R_{\max} = \left(\sum_{i=1}^{n} \sum_{j=1}^{n} R_i \rho_{ij} R_j \right)^{\frac{1}{2}}, \tag{A.3.2}$$

where

$$\rho_{ij} = \frac{8(\zeta_i \zeta_j \omega_i \omega_j)^{\frac{1}{2}} (\zeta_i \omega_i + \zeta_j \omega_j) \omega_i \omega_j}{(\omega_i^2 - \omega_j^2)^2 + 4\zeta_i \zeta_j \omega_i \omega_j (\omega_i^2 + \omega_j^2) + 4(\zeta_i^2 + \zeta_j^2) \omega_i^2 \omega_j^2},$$

in which ω_j is the natural frequency of the jth mode and ζ_j is the critical damping ratio for the jth mode.

The *double sum combination* (DSC) method for modal combination (Newmark and Rosenblueth, 1971) can be expressed as

$$R_{\max} = \left(\sum_{i=1}^{n} \sum_{j=1}^{n} R_i \rho_{ij} R_j \right)^{\frac{1}{2}}, \tag{A.3.3}$$

where

$$\rho_{ij} = \left[1 + \left(\frac{\omega_i' - \omega_j'}{\beta_i' \omega_i + \beta_j' \omega_j} \right)^2 \right]^{-1}, \quad \omega_j' = \omega_j \left[1 - (\beta_j')^2 \right]^{\frac{1}{2}}, \quad \beta_j' = \zeta_j + \frac{2}{T_S \omega_j},$$

in which T_S is the time duration of strong-motion segment of earthquake ground motion time-history (the subscript "S" standing for Strong). For recorded ground motions, T_S may be represented by the strong motion segment characterized by extremely irregular accelerations of roughly equal intensity. Since the formulation of the modal cross-correlation matrix in the DSC considers the strong-motion duration T_S, the DSC rule has the potential to provide better estimated peak response than the CQC rule. However, the selection of T_S is somewhat arbitrary when using seismic design spectra (Maison *et al.*, 1983).

The accuracy of each of the above modal combination rules in predicting the peak structural response depends on the characteristics of the earthquake ground excitation and the dynamic properties of the structure. The SRSS, CQC, and DSC rules are based on the theory of random vibration.

Two of the major assumptions used in the development of these rules are: (1) the excitation is a sample of stationary Gaussian random process with a wide frequency band (covering the natural frequencies of the structure) and (2) the vibration responses of the normal modes of the structure are also stationary. The simple form of the SRSS rule as compared to the CQC and DSC rules is a consequence of the additional assumption that the modal vibrations are statistically independent, i.e., the vibration of any mode is not correlated to that of any other modes (Maison *et al.*, 1983).

A.4 Fourier Spectral Analysis

While studying heat flow problems in the early nineteenth century, the French mathematician J.B.J. Fourier showed that any periodic function that meets certain conditions can be expressed as the sum of a series of sinusoids of different amplitude, frequency, and phase, which is known as the *Fourier series*. In earthquake engineering, Fourier series is often used to approximately represent recorded earthquake ground motions.

A.4.1 Fourier Series

Since a Fourier series is simply a summation of simple harmonic functions, it can be expressed using trigonometric notation. The general trigonometric form of the Fourier series representing a periodic function $x(t)$ with period T is

$$x(t) = a_0 + \sum_{k=1}^{\infty} (a_k \cos \omega_k t + b_k \sin \omega_k t), \tag{A.4.1}$$

where the *Fourier coefficients* are

$$a_0 = \frac{1}{T}\int_0^T x(t)\mathrm{d}t,$$
$$a_k = \frac{2}{T}\int_0^T x(t)\cos\omega_k t\mathrm{d}t, \quad k = 1, 2, \ldots, \tag{A.4.2}$$
$$b_k = \frac{2}{T}\int_0^T x(t)\sin\omega_k t\mathrm{d}t, \quad k = 1, 2, \ldots,$$

where $\omega_k = 2\pi k/T$. The term a_0 represents the average value of $x(t)$ over the range from $t = 0$ to T. The Fourier series represents a function exactly only for $k \to \infty$. If the series is truncated at some finite value of K, the Fourier series only approximates the function $x(t)$.

A.4.2 Discrete Fourier Transform

In earthquake engineering, recorded ground motions are described by a finite number of data points rather than by analytical functions. In such cases, the Fourier coefficients are obtained by summation rather than integration.

To use Fourier transform, the earthquake ground motion is assumed to be periodic with period $T = N\Delta t$, which is the duration of the time-history. For a time-history of N sampling points, the value of the mth sampling point can be expressed as

$$x_m = x(t)\big|_{t=m\Delta t} = x(m\Delta t), \quad m = 0, 1, 2, \ldots, N-1, \tag{A.4.3}$$

where Δt is sampling interval.

Based on the assumption that N is an even number, the Fourier series in equation (A.4.1) can be modified to represent the value of the mth sampling point of the time-history $x(t)$ as

$$x_m = \frac{a_0}{2} + \sum_{k=1}^{N/2-1}\left(a_k\cos\frac{2\pi km}{N} + b_k\sin\frac{2\pi km}{N}\right) + \frac{A_{N/2}}{2}\cos\frac{2\pi(N/2)m}{N},$$
$$m = 0, 1, 2, \ldots, N-1, \tag{A.4.4}$$

where the N Fourier coefficients are

$$a_0, a_1, a_2, \ldots, a_{N/2-1}, a_{N/2} \quad \text{and} \quad b_1, b_2, \ldots, b_{N/2-1},$$

which can be treated as N unknown constants in N equations (A.4.4).

Using the orthogonality property of trigonometric functions,

$$\begin{aligned}
\sum_{m=0}^{N-1} \cos\frac{2\pi lm}{N}\cos\frac{2\pi km}{N} &= \begin{cases} N/2, & k=l, \\ 0, & k\neq l, \end{cases} \\
\sum_{m=0}^{N-1} \sin\frac{2\pi lm}{N}\sin\frac{2\pi km}{N} &= \begin{cases} N/2, & k=l, \\ 0, & k\neq l, \end{cases} \\
\sum_{m=0}^{N-1} \sin\frac{2\pi lm}{N}\cos\frac{2\pi km}{N} &= 0,
\end{aligned} \tag{A.4.5}$$

equations (A.4.4) can be solved to obtain the N Fourier coefficients:

$$a_k = \frac{2}{N}\sum_{m=0}^{N-1} x_m \cos\frac{2\pi km}{N}, \quad k = 0, 1, 2, \ldots, \frac{N}{2}-1, \frac{N}{2}, \tag{A.4.6a}$$

$$b_k = \frac{2}{N}\sum_{m=0}^{N-1} x_m \sin\frac{2\pi km}{N}, \quad k = 1, 2, \ldots, \frac{N}{2}-1. \tag{A.4.6b}$$

The time-history $x(t)$ thus can be approximately represented by the Fourier series with $N/2$ harmonics as

$$\tilde{x}(t) = \frac{a_0}{2} + \sum_{k=1}^{N/2-1}\left(a_k \cos 2\pi f_k t + b_k \sin 2\pi f_k t\right) + \frac{A_{N/2}}{2}\cos 2\pi f_{N/2} t, \tag{A.4.7}$$

where the frequency of the kth harmonic of the series is given by

$$f_k = \frac{k}{N\Delta t}, \quad k = 1, 2, \ldots, \frac{N}{2}. \tag{A.4.8}$$

When $k=N/2$, $f_{N/2}=1/(2\Delta t)$ is the highest frequency valid for the time-history $x(t)$, known as the *Nyquist frequency*.

Using trigonometric identities, equation (A.4.7) can also be expressed as

$$\tilde{x}(t) = \frac{c_0}{2} + \sum_{k=1}^{N/2-1} c_k \cos(2\pi f_k t + \theta_k) + \frac{c_{N/2}}{2}\cos 2\pi f_{N/2} t, \tag{A.4.9}$$

where

$$c_k = \sqrt{a_k^2 + b_k^2}, \quad \theta_k = \tan^{-1}(-b_k/a_k), \quad k = 1, 2, \ldots, \frac{N}{2}. \tag{A.4.10}$$

In this form, c_k and θ_k are the amplitude and phase, respectively, of the kth harmonic. A plot of $N\Delta t\, c_k/2$ versus f_k is known as the *Fourier amplitude spectrum* and a plot of θ_k versus f_k gives the *Fourier phase spectrum*.